Rôle des pompes à calcium SERCA3 dans les fonctions plaquettaires

Ziane Elaib

Rôle des pompes ATPases SERCA3 dans les fonctions plaquettaires

Thèse de doctorat de l'Université Paris-Saclay
Préparée à l'UMR-S INSERM 1176: HEMOSTASE, INFLAMMATION ET THROMBOSE"

École doctorale n°**568**

Spécialité de doctorat: **SIGNALISATIONS ET RÉSEAUX INTÉGRATIFS EN BIOLOGIE (BIOSIGNE)**

Thèse présentée et soutenue au Kremlin Bicêtre, **le 29/09/2017**, par

Ziane Elaïb

Composition du Jury :

Pascale Gaussem PU-PH, INSERM UMR1140	Président
Martine Jandrot-Perrus Directeur de recherche, INSERM UMR1148	Rapporteur
Bela Papp Chargé de recherche, INSERM UMR978	Rapporteur
José Manuel Cancela Chargé de recherche, CNRS UMR9197	Examinateur
Jean-Philippe Rosa Directeur de recherche, INSERM UMR1176	Directeur de thèse
Régis Bobe Chargé de recherche, INSERM UMR1176	Co-Directeur de thèse

Titre : Role des pompes ATPases SERCA3 dans les fonctions plaquettaires

Mots clés : Sécrétion plaquettaire, ADP, signal calcique, thrombose.

Résumé : L'élévation de la concentration du calcium (Ca^{2+}) cytosolique est responsable de l'activation plaquettaire. Cette élévation est due à l'entrée du Ca^{2+} à partir du milieu extérieur (influx) ou sa translocation (mobilisation) dans le cytosol depuis ses réserves internes. Les **SERCAs** (**S**arco/**E**ndoplasmic **R**eticulum **Ca**$^{2+}$ **A**TPases) pompent le Ca^{2+} depuis le cytosol vers les réserves internes, maintenant le Ca^{2+} cytosolique bas (100 nM) et les plaquettes au repos. D'autre part elles assurent une concentration calcique élevée (≥1 mM) dans les réserves calciques permettant sa mobilisation, et enfin modulent l'intensité et la forme du signal calcique lors de l'activation. Mais les rôles respectifs des SERCAs plaquettaires, SERCA2b et SERCA3, sont encore mal définis d'où l'intérêt de mon projet qui a été de déterminer si SERCA3 avait un rôle fonctionnel précis et spécifique. Nous avons observé sur des souris SERCA3$^{-/-}$ un défaut de l'hémostase et s'accompagne d'une résistance à la thrombose dû à un déficit de sécrétion d'ADP, entrainant un défaut d'agrégation et d'adhérence. SERCA3 semble contrôler une voie de sécrétion initiale d'ADP capable d'agir en synergie avec une faible activation plaquettaire, aboutissant à un renforcement de la sécrétion et de l'agrégation. De plus, l'utilisation des inhibiteurs pharmacologiques préférentiels de SERCA2b (thapsigargine) ou SERCA3 (tBHQ), a montré que la sécrétion initiale d'ADP n'était pas dépendante de la mobilisation des réserves SERCA2b mais dépendait spécifiquement des réserves SERCA3. Nous avons retrouvé la même voie de sécrétion d'ADP dépendante de SERCA3 dans les plaquettes humaines.

Nous avons en particulier montré par le suivi d'une cohorte de patientes atteintes d'obésité morbide, un déficit d'agrégation, une faible mobilisation calcique et un taux faible de SERCA3 plaquettaire, revenus à la normale après retour à un poids normal après chirurgie bariatrique. Surtout nous avons retrouvé, dans les plaquettes de ces patientes obèses, un défaut de sécrétion d'ADP associé au défaut de SERCA3. Il s'agit du premier défaut de SERCA3 plaquettaire lié à une pathologie humaine. Nous avons ensuite montré que la sécrétion initiale d'ADP était rapide (5 sec) et entièrement dépendante de SERCA3. A l'aide d'une sonde calcique fluorescente membranaire (FURA2-NearMem-AM), nous avons démontré l'existence d'une mobilisation calcique juxta-membranaire spécifique de SERCA3, indépendante de l'ADP, correspondant donc à une sécrétion primaire. Cette mobilisation dépendante des réserves SERCA3 s'est avérée indépendante d'IP3, mais dépendante du NAADP, qui mobilise spécifiquement les réserves contrôlées par SERCA3 et non SERCA2b. En conclusion, nous avons mis en évidence une nouvelle voie d'activation plaquettaire, indépendante de l'IP3 mais dépendante du NAADP qui libère le Ca^{2+} des stocks internes dépendants de SERCA3 et spécifiquement engagés dans la libération précoce d'ADP lors de l'activation plaquettaire. Ces données identifient de nouvelles cibles avec un intérêt thérapeutiques anti-thrombotiques potentiel.

Title : Role of calcium pump SERCA3 in platelets function

Keywords: Platelet secretion, ADP, calcium signaling, thrombosis.

Abstract: The elevation of cytosolic calcium (Ca^{2+}) is responsible for platelet activation. This elevation is due to the entry of Ca^{2+} from the extracellular medium (influx) where its translocation (mobilization) into the cytosol from its Ca^{2+} stores. SERCAs (Sarco / Endoplasmic Reticulum Ca^{2+} ATPases) pump Ca^{2+} from the cytosol to the Ca^{2+} stores, maintaining low cytosolic Ca^{2+} (100 nM) and platelets at resting state. On the other hand, they ensure a high calcium concentration (≥ 1 mM) in the Ca^{2+} stores allowing its mobilization, and finally modulate the intensity and the shape of the Ca^{2+} signal during the activation. However, the respective roles of platelets SERCAs, SERCA2b and SERCA3, are still poorly defined. Hence the interest of my project which was to determine if SERCA3 had a precise and specific functional role. We observed in SERCA3$^{-/-}$ mice a defect in hemostasis that is accompanied by resistance to thrombosis due to ADP secretion deficiency, resulting in a lack of aggregation and adhesion. SERCA3 seems to control an initial pathway of ADP secretion able to acting in synergy with low platelet activation, resulting in increased secretion and aggregation. In addition, the use of specific pharmacological inhibitors of SERCA2b (thapsigargine) or SERCA3 (tBHQ) showed that the initial secretion of ADP was not dependent on the mobilization of SERCA2b stores, but was specifically dependent on SERCA3 stores. We found the same SERCA3-dependent ADP secretion pathway in human platelets.

In particular, we observed a defect of platelet aggregation, low Ca^{2+} mobilization and low platelet SERCA3 levels in a cohort of patients with morbid obesity compared to control subjects. Platelet functions and SERCA3 levels are restored after weight loss by a surgery bariatric. Above all, we found in the platelets of these obese patients, a defect of secretion of ADP associated with the defect of SERCA3. This is the first defect of platelet SERCA3 related to human pathology. We then showed that the initial secretion of ADP was rapid (5 sec) and entirely dependent on SERCA3. Using a membrane fluorescent Ca^{2+} probe (FURA2-NearMem-AM), we have demonstrated the existence of a juxta-membrane-specific calcium mobilization specific to SERCA3, independently of ADP, corresponding to primary secretion. This SERCA3 mobilization proved to be independent of IP3, but dependent on the NAADP, which specifically mobilizes the SERCA3 and not SERCA2b reserves. In conclusion, we have demonstrated a new platelet activation pathway, independent of IP3 but dependent on NAADP, which releases Ca^{2+} from SERCA3 dependent stores and specifically involved in the early release of ADP during platelet activation. These data identify new targets with a potential interest of anti-thrombotic therapy.

Université Paris-Saclay
Espace Technologique / Immeuble Discovery
Route de l'Orme aux Merisiers RD 128 / 91190 Saint-Aubin, France

Remerciements :

La thèse est une expérience à la fois scientifique et humaine. Je tiens donc à remercier dans cette partie toutes les personnes qui ont compté pour moi depuis mon arrivée au laboratoire U1176 alias U770.

Tout d'abord je voudrais remercier mon directeur de thèse, le docteur **Jean-Philippe Rosa,** pour les connaissances que tu m'as apprises, tout ce que tu m'as apporté, sur le plan scientifique et humain. Merci pour ton soutien, tes conseils, ta disponibilité, je garderai toujours un bon souvenir de toutes ces discussions qui se sont déroulées dans ton bureau. La thèse n'est pas une aventure facile et tu as permis à ce que mon travail se déroule dans les meilleures conditions possibles, ce fut un réel plaisir de travailler avec toi (tu es comme un deuxième père pour moi).

Régis Bobe mon Co-directeur de thèse, le grand frère, merci pour tout ce que tu as fait pour moi, pour ta patience, tes idées, tes conseils et de m'avoir appris à réfléchir comme un chercheur et surtout de m'avoir appris ce qu'est le calcium. Grâce à toi on pourra m'appeler le calciologue

Marijke Bryckaert, je ne te remercierais jamais assez de m'avoir enseigné la signalisation plaquettaire et de m'avoir fait aimer le domaine de l'hémostase

Eliane Berrou, Fréderic Adam, Maryline Lebret et Odile Issertial merci de vos conseils scientifiques et surtout de m'avoir formé et appris toutes les techniques que je maitrise maintenant.

Un grand merci à **Cécile Denis** de m'avoir accueillie dans son laboratoire et de m'avoir supporté pendant toutes ces années

Je remercie également tous les membres de mon jury d'avoir accepté d'évaluer mon travail de thèse, Mesdames les Professeurs et docteurs **Pascale Gaussem, Martine Jendrot-Perrus,** et Messieurs les Docteurs **Bela Papp** et **José Manuel Cancella.**

Je tiens à remercier aussi toutes les personnes qui ont croisé ma route au laboratoire. À **Vincent Muczynski**, pour ton aide en IF, tes idées originales que tu m'as apportées. À **Amine Bazaa et Alexandre Kauskot** pour vos conseils que vous avez pu me donner.

Un petit détour par le secrétariat à présent. **Florence Fragnet et Anne-lise Marville**, merci pour votre bonne humeur, pour m'avoir remonté le moral quand il le fallait, pour tous vos bons conseils, votre sagesse. Votre dynamisme à toute épreuve et caractère de feu feront toujours du secrétariat un endroit où l'on ne s'ennuie jamais, merci pour tout.

A **Valérie Proulle** et **Thomas Brungs** d'avoir été toujours disponible pour les prélèvements sanguins au service d'hémostase

Je remercie l'équipe 2, **François Saller**, **Allan**, **Christelle**, **Elsa**, **Tiffany** et surtout la directrice de l'équipe **Delphine Borgel**, Ta passion insatiable dans le domaine de la recherche m'impressionne et je m'en inspire, tes paroles encourageantes et ton esprit ouvert font de toi une Directrice hors pair.

Je remercie également toutes les personnes de l'équipe 1, notamment **Paulette Legendre**, **Cécile Loubiere**, **Peter Lenting** et **Olivier Christophe**, **François Moreau** c'était un réel plaisir de vous croiser tous les matins dans le long couloir.

J'arrive à présent au bureau, à commencer **Yasmine Bourti**, ton dynamisme et ton sourire et ta joie de vivre auront fait de ces années au labo de super moments. A **Mahita Razalanakolonnna**, tu es trop gentil, et je te remercie de m'avoir supporté cette derrière année et je m'excuse du dérangement et le débordement sur ton bureau, je te souhaite bon courage pour ta dernière année de thèse. **Marion**, **Fatou** et **Awat** je n'oublierai jamais les moments passés avec vous au bureau, à **Meriem Benseka**, t'as apporté la lumière au bureau, d'accord tu rangeais tout mais aussi t'as apporté un esprit d'équipe et le dynamisme dans notre laboratoire. **Aléria**, **Sandra**, **Abdallah et Stepheuun** vous êtes des gens extraordinaires, sans oublier **Miao** mon étudiante que je laisse derrière moi, j'espère que tu vas bien faire progresser le projet.

Je remercie enfin chaleureusement mes **Parents** qui m'ont toujours soutenu dans ma vie et dans mon parcours. Vous êtes la source d'énergie qui me permet d'avancer. **Mes sœurs et mon frère** qui croient que je suis un grand chercheur (les pauvres). Je vous remercie d'être toujours présent pour moi lorsque j'en ai besoin, merci pour ce que vous m'avez apporté, pour votre soutien à chaque instant, pour tout. Et à tous mes **Cousins** avec qui j'ai partagé de bons moments durant ma thèse, les voyages qu'on a faits ensemble m'ont permis de décompresser un peu. A la grande famille **Bouhara**, vous avez toujours été là pour moi et c'est un immense plaisir, et surtout je dis bien suuurtout ma tante **Fahima**, alors là toi t'as vraiment été là pour moi à chaque fois merci du fond du cœur de m'avoir soutenu, aidé, réveillé le matin pour aller travailler, et de m'avoir préparé des plats extraordinaires que je ramenais avec moi et dont tout le monde au labo avait envie d'y goûter.

Bien sûr, je ne peux terminer mes remerciements sans exprimer ma profonde gratitude pour ma chérie adorée et épouse **Meriem**, tu as su me supporter, m'épauler, me réveiller, me remonter le moral avec une patience infinie. Sans ton amour, sans tes encouragements, sans toi tous simplement, je n'y serais jamais arrivé.

Et pour finir, cher lecteur, je vous souhaite une bonne lecture

Table des matières :

Liste des figures

Liste des Abréviations

A

Aa	Acides aminés
AC	Adénylate cyclase
ADNc	Acide désoxyribonucléique complémentaire
ADP	Adénosine Di-Phosphate
AM	Acetoxymethylester
AMPc	AMP cyclique
ATP	Adénosine Tri-Phosphate
ARN	Acide ribonucléique messagers

C

Ca^{2+}	Calcium
Ca^{2+}-CaM	Calcium Calmoduline
cADPR	ADP-ribose cyclique
cADPR-AM	cADPR acetoxymethylester
CalDAG-GEFI	Calcium- and Diacylglycerol-Binding Guanine Nucleotide Exchange factor
CaM	Calmoduline
CaMKII	Calmoduline kinase
CD62-P	P-Sélectine
CICR	Calcium Induced Calcium release
Cox	Cyclo-oxygénase
CPA	Acide cyclopiazonique
C-terminale	Extrémité carboxyterminale

D

Da	Dalton
DAG	Diacylglycerol

E

EGTA	Ethylène glycol-bis (beta-aminoethyl ether)-N,N,N',N'-tetraacetic acid

F

$FeCl_3$	Chlorure de fer
Fg	Fibrinogène
FIB-SEM	Focused ion beam / scanning electron microscope

G

GA	Granules Acides
GAPDH	Glycéraldéhyde-3-phosphate
GC	Guanylate cyclase
GMPc	GMP cyclique
GP	Glycoprotéines
GPVI	Glycoprotéine VI

I

IMC	Indice de masse corporelle
IP3	Inositol trisphosphate
IP3R	Inositol trisphosphate Receptor
ITAM	Immuno-tyrosine based activation motifs

K

K^+	Potassium
Kb	kilobase
KDa	kiloDalton
K_d	Constante de dissociation
KO	Knockout

L

La^{3+}	Lanthane
LAMP	Lysosomal-associated membrane protein
LRO	Lysosome Related Organelles

M

MAPK	Mitogen activated protein kinase
MCU	Mitochondrial Calcium Uniport

MHCIIA	Non-Muscle Myosin Heavy Chain IIA
Min	Minute
MK	Megakaryocyte

N

Na^+	Sodium
NAADP	Nicotinic Acid Adenine Dinucleotide Phosphate
NAADP -AM	NAADP acetoxymethylester
NCX	Na^+/Ca^{2+} exchanger
NCKX	Na^+/Ca^{2+} K^+ dépendant
NFAT	Nuclear factor of activated T-cell
NF-κB	Nuclear factor κB
NK	Natural Killer
nNOS	NO-synthase neuronale
NO	Monoxyde d'azote
NOS 3	NO synthase endothéliale
N-terminale	Extrémité aminoterminale

O

OAG	1-oléoyl-2-acétyl-sn-glycerol
ORAI	Calcium Release-Activated Calcium Modulator
OsO_4	Tétra-oxyde d'osmium

P

PAR	Protase Activator Receptor
Pb	Paire de base
PF4	Facteur plaquettaire-4
PGI2	Prostacycline
PGE1	Prostaglandines
Pi	Phosphate inorganique
PI	Phosphatidyl Inositol
PI3K	Phosphatidylinositide 3-kinase

PKA Protéines kinases A

PKC Protéines kinases C

PL Phospholipide

PLA_2 Phospholipase A_2

PLCβ Phospholipase β

PLCγ2 Phospholipase Cγ2

PLN Phospholamban

PMCA Plasma Membrane Ca^{2+} ATPase

PS Phosphatidyl Serine

R

RCPG Récepteurs couplés à des protéines G

RE Reticulum endoplasmic

RIAM Rap1-GTP-interacting Adaptor Molecule

R-IP_3 IP_3 receptor

ROC Receptor-operated channel

RT-PCR Reverse Transcription-Polymerase Chain Reaction

RyR Récepteur a la Ryanodine

S

SCO Système canaliculaire ouvert

SERCA Sarco-Endoplasmic Reticulum Ca^{2+} ATPase

SLN Sarcolipine

SMOC Second messenger-operated channel

SOCe Store Operated Calcium entry

SOC Store Operated Calcium

SPCA Secretory pathway Ca^{2+}ATPase

STD Système tubulaire dense

STIM1 Stromal interaction molecule 1

STK16 Serine/thréonine kinase 16

T

tBhQ	2,5-di-(*tert*-butyl)-1,4-benzohydroquinone
TEM	Microscopie électronique à transmission
Tg	Th apsigargine
TIRF	Total Internal Reflection Fluorescence microscopy
TRPC	Transient Receptor Potential Cation
TPC	Two Pore Chanel
TRPLM	Melastatin-like transient receptor potential
TSP1	Thrombospondine 1
TXA2	Thromboxane A2

V

VDAC	Voltage Dependent Anion Selective Channel
TFAM	The mitochondrial transcription Factor A
VOC	Voltage operated channel
$[VO_3(OH)]^{2-}$	Orthovanadate vWF
vWF	Facteur von Willebrand

W

WB	Immunoempreinte

Y

YPS	Syndrome de York

Généralités sur les plaquettes sanguines

Les plaquettes sont des éléments anucléés du sang importants dans l'hémostase dite primaire, où elles seront les premiers éléments à intervenir dans l'arrêt du saignement. Ces cellules sont dérivées de mégacaryocytes de la moelle osseuse. Les plaquettes au repos ont une structure discoïde biconvexe de 0,5 µm d'épaisseur et 2 µm de diamètre, d'un volume de 7 à 10 fL chez l'Homme, 4 à 6 fL chez la souris. La valeur normale du taux de plaquettes circulantes est comprise entre 150 000 et 400 000 par mm^3 (ou 150-400G/L), chez l'Homme, et de 400 000 à 1 600 000/mm^3 (moyenne: 1000 000/mm^3) chez la souris (1)

L'étude de la morphologie plaquettaire par microscopie électronique permet de distinguer trois zones principales (Figure 1 ; page 15) : **1)** la zone périphérique qui comprend la membrane plasmique, le système canaliculaire ouvert (SCO) et le système tubulaire dense (STD). **2)** la zone des organelles comprenant des granules de sécrétion (alpha (α), denses et lysosomes), des grains de glycogène, des mitochondries, des peroxysomes et l'appareil de Golgi. **3)** la zone du cytosquelette comprenant des microtubules et des filaments d'actine (2).

A) La membrane plasmique

La membrane plasmique plaquettaire est caractérisée par une distribution asymétrique des phospholipides avec un feuillet interne riche en charges négatives (Phosphatidyl Serine, (PS) et Phosphatidyl Inositol (PI)). Les lipides de la membrane plasmique sont riches en cholestérol libre qui permet d'assurer une certaine stabilité et rigidité des membranes. Au cours de l'activation plaquettaire, les charges négatives des phospholipides anioniques vont être externalisées vers le feuillet externe et vont permettre ainsi l'interaction des protéines de la coagulation avec la membrane. Sont également insérés dans cette bicouche lipidique différents récepteurs dont les glycoprotéines (GP) (60% des protéines totales) impliquées dans les fonctions plaquettaires: les interactions cellules-cellules, la détection de molécules extra-cytoplasmiques et la transduction des signaux. Le système canaliculaire ouvert, ou SCO, correspond à des invaginations profondes de la membrane externe au travers du cytoplasme et est en continuité avec la surface cellulaire. Ce réservoir de membranes facilite l'étalement des plaquettes lors de leur activation en leur permettant de disposer d'une surface membranaire importante en contact avec l'extérieur. Au cours de l'activation plaquettaire, la membrane des granules fusionne avec le SCO facilitant ainsi la libération du contenu granulaire. Le système tubulaire dense, ou STD, est un réseau analogue au réticulum endoplasmique. Le STD contient

essentiellement du Ca^{2+}, des enzymes du métabolisme lipidique (essentiellement prostaglandines (PGE1)) comme la peroxydase plaquettaire, mais aussi des ATPases calcium (Ca^{2+}) dépendantes, ces pompes calciques sont ancrées dans la membrane du STD pour la régulation du transport du Ca^{2+} intracellulaire.

B) La zone des organelles

La zone des organelles comprend des mitochondries, des peroxysomes, des grains de glycogène et des granules de sécrétion (granules denses ou δ, granules α, granules acides et les lysosomes ou granules γ). Lors de l'activation plaquettaire, les granules sécrètent leur contenu par un mécanisme d'exocytose.

I) Les granules denses

Les granules denses sont un sous-type d'organites analogues aux lysosomes (Lysosome Related Organelles ou "LRO"), au nombre 3 à 6 par plaquette humaine et 8 par plaquette murine (3) (4) et ils ont un diamètre variant de 100 à 300 nm (5). Une pompe à protons H^+-ATPase vésiculaire maintient le contenu de ces granules à un pH ~ 5,4 (6). Ils sont denses aux électrons en microscopie électronique, donc visibles en l'absence de coloration. Ceci est dû, notamment, à leur contenu très riche en Ca^{2+} (~2 M) (7). Ils contiennent également de l'Adénosine Di-Phosphate (ADP) (~650 mM), de l'Adénosine tri-Phosphate (ATP) (~450 mM), du pyrophosphate (~300 mM), de la sérotonine (~65 mM), de l'adrénaline et de la noradrénaline (8) (9), et récemment la présence des poly-phosphates a été mise en évidence (10). La membrane des granules denses contient en faible quantité la P-Sélectine ou (CD62-P), GPIb, l'intégrine αIIbβ3 et des protéines lysosomales: LAMP-2 et LAMP-3 (CD63) (lysosomal-associated membrane protein) (11). Les granules denses jouent un rôle crucial dans le processus de l'hémostase primaire en sécrétant de l'ADP qui par l'intermédiaire de ses récepteurs ($P2Y_1$ et $P2Y_{12}$) permet d'amplifier l'activation plaquettaire.

Il a été montré que la sécrétion de la sérotonine contenue que dans les granules denses survient avant la sécrétion du facteur plaquettaire 4 (PF4) contenu dans les granules α ou avec la sécrétion de β-hexosaminidase depuis les lysosomes, quel que soit l'activateur utilisé pour stimuler les plaquettes (12) (13). Ces résultats suggèrent que les granules denses sont sécrétés avant les granules α.

II) Les granules α

Les granules α sont plus abondants (50 à 80 par plaquette humaine, 37 à 45 par plaquette murine) (3). Ils mesurent entre 200 et 500 nm de diamètre et représentent environ 10% du volume des plaquettes. Les granules α contiennent une variété de protéines membranaires qui leur donnent une apparence distincte lorsqu'ils sont colorés par le tétra-oxyde d'osmium (OsO_4) puis observés par microscopie électronique à transmission (TEM), où ils apparaissent avec un contenu grisé, et souvent un noyau plus foncé ou nucléoïde, correspondant probablement à des protéines cristallisées. Les granules α contiennent des protéines adhésives importantes pour l'hémostase primaire telles que le fibrinogène (Fg), le facteur von Willebrand (vWF), la thrombospondine 1 (TSP1), la fibronectine, la vitronectine, mais aussi un grand nombre de facteurs de la coagulation, de l'inflammation, de l'angiogenèse, ainsi que des facteurs de croissance (VEGF), des cytokines (TGFβ), des chimiokines (PF4), ou encore des protéines membranaires comme l'intégrine αIIbβ3, le complexe GPIb-IX-V, la P-selectine. Une étude a montré par immunofluorescence que le facteur vWF et le Fg n'étaient pas contenus dans les mêmes granules α, suggérant ainsi l'existence de sous-populations de ces granules (14).

III) Les lysosomes

Les lysosomes ou granules λ, sont des petits organites de structures arrondies de 175 à 250 nm de diamètre. Les plaquettes possèdent des lysosomes qui deviennent actifs après intégration de l'élément à dégrader. Le recyclage des macromolécules ou particules endocytées fait aussi partie de leur fonction (15). Les lysosomes contiennent principalement des enzymes (par exemple des protéases, lipases, glycosidases, nucléases) ainsi que des protéines membranaires comme celles de la famille LAMP (LAMP-1, LAMP-2 et LAMP-3). Ces lysosomes sont des organites sécrétables après activation plaquettaire (16).

C) Le cytosquelette

La membrane plasmique est supportée par un cytosquelette très développé, constitué par différents systèmes fibrillaires: les microtubules, les microfilaments d'actine et de filaments intermédiaires (kératine). Ce cytosquelette joue un rôle important dans le maintien et le changement de forme des plaquettes observé au cours de l'activation et de l'agrégation. L'actine représente 20% des protéines totales plaquettaires et elle est nécessaire à la contraction, la sécrétion, la rétraction du caillot, l'émission de filopodes et la formation des lamellipodes. Au repos, 40% de l'actine est sous forme polymérisée en longs filaments (actine F). Lors de l'étalement plaquettaire, l'actine se réorganise et la proportion de sa forme polymérisée atteint

80% des protéines plaquettaires totales . Ce remodelage de l'actine plaquettaire est sous le contrôle de différentes protéines, notamment certaines protéines G de la famille Rho (Cdc42, Rac1 et RhoA). En effet, Cdc42 joue un rôle dans la régulation de la sécrétion des granules denses et peut être en partie responsable de la formation des filopodes plaquettaires. La protéine Rac1 est impliquée dans la formation des lamellipodes après interactions collagène-Glycoprotéine VI (GPVI) et thrombine-PAR (Protase Activator Receptor), en formant un réseau fin d'actine lors de l'étalement. Enfin, RhoA est également impliquée dans la régulation de la formation des lamellipodes, mais aussi dans la génération des fibres de stress à la suite de l'activation des intégrines.

Au repos, les microtubules périphériques confèrent aux plaquettes leur forme discoïde (Figure 1). Il est possible qu'un seul microtubule faisant plusieurs tours, agisse comme un ressort écarteur, d'où la forme en lentille aplatie des plaquettes. Lors de l'activation plaquettaire, ce microtubule se dépolymérise. Alors, plusieurs microtubules se reforment au centre de la plaquette et leur contraction permet la centralisation et l'exocytose des granules (17).

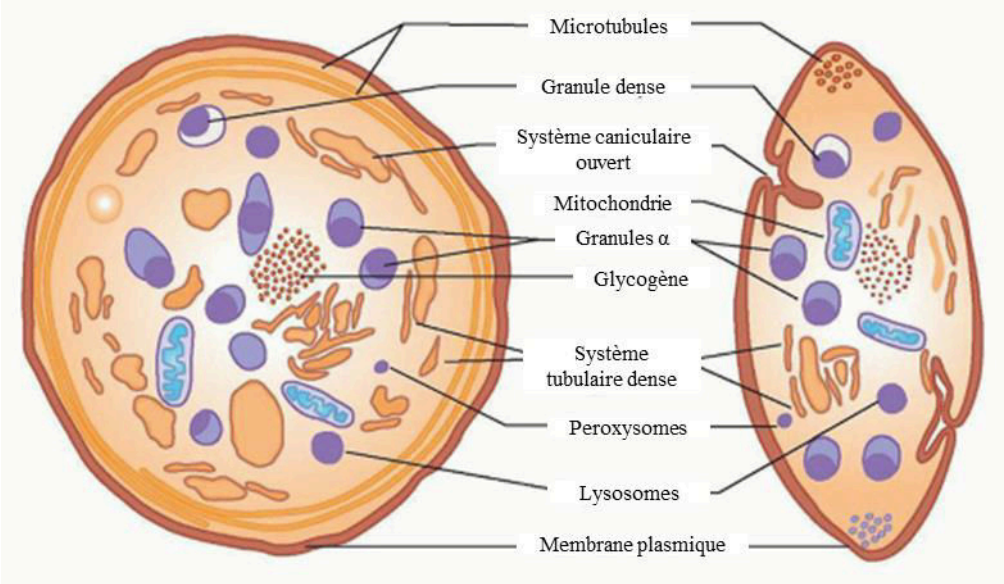

Figure 1 : Diagramme d'une plaquette humaine présentant des composants visibles par microscopie électronique et cytochimie (d'après (15)**)**

Les plaquettes sont composées d'une partie membranaire (membrane plasmique, SCO relié à la surface et STD), elles sont aussi composées de mitochondries, microtubules et de glycogène. Trois types d'organites de stockage sont identifiés: granules α, granules denses et lysosomes.

Fonctions plaquettaires

La fonction majeure des plaquettes est de participer aux mécanismes de l'hémostase primaire car elles sont les premières à intervenir dans l'arrêt du saignement. L'hémostase est un processus physiologique qui permet de maintenir la fluidité du sang et d'empêcher le saignement lors d'une lésion vasculaire. Elle est assurée par deux phénomènes: l'activation plaquettaire et la coagulation. Dans les conditions physiologiques, les plaquettes circulent sous forme discoïde dans un état de non activation dans le système vasculaire bordé par une monocouche de cellules endothéliales intactes. Ces cellules endothéliales ont des propriétés anti-thrombotiques et sécrètent des molécules anti-agrégantes : la prostacycline (PGI_2) et le monoxyde d'azote (NO). La PGI_2 sécrétée par l'endothélium stimule l'adénylate cyclase (AC) et la production intracellulaire d'AMP cyclique (AMPc) dans les plaquettes, tandis que le NO inhibe les plaquettes en stimulant une guanylate cyclase (GC) et la production de GMP cyclique (GMPc) (18) (19).

Lors d'une lésion vasculaire, la désendothélialisation du vaisseau expose au sang circulant de nombreuses protéines du sous-endothélium : le vWF, différents types de collagènes, la fibronectine, des laminines, et chacune de ces protéines interagit avec des récepteurs de la membrane des plaquettes. Les plaquettes adhèrent alors rapidement au site lésé pour former un thrombus permettant de prévenir le saignement. Ce processus est dépendant de la capacité d'adhésion des plaquettes à la matrice sous-endothéliale, ainsi que de leur faculté à changer rapidement de forme, de s'étaler, sécréter, s'agréger et développer une activité pro-coagulante. Toutes ces étapes aboutissent à la formation d'un clou hémostatique et l'arrêt du saignement (Figure 2) (20)

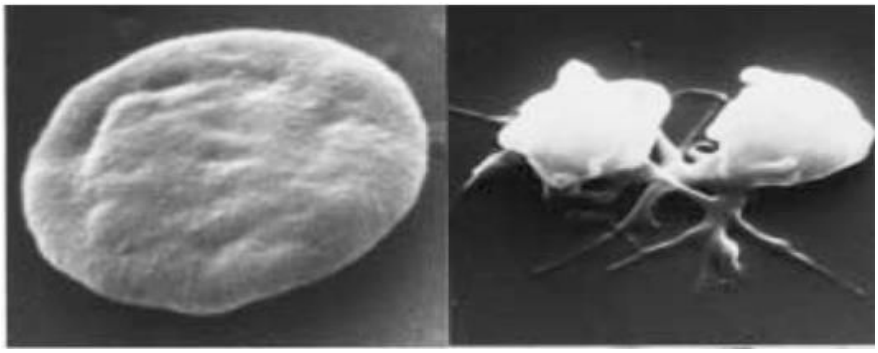

Figure 2: Image de microscopie électronique à balayage de paquette humaine.

A) *Une plaquette au repos avec une forme discoïde.* ***B)*** *des plaquettes activées qui commencent à former des filopodes et à s'agréger entre elles* (21).

Recrutement et activation des plaquettes

Lors d'une brèche vasculaire, les plaquettes adhèrent à la matrice sous-endothéliale exposée, d'abord de façon transitoire, puis stable. Par la suite, les plaquettes activées sécrètent des activateurs secondaires qui stimulent les plaquettes circulantes du voisinage, et les recrutent en formant des liens entre elles. Au cours de ce processus, les plaquettes exposent des lipides anioniques à leur surface. Ces derniers se lient aux facteurs de la coagulation qui génèrent les quantités appropriées de thrombine. La thrombine renforce l'activation des plaquettes et induit la coagulation par transformation du fibrinogène en fibrine insoluble, consolidant ainsi la formation d'un thrombus nécessaire à l'occlusion de la brèche vasculaire et à l'arrêt du saignement (Figure 3).

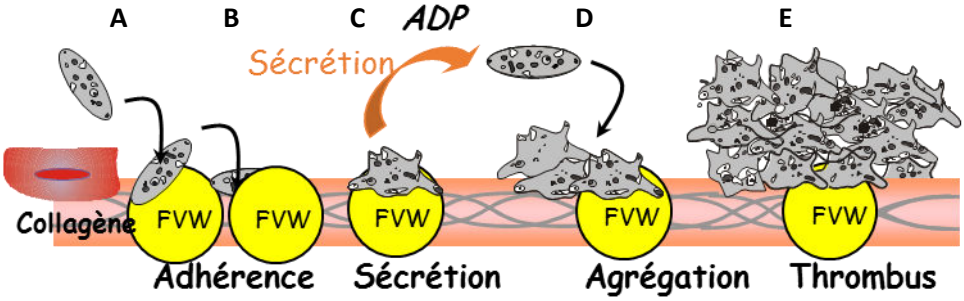

Figure 3: Formation d'un thrombus au niveau de la lésion vasculaire

A) *Les plaquettes sanguines circulent dans le sang à proximité de l'endothélium.* ***B)*** *Suite à une lésion vasculaire, les plaquettes interagissent rapidement avec le sous endothélium de façon transitoire* ***C)*** *les plaquettes interagissent de façon stable avec le sous endothélium, changent de forme, s'étalent sur la surface et sécrètent des activateurs secondaires tel que l'ADP contenu dans les granules* ***D)*** *Activation des plaquettes circulantes par l'ADP et agrégation* ***E)*** *formation d'un clou hémostatique composé principalement de plaquettes mais aussi de fibrine produite au contact des plaquettes activées par la thrombine générée localement et arrêt du saignement.*

L'interaction initiale plaquette-matrice se fait entre le complexe glycoprotéique GPIb-V-IX des plaquettes et son ligand, le vWF, lié au collagène du sous-endothélium. Cette liaison ne se fait qu'à fort taux de cisaillement ($\geq$1200 s^{-1} dans le compartiment artériel) qui rend le vWF actif par dépliement (22). Cette liaison est réversible, mais semble se répéter plusieurs fois pour une plaquette parcourant la matrice. Cette succession de liaison-dissociation dans des conditions de flux physiologiques aboutit à un ralentissement des plaquettes sur la matrice (22). Ce ralentissement semble un prérequis pour permettre ensuite une liaison forte des plaquettes avec le collagène auquel elles vont adhérer de façon irréversible. L'interaction avec le collagène se fait via deux récepteurs : l'intégrine α2β1, impliquée dans l'adhérence et le contact mécanique, et le récepteur GPVI qui initie l'activation plaquettaire. L'activation de GPVI entraîne, par l'intermédiaire de son motif ITAM (immuno-tyrosine based activation motifs) (23), des voies de signalisation liées à des kinases de la famille Src (Fyn, Lyn). Ces dernières recrutent la tyrosine kinase Syk qui aboutit, par une série de réactions de phosphorylation de divers substrats et effecteurs, à l'activation de la phospholipase Cγ2 (PLCγ2) nécessaire à la production de l'inositol tris-phosphate (IP3) puis à la mobilisation calcique vers le cytosol à partir des stocks intracellulaires. Ce Ca^{2+} cytosolique est fondamental pour la sécrétion du contenu granulaire.

L'adhérence stable des plaquettes au sous-endothélium est consolidée par l'interaction entre les intégrines plaquettaires et les composants de la matrice (α5β1-fibronectine, α6β1-laminine, αIIbβ3-fibrinogène ou fibrine) (24).

En parallèle, la libération du facteur tissulaire présent dans la paroi vasculaire aboutit à la formation de la thrombine par une succession de réactions protéolytiques. La thrombine formée est l'activateur le plus puissant des plaquettes : elle active par clivage protéolytique ses récepteurs PAR1 et PAR4 chez l'homme (25). Chez la souris, il n'y a pas de PAR1, et PAR4 est le principal récepteur impliqué dans la signalisation de la thrombine. En effet, les plaquettes de souris expriment PAR3 et PAR4, mais PAR3 est incapable d'induire des signaux par lui-même. Il présente un site de liaison à la thrombine et agit comme cofacteur du clivage activant PAR4 (26). Ces récepteurs à sept domaines transmembranaires sont couplés à des protéines G hétérotrimériques (RCPG) qui sont des commutateurs moléculaires de la transduction des signaux (27). Dans les plaquettes, en aval des RCPG, trois voies principales agissent de façon synergique. La voie initiée par la protéine Gq active la phospholipase β (PLCβ) et mobilise des stocks intracellulaires de Ca^{2+} nécessaire à l'activation de protéines kinases C (PKC). La voie $G_{12/13}$ mène à la phosphorylation de la chaîne légère de la myosine et à l'activation de la GTPase

RhoA responsable notamment des phénomènes contractiles et de l'étalement plaquettaire. Enfin, la voie Gi inhibe la formation d'AMPc, un second messager inhibiteur des fonctions plaquettaires, et active la phosphatidylinositide 3-kinase (PI3K) (28). Les deux récepteurs PARs de la thrombine sont couplés aux protéines Gq et $G_{12/13}$.

L'activation plaquettaire via la thrombine ou le collagène conduit à la mobilisation du Ca^{2+} à partir des stocks calciques. Le Ca^{2+} est nécessaire à la sécrétion des activateurs secondaires tels que le thromboxane A2 (TxA2) dérivé de l'acide arachidonique, ou l'ADP des granules denses. Ces médiateurs aux effets autocrines et paracrines, agissent par l'intermédiaire de récepteurs, eux aussi de type RCPG.

Le rôle de l'ADP est de renforcer l'activation plaquettaire et la stabilisation du thrombus (29) (30). Les plaquettes sanguines possèdent deux récepteurs à l'ADP, $P2Y_1$ et $P2Y_{12}$. On compte environ 150 copies de $P2Y_1$ par plaquette. Ce récepteur est couplé à une protéine Gq, responsable de l'activation des PLCβ, de la mobilisation calcique, et donc des PKC. $P2Y_1$ est responsable des changements morphologiques et régule la réactivité des plaquettes en réponse à l'ADP en se désensibilisant transitoirement (31) (32). $P2Y_{12}$ est plus exprimé à la surface des plaquettes, avec près de 500 à 800 copies. Il présente un rôle d'amplificateur des réponses plaquettaires. Ce récepteur est couplé à une protéine Gi, responsable de l'inhibition de la formation d'AMPc, ce qui lève l'inhibition plaquettaire (33). De plus, au-delà de cette fonction, les voies de signalisation liées à $P2Y_{12}$ impliquent aussi les PI3K, des kinases de type Akt, la petite GTPase de la famille Ras Rap1b et son facteur d'échange GDP-GTP CalDAG-GEFI (Calcium- and Diacylglycerol-Binding Guanine Nucleotide Exchange Factor I) (34).

L'absence d'ADP dans les granules denses ou l'inhibition pharmacologique de ces récepteurs plaquettaires se traduisent par une réponse diminuée à toutes les formes de stimulation, que ce soit par la thrombine ou le collagène (35) (36) .

Le TXA2 est à la fois un activateur des plaquettes et un puissant vasoconstricteur. Lors de l'activation plaquettaire, le TXA2 est produit par la thromboxane synthétase à partir des endopéroxydes, eux-mêmes synthétisés par la cyclo-oxygénase 1 (Cox1) à partir de l'acide arachidonique issu du clivage des phospholipides membranaires par la phospholipase A_2 (PLA_2) activée après la mobilisation calcique (37). Une fois libéré, le TxA2 diffuse à l'extérieur de la plaquette, et interagit avec son récepteur membranaire TP_1 ou TP_2. Ces récepteurs sont couplés à des protéines G de type Gq et $G_{12/13}$. L'aspirine bloque la synthèse du TxA2 en inhibant la Cox1 (38).

L'ensemble de ces voies de signalisation conduit à l'agrégation et à la formation du thrombus, à la suite de l'activation de l'intégrine $\alpha_{II}b\beta_3$, appelée aussi GPIIbIIIa. Cette intégrine est majoritaire dans les plaquettes (on en compte près de 50 000 à 100 000 copies par plaquette). Elle joue un rôle central dans l'agrégation plaquettaire. En effet, la mobilisation du Ca^{2+} et la production du Diacyl-glycerol (DAG) par la PLC permettent l'activation de la protéine CalDAG-GEFI, protéine essentielle pour l'activation de Rap1b, une des petites protéines G les plus abondantes (90% des Rap totales) dans les plaquettes. Rap1b fonctionne comme un commutateur moléculaire entre l'état inactif Rap-GDP et l'état actif Rap-GTP sous le contrôle de CalDAG-GEFI qui échange une molécule de GDP par une molécule GTP (39). Rap1b activé interagit avec Rap1-GTP-interacting Adaptor Molecule (RIAM) qui, à son tour, régule la polymérisation de l'actine et recrute au niveau de la membrane plasmique la taline et la kindline, deux protéines adaptatrices du cytosquelette. Ce recrutement favorise l'association de ces deux protéines avec la région cytoplasmique de la sous-unité β3 de l'intégrine αIIbβ3, induisant un changement de sa conformation et son activation (40). Ce processus d'activation est communément appelé signal « Inside-out » (Figure 4). $\alpha_{II}b\beta_3$ activée est responsable des interactions plaquette-plaquette, en liant le fibrinogène (ou vWF en conditions de flux) pour former des ponts entre les plaquettes et permettre la formation d'un thrombus en flux conduisant ainsi à l'arrêt du saignement.

De plus, lorsque l'intégrine αIIbβ3 activée lie son ligand, une signalisation de l'extérieur vers l'intérieur de la plaquette se met en place. Ce phénomène est appelé signal «Outside-in ». Ce signal est important pour la fonction hémostatique des plaquettes et le renforcement de l'activation plaquettaire car il régule les fonctions liées à l'ancrage et à l'étalement des plaquettes aux protéines de la matrice sous-endothéliale, la stabilité de l'agrégat plaquettaire, et la rétraction du caillot. Ces mécanismes de signalisation font intervenir des tyrosines kinases de type Syk, des kinases de la famille Src, des lipides kinases et des phosphatases qui aboutissent à la polymérisation d'actine, la sécrétion, le renforcement d'$\alpha_{II}b\beta_3$ au cytosquelette, et la contraction (rétraction du caillot).

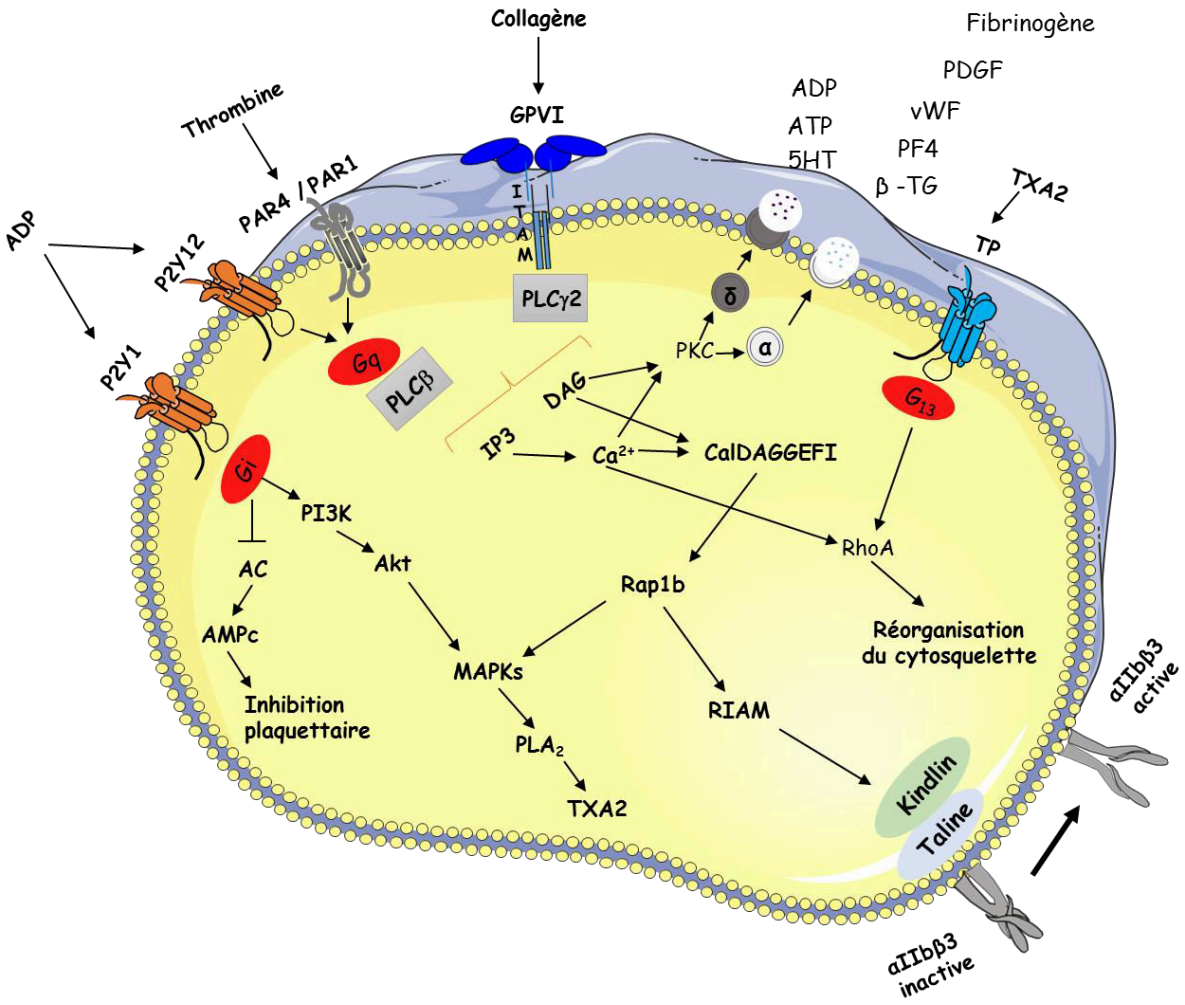

Figure 4 : schématisation des grandes voies d'activation plaquettaire (adapté de Gachet *et al Natl Méd.*, 2013 Feb;197(2):361-73.)

Les phénomènes d'adhérence, d'activation plaquettaire et de son amplification par des médiateurs solubles tels que l'ADP ou le TxA2 libérés lors de l'activation. Les phénomènes d'adhérence font essentiellement intervenir des protéines adhésives comme le collagène, le vWF, le Fg, comme ligands de glycoprotéines membranaires qui empruntent des voies de signalisation aboutissant à l'activation de la phospholipase γ2 (PLCγ2). Les médiateurs solubles comme la thrombine activent principalement des récepteurs couplés aux protéines G hétérotrimériques (RCPG) de type Gq qui activent la phospholipase β (PLC β). Les deux PLC produisent de l'inositol trisphosphate (IP3) qui mobilise le calcium (Ca^{2+}) et le Diacylglycerol (DAG). Ces derniers activent les PKC responsables de la sécrétion des granules denses δ contenant de l'ADP, ATP et sérotonine (5HT), mais aussi les granules alpha α qui contiennent du Fg, vWF et lePF4. La voie $G_{12/13}$ mène à la phosphorylation de la chaîne légère de la myosine et la voie Gi inhibe la formation d'AMPc, second messager inhibiteur des fonctions plaquettaires, et active la phoshatidylinositide 3-kinase.

Rôle du Ca^{2+} dans les plaquettes

A) Homéostasie calcique

L'homéostasie du Ca^{2+} cytosolique est un élément essentiel en biologie cellulaire. Dès les années 1880, les observations de Ringer ont révélé l'importance du Ca^{2+} dans la physiologie cellulaire (41). Ce cation divalent est un second messager pour un grand nombre de fonctions cellulaires. En effet, il est impliqué dans plusieurs processus cellulaires fondamentaux comme la contraction musculaire, la sécrétion, la transcription des gènes, la différenciation, la prolifération, la plasticité neuronale, la fertilisation ainsi que le métabolisme (Figure 5). Le Ca^{2+} permet aussi la régulation d'enzymes, notamment des enzymes comme les kinases, les déshydrogénases, les phospholipases, les protéases et les endonucléases, ainsi que des facteurs de transcription tels que NF-κB (nuclear factor-κB) et NFAT (nuclear factor of activated T-cells) (42–44).

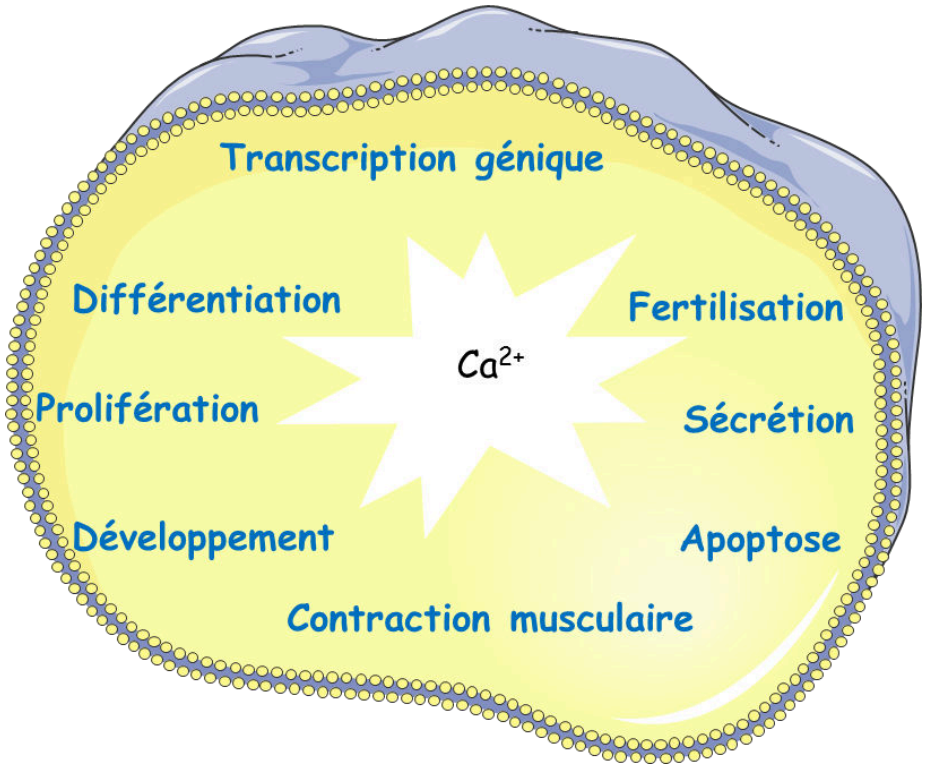

Figure 5 : Rôle du calcium dans la vie cellulaire

Dans la plaquette au repos, la concentration du Ca^{2+} cytosolique se situe entre 10 et 100 nM (45–47) ce qui est très faible par rapport au Ca^{2+} disponible dans les réserves intra-plaquettaires ou dans le milieu extracellulaire et qui est de l'ordre du mM (42) (48).

Une augmentation importante de la concentration du Ca^{2+} cytosolique survient lors de l'activation plaquettaire : cette activation survient après sortie du Ca^{2+} à partir des réserves intraplaquettaires, en particulier du STD, vers le cytosol (« mobilisation »). De plus, la déplétion des réserves calciques induit l'activation d'un processus appelé « Store Operated Calcium Entry » (ou SOCE) qui permet l'entrée du Ca^{2+} à partir du milieu extracellulaire, à travers la membrane plasmique vers le cytosol (« influx »), processus au cours duquel les stocks internes vont se reconstituer.

La diminution de la concentration calcique dans les plaquettes est contrôlée par l'action de transporteurs calciques qui permettent l'extrusion du Ca^{2+} cytosolique dans le milieu extracellulaire ou son incorporation dans les organites de stockage (appelés aussi réserves intra-plaquettaires) (Figure 6). La régulation coordonnée de ces protéines effectrices module le profil des élévations calciques intra-cytoplasmiques, à distance et à proximité (micro domaines) des organelles subcellulaires, et permet la transmission du signal calcique (49).

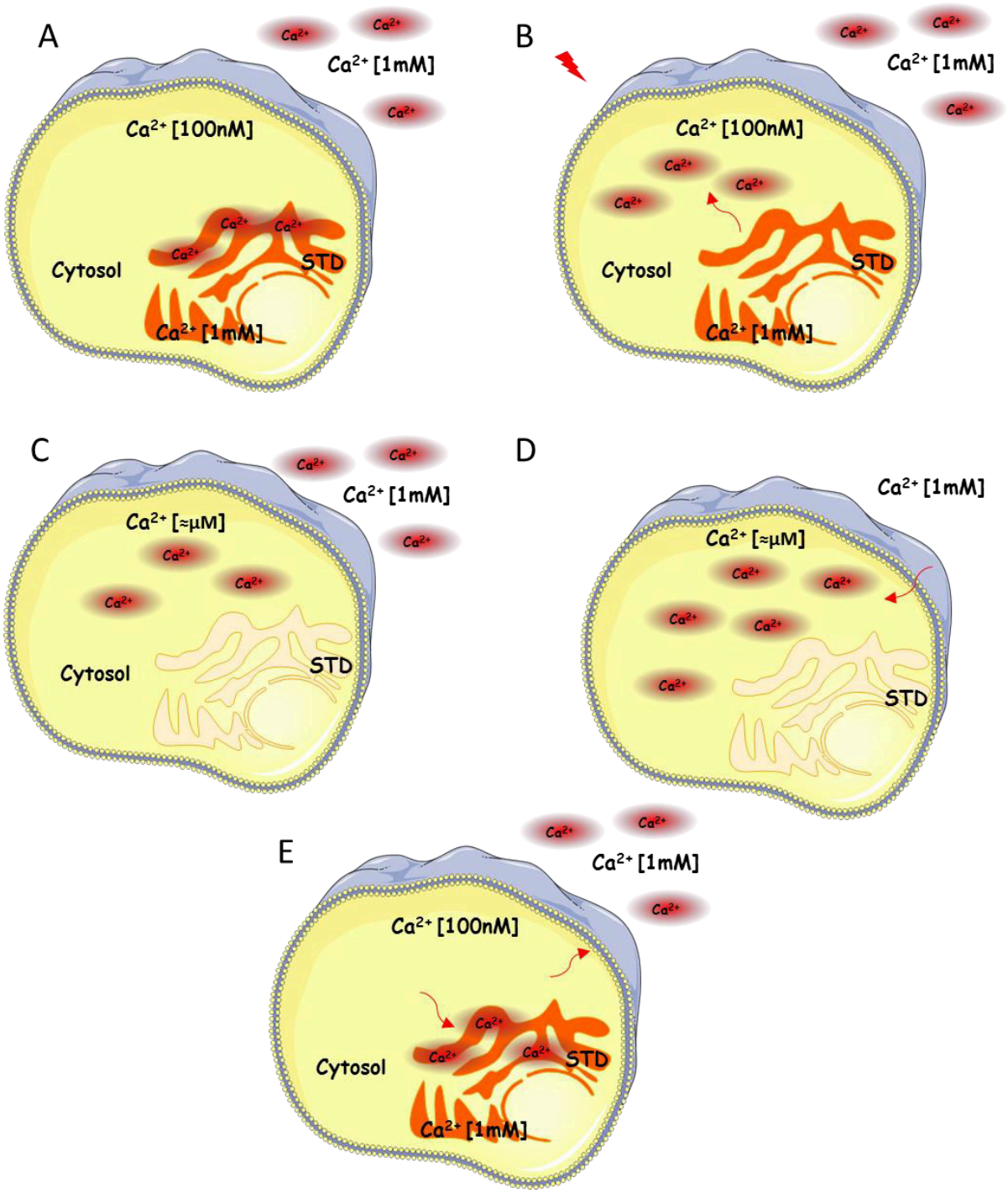

Figure 6 : Représentation schématique de l'augmentation et de la diminution de la concentration calcique dans les plaquettes. ***A)*** *plaquette au repos avec un Ca^{2+} cytosolique [100nM] faible par rapport au Ca^{2+} extracellulaire et celui du STD [1mM].* ***B)*** *après activation plaquettaire il y a mobilisation du Ca^{2+} du STD vers le cytosol ce qui augmente sa concentration dans ce compartiment.* ***C)*** *Déplétion du STD.* ***D)*** *Entrée du Ca^{2+} extracellulaire dans le cytosol.* ***E)*** *Diminution de la concentration du Ca^{2+} cytosolique par restockage à l'intérieur du STD ou élimination vers le milieu extracellulaire.*

B) Les organites subcellulaires impliqués dans la régulation de la signalisation calcique

Plusieurs organites subcellulaires sont impliqués dans le stockage du Ca^{2+} plaquettaire. Ils sont considérés à la fois comme des réserves pouvant libérer leur Ca^{2+} dans le cytosol et comme des régions où la concentration de Ca^{2+} conditionne de nombreuses activités enzymatiques (50) (51). En plus des granules denses déjà décrits plus haut, plusieurs compartiments intra-plaquettaires contiennent du Ca^{2+}, comme le STD ou les mitochondries.

I) Le Système tubulaire dense (STD)

Le STD peut stocker du Ca^{2+} en quantité très importante (52). C'est une des raisons qui fait considérer qu'il s'agit d'un équivalent du réticulum endoplasmique (RE). Il est couramment appelé « réserve intracellulaire de Ca^{2+} ». Il contient des systèmes d'incorporation et de libération du Ca^{2+}. De fait, il est considéré comme le principal compartiment contenant du Ca^{2+} mobilisable au cours de l'activation cellulaire, et fait donc partie de la dynamique du signal calcique. L'échange de Ca^{2+} entre le cytosol et le STD s'effectue grâce à différents transporteurs de Ca^{2+} insérés dans la membrane du STD. Le Ca^{2+} contenu dans le STD n'est pas exclusivement sous forme libre, il peut être lié à des protéines de stockage ou «Ca^{2+}-binding proteins» : on peut citer la calréticuline, qui possède une faible affinité pour le Ca^{2+} mais du fait de sa concentration élevée présente une forte capacité de stockage et par ce biais contrôle la concentration de Ca^{2+} dans le STD (53).

II) Les mitochondries

Les mitochondries sont des organites multifonctionnels qui contrôlent un grand nombre de processus cellulaires. Leur rôle principal est de produire de l'ATP, forme d'énergie nécessaire à la cellule. La paroi des mitochondries est composée de deux membranes: une membrane externe contenant les canaux VDAC (Voltage Dependent Anion Selective Channel) qui assurent la diffusion de petites molécules hydrophiles telles que l'ADP et l'ATP; et une membrane interne, imperméable, à travers laquelle le transport du Ca^{2+} se fait via le complexe MCU (Mitochondrial Calcium Uniport). Les mitochondries peuvent ainsi accumuler le Ca^{2+} dans leur matrice jusqu'à atteindre des concentrations de 0,5 mM mais seulement lorsque la concentration du Ca^{2+} cytosolique dépasse le seuil de 0,5 µM (54) (55). On peut parler de "vase d'expansion" empêchant le dépassement du seuil calcique cytosolique pouvant déclencher l'apoptose. L'accumulation du Ca^{2+} dans les mitochondries est favorisée par l'élévation

localisée de la concentration calcique dans le cytosol à proximité des canaux calciques de la membrane cytoplasmique et de la membrane du STD.

III) Les granules acides

Ces compartiments calciques maintiennent un gradient de protons à travers leur membranes et sont majoritairement identifiés comme des organites qui ressemblent aux lysosomes (56). Dans les plaquettes, la présence de deux compartiments calciques contrôlés par deux pompes ATPases différentes a été proposée pour la première fois en 1995 par Cavallini *et al.* (57), sur la base d'expériences utilisant des inhibiteurs pharmacologiques bloquant l'activité de ces pompes.

C) Acteurs des variations de la concentration de Ca^{2+} intracellulaire

Le signal calcique a été exploré dans les plaquettes humaines et murines, où la machinerie de l'homéostasie calcique est finement régulée. Lors de l'activation plaquettaire, le Ca^{2+} est mobilisé à partir des stocks internes via différents seconds messagers comme l'IP3 produit par la PLC ou l'ADP-ribose cyclique (cADPR) ou le NAADP (Nicotinic Acid Adenine Dinucleotide Phosphate) produit par l'enzyme CD38 (58–60). De plus, la déplétion des réserves internes en Ca^{2+} active les protéines sensorielles (STIM1) (Stromal interaction molecule 1) ancrées au niveau de la membrane du STD et des granules acides (61) (62). STIM1 activé, se fixe sur Orai (Calcium Release-Activated Calcium Modulator, le nom Orai provient de la mythologie grecque, ce sont les gardiens de la porte du paradis) (63) situé au niveau de la membrane plasmique. Ces deux protéines forment alors un canal appelé SOC (Store Operated Channels) permettant l'entrée du Ca^{2+} à partir du milieu extracellulaire vers le cytosol. Il existe d'autres canaux impliqués dans l'entrée du Ca^{2+} comme les TRPC (Transient Receptor Potential Cation) (64), (65) ou $P2X_1$, le récepteur canal de l'ATP.

L'augmentation de la concentration calcique est importante pour l'activation plaquettaire, mais l'élévation du Ca^{2+} dans le cytosol devient toxique pour la cellule et est alors capable d'activer des cibles moléculaires impliquées dans le programme de la mort cellulaire par apoptose (66–68).

L'élimination du Ca^{2+} cytosolique survient après activation de plusieurs mécanismes, incluant le re-pompage du Ca^{2+} du cytosol vers les stocks internes et son élimination vers le milieu extracellulaire. Le re-pompage vers les stocks internes est contrôlé par des pompes

ATPases appelées SERCA (Sarco-Endoplasmic Réticulum Ca^{2+} ATPase), incluant les isoformes SERCA2b et SERCA3 (69). Ces pompes transportent le Ca^{2+} du cytosol vers l'intérieur des réserves. L'élimination du Ca^{2+} vers le milieu extracellulaire est contrôlée par d'autres pompes ATPases ancrées dans la membrane plasmique. Ces pompes sont appelées PMCA (Plasma Membrane Ca^{2+} ATPase) et transportent le Ca^{2+} du cytosol vers le milieu extracellulaire. Les plaquettes expriment les isoformes PMCA1b et PMCA4b (70–72). L'élimination du Ca^{2+} vers le milieu extracellulaire est aussi contrôlée par l'échange du Ca^{2+} avec Na^{+} par les échangeurs Na^{+}/Ca^{2+}(NCX) (73) (Figure 7).

D'importantes différences entre les plaquettes humaines et murines ont été décrites aussi bien au niveau du compte plaquettaire qu'au niveau de leur taille (environ deux fois plus petite chez la souris) et l'expression de certaines protéines. Ces différences n'empêchent pas l'utilisation du modèle murin pour étudier l'homéostasie calcique dans les plaquettes. En revanche, ces différences poussent les chercheurs à être prudents dans l'extrapolation des résultats trouvés chez la souris sur les plaquettes humaines concernant la régulation du signal calcique.

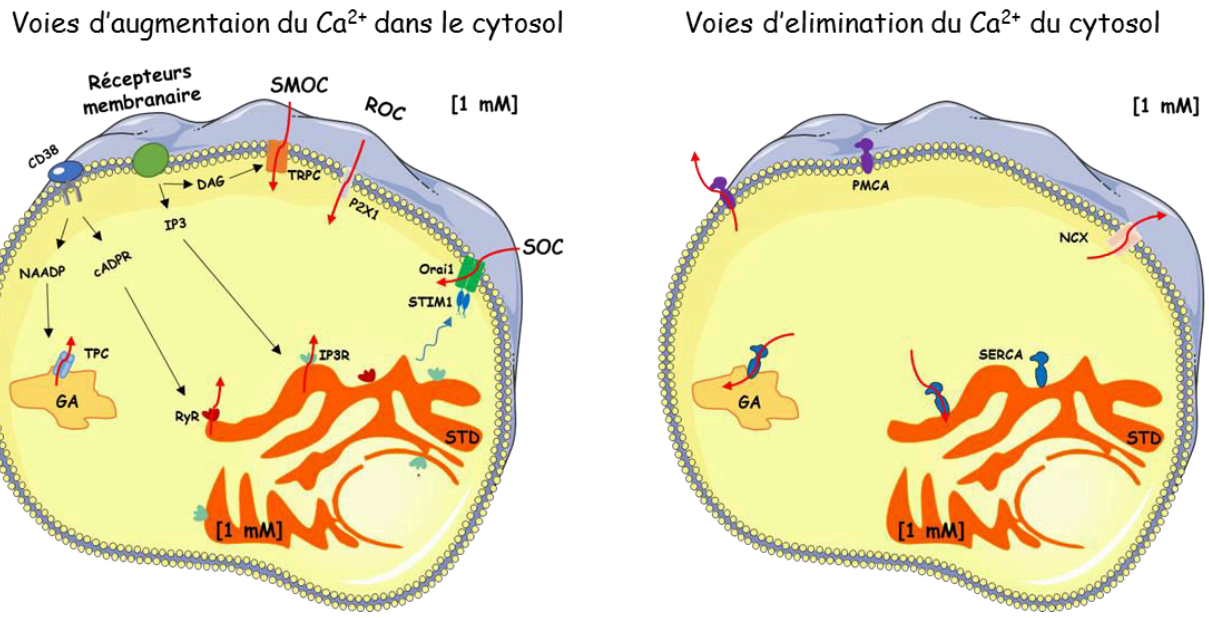

Figure 7 : Les voies d'augmentation et d'élimination du calcium du cytosol

L'augmentation de la concentration calcique survient en aval de l'activation d'un récepteur plaquettaire (PAR, GPVI ...) qui induisent la production d'IP3 et DAG, mais aussi l'exonuclease CD38 qui synthétise le NAADP et le cADPR. IP3 mobilise le Ca^{2+} à partir du STD après sa fixation sur son récepteur canal IP3R. Le cADPR mobilise le Ca^{2+} à partir du STD après sa fixation dur son récepteur (RyR). Le NAADP mobilise le Ca^{2+} à partir des granules acides (GA). De plus, le DAG active canal TRPC afin de permettre l'entrée du Ca^{2+} du milieu extra cellulaire vers le cytosol. TRPC fait partie de la famille des canaux SMOC (second Messenger Operated Calcium) D'autre part la déplétion du STD en calcium induit l'activation de la protéine sensorielle STIM1 qui a son tour vient activer Orai1 inséré dans la membrane plasmique, cette interaction permet la formation d'un canal appelée SOC (Store Operated Channel). Il existe d'autres canaux impliqués dans l'influx calcique, $P2X_1$ récepteur de l'ATP qui fait partie des canaux ROC (Receptor Operated Calcium).

I) Augmentation de la concentration du Ca^{2+} cytosolique :

Il existe deux composantes de l'élévation de la concentration du Ca^{2+} cytosolique, sa mobilisation à partir des stocks internes via IP3, cADPR et NAADP, mais aussi son influx depuis le milieu extracellulaire à travers différents canaux calciques (SOC, TRPC, $P2X_1$).

i.) Libération du Ca^{2+} des réserves intracellulaires : mobilisation calcique

a) Les IP3-R

Ce récepteur canal découvert en 1984 (74) est activé par son interaction avec son ligand IP3. Cette liaison permet l'ouverture du canal et l'efflux vers le cytosol du Ca^{2+} contenu dans les stocks intracellulaires. Dans la majorité des cellules, l'IP3-R est situé au niveau du RE.

Chez les mammifères, il y a trois isoformes du récepteur de l'IP3 (IP3-R1, IP3-R2 et IP3-R3) insérées dans la membrane du RE. Les trois types de récepteurs sont codés par des gènes homologues et sont structurellement similaires avec un niveau d'expression variable selon les tissus (75–77). Chaque récepteur se distingue notamment par son affinité différente vis-à-vis de l'IP_3 (IP3-R2> IP3-R1> IP3-R3) (78) (79).

Des souris knockout (KO) pour ces trois gènes ont été réalisées et les souris KO pour les IP3-R2 et IP3-R3 ne présentent pas de phénotype majeur. En revanche, concernant les souris KO pour l'IP3-R1, très peu d'entre elles survivent à la naissance, et celles qui survivent présentent des troubles neurologiques sévères et des défauts physiologiques. Ceci indique que IP3-R1 joue un rôle important au cours du développement embryonnaire, qui n'est pas ou peu compensé par les autres IP3R, alors qu'inversement IP3R1 pourrait compenser les autres (80).

D'un point de vue structurel, les IP3-R sont composés de trois domaines différents : le domaine N-terminal correspondant au domaine de fixation à l'IP3, le domaine C-terminal cytoplasmique qui permet la régulation de l'activité du récepteur, et un domaine central qui comprend six domaines transmembranaires portant la fonction canal. Ce récepteur est un tétramère composé de quatre sous-unités d'IP3-R qui forment un pore canal central (81) (Figure 8). L'IP3-R est une très grosse protéine d'environ 1000 kDa. Son activité peut être régulée par sa phosphorylation dans le domaine intermédiaire, par les PKC, les PKA (protéine kinase A) ou la Ca^{2+}/Calmoduline kinase (CaMKII) (82–85). De plus, cette activité est aussi modulée par le Ca^{2+} cytosolique et celui stocké dans les réserves. Sa sensibilité au Ca^{2+} joue un rôle très important dans le signal calcique (86). En effet, l'augmentation de la concentration du Ca^{2+} dans l'environnement du récepteur potentialise sa capacité d'ouverture et inversement une forte

diminution de la concentration réticulaire favorise la fermeture du canal. Par ailleurs, une très forte concentration de Ca^{2+} cytosolique peut inhiber les IP3-R (87). Ce mécanisme appelé CICR (Calcium Induced Calcium release) est impliqué dans la propagation du signal calcique à travers de nombreux types cellulaires (88).

Dans les plaquettes, les IP3-R sont décrits comme étant les principaux récepteurs de la mobilisation calcique (89) (90) (91). Les trois isoformes sont retrouvées, mais IP3R-1 et IP3R-2 sont prédominantes (92) (93). La liaison avec une forte affinité d'une molécule d'IP3 sur chaque sous-unité du récepteur, permet l'ouverture du canal entraînant une libération de Ca^{2+} depuis le STD vers le cytosol.

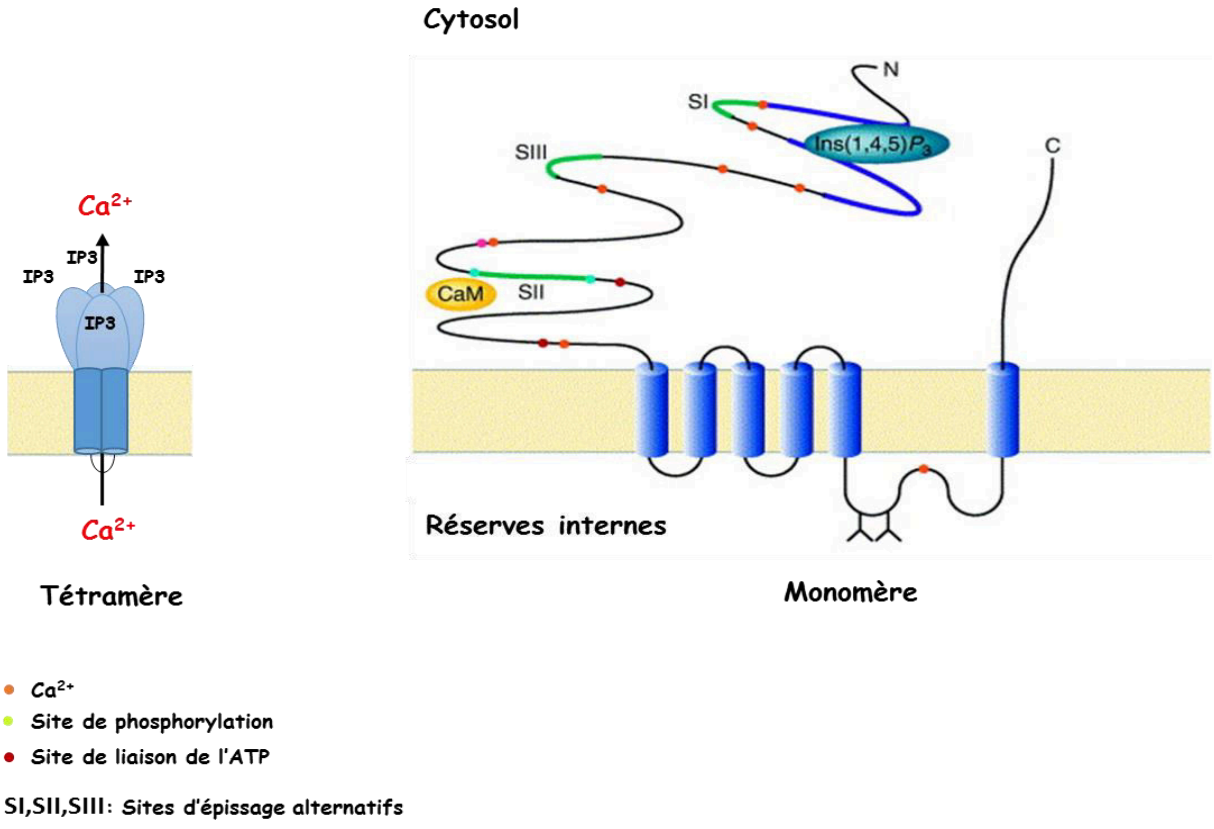

Figure 8 : Structure du récepteur a l'inositol (1, 4, 5) - trisphosphate IP3.

Le récepteur IP3-R est un tétramère (homo ou hétéro) et chaque sous-unité est constituée d'un domaine de liaison au ligand N-terminal (région violette) suivi d'un domaine régulateur et d'une chaine C-terminal (composée de six domaines transmembranaire). Les sites de liaison du Ca^{2+} sont représentés sous forme de cercles orange, les sites de liaison à l'ATP sont représentés sous forme de cercles roux foncés, et les sites de phosphorylation sont représentés sous forme de cercles bleus. La calmoduline (CaM) se lie sur l'un des sites de phosphorylation. Les sites d'épissage alternatif SI, SII et SIII sont représentés en vert. Les sites de N-glycosylation sont également présents).

b) Les R-NAADP et RyR

Comme évoqué plus haut, il existe, en plus de l'IP3, deux autres messagers secondaires qui libèrent du Ca^{2+} à partir d'autres réserves intracellulaires : le cADPR (94) et le NAADP (95). Ces deux messagers secondaires sont synthétisés après activation plaquettaire par une exonucleotide synthase (CD38) présente dans la membrane plasmique des plaquettes. Cette enzyme possède une activité synthase (S) et une activité hydrolase (H) (96) (Figure 9). Il a été montré que dans les cellules immunitaires (Natural Killer NK), l'association de CD38 avec MHCIIA (Non-Muscle Myosin Heavy Chain IIA), la tyrosine kinase Lck, et les PKC permet son internalisation et son activation (97). La découverte de ces deux seconds messagers a permis de mieux comprendre comment les signaux complexes de Ca^{2+} sont générés.

Le cADPR est un modulateur des récepteurs à la Ryanodine (RyR) qui pourraient être présents dans le STD (58). Seuls les travaux de Mazhar Mushtaq *et al* suggèrent la présence de RyR de type 2 dans les plaquettes humaines (58). Cependant, dans cette publication, la pureté de la préparation plaquettaire utilisée en expériences d'immunoempreinte (WB) et RT-PCR n'a pas été démontrée. De plus, aucune démonstration directe de l'effet du cADPR sur la mobilisation calcique n'a été apportée. Enfin, les auteurs montrent que l'utilisation de l'inhibiteur du cADPR (8-Br-cADPR) affecte la mobilisation calcique en réponse à la thrombine. Mais comme cette molécule inhibe à la fois la production du cADPR et du NAADP, l'existence dans les plaquettes d'une signalisation calcique cADPR dépendante reste à établir.

Le rôle du NAADP dans la mobilisation calcique est maintenant bien documenté (98–104). Une des premières démonstrations du rôle du NAADP dans la mobilisation calcique a été décrite par Lee *et al* (95). La production du NAADP acetoxymethylester (NAADP-AM) (pouvant traverser la membrane des cellules) (105) et l'utilisation de la molécule chimique Ned-19, un analogue du NAADP qui inhibe sa signalisation (106), ont permis l'avancée rapide de ces recherches. Depuis, il a été démontré que le NAADP mobilise du Ca^{2+} à partir des réserves acides, des granules de sécrétion et des lysosomes (99) (107) dans les cellules acinaires pancréatiques (100), les microsomes issus à partir de cerveau de rats (108), les cellules bêta pancréatiques (109) (110), les cellules musculaires lisses artérielles (99), les astrocytes (111), mais aussi les plaquettes (9) (112).

Le récepteur ou/et le canal mobilisé par le NAADP reste à identifier. Le récepteur RyR a été proposé comme récepteur pour le NAADP, mais ces observations n'ont été faites que pour les lymphocytes T (113) (114). Cependant, dans les spermatozoïdes humains, l'utilisation de

cADPR-AM et de NAADP-AM a montré que seul le NAADP pouvait mobiliser du Ca^{2+} (104), ce qui indique que le NAADP est capable de cibler des récepteurs autres que les RyR.

Les Two Pore Channels (TPC) pourraient constituer un autre type de récepteurs pour le NAADP. En 2009, plusieurs études ont montré que les membres de la famille des canaux TPC, TPC1 (115) et TPC2 (116), libèrent du Ca^{2+} à partir des granules acides après stimulation par le NAADP (117). De plus, la surexpression ou la diminution de l'expression de TPC1 ou TPC2 affecte la réponse au NAADP (118). Néanmoins, il n'y a pas d'évidence directe que les TPC soient les récepteurs du NAADP. A contrario, il a été proposé que le NAADP se fixe sur la mucolipine (TRPLM) et cette association induirait l'activation des canaux TPC (118).

Si l'expression des TPC dans les plaquettes n'a pas été mise en évidence directement, des analyses par RT-PCR et immunomarquage ont révélé l'expression de TPC1 et TPC2 dans les lignées MEG01 (Lignée mégacaryocytaire humaine) (9) (119) (120). Dans les plaquettes, il a été proposé que le NAADP mobilise du Ca^{2+} à partir des réserves acides. Les réserves acides seraient également sous le contrôle des pompes ATPase SERCA de type 3 (60). Ce Ca^{2+} mobilisé pourrait induire à son tour, par le mécanisme du CICR, une libération du Ca^{2+} depuis le STD qui est sous le contrôle des SERCA de type 2 (98–103).

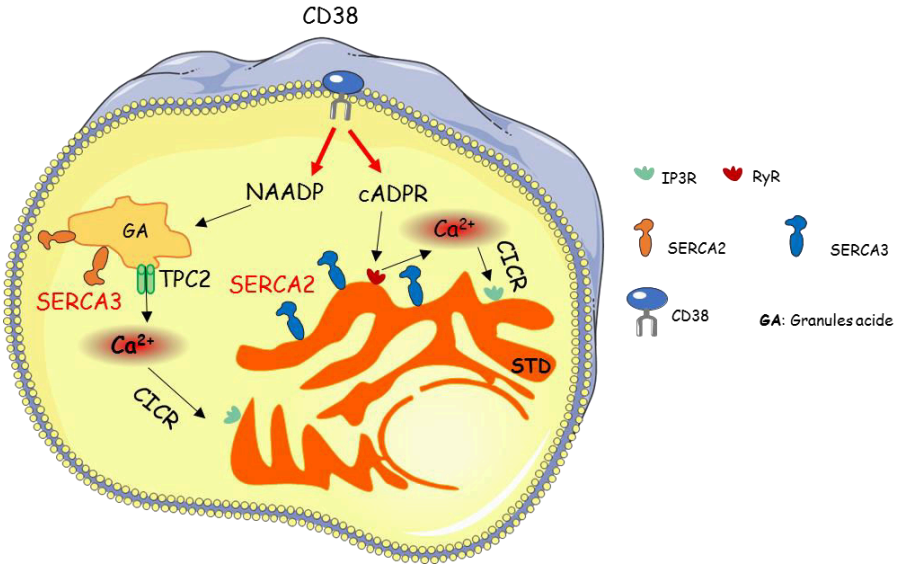

Figure 9: schéma illustrant la signalisation en aval de CD38.

CD38 synthétise du NAADP (Nicotinic Acide Adenine Dinucleotide Phosphate) et le cADPR (cyclique ADP ribose) qui mobilisent respectivement le Ca^{2+} à partir des granules acides (GA) via TPC2 et le système tubulaire dense (STD) via le récepteur d'IP3 (IP3R) et RyR (récepteur de la ryanodine). Ce Ca^{2+} mobilisé pourrait induire à son tour, par le mécanisme du CICR (Calcium induced Calcium release) une libération du Ca^{2+} depuis le STD et les GA contrôlés respectivement par SERCA2 et SERCA3.

ii.) Entrée de Ca^{2+} du milieu extracellulaire: (influx calcique)

Les mécanismes par lesquels l'entrée du Ca^{2+} est régulée dans les plaquettes ne sont encore qu'incomplètement connus, mais au moins trois voies d'entrée du Ca^{2+} pouvant opérer ensemble après stimuli physiologiques ont été décrites :

a) Les canaux ROC (Receptor Operated Calcium)

Ce mécanisme d'influx calcique est directement induit par l'activation d'un récepteur, comme le $P2X_1$ (121). Ce récepteur canal à l'ATP est de type cationique mixte, c'est-à-dire perméant à la fois au Ca^{2+}, au sodium (Na^+) et au potassium (K^+). Son activation par l'ATP se traduit par l'ouverture du canal ionique, suivi d'un courant très rapide de Ca^{2+} et de sa désensibilisation. Ce récepteur semble important car il est impliqué dans plusieurs fonctions plaquettaires comprenant le changement de forme (122), la régulation de l'activation par le collagène, l'adrénaline, le thromboxane A2 (TXA2) et la thrombine (123–126). De plus, il a été montré que la stimulation des récepteurs plaquettaires $P2X_1$ peut entrer en synergie avec les récepteurs à l'ADP ($P2Y_1$) et d'autres RCPG dépendants de Gq comme les PARs, et potentialiser la mobilisation calcique ainsi que l'agrégation (126–128).

Cependant, des études *in vivo* utilisant un modèle de souris déficientes en $P2X_1$ ont montré que bien que ce récepteur soit impliqué dans la formation du thrombus, aucune différence significative n'a été observée pour le compte plaquettaire, l'expression des principaux récepteurs plaquettaires et le temps de saignement (106) (129) (130), ce qui relativise son importance physiologique.

b) Les canaux SMOC (Second Messenger Operated Calcium)

L'entrée du Ca^{2+} à partir de ces canaux est un mécanisme décrit dans les plaquettes et d'autres types cellulaires. L'activation des plaquettes permet la production du DAG, ce dernier pouvant agir comme un second messager pour activer les canaux calciques tels que les TRPC6 (Transient Receptor Potential Cation), entrainant un influx de Ca^{2+}. Ce mécanisme a été établi dans les plaquettes humaines et murines à l'aide d'un analogue du DAG, le 1-oléoyl-2-acétyl-sn-glycerol (OAG) (131) (132).

Des études par RT-PCR ont montré la présence d'ARN messagers (ARNm) correspondant à différents TRPC (TRPC1, TRPC2, TRPC3, TRPC4 et TRPC6) dans les lignées mégacaryocytaires (MEG-01, DAMI) et les plaquettes (123) (133). L'expression des protéines TRPC1 et TRPC6 dans les plaquettes humaines, ainsi que l'implication de TRPC6 dans l'entrée

non capacitive du Ca^2, ont été ensuite démontrées par Hassock *et al* en 2002 (124). Les auteurs suggéraient que ces deux protéines ont une localisation subcellulaire distincte: TRPC1 serait localisé dans les membranes des réserves intraplaquettaires et pourrait s'activer en s'associant au IP3-R2 au cours de la déplétion de ces réserves (130), alors que TRPC6, l'isoforme majoritaire des plaquettes, serait localisée dans la membrane plasmique (134).

Rôle des canaux TRPC dans la thrombose et l'hémostase

Il n'existe pas d'étude reliée au domaine de la thrombose et de l'hémostase sur des patients ayant une mutation de TRPC. Néanmoins, une association entre une surexpression de TRPC6 et une hypertension artérielle pulmonaire idiopathique a été mise en évidence (135).

La fonction des canaux TRPC a été étudiée à partir de plusieurs modèles murins déficients, mais celle-ci reste encore à être élucidée. Alors qu'il a été montré que les fonctions plaquettaires sont normales chez les souris déficientes en TRPC1 et que l'influx calcique n'est pas altéré (136), le rôle de TRPC6 dans la thrombose et l'hémostase chez la souris est controversé. En effet, l'équipe de Bernard Nieswandt a montré que les souris déficientes en TRPC6 n'avaient aucun trouble de l'hémostase mais une diminution de l'influx calcique en réponse à l'OAG (132), tandis qu'à l'inverse, l'équipe de Khasawneh (125) a observé un temps de saignement allongé et un temps d'occlusion retardé chez ces mêmes souris. Ils ont aussi démontré l'implication de TRPC6 dans la rétraction du caillot et la régulation de la signalisation du T_XA2 (134). La raison de ces résultats opposés reste obscure, d'autant qu'il s'agit de la même souche de souris (fournis par le Dr Lutz Birnbaumer). Néanmoins, il existe beaucoup de différences au niveau des procédures expérimentales qui pourraient expliquer ces contradictions : par exemple, pour mesurer le temps de saignement, l'équipe de B. Nieswandt coupe 1 mm de l'extrémité de la queue des souris, tandis que l'équipe de T. Khasawneh coupe 5 mm).

c) Les canaux SOC (Store Operated Channels)

En plus de l'influx calcique, conduit par les canaux ROC et SMOC qui agissent de façon indépendante des réserves intra-plaquettaires ou "entrée non capacitive du Ca^{2+}", il existe d'autres canaux d'entrée du Ca^{2+} qui sont activés après la déplétion des réserves intra-plaquettaires. Ce mécanisme est aussi appelé "entrée capacitive du Ca^{2+}" ou "Store Operated Calcium entry" (SOCe), et est opéré par les canaux SOCs. Cette entrée de Ca^{2+} est conditionnée par la déplétion du STD et des granules acides, consécutive à une mobilisation calcique induite par IP3 et NAADP (137). En effet, la déplétion en Ca^{2+} des réserves intra-plaquettaires et la

diminution de sa concentration est détectée par la protéine STIM1, qui s'active de façon inversement proportionnelle à la concentration en Ca^{2+} intraluminal. Ce senseur calcique de 77 kDa a été découvert en 2006 chez l'homme et 1 an après chez la souris (138)(139). STIM1 est ancré dans la membrane du STD et des granules acides. Lorsque qu'elles sont activées, les protéines STIM1 se dimérisent et s'oligomérisent. Ces complexes migrent ensuite vers les jonctions de contact entre les réserves intraplaquettaires et la membrane plasmique, où ils recrutent et s'associent avec Orai1 ancrée dans la membrane plasmique. Cette association STIM1-Orai1 forme un complexe appelé SOC qui permet l'entrée du Ca^{2+} du milieu extracellulaire vers le cytosol. Les régions où la membrane des réserves de Ca^{2+} est en contact étroit avec la membrane plasmique est aussi appelée "puncta". Ces complexes STIM1-Orai1 peuvent-être associés avec les TRPCs (140).

Rôle de STIM1 et Orai1 dans la thrombose et l'hémostase

Comme mentionné ci-dessus, les membres de la famille de STIM et Orai sont considérés comme les composants majoritaires des SOCs. Dans le cas des protéines STIM, il n'existe pas de résultats convaincants sur le rôle de STIM2 dans les fonctions plaquettaires aussi bien chez l'homme que chez la souris déficiente en STIM2 en physiologie plaquettaire et en hémostase (141). Par contre l'absence de STIM1 joue un rôle déterminant dans la physiologie plaquettaire puisque l'influx calcique, l'exposition des PS et la génération de thrombine sont diminués *in vitro* en réponse à l'activation de GPVI (141) et qu'une absence d'occlusion des vaisseaux est observée lors d'une lésion vasculaire au chlorure de fer ($FeCl_3$) *in vivo* (142) (143). De plus, une mutation causant une sur-activation de STIM1 se traduit par une entrée excessive de Ca^{2+} dans les plaquettes induisant leur activation précocement, une exposition constitutive des PS à leur surface, une thrombopénie et des troubles de l'hémostase. Tous ces disfonctionnements sont probablement la cause du syndrome de Stormorken chez l'homme (144) (145). Les mutations hétérozygotes gain de fonction de STIM1 sont souvent associées au syndrome de York (YPS). Chez l'homme, ce syndrome est caractérisé par une thrombopénie et une absence de Ca^{2+} au niveau des granules plaquettaires (146).

Les patients présentant des mutations induisant la perte de fonction de STIM1ont un allongement du temps de saignement avec une diminution de l'activité des SOCs dans les plaquettes, ainsi qu'une diminution de la sécrétion des granules denses et alpha après stimulation par la thrombine. L'agrégation plaquettaire est également diminuée après stimulation par d'adrénaline (142).

Dans le cas de la famille Orai, il a été rapporté qu'une mutation entrainant une augmentation de l'activité d'Orai1 donne un phénotype similaire à celui du syndrome de Stormorken chez l'Homme ; cette mutation se traduit par une altération de l'hémostase et de la formation du thrombus (147). Les mutations menant à une altération de l'activité d'Orai1 se traduisent par une thrombopénie (148). L'utilisation de souris KO pour Orai1 spécifiquement dans les plaquettes révèle que l'absence d'Orai1 se traduit par une diminution de l'influx calcique conduisant à une instabilité du thrombus (149). De même, les plaquettes de souris exprimant un mutant perte-de-fonction d'Orai1 (R93W) montrent une diminution de l'influx calcique de type SOCE (150).

Ces observations étant similaires à celles observées dans les plaquettes $STIM1^{-/-}$, elles suggèrent fortement qu'Orai1 et STIM1 participent à la même voie de signalisation et que les SOCs jouent un rôle plus important dans la formation du thrombus que dans l'hémostase (141) (150) (151).

Le fait que, chez la souris, STIM1 et Orai1 (SOCs) jouent un rôle important dans la formation du thrombus et sa stabilisation mais pas dans l'hémostase primaire, suggère que les thérapies dirigées contre les canaux SOCs et ces deux protéines au cours d'une ischémie myocardique ou cérébrovasculaire pourraient améliorer significativement les thérapies traditionnelles anti-thrombotiques (152). (Figure 10)

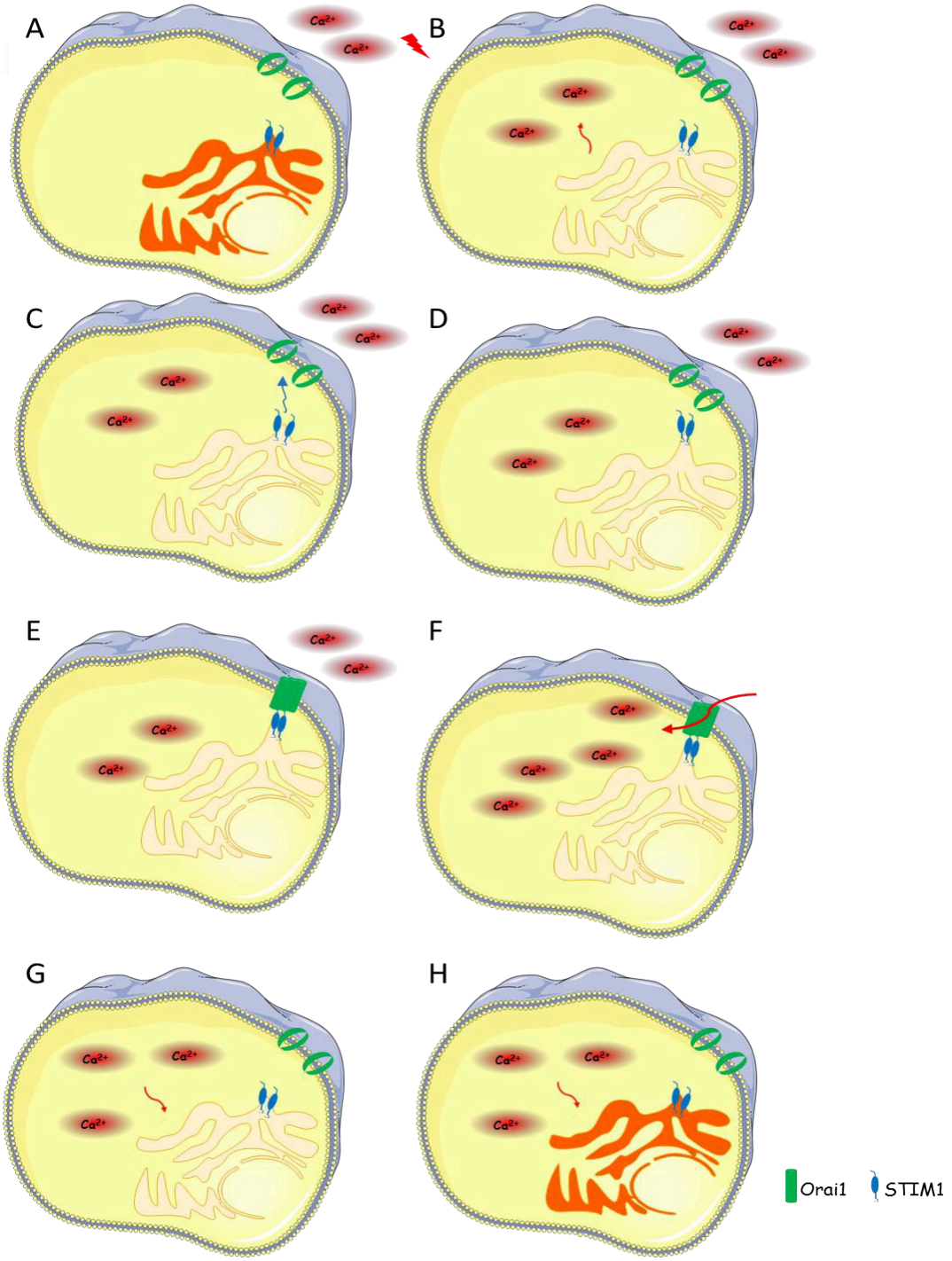

Figure10 schématisation du mécanisme de l'influx calcique

A) *STIM1 est localisé sur la membrane du STD et Orai1 sur la membrane plasmique* ***B)*** *activation plaquettaire, mobilisation calcique et déplétion du STD en* Ca^{2+} ***C)*** *STIM1 se rapproche de la membrane* ***D)*** *STIM1 se fixe sur Orai1* ***E)*** *les deux molécules forment un canal appelé SOC* ***F)*** *le canal SOC permet la rentrée du* Ca^{2+} *du milieu extracellulaire vers le cytosol et augmente sa concentration dans ce compartiment* ***G)*** *stockage du* Ca^{2+} *à l'intérieur du STD* ***H)*** *remplissage des réserves.*

II) Diminution de la concentration du Ca^{2+} cytosolique

Le retour à l'état de repos des cellules ou encore la terminaison du signal se fait par la diminution de la concentration du Ca^{2+} cytosolique. Cette diminution est assurée par la présence de systèmes permettant d'une part la séquestration du Ca^{2+} dans les réserves intraplaquettaires, et d'autre part son expulsion vers le milieu extracellulaire. Cette diminution est contrôlée par les pompes ATPases et les échangeurs.

Le système de transport du Ca^{2+} à partir du cytosol vers le milieu extracellulaire comprend les pompes ATPase de type PMCA, et l'échangeur de Ca^{2+} contre Na^{+}, tous les deux ancrés dans la membrane plasmique. Le transport du Ca^{2+} à partir du cytosol vers les réserves intraplaquettaires est effectué par les pompes ATPases de type SERCA (Sarco-Endoplasmique Réticulum Calcium ATPase) ancrées dans la membrane du STD ou du RE dans d'autres cellules.

a) Les échangeurs Na^{+}/Ca^{2+} :

Les échangeurs Na^{+}/Ca^{2+} sont exprimés au niveau de la membrane plasmique. Ces transporteurs bidirectionnels jouent un rôle important dans le maintien de la concentration du calcium cytosolique des plaquettes. Ce transport se produit par l'éjection d'un ion Ca^{2+} vers le milieu extracellulaire couplée à l'influx de trois ions Na^{+}, et peut également s'effectuer en mode inverse lorsque la concentration du Na^{+} est augmentée dans le cytosol. Les échangeurs Na^{+}/Ca^{2+} sont codés par 5 gènes *(NCX1-5)* avec différentes isoformes produites par épissage alternatif (153). Il existe deux classes d'échangeurs Na^{+}/Ca^{2+}: les Na^{+}/Ca^{2+} K^{+} indépendants *(NCX)* et les Na^{+}/Ca^{2+} K^{+} dépendants *(NCKX)*.

b) Les pompes calcique de type PMCA :

Les PMCAs sont des pompes calciques localisées dans la membrane plasmique où elles assurent le transport actif du Ca^{2+} depuis le cytosol vers le milieu extracellulaire permettant ainsi la diminution de la concentration du Ca^{2+} cytosolique. Ces pompes sont la voie principale d'élimination du Ca^{2+} vers le milieu extracellulaire dans les plaquettes (154), et elles ont été retrouvées dans toutes les cellules de mammifères. Les PMCAs sont codées par quatre gènes qui donnent 30 isoformes par épissages alternatifs (83). Les plaquettes expriment en majorité l'isoforme PMCA4b ainsi que PMCA1b en moindre quantité (70) (155).

En plus de leur activité d'élimination de Ca^{2+}, les PMCAs peuvent jouer un rôle important dans la signalisation. Par exemple, elles interagissent avec la NO-synthase neuronale (nNOS)

contenant un domaine PDZ qui leur permet d'avoir un effet important sur la fonction cardiaque (156). Dans les plaquettes, les PMCA interagissent avec le cytosquelette d'actine et sont localisées dans les filopodes pendant l'activation plaquettaire. Au repos les PMCAs possèdent une faible affinité pour le Ca^{2+}. Lors d'une activation, l'augmentation rapide de la concentration calcique dans le cytosol permet l'interaction des PMCAs avec la calmoduline (CaM) et les phospholipides. Ces interactions augmentent l'affinité des PMCAs pour le Ca^{2+} et activent le transport de cet ion (157). En 2010, Jones *et al.* ont montré que les plaquettes de souris déficientes en PMCA4 ont une diminution de la mobilisation calcique qui se traduit par un défaut de sécrétion et d'agrégation plaquettaire (158). Ce défaut d'activation plaquettaire pourrait être dû au repompage du Ca^{2+} vers le STD afin qu'il soit rapidement éliminé du cytosol, ce qui diminuerait aussi l'activation des SOCS dépendant de la déplétion du Ca^{2+} disponible dans le STD. En revanche l'invalidation du gène Pmca1 est létale chez la souris à l'état homozygote, suggérant que cette isoforme assure des fonctions de type « housekeeping ».

c) Les pompes calciques de type SERCA :

Les SERCAs sont des pompes ATPase de type P, localisées au niveau de la membrane du RE (ou le STD dans les plaquettes). Le premier système de transport actif du calcium utilisant l'ATP a été mis en évidence en 1961 sur le muscle squelettique (159) (160). En assurant un transport actif du Ca^{2+} cytosolique vers l'intérieur des réserves intraplaquettaires, les SERCAs maintiennent à la fois l'homéostasie calcique des réserves [1 mM] et du cytosol [100 nM]. Ce transport actif se fait contre un gradient de concentration en utilisant l'énergie de l'ATP, et en relarguant de l'ADP dans le cytosol (et H^+ dans les réserves) (161). En contrôlant la concentration du Ca^{2+} dans la cellule, les SERCAs jouent donc un rôle dans la création du signal Ca^{2+} et sa terminaison après activation cellulaire. Les SERCAs sont codées par trois gènes, donnant plusieurs isoformes par épissages alternatifs. Ces isoformes sont exprimées de façons spécifique dans les tissus avec une variabilité d'expression selon le stade de développement (162). Des différences biochimiques bien distinctes ont été démontrées entre les isoformes de SERCAs notamment vis-à-vis de leur affinité pour le Ca^{2+} (163). L'existence d'une spécificité propre à chaque isoforme permet une régulation fine de l'homéostasie calcique de la cellule selon son stade de différenciation et ses fonctions spécialisées (164). L'activité de séquestration du Ca^{2+} par les SERCAs est régulée au niveau du contenu en protéine, et elle est par ailleurs modulée principalement par deux protéines endogènes, le phospholamban (PLN) et la sarcolipine (SLN) (165).

Les différentes isoformes SERCAs :

Tout comme les PMCAs, les SERCAs sont codées par une famille de trois gènes: SERCA1 *(ATP2A1)*, SERCA2 *(ATP2A2)*, SERCA3 *(ATP2A3)* qui codent de multiples isoformes par épissage alternatif.

SERCA1 :

Chez l'Homme, le gène *ATP2A1* est localisé sur le chromosome 16p12.2 (166) et sa taille est de 26 kb pour 23 exons (167). L'analyse des transcrits SERCA1 a permis de montrer l'existence de deux ARNms: SERCA1a, transcrit complet, retrouvé chez l'adulte, et SERCA1b, présent que chez les nouveaux-nés. L'avant-dernier exon (exon 22 de 42 pb) de l'isoforme SERCA1a, est excisé pour SERCA1b. Au niveau protéique, les isoformes SERCA1a et SERCA1b ne diffèrent donc que par leurs parties C-terminales. L'exon supplémentaire présent dans SERCA1a contient un codon STOP et code pour un seul acide aminé (aa) Gly en position 994. La taille de la protéine SERCA1a est de 110 kDa. A ce jour, SERCA1 est la seule ATPase de type P pour laquelle la structure tridimensionnelle à haute résolution est connue (168).

Les protéines SERCA1 sont différemment exprimées principalement dans les muscles squelettiques rapides. L'isoforme SERCA1a, très abondante dans le RE de ces cellules, y représente 70 à 80% des protéines membranaires. De plus, SERCA1a représente aussi 99% des SERCA1, et est exprimée dans le muscle squelettique adulte, tandis que SERCA1b prédomine dans le muscle squelettique néonatal (169).

L'expression des deux protéines dans les cellules COS n'a pas permis de les différencier fonctionnellement. La raison de leur coexistence dans les muscles squelettiques reste donc obscure (170).

La déficience en SERCA1 chez la souris se traduit par un phénotype sévère qui mène à une mortalité précoce des souris. Cette mortalité rapide est causée par des difficultés respiratoires. Au stade embryonnaire, aucune anomalie n'est relevée. Aucune compensation n'a été observée en termes d'expression des autres SERCAs.

Des mutations du gène *ATP2A1* chez l'homme peuvent être à l'origine de la maladie de Brody, une maladie héréditaire caractérisée par une altération de la relaxation musculaire après un exercice, une rigidité corporelle, et des crampes musculaires durant l'effort (171). Ces symptômes s'expliquent par une diminution de l'activité de SERCA1a (172). Les signes cliniques du syndrome de Brody sont souvent bénins, du fait de l'expression compensatoire des autres pompes, contrairement à la souris.

SERCA2 :

En 1986, Brandl *et al*, ont montré l'existence d'un deuxième gène codant pour une pompe ATPase connue sous le nom d'*ATP2A2*, qui code pour 3 isoformes, SERCA2a, b et c. Ces isoformes se distinguent par leur extrémité C-terminale. Ce gène localisé au niveau du chromosome 12q24, est composé de 22 exons et sa taille est de 70 kb. Son organisation est similaire à celle de *ATP2A1* (173) (174).

La séquence des 993 premiers acides aminés (aa) est identique entre les 3 isoformes codées par le même gène. Les 4 aa de la partie C terminale de SERCA2a sont remplacés par 49 aa dans l'isoforme SERCA2b et 6 dans l'isoforme SERCA2c (175).

L'isoforme SERCA2a est majoritairement exprimée dans les cardiomyocytes (176), à la fois aux stades adultes et néonataux du développement cardiaque (177), mais aussi dans les cellules musculaires lisses (178), les cellules épithéliales pancréatiques, et faiblement dans le cervelet (179) ou dans les cellules polarisées (cellules du pancréas et glandes salivaires) (180).

L'isoforme SERCA2b a été détectée dans la membrane du RE de toutes les cellules testées à ce jour. Comme les PMCA1a et PMCA4b, SERCA2b est ubiquitaire y compris dans les cellules non musculaires comme les plaquettes (181) (182). La partie C-terminale de SERCA2b contient une séquence hautement hydrophobe pouvant donner un domaine transmembranaire additionnel (175). *G. Shull et coll.* ont proposé que la calréticuline, une protéine chaperonne, interagit avec ce domaine et module l'activité de SERCA2b.

La troisième isoforme, SERCA2c a été détectée dans les cellules non-musculaires. Elle est retrouvée dans les cellules mésenchymateuses et hématopoïétiques. L'ARNm de SERCA2c est présent dans les monocytes où son niveau d'expression est régulé au cours des phases de différenciation (174). Il a aussi été montré que l'ARNm de SERCA2c est présent dans le ventricule gauche du cœur au stade fœtal, suggérant un rôle fonctionnel important (183) (184). Les mutations du gène *ATP2A2* entraînent une maladie cutanée rare caractérisée par une hyperkératose. Cette maladie à transmission autosomique dominante, est connue sous le nom de la maladie de Darier (185). En 2004, Hovnanian *et al.* ont recensé plus de 120 mutations du gène *ATP2A2* responsables de cette maladie (186). Ces mutations entraînent une invalidation de l'activité de SERCA2 dans le tissu épidermique humain, ce qui se traduit par une affinité réduite pour le Ca^{2+}, suivi par une diminution des stocks calciques dans ces cellules. Cette diminution est liée à la dissociation facile des cellules épidermiques et la formation d'agrégats tissulaires dans l'épiderme chez les patients atteints de cette maladie (187). Il reste à élucider pourquoi la maladie de Darier est limitée à l'épiderme et à des régions spécifiques de la peau.

L'hypothèse la plus probable est une compensation du déficit par d'autres ATPases dans les autres tissus (188).

Des études d'invalidation du gène codant pour SERCA2 chez la souris ont montré qu'il n'était pas possible d'obtenir des homozygotes KO ($SERCA2^{-/-}$), suggérant que ce gène joue un rôle vital, probablement du fait du caractère ubiquitaire de SERCA2b (189). En revanche, les souris hétérozygotes ($SERCA2^{+/-}$) sont viables et présentent des défauts physiologiques: une diminution du stockage du Ca^{2+} dans le RE des cardiomyocytes, ce qui se traduit par une augmentation du Ca^{2+} cytosolique et une diminution de la pression intra-ventriculaire gauche (190). Cependant ce déficit en SERCA2 peut être partiellement compensé par une augmentation de l'expression des NCX (191). Une étude dans laquelle SERCA2a a été surexprimée dans les cellules musculaires lisses montre qu'après leur stimulation par la thrombine, le Ca^{2+} mobilisé dans le cytosol est rapidement capturé par ces pompes. Cette recapture rapide empêche l'activation des SOCs et donc l'influx calcique. Dans cette étude, les auteurs indiquent que l'origine du Ca^{2+} (extracellulaire ou intracellulaire), ainsi que sa disponibilité dans le cytosol (élimination rapide ou plus lente) jouent un rôle important dans la physiologie de la cellule (192).

SERCA3 :

Une troisième pompe ATPase a été mise en évidence par Burck et ses collaborateurs en 1989 chez le rat (193) puis chez l'homme par Wuytack *et al* en 1994 (194), mais ce n'est qu'en 1996 qu'ils ont identifié et cloné le gène *ATP2A3* (195). Le gène humain est localisé sur le chromosome 17p13.2 et sa taille est de 90 kb dont 50 kb sont codante (196) Ce gène possède un degré de complexité très élevé, non observé pour SERCA1 et SERCA2, avec l'existence d'isoformes spécifiques à chaque espèce. Il a été montré que chez l'homme, ce gène code pour 6 isoformes (SERCA3a, 3b, 3c, 3d, 3e & 3f) (Figure 13 ; page 47) (197) (198) alors que chez la souris il code seulement pour trois isoformes (SERCA3a, 3b, 3c) et pour deux chez le rat (3a et 3b/c) (Figure 11).

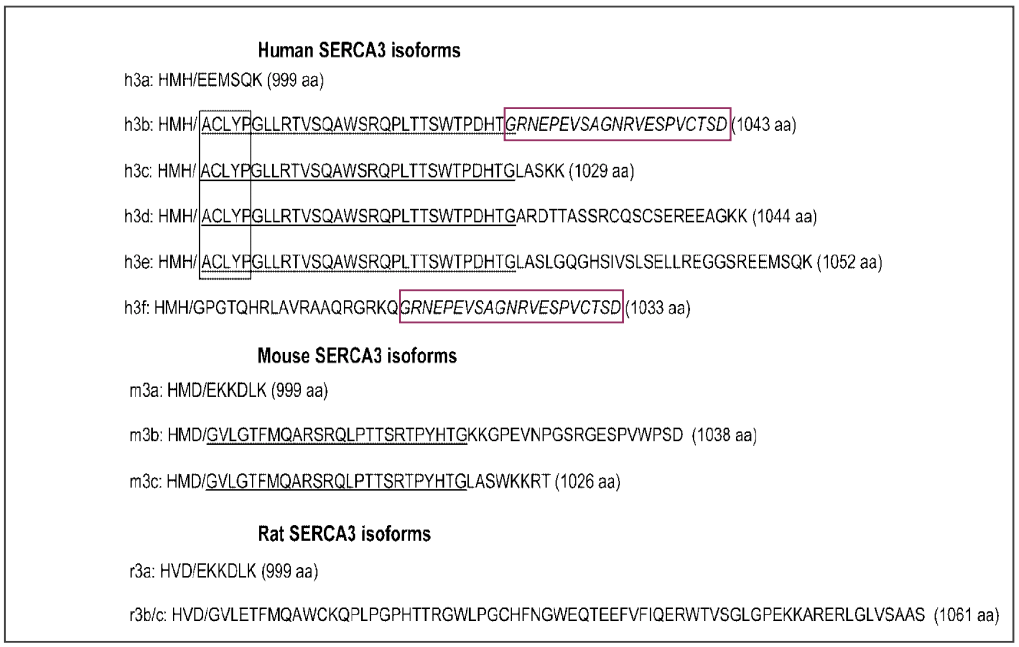

SERCA3 (Bobe, 2004; Martin, 2002).

Figure 11 : Représentation des séquences C-terminales des différentes isoformes de SERCA3

La partie C-terminale des différentes isoformes SERCA3 connues chez l'humain, la souris et le rat. La séquence ACLYP encadrée est absente dans la partie 5' de l'exon 21 de souris et du rat. Les séquences d'acides aminés soulignés sont communes aux isoformes SERCA3b, 3c, 3d et 3e humaines et de SERCA3b et 3c de souris. Les séquences en italique représentent les acides aminés communs aux deux isoformes humaines SERCA3b et SERCA3f. Les nombres indiquent la taille de chaque isoforme en acides aminés.

En 1998, Dode *et al* ont identifié 3 variants d'épissage de SERCA3 qui codent pour des protéines de 999, 1043 et 1024 aa. Ces protéines, que les auteurs ont appelées respectivement, SERCA3a, SERCA3b et SERCA3c, ne divergent qu'au niveau de leur extrémité C-terminale. Chez la souris, ces trois isoformes sont également exprimées avec des tailles similaires à celles des isoformes humaines. Les 6 derniers aa de la partie C-terminale de SERCA3a sont remplacés chez la souris et l'homme, respectivement par une extension protéique de 45 et 50 aa pour l'isoforme SERCA3b ou par 33 et 36 aa pour l'isoforme SERCA3c.

En 2002, Martin et ses collaborateurs ont identifié et cloné dans les plaquettes humaines deux nouvelles isoformes de SERCA3 (SERCA3d et SERCA3e) codant respectivement pour deux protéines qui contiennent 1044 et 1052 aa. Ces deux nouveaux ARNm utilisent le même signal de poly-adénylation que les ARNm des isoformes précédemment identifiées et ne diffèrent seulement par leurs extrémités C-terminales. Les deux nouveaux messagers humains SERCA3d et SERCA3e proviennent respectivement de l'insertion d'un nouvel exon de 58 pb. De plus Martin *et coll* ont détecté par RT-PCR les 5 isoformes des SERCA3 dans les plaquettes, les poumons et le pancréas. Le cœur, le cerveau, le placenta et les reins expriment 4 isoformes, alors que les muscles squelettiques expriment seulement une seule isoforme (199).

Enfin en 2004, Bobe *et coll* ont identifié un sixième variant, l'isoforme SERCA3f. L'ARNm de SERCA3f provient de l'excision de l'exon 21 et l'insertion de l'exon 22. Il a été également montré que l'isoforme SERCA3f est très proche de l'isoforme SERCA3b, ne divergeant de SERCA3b que par une séquence de 29 aa (provenant de l'exon 21) qui est remplacée par une séquence de 19 aa pour SERCA3f (provenant de l'exon 22). Les derniers 21 aa (provenant de l'exon 23) de ces deux protéines sont identiques (197).

L'expression des ARNm de SERCA3 a été explorée dans différents tissus humains et différentes lignées cellulaires. Une étude a montré que SERCA3 est principalement exprimée dans les tissus non musculaires : les cellules lymphoïdes, dans les cellules endothéliales, les cellules épithéliales de la trachée, des glandes salivaires, de l'intestin, mais aussi dans le cœur et les cellules de Purkinje du cervelet. Une forte expression de tous ces messagers a été démontrée aussi dans le poumon et le pancréas (176) (180) (199) (200).

L'expression de SERCA3 peut varier selon le type et l'état de différenciation cellulaires. D'ailleurs, SERCA3 est fortement exprimée dans les cellules épithéliales coliques normales alors que dans les cancers coliques, son expression est très diminuée ou nulle (201). Les ARNm de SERCA3b et SERCA3c sont principalement exprimés dans le rein, le pancréas et le poumon, mais à un faible niveau d'expression par rapport au ARNm de SERCA3a. Il a aussi été montré que les trois isoformes SERCA3a, 3b et 3c sont exprimées dans les cardiomyocytes et l'aorte thoracique de souris. Par ailleurs, SERCA3d et SERCA3f sont retrouvés dans tous les tissus musculaires et non-musculaires testés, et à des taux comparables (Figure 12). Elles pourraient correspondre à des SERCA3 ubiquitaires, tout comme SERCA2b.

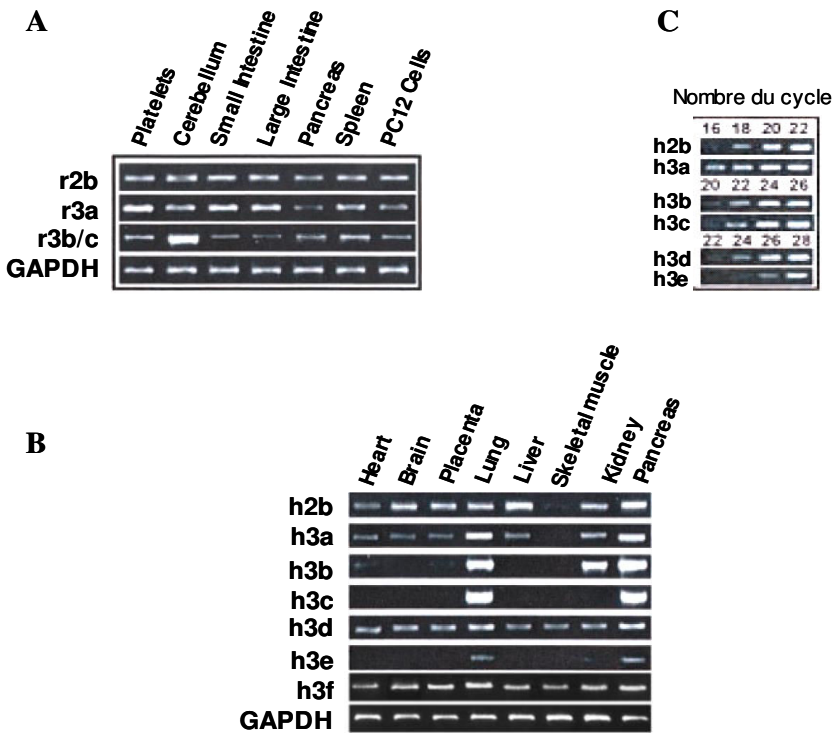

Figure 12 : Expression tissulaire des différents messagers SERCA3 (Bobe, 2004; Martin, 2002).

*Distribution des ARNm de SERCA3 dans différents tissus de rat (**A**) et humains (**B**). (**C**) Le nombre de cycles de PCR utilisés peut varier d'une isoforme à l'autre mais est invariant pour une isoforme donnée. Pour comparaison, l'expression de SERCA2b et de la GAPDH (glycéraldéhyde-3-phosphate, enzyme ubiquitaire) a également été analysée.*

En 1997, l'équipe de G. Shull a invalidé le gène codant pour SERCA3 chez la souris (202). Cette invalidation a été réalisée par insertion du gène de résistance à la néomycine au niveau de l'exon 5 du gène. Les souris homozygotes sont viables, fertiles et ne présentent aucune pathologie décrite à l'exception d'une altération du sens gustatif récemment observée (203). Par ailleurs, les travaux initiaux ont montré *in vitro* qu'au niveau des cellules musculaires aortiques et celles de la trachée (204), un défaut de relaxation dépendant de l'endothélium est lié à la diminution de la production du NO par la NO synthase endothéliale (NOS 3). L'analyse de cellules endothéliales isolées indique une perturbation dans la signalisation calcique contrôlant l'activation de la NOS3. Cette enzyme est localisée dans les caveolae et son activation par le Ca^{2+} dépend des réserves associées aux SERCA3. D'ailleurs, un compartiment calcique sous-membranaire a été décrit dans les cellules endothéliales artérielles, et une étude montre qu'il peut être responsable de l'activation de la NOS3 (205). Ces résultats suggèrent aussi une localisation de SERCA3 dans le RE sous-jacent à la membrane plasmique dans ce type cellulaire.

Chez l'homme, des mutations de SERCA3 ont été trouvées dans plusieurs types de cancer (poumon, colon, cerveau) (206)(207). Il existe également une perte d'expression de SERCA3 dans certaines tumeurs, comme observé au niveau du plexus choroïde (208). Des mutations de SERCA3 humaine sont associées au diabète de type II (209). De plus, l'équipe de P. Gilon *et coll* a montré que les SERCAs participent à la signalisation après stimulation par le glucose dans les cellules pancréatiques, et *in vitro* ils ont montré sur des ilots β une sécrétion d'insuline altérée (210 –212). Dans le diabète de type II, une diminution de l'expression de SERCA3 est également retrouvée dans les cellules pancréatiques (213). Tous ces résultats suggèrent un rôle spécifique de SERCA3 dans la signalisation calcique.

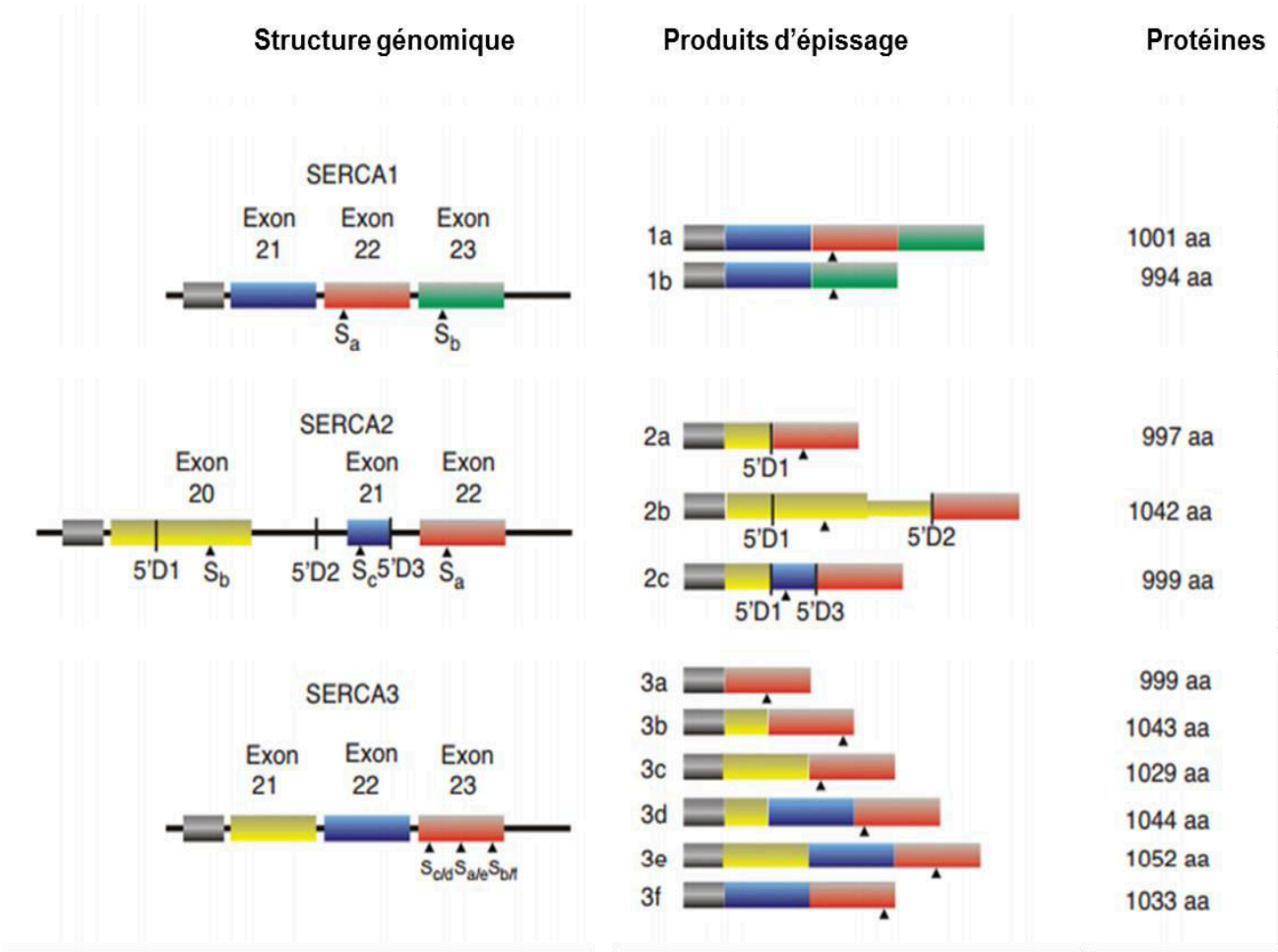

Figure 13 : épissage alternatif des trois gènes codant pour les SERCA

Génération d'isoformes SERCA multiples par épissage alternatif des gènes ATP2A1-3 humains. Les exons sont représentés par des boîtes colorées, les introns par la ligne noire. La boîte étroite de l'isoforme SERCA2b représente le pseudo exon non traduit.5'D1, 5'D2 et 5'D3 indiquent les sites donneurs d'épissage optionnels pour les transcrits SERCA2a, SERCA2b et SERCA2c, respectivement. Sa-f indique la position des différents codons Stop pour les isoformes de protéines correspondantes. La taille des produits protéiques est indiquée sur la droite. Les représentations des gènes ne sont pas à l'échelle.

Structure des SERCAs :

Les Ca^{2+} ATPases ont une structure asymétrique avec trois domaines fonctionnellement différents :

I) Le domaine cytoplasmique :

Ce domaine contient les sites de fixation de l'ATP et de phosphorylation. Il est divisé en trois régions, le plus petit est appelé domaine A pour « actuator domain » qui contient la séquence TGES très conservée dans l'ensemble des ATPase de type P. Ce domaine joue un rôle dans le contrôle de l'accessibilité des ions Ca^{2+} à leurs sites de fixation, ainsi que dans la déphosphorylation de l'enzyme. Le domaine P « phosphorylation Domain » qui contient le site d'autophosphorylation. Enfin, le troisième domaine N «nucleotide binding domain », impliqué dans la liaison des nucléotides ATP/ADP.

II) Le domaine transmembranaire :

Ce domaine contient les sites de haute affinité pour le calcium. Il est composé de 10 hélices α qui participent à la formation du pore calcique. Les hélices M4, M5, M6 et M8 sont impliquées dans la fixation du Ca^{2+} ; ces hélices contiennent essentiellement des résidus acides. La cinquième hélice (M5) est un élément essentiel dans le fonctionnement de l'enzyme car elle relie le domaine transmembranaire au domaine cytoplasmique et le domaine luminal. Ce domaine transmembranaire est connecté aux deux régions A (M1, M2 et M3) et P (M4 et M5) du domaine cytoplasmique, tandis que le domaine N est relié au domaine P (214).

III) Le domaine luminal

C'est le plus petit domaine de la molécule, il ne représente que 3 % de la taille totale de la protéine. Il est en contact avec la lumière du RE. Des mutations au niveau de ce domaine induisent une perte complète de l'activité de transport du Ca^{2+} (215) (Figure 14).

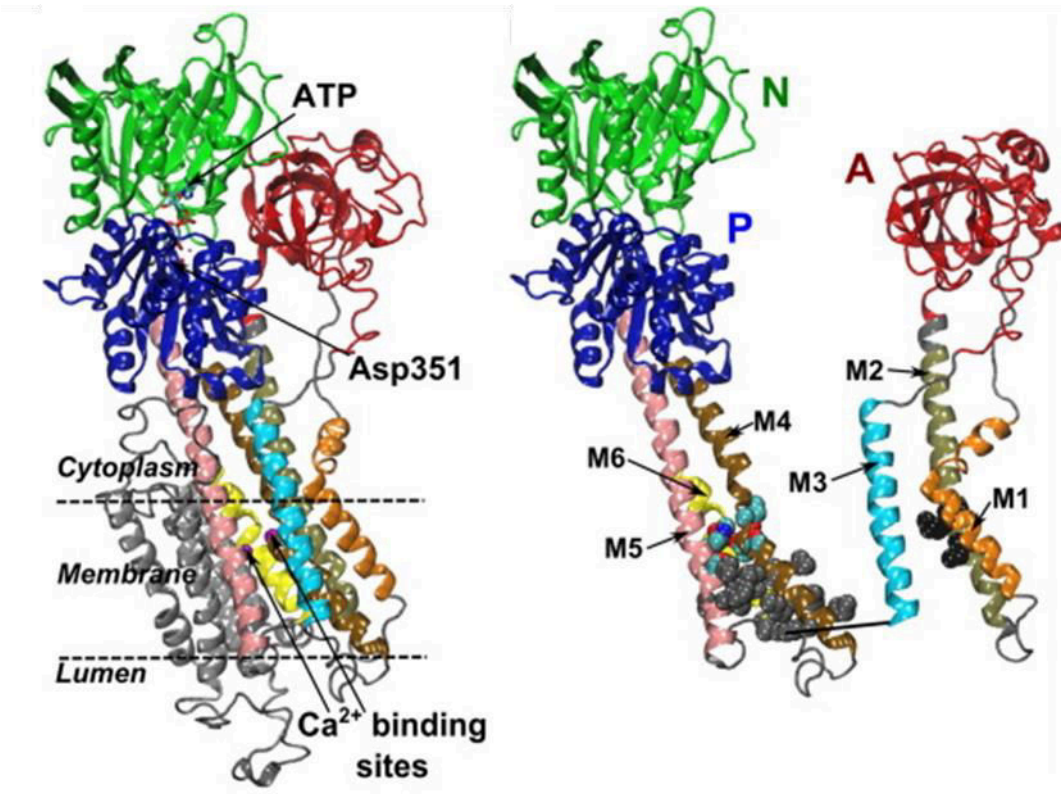

Figure 14 : Structure tertiaire des SERCAs d'après (Das et al 2017)

Topologie globale de la pompe à calcium ATPase de type P SERCA. A) le domaine cytoplasmique comprend les domaines de liaison nucléotidique (N), de phosphorylation (P) et d'actionneur (A). L'ATP se lie au domaine (N). Le domaine (P) contient l'acide aspartique (Asp351) hautement conservé qui peut se phosphoryler. Les sites de liaison au calcium sont situés dans le domaine transmembranaire (TM) qui est constitué de 10 hélices (M1 à M10). B) Le domaine A est lié de manière covalente aux hélices M1, M2 et M3, et le domaine P est lié aux hélices M4 et M5.

Mécanisme d'action des SERCAs:

La compréhension du mécanisme de transport du Ca^{2+} par les SERCAs a fait l'objet de nombreuses études. Dès 1970, Makinos *et al*. ont proposé un modèle décrivant le transport du Ca^{2+} qui est toujours d'actualité (216).

Le cycle de transport du Ca^{2+} est initié par la formation d'un complexe aspartyl (Asp 351) des SERCA et le phosphate terminal de l'ATP. Ce complexe permet de fournir l'énergie de l'ATP nécessaire pour le transport actif du Ca^{2+}. La transphosphorylation de l'Asp permet la liaison de deux ions Ca^{2+} aux deux sites localisés dans le domaine transmembranaire, probablement par remaniement conformationnel. Ces deux sites sont situés côte à côte près de la surface cytoplasmique de la bicouche lipidique membranaire. Le premier site (I) est situé entre M5 et M8, alors que le site (II) est localisé entre M4 et M6. Dans les deux sites, le Ca^{2+} coordonne sept atomes d'oxygène provenant de résidus qui se trouvent dans les hélices M4, M5, M6 et M8. A partir de ces sites I et II, les deux ions Ca^{2+} sont ensuite transportés vers la lumière des réserves intraplaquettaires. Cette voie moléculaire de transport de Ca^{2+} à travers les pompes ATPases a été maintenant cartographiée, et implique probablement l'hélice M5, qui s'étend de la surface luminale de la membrane jusqu'au domaine P cytoplasmique. Alors que les hélices M1 à M6 se déplacent considérablement durant le cycle de réaction, les hélices M7 à M10 ne bougent pas, jouant sûrement le rôle d'ancrage à la membrane. Le domaine P est situé dans la partie centrale du domaine cytoplasmique, et est composé de deux régions : une courte région N-terminale connectée à l'hélice M4 qui contient le résidu aspartyl (Asp 351) et une partie C-terminale plus longue connectée à l'hélice M5. Il est important de noter que la séquence TGES (Threonine, Glycine, Glutamic Acid, Serine) du domaine A joue un rôle important dans l'hydrolyse de Asp351 phosphorylé.

Les SERCAs alternent entre deux conformations majeures (E1 et E2) non phosphorylées et deux conformations phosphorylées (E1~P, E2~P). L'état E1 représente la conformation à haute affinité pour le Ca^{2+} (K_d=10^{-7} à 10^{-6} M) et lie les ions de Ca^{2+} à partir du cytosol. Cette liaison ($2Ca^{2+}$E1) entraine une transition conformationnelle de la pompe permettant la fixation de la molécule d'ATP suivie d'une autophosphorylation de l'enzyme ($2Ca^{2+}$E1~P) sur le résidu Asp 351 en présence de Mg^{2+} pour stabiliser le phosphate. Le changement de conformation $2Ca^{2+}$E1~P ➔ E2~P se transmet du site catalytique au domaine transmembranaire de liaison du Ca^{2+}, ce qui induit un réarrangement des sites de liaison qui deviennent inaccessibles depuis le cytosol mais accessibles depuis le lumen des réserves intraplaquettaires. Par la suite, les sites de haute affinité disparaissent pour laisser place à des sites de faible affinité pour le Ca^{2+}

(K_d=10^{-4} a 10^{-3}M). La déphosphorylation de E2~P libère un phosphate inorganique (Pi) pour un changement de conformation (E2).

Le retour à l'état E1 est réalisé par le contre transport de deux protons H^+ à la place des ions Ca^{2+} (217–219) (Figure 15) (Figure 16)

Les deux autres pompes ATPases de type P, PMCA et SPCA, ne contiennent pas de résidu acide dans leur domaine transmembranaire M5, et n'ont qu'un site de fixation du Ca^{2+}, correspondant au site (II) des pompes SERCAs. Par conséquent, la stœchiométrie du transport Ca^{2+}/ATP est de 2 chez les pompes SERCA et de seulement 1 dans les pompes PMCA et SPCA.

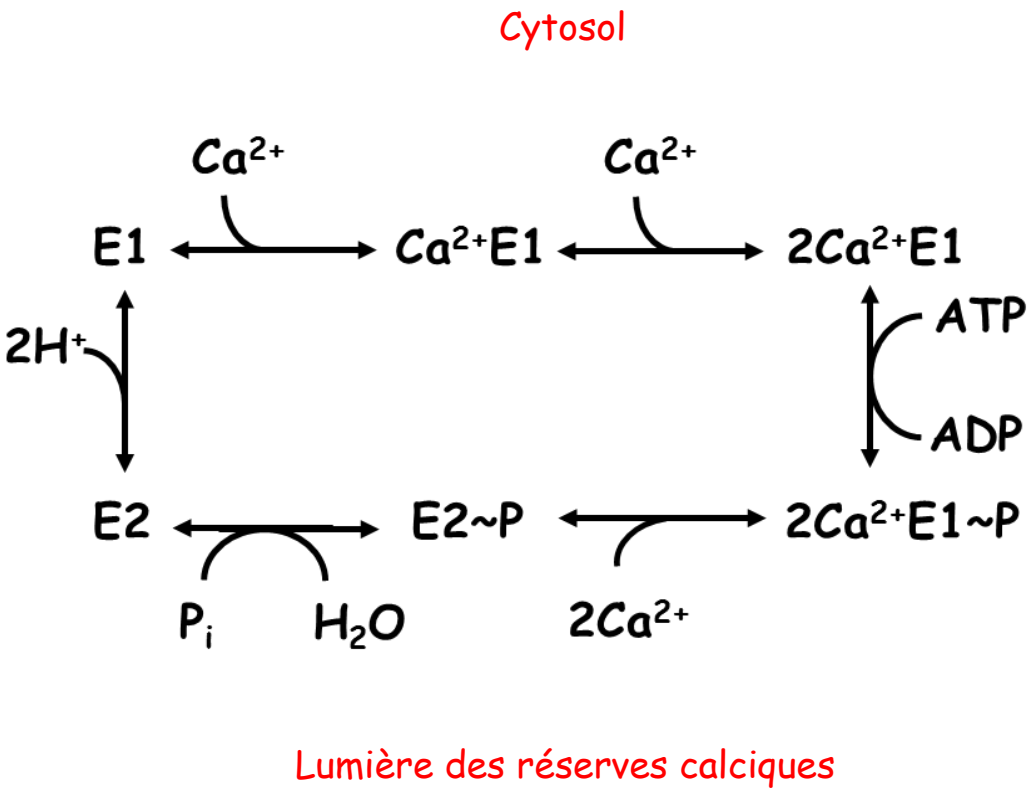

Figure 15 : Cycle catalytique des pompes Ca^{2+}-ATPases SERCA.

Les pompes existent dans deux états conformationnels principaux: E1 lie le Ca^{2+} avec une forte affinité sur le site cytosolique; E2 a une faible affinité pour le Ca^{2+} et le libère donc sur le site opposé de la membrane. Le cycle catalytique a plusieurs autres conformations qui sont simplifiées ici mais qui sont discutées dans le texte. L'ATP phosphoryle un résidu d'acide aspartique hautement conservé permettant la translocation de Ca^{2+}.

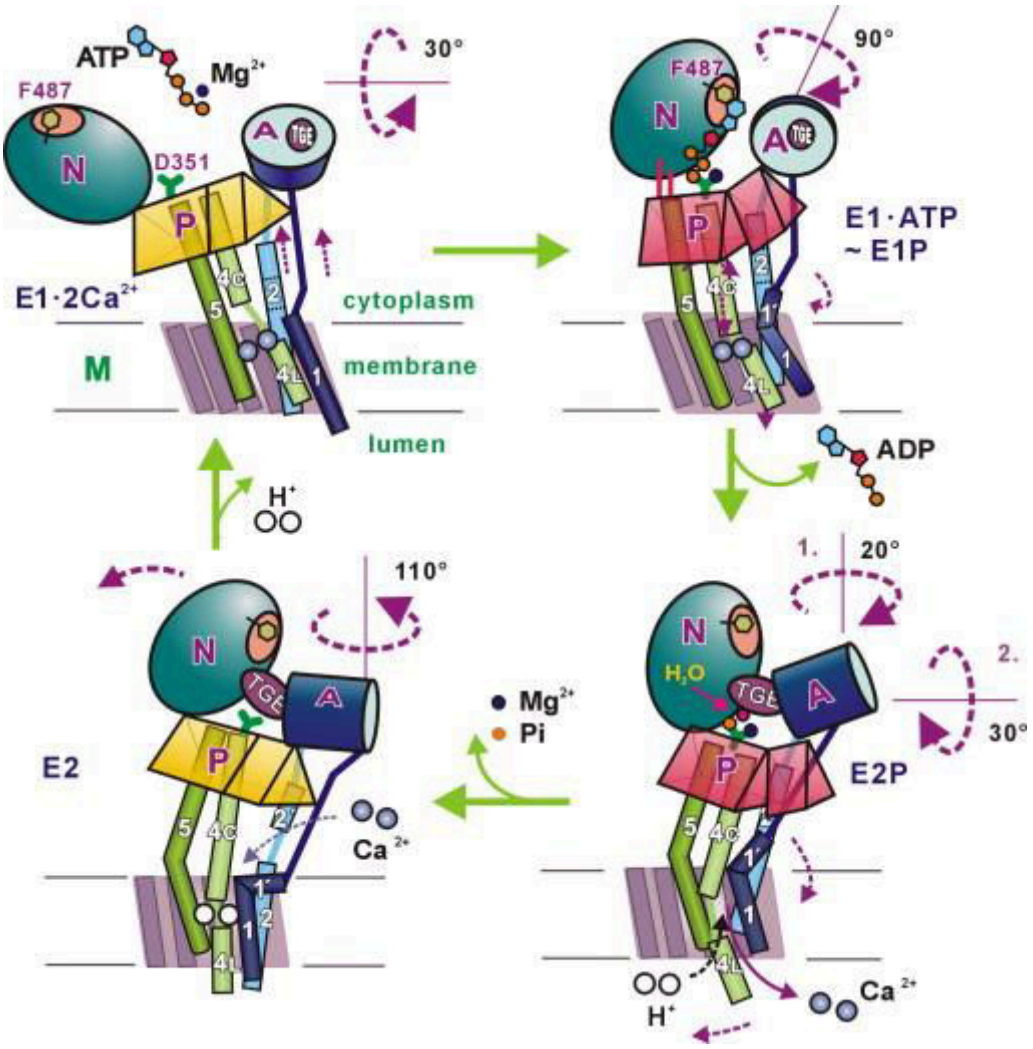

Figure 16 : Les changements conformationnels majeurs de la structure de l'enzyme SERCA au cours du cycle de transport du Ca^{2+} (Toyoshima, 2008; (220))

Différences fonctionnelles entre les différentes isoformes de SERCA:

Bien que le cycle catalytique et la structure des SERCAs soient similaires, ces enzymes présentent des propriétés biochimiques distinctes. En effet, les propriétés des différentes SERCAs ont été établies *in vitro,* après transfection de leur ADN complémentaire (ADNc) dans les cellules COS-1 ou HEK-293, par comparaison de la mesure du transport de Ca^{2+}, de la concentration du Ca^{2+} cytosolique, et de la mobilisation du Ca^{2+} induite par l'ionophore calcique ionomycine (221). Les deux isoformes SERCA1 et SERCA2a ont la même affinité pour le Ca^{2+}, tandis que SERCA2b possède une affinité plus forte, et SERCA2c plus faible. Par ailleurs, SERCA2a a une capacité de transport supérieure à celle SERCA2b. Les isoformes SERCA3 présentent des différences importantes par rapport aux autres SERCAs. Des études comparatives ont montré que SERCA3 a une affinité pour le Ca^{2+} considérablement inférieure à celle de SERCA2 ($K_{1/2}$ ~0. 27 µM pour SERCA2 contre 1 µM pour SERCA3) mais une capacité de transport plus forte (21 nmol/min/mg pour SERCA3 contre 7nmol/min/mg pour SERCA2) (164) (221).

A) Les régulateurs physiologiques et inhibiteurs pharmacologiques des SERCAs :

Les aspects de régulation sont plutôt mieux connus pour l'isoforme SERCA2. La régulation de SERCA2 se fait à plusieurs niveaux: au niveau génique et protéique. Au niveau du gène, l'activité transcriptionnelle du promoteur du gène ATP2A2 est régulée par plusieurs facteurs de transcription dont TFAM et TFB2M (223).

Au niveau protéique, l'activité des SERCA2 et SERCA1 est inhibée par le PLN. Cette protéine de 52 aa localisée dans le RE a été découverte dans le cœur il y a plus de quarante ans (224). Lorsque la concentration du Ca^{2+} cytosolique est faible, PLN interagit avec SERCA2 et SERCA1 et diminue leur affinité pour le Ca^{2+}. En revanche, PLN n'interagit pas avec SERCA3. La structure tertiaire du PLN montre qu'il existe une partie C-terminale hydrophobe hélicoïdale s'ancrant dans la membrane des réserves intracellulaires et une partie cytosolique N terminale. Sous sa forme non phosphorylée, PLN se lie à la pompe et l'inhibe en réduisant son affinité pour le Ca^{2+}. On suppose que la phosphorylation de la partie hydrophile du PLN par la PKA induit son détachement de la pompe, ce qui augmente l'affinité de la pompe pour le Ca^{2+} induisant l'augmentation de son transport. Cependant il a été proposé que le PLN ne se détache pas complètement de la pompe mais reste attaché au domaine N cytoplasmique (225).

A forte concentration, le Ca^{2+} induit un changement de conformation de la CaM et forme un complexe avec lui (Ca^{2+}-CaM). Ce complexe permet l'activation de la CaMKII, une sérine/thréonine kinase qui phosphoryle le PLN au niveau du résidu thréonine 17 et bloque ces fonctions inhibitrices (226).

La suppression de l'expression de PLN dans des souris transgéniques entraine une augmentation de la contraction cardiaque et de l'affinité de SERCA2a pour le Ca^{2+}, alors que la surexpression de PLN dans le cœur est associée à une altération des fonctions cardiaques (227) (228).

La SLN est une autre protéine transmembranaire de 31 aa. Cette protéine homologue du PLN est également inhibitrice de SERCA1 et SERCA2. A la différence de PLN elle est inhibée par la serine/thréonine kinase 16 (STK16) et pas par CaMKII (229)(230). L'expression de SLN est augmentée chez les patients atteints de maladies cardiovasculaires. La co expression de SLN et PLN dans un modèle cellulaire induit une très forte inhibition de la pompe (161).

En jouant un rôle dans la régulation de la concentration de Ca^{2+} dans les réserves intracellulaires, les SERCAs peuvent donc être essentielles pour la maturation des protéines produites dans le RE. Certaines protéines présentes dans le RE se lient au Ca^{2+} et régulent l'activité des SERCAs. La calréticuline et la calnexine, des protéines chaperons, régulent l'activité des SERCAs. Il a été suggéré que la calréticuline interagit fonctionnellement avec SERCA2b mais pas avec SERCA2a (231). SERCA2b contient un site de N-glycosylation dans sa partie C-terminale luminale. Ainsi, les différences fonctionnelles des deux isoformes pourraient être liées à l'interaction du domaine lectine de la calréticuline ou de la calnexine avec le résidu glycosylé dans SERCA2b. Cependant, la glycosylation de SERCA2b n'a pas été clairement démontrée (232).

Il existe aussi des inhibiteurs pharmacologiques pour les Ca^{2+} ATPases. En se fixant aux SERCAs, ces inhibiteurs déclenchent un relargage du Ca^{2+} stocké dans les réserves intracellulaires vers le cytosol. Parmi les inhibiteurs pharmacologiques des pompes ATPases, on trouve le lanthane (La^{3+}) et l'orthovanadate $[VO_3(OH)]^{2-}$. Ces molécules inhibent toutes les pompes ATPases (SERCA, PMCA, SPCA) (233) (mais également d'autres enzymes), mais d'autres inhibiteurs sont spécifiques des SERCAs : la thapsigargine (Tg) (isolée des racines de la plante thapsia garganica) (234), l'acide cyclopiazonique (CPA) (produit par Aspergillus et Penicillium) une mycotoxine (235) et le 2,5-di-(*tert*-butyl)-1,4-benzohydroquinone (tBHQ), un anti-oxydant (236). La curcumine (différuloylméthane ou 1,7-bis (4-hydroxy-3-

méthoxyphénol) -1,6-hepatadiene-3,5-dione), un composé dérivé du curcuma, inhibe également les pompes SERCAs, probablement en inhibant la liaison ATP. Cependant, sa spécificité est inférieure à celle des autres inhibiteurs, car elle peut également agir sur des canaux de libération de Ca^{2+} intracellulaires.

CPA et tBHQ ont une affinité plus faible pour les pompes ATPase par rapport à la Tg (Kd plus faible). L'inhibition par CPA ou tBHQ est réversible et disparaît après leur élimination du milieu. Les aspects moléculaires du mécanisme d'inhibition par la Tg sont mieux connus grâce à la modélisation obtenue après cristallographie. La Tg se lie aux SERCAs de manière stœchiométrique et non-compétitive avec une affinité très élevée (valeurs de K_d de l'ordre du subnanomolaire) (237) sur le résidu phénylalanine 256 (F256) de l'hélice M3 (238). Cette liaison induit le blocage de la pompe dans un état irréversible. La Tg interagit préférentiellement avec la pompe sans Ca^{2+}. L'utilisation de la Tg a permis d'obtenir une structure 3D de la pompe à l'état Ca^{2+}~ E2) (239). La CPA et la Tg ont d'abord été proposés pour se lier à des sites similaires sur les SERCAs (240), mais les derniers travaux structurels suggèrent qu'ils ont probablement des sites d'interaction différents (241) (242). Un effet antagoniste de la liaison CPA contre la liaison ATP a été proposé, en accord avec les modèles précédents: il a été constaté que la poche de liaison au CPA est formée par les segments transmembranaires M1, M2, M3 et M4. Il a été également démontré que la liaison est assurée par des cations divalents (243). En ce qui concerne la Tg, son site de liaison a été identifié comme une cavité entourée par les hélices M3, M5 et M7 près de la surface cytoplasmique des hélices membranaires par liaison hydrogène avec Ile 829 (Figure 17). Dans la conformation E1 Ca^{2+}, la cavité devient plus petite et la surface n'est plus complémentaire à la Tg en raison du décalage de M3. Le clonage des ADNc de la pompe SERCA (169) (173) (193) (202) a permis un certain nombre de conclusions sur le mécanisme moléculaire de la pompe : par exemple, la proposition selon laquelle l'enzyme est organisée dans la membrane avec dix domaines hélicoïdaux transmembranaires (M1-M10). Le tBHQ se fixe au domaine membranaire de l'enzyme, en se plaçant entre les hélices M3 et M4, par des liaisons hydrogène (Figure 18).

A 1µM, la thapsigargine inhibe toutes les SERCAs alors qu'à faibles concentrations (200 nM) elle inhibe préférentiellement SERCA2. Le tBHQ (10 à 20 µM) inhibe spécifiquement les SERCA3 (56) (60) (245).

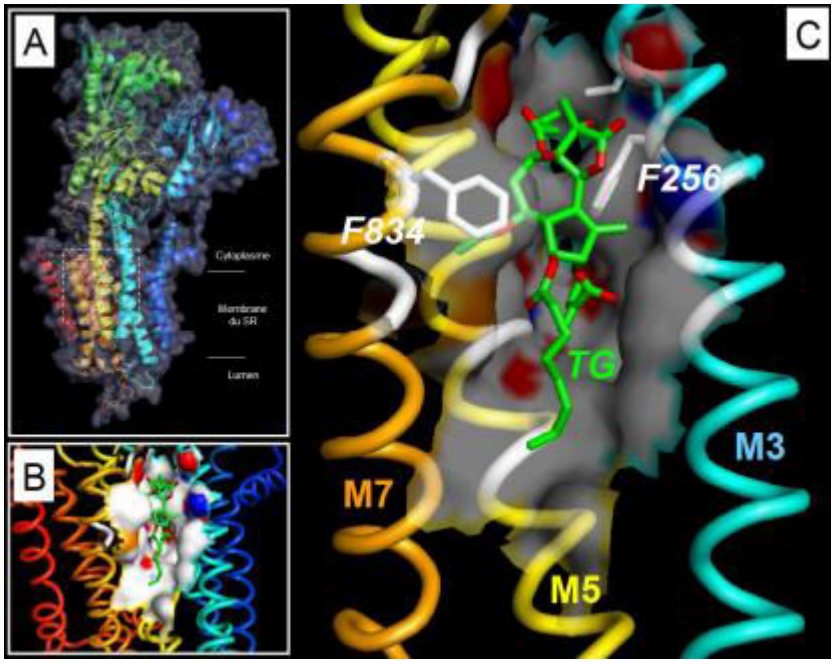

Figure17: Site de fixation de la thapsigargine (TG). ***A)*** *représentation de la structure à résolution atomique de l'ATPase-Ca^{2+} obtenue en présence de la thapsigargine, avec sa chaine polypeptidique représentée par des rubans colorés (du bleu au rouge, du N-vers le C-terminal) et son volume total en gris. La thapsigargine est fixée dans le domaine membranaire, entre les hélices M3 (bleu ciel), M5 (jaune) et M7 (orangée).* ***B)*** *agrandissement de la zone pointillée du panneau A. La TG est fixée au sein d'une poche hydrophobe. Les atomes formant la poche sont colorés en rouge pour les oxygènes, bleu pour les azotes et blanc pour les carbones : la poche est essentiellement hydrophobe. La TG est aussi colorée selon la nature des atomes (ici, dans un souci de clarté, le vert remplace le blanc pour les carbones).* ***C)*** *Image identique à B mais seules les hélices M3, M5 et M7 sont maintenant représentées, par souci de simplification. Les chaines latérales des phénylalanines 256 (F256) et 834 (F834) enserrent la TG et interagissent via leurs cycles avec la sesquiterpène-lactone de la TG* (239)

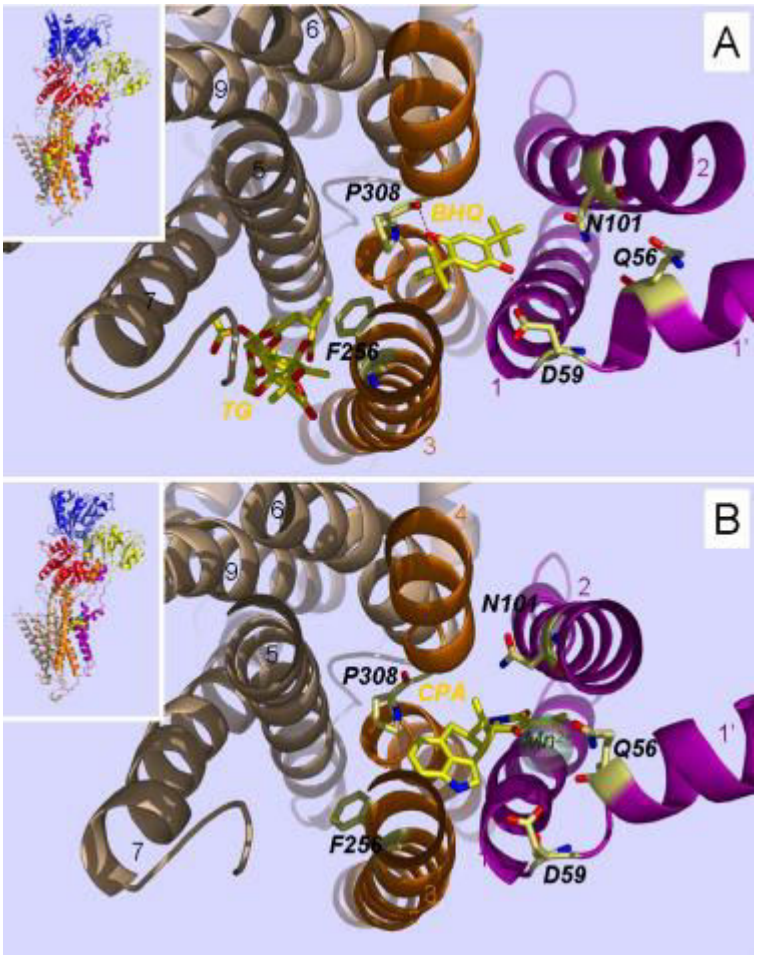

Figure 18 : Site de fixation de la 2,5-di (t-butyl) hydroquinone (tBHQ) et de l'acide cyclopiazonique (CPA). *Les « E2TG. TBHQ » et « E2 CPA » sont représentées en rubans avec la même orientation pour leurs domaines C-terminaux (hélices transmembranaires M7à M10). Le domaine membranaire représenté ici est observé depuis le cytosol, selon un axe perpendiculaire à la membrane (le domaine cytosolique a été masqué). Les hélices transmembranaires M1 à M9 sont visibles et annotées de 1 à 9 ainsi que la partie 1' de M1 orientée dans un plan parallèle à la membrane dans ces conformations (M1 et M2 en violet, M3 et M4 en orangé, M5 et M 6 à M10 en grisé). Les chaines latérales des acides aminés sont indiquées en gras et italique et les atomes sont colorés en rouge pour les oxygènes, en bleu pour les azotes et en blanc pour les carbones. Les inhibiteurs TG, tBHQ et CPA sont indiqués en coloré en orange et les carbones en jaune.* ***A)*** *la TG occupe, comme décrit plus haut, la poche formée par les hélices M3, M5 et M7, avec une interaction majeure avec la phénylalanine F256. Le tBHQ est enchâssé au sein des hélices M1 à M4, et est lié aux deux hélices M1 et M4 via une liaison hydrogène avec les résidus aspartate D59 (M1) et proline P308 (M4), ce qui semble stabiliser les coudes présents dans ces deux hélices.* ***B)*** *En présence de CPA, les hélices M1 et M2 sont réorganisées de manières subtile mais significative. La CPA se positionne également entre les hélices M1 et M4 et bloque la protéine en stabilisant un réseau de liaisons hydrogènes, via les molécules d'eau non représentées ici, avec le résidu asparagine N101*(246).

B) Rôle physiologiques des SERCA2 et SERCA3:

Nous avons vu que les isoformes SERCA2 et SERCA3 présentaient des différences d'affinité, de fonction, d'expression tissulaire et de régulateurs physiologiques, mais ces deux isoformes sont co-exprimées dans de nombreux types cellulaires (cardiomyocytes, plaquettes). Sachant que SERCA2b est exprimée de façon ubiquitaire, la présence de SERCA3 dans les mêmes cellules suggère qu'elle remplit un rôle diffèrent, spécifique, précis et une compartimentalisation dans des réserves calciques dont la charge en Ca^{2+} serait contrôlée par une isoforme particulière. D'ailleurs, plusieurs études sont en accord avec cette hypothèse, la première ayant notamment montré une organisation réticulaire dans les plaquettes à partir de vésicules membranaires intra-plaquettaires purifiées, et l'existence de plusieurs réserves de Ca^{2+} de sensibilité différente à la TG et au tBHQ qui respectivement inhibent préférentiellement SERCA2 et SERCA3 (247). Cette observation a été confirmée depuis dans les plaquettes entières par les travaux de l'équipe de Rosado qui a montré par une approche pharmacologique une association des isoformes de SERCA3 avec les granules acides de type lysosomial et avec les réserves possédant les récepteurs du NAADP (56)(60), Ces données suggèrent différentes fonctions des isoformes de SERCAs présentes dans un même type cellulaire. De plus, Kovacs et coll ont montré par immuno-électromicroscopie une localisation périphérique, voire membranaire plasmique de SERCA3 (248); mais ces observations méritent d'être confirmées puisque les images publiées montrent un fort bruit de fond, rendant les interprétations délicates.

Objectif de la thèse

Le Ca^{2+} est très important dans les processus d'activation plaquettaire, tout d'abord dans la sécrétion contrôlée par les PKC, elles-mêmes pour la plupart dépendantes du Ca^{2+}. Le Ca^{2+} est aussi impliqué dans l'activation de l'intégrine αIIbβ3, responsable de l'agrégation plaquettaire. Ce Ca^{2+} est aussi important pour la réorganisation du cytosquelette. L'implication du Ca^{2+} dans un nombre important de fonctions plaquettaires suggère une régulation spatiale et temporelle précise du signal calcique. L'homéostasie du Ca^{2+} est un processus dynamique mettant en jeu des mouvements permanents du Ca^{2+} à travers les différentes membranes plaquettaires. Dans les plaquettes au repos, la concentration du Ca^{2+} cytosolique est maintenue aux alentours de 100 nM ce qui est très faible par rapport au Ca^{2+} disponible dans le milieu extracellulaire ou dans les stocks internes.

L'activation plaquettaire passe par une élévation du Ca^{2+} cytosolique. Cette élévation est due à l'entrée du Ca^{2+} à partir du milieu extracellulaire ("influx") ou sa translocation ("mobilisation") dans le cytosol depuis les réserves internes. L'homéostasie calcique est finement contrôlée entre autres par les pompes ATPases ancrées dans les membranes internes, les SERCAs. Les SERCAs pompent le Ca^{2+} depuis le cytosol vers les réserves internes, maintenant le Ca^{2+} cytosolique bas et assurent ainsi une concentration en Ca^{2+} élevée (≥1 mM) dans les réserves internes permettant la mobilisation. Les plaquettes expriment l'isoforme ubiquitaire SERCA2b et plusieurs isoformes de SERCA3. Ces pompes modulent l'intensité et la forme du signal calcique lors de l'activation. Cependant, les rôles respectifs des SERCAs plaquettaires, SERCA2b et SERCA3, sont encore mal définis. Est-ce que ces différentes isoformes jouent un rôle redondant ou au contraire ont un rôle précis dans la fonction plaquettaire ?

L'objectif de ma thèse a été d'une part de déterminer si les SERCA3 jouaient un rôle dans les fonctions plaquettaires et d'autre part de discriminer les voies de signalisation dépendantes de SERCA3 et celles dépendantes de SERCA2b. Nous avons utilisé un modèle de souris déficientes en SERCA3 que nous avons caractérisé en hémostase primaire (temps de saignement, thrombose *in vivo* et *in vitro*, agrégation, sécrétion plaquettaire, mobilisation calcique) (Article I et III). En parallèle, nous avons mené une étude sur des patients atteints d'obésité morbide, une pathologie où nous avons découvert un défaut fonctionnel plaquettaire associé à un taux d'expression de SERCA3 fortement diminué (Article II), confirmant donc chez l'Homme les observations sur le modèle murin.

Résultats

Article I

Rôle de SERCA3 dans les fonctions plaquettaires chez la souris

Article II

Rôle de SERCA3 dans les fonctions plaquettaires chez l'homme

Article III

La sécrétion primaire d'ADP dépend de SERCA3 et du NAADP

Article I

Rôle de SERCA3 dans les fonctions plaquettaires chez la souris

Dans cette première partie de mon travail de thèse, j'ai caractérisé en hémostase un modèle de souris déficientes en SERCA3 (SERCA3$^{-/-}$). Aucune différence avec des souris sauvages n'a été observée dans la formule sanguine, au niveau de l'expression des récepteurs plaquettaires ou de l'ultrastructure plaquettaire en microscopie électronique. Par contre les souris SERCA3$^{-/-}$ ont montré une tendance à l'allongement du temps de saignement associée à une reprise de saignement. Ce défaut de l'hémostase est cohérent avec un retard du temps d'occlusion associé à une instabilité des thrombi observés dans un modèle de thrombose in vivo (dite "au $FeCl_3$") chez les souris SERCA3$^{-/-}$. Ces résultats suggèrent que SERCA3 joue un rôle positif dans la formation du thrombus. L'invalidation de SERCA3 dans ces souris n'étant pas restreinte qu'aux plaquettes, la composante vasculaire (cellules endothéliales) pourrait aussi jouer un rôle dans la formation du thrombus. Pour vérifier directement l'impact du déficit de SERCA3 sur les plaquettes, nous avons étudié la formation des thrombi plaquettaires *in vitro* en capillaires, et en conditions de flux sur matrice de collagène. L'adhérence plaquettaire est diminuée de 50 % pour les plaquettes des souris SERCA3$^{-/-}$ par rapport à celles des souris sauvages. L'adhérence en flux au collagène étant dépendante de la sécrétion d'ADP plaquettaire à partir de ses stocks granulaires, nous avons postulé un défaut de sécrétion d'ADP dans les souris SERCA3$^{-/-}$. En présence d'apyrase, enzyme dégradant l'ADP, l'adhérence plaquettaire des souris sauvages est diminuée et rejoint celle des souris SERCA3$^{-/-}$ qui reste inchangée. Ces résultats confirment que l'absence de SERCA3 a un effet direct sur la fonction plaquettaire et d'autre part suggèrent un défaut de sécrétion d'ADP dans ce modèle. J'ai donc analysé les fonctions des plaquettes isolées et aux faibles doses d'activateurs (thrombine, collagène, AP-PAR4), j'ai observé chez les souris SERCA3$^{-/-}$ un défaut d'agrégation plaquettaire, de sécrétion des granules denses et alpha, et d'activation de l'intégrine $\alpha_{IIb}\beta_3$ (nécessaire à la liaison de son ligand, le fibrinogène, et à la formation de ponts inter-plaquettaires). J'ai confirmé un défaut de sécrétion d'ADP dans les plaquettes SERCA3$^{-/-}$ par l'apyrase qui inhibe complètement l'agrégation plaquettaire chez les plaquettes de souris SERCA3$^{-/-}$ et sauvages, et surtout par l'addition d'ADP exogène aux activateurs qui permet de restaurer une agrégation normale dans les plaquettes de souris SERCA3$^{-/-}$ (sans effet additif chez les souris sauvages). De plus, l'addition d'ADP aux activateurs permet de restaurer la sécrétion des granules denses et alpha ainsi que l'activation de l'intégrine $\alpha_{IIb}\beta_3$.

J'ai ensuite montré que l'agrégation par l'ADP était normale dans les plaquettes SERCA3$^{-/-}$ et que le contenu des granules denses était normal (ATP, sérotonine), invalidant la possibilité d'un défaut de stockage granulaire. Ces résultats suggèrent donc que l'absence de SERCA3 affecterait directement la sécrétion d'ADP, essentielle pour l'activation complète des plaquettes. Par ailleurs, lorsque l'activité de SERCA3 est bloquée dans les plaquettes sauvages par l'inhibiteur spécifique tBHQ (10µM), la sécrétion diminue au même niveau que celle de plaquettes SERCA3$^{-/-}$. Par contre l'inhibition de SERCA2b par la thapsigargine (200 nM) n'affecte pas la sécrétion des plaquettes sauvages et la différence de sécrétion reste maintenue avec les plaquettes SERCA3$^{-/-}$. Ces résultats indiquent que c'est l'activité de SERCA3 qui est impliquée spécifiquement dans la régulation de la sécrétion d'ADP indépendamment de l'activité de SERCA2b, et suggèrent donc que ce sont les réserves calciques dépendantes de SERCA3 qui sont importantes fonctionnellement pour la sécrétion d'ADP.

L'absence de SERCA3 ou son inhibition se traduit par un défaut de mobilisation des stocks calciques après stimulation par la thrombine. Ce défaut de mobilisation, dans les 2 cas, est dû au défaut de sécrétion d'ADP, puisque l'apyrase abaisse la mobilisation calcique des plaquettes sauvages au niveau de celui des plaquettes SERCA3$^{-/-}$, et réciproquement l'addition d'ADP exogène à la thrombine élève la mobilisation calcique des plaquettes SERCA3$^{-/-}$ et des plaquettes sauvages traitées avec le tBHQ, au niveau de celui des plaquettes sauvages témoins. Il apparait donc que SERCA3 (contrairement à SERCA2b) contrôle une sécrétion d'ADP, importante pour la mobilisation calcique et l'activation plaquettaire.

Ces résultats nous ont permis de proposer un nouveau mécanisme d'activation plaquettaire où un activateur déclenche une sécrétion rapide d'un stock granulaire d'ADP, sous le contrôle de SERCA3. Cette première vague d'ADP sécrétée viendrait renforcer en synergie la signalisation du premier activateur permettant une mobilisation calcique normale suivie d'une activation de l'intégrine $\alpha_{IIb}\beta_3$ et d'une sécrétion du reste des granules aboutissant à une agrégation normale. Ce travail a fait l'objet de l'article ci-joint (Elaib et coll, 2016, Blood, *Full activation of mouse platelets requires ADP secretion regulated by SERCA3 ATPase-dependent calcium stores. Blood 128, 1129–1138*) et d'un commentaire éditorial (Flaumenhaft, R, 2016 Blood. *SERCAmnavigating calcium signaling in platelets. Blood 128, 1034–1035*.).

Regular Article

blood

PLATELETS AND THROMBOPOIESIS

Full activation of mouse platelets requires ADP secretion regulated by SERCA3 ATPase–dependent calcium stores

Ziane Elaïb,[1] Frédéric Adam,[1] Eliane Berrou,[1] Jean-Claude Bordet,[2,3] Nicolas Prévost,[4] Régis Bobe,[1,*] Marijke Bryckaert,[1,*] and Jean-Philippe Rosa[1,*]

[1]INSERM Unité Mixte de Recherche–Santé 1176, Université Paris-Sud, Université Paris-Saclay, Le Kremlin-Bicêtre, France; [2]Unité d'Hémostase Clinique, Lyon, France; [3]CeCILE-SFR/Centre Commun d'Imagerie de Lyon-Est–Structure Fédérative de Recherche, Université de Lyon, Lyon, France; and [4]Kyoto Gakuen University, Kameoka, Japan

Key Points

- Defect in thrombus formation, platelet aggregation, and ADP secretion induced by ablation or inhibition of SERCA3$^{-/-}$.

The role of the sarco-endoplasmic reticulum calcium (Ca^{2+}) adenosine triphosphatase (ATPase) 3 (SERCA3) in platelet physiology remains poorly understood. Here, we show that SERCA3 knockout (SERCA3$^{-/-}$) mice exhibit prolonged tail bleeding time and rebleeding. Thrombus formation was delayed both in arteries and venules in an in vivo ferric chloride–induced thrombosis model. Defective platelet adhesion and thrombus growth over collagen was confirmed in vitro. Adenosine 5′-diphosphate (ADP) removal by apyrase diminished adhesion and thrombus growth of control platelets to the level of SERCA3$^{-/-}$ platelets. Aggregation, dense granule secretion, and Ca^{2+} mobilization of SERCA3$^{-/-}$ platelets induced by low collagen or low thrombin concentration were weaker than controls. Accordingly, SERCA3$^{-/-}$ platelets exhibited a partial defect in total stored Ca^{2+} and in Ca^{2+} store reuptake following thrombin stimulation. Importantly ADP, but not serotonin, rescued aggregation, secretion, and Ca^{2+} mobilization in SERCA3$^{-/-}$ platelets, suggesting specificity. Dense granules appeared normal upon electron microscopy, mepacrine staining, and total serotonin content, ruling out a dense granule defect. ADP induced normal platelet aggregation, excluding a defect in ADP activation pathways. The SERCA3-specific inhibitor 2,5-di-(*tert*-butyl)-1,4-benzohydroquinone diminished both Ca^{2+} mobilization and secretion of control platelets, as opposed to the SERCA2b inhibitor thapsigargin. This confirmed the specific role of catalytically active SERCA3 in ADP secretion. Accordingly, SERCA3-dependent Ca^{2+} stores appeared depleted in SERCA3$^{-/-}$ platelets. Finally, $\alpha_{IIb}\beta_3$ integrin blockade did not affect SERCA3-dependent secretion, therefore proving independent of $\alpha_{IIb}\beta_3$ engagement. Altogether, these results show that SERCA3-dependent Ca^{2+} stores control a specific ADP secretion pathway required for full platelet secretion induced by agonists at low concentration and independent of $\alpha_{IIb}\beta_3$. (*Blood*. 2016;128(8):1129-1138)

Introduction

Among regulatory mechanisms of Ca^{2+} intracellular signaling in platelets, the sarco-endoplasmic Ca^{2+} adenosine triphosphatases (SERCAs) that pump Ca^{2+} into intracellular stores are particularly relevant.[1] SERCAs are encoded by 3 genes, *ATP2A1*, *ATP2A2*, and *ATP2A3*, which produce several alternate transcripts and protein isoforms: SERCA1a/b, SERCA2a-c, and SERCA3a-f. They are found in multiple tissues, but platelets exhibit only SERCA2b and SERCA3 isoforms.[2-4] SERCAs maintain a Ca^{2+} concentration gradient between the cytosol (100 nM) and the endoplasmic reticulum (1 mM), requiring degradation of adenosine triphosphate (ATP)[5] into adenosine 5′-diphosphate (ADP) then released into the cytosol.[6]

SERCA enzymes share similar structures with distinct intrinsic activities: higher Ca^{2+} affinity for SERCA2b than for SERCA3 ($K_{1/2}$ ~0.27 μM vs 1 μM) but a lower Ca^{2+} uptake (7 nmol/min per mg of protein vs 21 nmol/min per mg)[7,8] allowing cytosolic Ca^{2+} to be maintained at low levels in the resting cells.[9]

Pathologies and mouse models provide insight into SERCA2b and SERCA3 functions. Mutations in the human *ATP2A2* gene affecting SERCA2 lead to Darier syndrome in humans, a dermatological syndrome.[10,11] SERCA mutations are associated with some cancers,[12-14] suggesting involvement in cell differentiation.[15] SERCA3 human mutations seem associated with type 2 diabetes.[16] Mouse SERCA2 knockouts are not viable at the homozygous state, but heterozygotes exhibit SERCA2a-type (defect in heart contractility and relaxation)[17] and SERCA2b-type defects, evocative of Darier syndrome.[18] Mouse SERCA3 knockout (SERCA3$^{-/-}$) mice exhibit no phenotypic alterations,[19] except for an altered gustatory nerve response.[20] Impaired relaxation of SERCA3$^{-/-}$ aorta rings was reported, with defective relaxation of vascular smooth muscle cells, altered Ca^{2+} signaling, and low nitric oxide production.[19] In vitro, low insulin secretion and altered Ca^{2+} oscillations were reported.[21-23] Altogether these results point to a potential specific role for SERCA3 in Ca^{2+} signal modulation.

Among other differences in platelets is a different topology, peripheral for SERCA3, more central for SERCA2b.[24] SERCA3 is specifically associated with acidic Ca^{2+} stores,[25] and with STIM1 (the

Submitted October 28, 2015; accepted June 1, 2016. Prepublished online as *Blood* First Edition paper, June 14, 2016; DOI 10.1182/blood-2015-10-678383.

*R.B., M.B., and J.-P.R. contributed equally to this study.

The online version of this article contains a data supplement.

There is an Inside *Blood* Commentary on this article in this issue.

The publication costs of this article were defrayed in part by page charge payment. Therefore, and solely to indicate this fact, this article is hereby marked "advertisement" in accordance with 18 USC section 1734.

Ca^{2+} sensor of the store operated Ca^{2+} entry [SOCE]).[26] To assess the role of SERCA3 in platelets, we have decided to assess the hemostasis status of SERCA3$^{-/-}$ mice. Here, we report the analysis of both in vivo and in vitro hemostasis features of SERCA3$^{-/-}$ mice and show that ablation of SERCA3 lowers in vivo hemostatic and thrombotic responses, as well as platelet adhesive and secretory functions in vitro. Moreover, we find that thrombin or collagen activation is affected because of low dense granule secretion. Importantly, mobilization and secretion are rescued by ADP addition, consistent with a role for SERCA3 in ADP secretion. Confirming a specific role for SERCA3, pharmacological inhibition of SERCA3, but not of SERCA2b, in control platelets recapitulates the same defect in secretion in vitro, definitely pointing to SERCA3 as specifically involved in the regulation of such a secretion. Finally, SERCA3-dependent secretion appears independent of $\alpha_{IIb}\beta_3$ integrin engagement. These results thus point to an as yet unreported role of SERCA3 in hemostasis and in positive regulation of platelet dense granule and ADP secretion.

Materials and methods

Material

Fibrillar collagen (equine type I) and ADP were obtained from Kordia (Leiden, The Netherlands). Apyrase (grade 7), rhodamine 6G, bovine thrombin, ferric chloride, indomethacin, and the SERCA inhibitors thapsigargin (Tg) and 2,5-di-(*tert*-butyl)-1,4-benzohydroquinone (tBHQ) were obtained from Sigma (St. Louis, MO). We purchased D-Phe-Pro-Arg chloromethylketone dihydrochloride from Calbiochem-VWR (Fontenay-sous-Bois, France). The protease-activated receptor (PAR) agonist peptide (PAR4-AP; AYPGKF-NH_2) was purchased from Bachem (Weil am Rheim, Germany). Mepacrine (quinacrine dihydrochloride) was from Sigma-Aldrich (St. Louis, MO). Alexa Fluor 488-labeled phalloidin was from Invitrogen (Cergy Pontoise, France). Phycoerythrin-labeled rat anti-mouse integrin $\alpha_{IIb}\beta_3$ monoclonal antibody (mAb; JON/A), fluorescein isothiocyanate–labeled rat anti-mouse CD62P (P-selectin) mAb (Wug.E9) and purified rat anti-mouse integrin $\alpha_{IIb}\beta_3$ mAb (Leo.H4) were from Emfret Analytics (Würzburg, Germany). Oregon Green 488 BAPTA1-AM was from Molecular Probes (Eugene, OR). Polyclonal antibodies specific for SERCA2b[27] and for SERCA3 (N89)[28] were generous gifts from F. Wuytack (Katholieke Universiteit Leuven, Leuven, Belgium). The antibody directed against 14-3-3ζ, was obtained from Santa Cruz Biotechnology (Santa Cruz, CA). Phospho-(Ser) protein kinase C substrate antibody was from Cell Signaling Technology (Danvers, MA).

SERCA3$^{-/-}$ mice. The Black Swiss SERCA3$^{-/-}$ mice originally generated by G. E. Shull (University of Cincinnati, OH)[19] were crossed with C57BL/6 mice and kindly provided by P. Gilon (University of Louvain, Belgium) with the authorization of G. E. Shull. Wild-type (WT) littermate mice were provided as well and served as controls. Transferred wt/- heterozygous mice were intercrossed and homozygotes were detected by polymerase chain reaction, using published oligonucleotide primers.[19] All experimental procedures were carried out in accordance with the European legislation concerning the use of laboratory animals and approved by the Animal Care and Ethical Committee of Université Paris-Sud (agreement #00243-02).

Hematologic analysis and bleeding time. Blood counts were determined with an automatic cell counter (scil Vet abc Plus; Horiba Medical, France). Bleeding time assays were performed as previously described,[29] on 8- to 12-week-old mice.

Measurement of intracellular calcium. Mouse platelets (3×10^7 platelets per mL) were loaded with the Ca^{2+}-sensitive dye Oregon Green 488 BAPTA1-AM (1 mM) for 45 minutes at 20°C. Ca^{2+} mobilization induced by thrombin was analyzed in Ca^{2+} free medium and in the presence of 0.5 mM EGTA using an Accuri C6 flow cytometer. Changes in Ca^{2+} signal intensity were calculated as the ratios of fluorescence of activated over nonactivated platelets and the area below the curve for 2 minutes after agonist addition was chosen as an indicator of the calcium response. Fluorescence calibration in nanomolar Ca^{2+} was established as described in the supplemental Methods (available on the *Blood* Web site).

In vitro thrombus formation under flow conditions. Thrombus formation was evaluated in a whole blood perfusion assay on a fibrillar collagen matrix (50 μg/mL) at various shear rates (150 s^{-1} and 1200 s^{-1}) and recorded and analyzed as previously described.[29] Thrombus formation was evaluated by assessment of platelet adhesion quantitated by measurement of the mean percentage of the total area covered by thrombi.

Ferric chloride–induced thrombosis model. Ferric chloride ($FeCl_3$) injury was induced in 4- to 5-week-old mice, as previously described.[30] Briefly, rhodamine 6G (3.3 mg/kg) was injected into the retro-orbital plexus of anesthetized mice (to label platelets). After topical deposition on the mesenteric vessels of $FeCl_3$ solution (10%), thrombus growth was monitored in real-time with an inverted epifluorescent microscope (×10) (Nikon Eclipse TE2000-U).

Serotonin assay. Platelet serotonin (5HT) was assessed using the Serotonin Enzyme-Linked Immunosorbent Assay Kit from Abcam (Cambridge, UK). The 5HT was assayed in platelets supernatants or in platelet lysate (after 4 freeze-thaw cycles) to determine platelet total 5HT content.

Statistical analysis. Statistical significance was evaluated with the Student *t* tests or 1-way analysis of variance (ANOVA) followed by the Tukey pairwise test as indicated, using GraphPad Prism (San Diego, CA).

Results

Prolonged bleeding time and delayed in vivo thrombosis in SERCA3$^{-/-}$ mice

We first confirmed in our mouse colony the deletion of *Atp2a3*, the mouse *SERCA3* gene, by polymerase chain reaction (data not shown) and the absence of the SERCA3 protein in platelets by western blotting (Figure 1A). Note that platelet SERCA2b is expressed at the same level as controls. The tail clipping bleeding time assay was found significantly increased in SERCA3$^{-/-}$ vs WT mice (142 ± 12 s for SERCA3$^{-/-}$ mice vs 67 ± 5 s for controls, $P < .001$; Figure 1B). Moreover, a marked rebleeding tendency was noted with 75% rebleeding within 1 minute of bleeding arrest vs 10% for controls (Figure 1C). Platelets were normal morphologically (Figure 1D), slightly larger in size (5.82 ± 0.08 compared with 4.99 ± 0.04 fL; Table 1), and in slightly lower numbers than controls (average 778.2 ± 0.31 × 10^9/L vs 914.5 ± 0.33 × 10^9/L, n = 21 and 18, respectively; Table 1), not low enough to explain the prolonged bleeding time. Other blood cell counts were normal.

Ferric chloride-induction of thrombosis in mesenteric vessels showed delayed thrombus formation (often no occlusion at 60 minutes) in both venules and arterioles of SERCA3$^{-/-}$ mice compared with controls (30 minutes occlusion time for controls; Figure 1E-F). Thrombus instability in SERCA3$^{-/-}$ mice was frequent with 3 times more venule or arteriole emboli than in controls (Figure 1G). These results indicate that SERCA3 ablation affects hemostasis, thrombus formation, and stability in vivo.

Evidence for an ADP secretion defect of SERCA3$^{-/-}$ platelets in in vitro flow adhesion and aggregation

To confirm a platelet defect, we next assessed adhesion and thrombus formation of SERCA3$^{-/-}$ platelets on a collagen matrix in both low (150 s^{-1}; Figure 2A-B) and high (1200 s^{-1}; Figure 2C-D) shear conditions, which were both significantly lower in SERCA3$^{-/-}$ platelets compared with controls. Adhesion and thrombus size (in both low and high shear conditions) of control platelets was diminished to the level of SERCA3$^{-/-}$ platelets after secretion inhibition by apyrase and indomethacin. Altogether these results indicate that SERCA3 ablation affected platelets, most likely through alteration of ADP secretion.

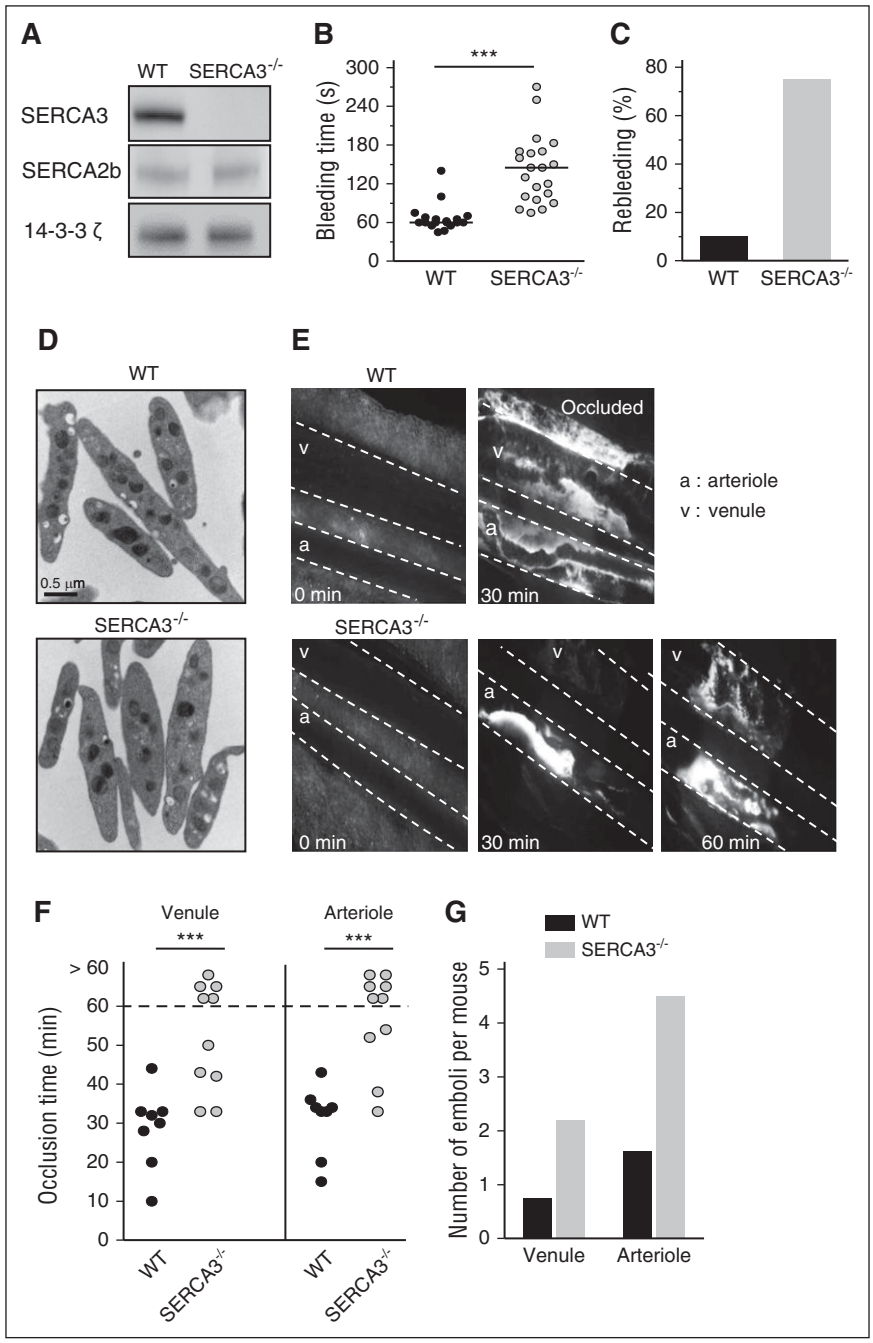

Figure 1. Characterization of hemostasis and in vivo thrombosis in SERCA3$^{-/-}$ mice. (A) Western blot of SERCAs in mouse platelets. Control (WT) and SERCA3$^{-/-}$ mouse platelets were collected and solubilized and subjected to sodium dodecyl sulfate polyacrylamide gel electrophoresis, prior to transfer to nitrocellulose and detection by antibodies specific for SERCA3 or SERCA2b.[28] After addition of a secondary antibody coupled to horse radish peroxidase, bands were revealed by chemiluminescence. The 14-3-3ζ adaptor was used as an internal standard for normalization. Note the absence of SERCA3 in SERCA3$^{-/-}$ platelets and the same levels of SERCA2b in both control and SERCA3$^{-/-}$ platelets. (B) Tail bleeding time. Tail bleeding was performed as indicated in "Materials and methods," and bleeding time assessed both on control (WT) and SERCA3$^{-/-}$ mice. Results are presented as mean ± SEM, using the Student *t* test; ***$P < .001$. (C) Rebleeding was assessed for 1 minute following initial bleeding arrest. A total of 18 control and 21 SERCA3$^{-/-}$ mice were used. (D) Transmission electron microscopy of resting control and SERCA3$^{-/-}$ platelets. Platelets were subjected to standard transmission electron microscopy. Upper panel, control (WT); lower panel, SERCA3$^{-/-}$ platelets. The scale bar (0.5 μm) is shown in the lower left corner of the WT panel. (E) Kinetics of in vivo ferric chloride-induced thrombosis of mesenteric vessels. Venules (v) or arterioles (a) are shown by fluorescence microscopy (limits outlined with white dashed lines), thrombi being visualized by rhodamine 6G–labeled platelets. Images at 0, 30, and 60 minutes are shown. (F) Quantification of thrombus formation. Time to occlusion was noted for 18 control (WT, closed circles) and 21 SERCA3$^{-/-}$ (open circles) mice up to 60 minutes, the maximal time assessed. Results were analyzed using 1-way ANOVA followed by Tukey's multiple comparison test; ***$P < .001$. (G) Quantification of emboli. The number of emboli shedding from thrombi was assessed for 60 minutes, both in venules and arterioles of control and SERCA3$^{-/-}$ mice.

Confirming platelet involvement, aggregation of SERCA3$^{-/-}$ platelets was impaired, when induced by low levels of collagen (0.8 μg/mL) (Figure 3A), thrombin (40 mU/mL) (Figure 3B), or PAR4-AP peptide (activator peptide of the PAR-4 thrombin receptor, a G-protein coupled receptor) (supplemental Figure 2A). Higher doses of agonist essentially normalized aggregation levels. ADP scavenging by apyrase abolished aggregation responses of both control and SERCA3$^{-/-}$ platelets (Figure 3C; supplemental Figure 2B). This strengthened the hypothesis of an ADP secretion defect in SERCA3$^{-/-}$ platelets. Moreover aggregation of SERCA3$^{-/-}$ platelets was rescued by 10 μM ADP (not promoting aggregation alone in absence of added fibrinogen, not shown) addition to either collagen or thrombin (Figure 3D).

Secretion of the ADP storage organelles dense granules, as monitored by ATP release during aggregation appeared strongly diminished in SERCA3$^{-/-}$ compared with control platelets (Figure 4A-B; supplemental Figure 2C). Confirming a dense granule secretion defect, serotonin (5HT) release was also markedly altered in SERCA3$^{-/-}$ platelets (supplemental Figure 3C). Conversely, dense granule secretion was almost completely rescued by addition of 10 μM ADP, as assessed by ATP or 5HT secretion (Figure 4A; supplemental Figure 3C, respectively). ADP alone (Figure 4A-B) did not elicit dense granule secretion in control or SERCA3$^{-/-}$ platelets. Thus, SERCA3$^{-/-}$ platelets exhibit a defect because of alteration of dense granule secretion.

P-selectin exposure of stimulated SERCA3$^{-/-}$ platelets (Figure 4C; supplemental Figure 2E) was significantly diminished compared with control platelets. Not shown, a defect in P-selectin exposure was also observed in convulxin-stimulated SERCA3$^{-/-}$ unstirred platelets.

Table 1. Blood cell analysis of SERCA3$^{-/-}$ mice

	WT	SERCA3$^{-/-}$
Leukocytes (10^9/L)	5.63 ± 0.30	6.35 ± 0.33
Red blood cells (10^{12}/L)	10.84 ± 0.16	10.33 ± 0.25
Hematocrit (%)	48.24 ± 0.7	44.57 ± 1.15
Platelets (10^9/L)	914.5 ± 0.33	778.2 ± 0.31
MPV (fL)	4.99 ± 0.04	5.82 ± 0.08

Cell counts in whole blood were determined by an automated cell counter (see "Materials and methods"), and values are expressed as means ± standard error of the mean (SEM). Units are shown in parentheses.

MPV, mean platelet volume.

Apyrase treatment nearly suppressed P-selectin exposure of control and SERCA3$^{-/-}$ platelets, stimulated with low thrombin concentration, whereas ADP addition to thrombin restored normal P-selectin exposure on SERCA3$^{-/-}$ platelets (Figure 4C). This indicated that α-granule exocytosis is likely to be secondary to ADP secretion and thus only indirectly dependent on SERCA3.

Finally, aggregation to ADP of SERCA3$^{-/-}$ platelets (in platelet-rich plasma, to provide fibrinogen), was normal compared with control (Figure 5C). Thus, SERCA3$^{-/-}$ ablation does not affect platelet activation by ADP but specifically acts on ADP secretion.

Dense granule content is not affected in SERCA3$^{-/-}$ platelets

To check that defective secretion was not because of a dense granule defect, platelets were labeled with the fluorescent reporter mepacrine, which accumulates specifically in dense granules.[31] Flow cytometry showed that mepacrine was stored to the same extent in control and SERCA3$^{-/-}$ platelets (supplemental Figure 3A), strongly suggesting a normal content in dense granules. In addition ATP release after maximal platelet stimulation (thrombin 2 U/mL) of SERCA3$^{-/-}$ platelets reached ~70% of controls (supplemental Figure 3B), but reached 100% ATP secretion compared with control platelets upon ADP addition to thrombin. Most significantly, total 5HT content was identical between control and SERCA3$^{-/-}$ platelets (supplemental Figure 3C).

Thus, the dense granule secretion defect observed in SERCA3$^{-/-}$ platelets is not because of a defect in number or content.

5HT does not restore the functional defect of SERCA3$^{-/-}$ platelets

To test whether rescue is specific for ADP, and may not be induced just by any weak agonist, we analyzed aggregation and secretion rescue induced by 5HT (another weak agonist and dense granule cargo). At concentrations within the same range as ADP, 5HT did not induce aggregation (supplemental Figure 3D), nor did it rescue aggregation (supplemental Figure 3E), ATP secretion (supplemental Figure 3F), $\alpha_{IIb}\beta_3$ activation, or P-selectin exposure (data not shown) elicited by 40 mU/mL thrombin. These data, together with the defects induced by apyrase (flow adhesion, platelet aggregation, and secretion) in control platelets, confirm that ADP is most likely the only agonist involved in SERCA3$^{-/-}$ platelet defect.

SERCA3 ablation alters ADP-dependent $\alpha_{IIb}\beta_3$ activation

Platelet secretion is elicited by agonist-induced receptor activation and $\alpha_{IIb}\beta_3$ integrin engagement (outside-in signaling). To examine a potential link between SERCA3-dependent ADP secretion and $\alpha_{IIb}\beta_3$, SERCA3$^{-/-}$ platelets were activated by thrombin in the presence of the mAb JON/A, specific for the active form of mouse $\alpha_{IIb}\beta_3$,[32] and analyzed by flow cytometry. SERCA3$^{-/-}$ platelets exhibited lower

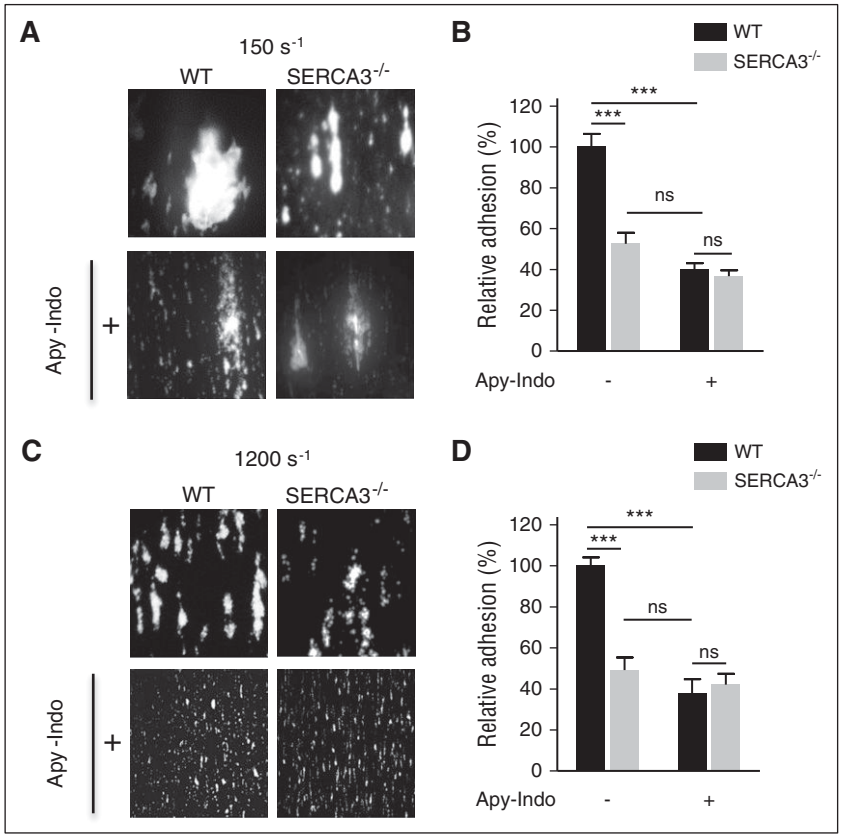

Figure 2. In vitro thrombus formation of SERCA3$^{-/-}$ platelets compared with controls. Rhodamine 6G–labeled platelets were injected into capillaries precoated with collagen (50 μg/mL) at low (150 s^{-1}; A) or at high (1200 s^{-1}; C) shear rates in absence or in presence of both apyrase (5 U/mL) and indomethacin (5 μM), noted "Apy-Indo." Images show platelet adhesion and thrombus formation after 3 minutes of perfusion, and plots (B, D) represent the quantification of platelet adhesion, expressed as covered surface area relative to controls given as 100%. Absence or presence of Apy-Indo is noted "-" or "+" below plots. Data were calculated using 1-way ANOVA followed by Tukey's multiple comparison test; ns, not significant; ***$P < .001$.

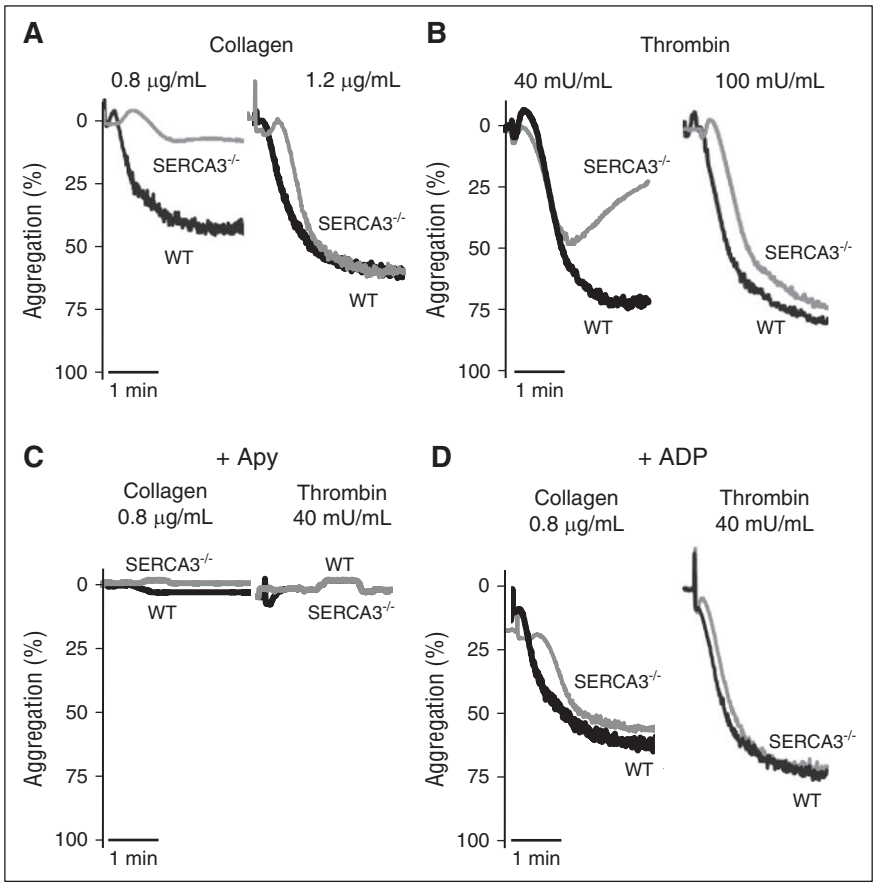

Figure 3. Aggregation of washed platelets from control or SERCA3$^{-/-}$ mice. Washed platelets from controls (WT, black line) or SERCA3$^{-/-}$ (gray line) mice were stimulated with collagen (A; 0.8 or 1.2 μg/mL) or with thrombin (B; 40 and 100 mU/mL) and recorded for aggregation for 3 minutes. Aggregation intensities are expressed as percent of light transmitted, 100% corresponding to buffer alone. Note the low aggregation rate of SERCA3$^{-/-}$ platelets at 0.8 μg/mL of collagen and 40 mU/mL thrombin. These tracings are representative of 5 experiments. (C) Aggregation induced by collagen (0.8 μg/mL) or thrombin (40 mU/mL) of control (WT) and SERCA3$^{-/-}$ platelets was carried out in the presence of apyrase (5 U/mL, noted "Apy"). (D) Aggregation rescue was conducted on control and SERCA3$^{-/-}$ washed platelets by addition of 10 μM ADP following stimulation by either collagen (0.8 μg/mL) or thrombin (40 mU/mL). These tracings are representative of 3 experiments.

$\alpha_{IIb}\beta_3$ activation [but normal total level (supplemental Figure 1)] than controls (Figure 5A). ADP scavenging by apyrase almost completely abrogated $\alpha_{IIb}\beta_3$ activation in both control and SERCA3$^{-/-}$ platelets (Figure 5A). Conversely, addition of ADP rescued $\alpha_{IIb}\beta_3$ activation in both cases, confirming that the lower activation level of $\alpha_{IIb}\beta_3$ in SERCA3$^{-/-}$ platelets is because of reduced ADP secretion. Blockade of $\alpha_{IIb}\beta_3$ by the antibody Leo. H4,[33] which prevents $\alpha_{IIb}\beta_3$ engagement, reduced secretion equally in both control and SERCA3$^{-/-}$ platelets, corresponding to $\alpha_{IIb}\beta_3$-dependent secretion, but the difference in secretion remained unchanged (Figure 5B). Importantly, ADP addition rescued secretion in SERCA3$^{-/-}$ platelets (unchanged in control platelets) despite $\alpha_{IIb}\beta_3$ blockade. Thus, the altered secretion in SERCA3$^{-/-}$ platelets is $\alpha_{IIb}\beta_3$ independent.

SERCA3 ablation or inhibition alters Ca^{2+} signaling and dense granule secretion

SERCA3 and SERCA2b[34] regulate Ca^{2+} mobilization from intracellular stores, essential to platelet activation and secretion.[35] Flow cytometry of unstirred Oregon Green BAPTA1-AM loaded platelets preincubated with EGTA (no extracellular Ca^{2+} to avoid Ca^{2+} influx) and stimulated with thrombin showed a lower Ca^{2+} mobilization (50%, as measured by the area below the curve for 2 minutes) in SERCA3$^{-/-}$ platelets compared with controls, at 40 mU/mL (Figure 6A,E, left panels), but not at 100 mU/mL (supplemental Figure 4A). Ca^{2+} influx induced by extracellular Ca^{2+} (1 mM) was stronger in SERCA3$^{-/-}$ (30% to 40% increase as assessed by areas under curves) than control platelets (Figure 6A-B,E; supplemental Figure 4A). Interestingly, stimulation of SERCA3$^{-/-}$ platelets with thrombin in the presence of extracellular Ca^{2+} showed a similar fluorescence increase compared with control platelets, suggesting compensation of low Ca^{2+} mobilization by high Ca^{2+} influx (Figure 6A, right panel). Importantly, in the presence of apyrase, Ca^{2+} mobilization of control platelets at 40 mU/mL of thrombin was lowered to the level of SERCA3$^{-/-}$ platelets, unaffected by ADP scavenging (Figure 6B,E). Conversely, addition of ADP to thrombin raised Ca^{2+} mobilization in SERCA3$^{-/-}$ platelets to the level of control platelets (Figure 6B,E). In contrast, Ca^{2+} influx remained unaffected by apyrase pretreatment or after addition of ADP, for both control and SERCA3$^{-/-}$ platelets (Figure 6B,E), suggesting that contrary to mobilization, influx is independent of ADP. These results are thus consistent with SERCA3-dependent Ca^{2+} mobilization in low agonist conditions being secondary to secreted ADP.

To confirm the role of SERCA3 and its catalytic activity, platelets were challenged with tBHQ specific for SERCA3.[3] In control platelets, 10 μM tBHQ (specific for SERCA3, because inducing Ca^{2+} mobilization in control but not in SERCA3$^{-/-}$ platelets; supplemental Figure 4C) lowered thrombin-induced Ca^{2+} mobilization (Figure 6C) comparatively to control (Figure 6A). Ratios of areas under curves of WT over SERCA3$^{-/-}$ Ca^{2+} mobilization dropped from 2 in absence of tBHQ to 1 in the presence of the antagonist. tBHQ elicited partial inhibition of thrombin-induced aggregation (Figure 6F) and secretion (Figure 6G) of SERCA3$^{-/-}$ platelets, which were both rescued by ADP. In contrast, specific inhibition of SERCA2b with 200 nM Tg (supplemental Figure 5A) partially inhibited thrombin-induced Ca^{2+} mobilization in control

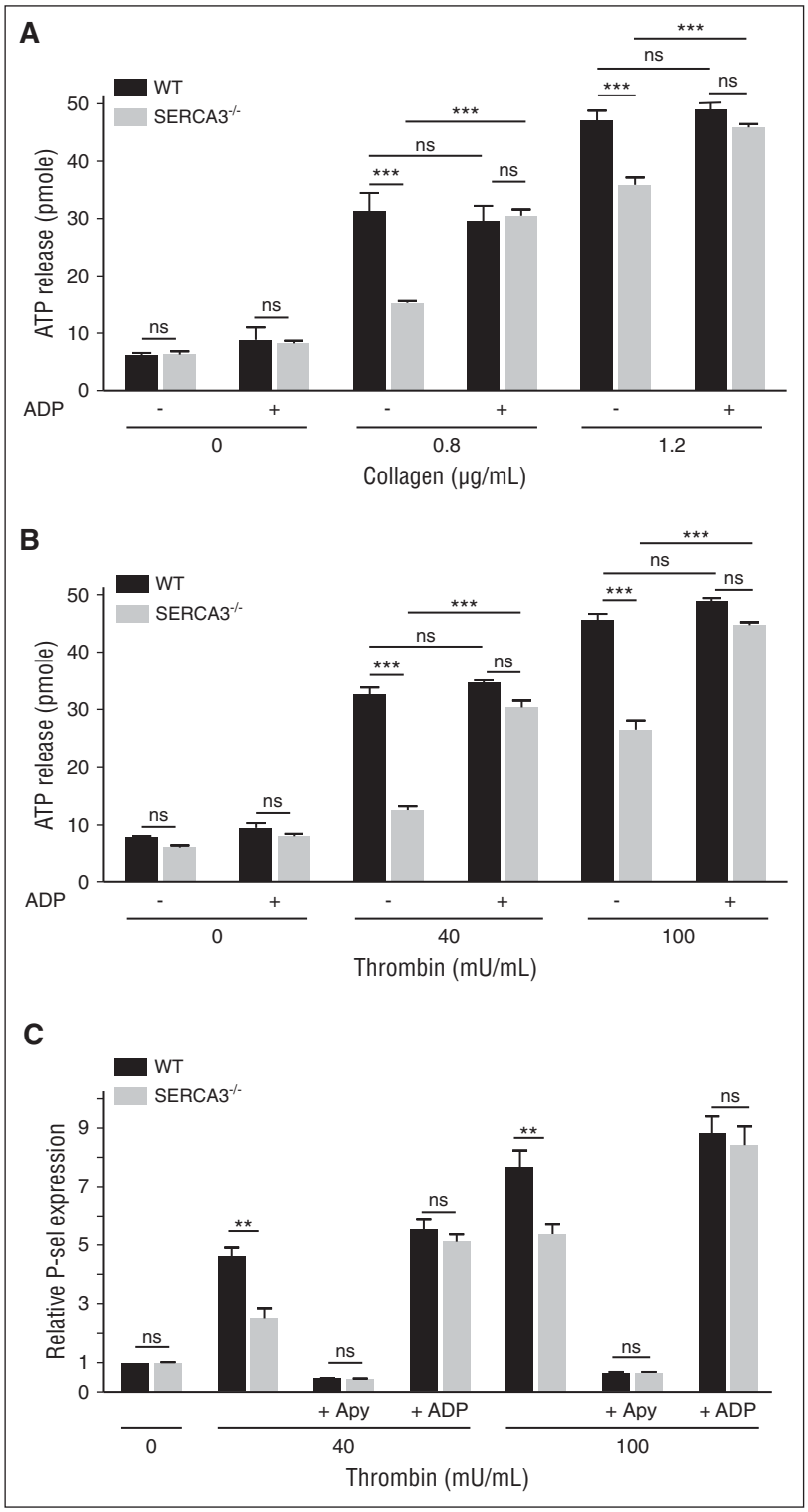

Figure 4. Platelet secretion of washed platelets from control or SERCA3$^{-/-}$ mice. Dense granule secretion from platelets aggregated in the presence of collagen (A; 0.8 or 1.2 μg/mL) or thrombin (B; 40 or 100 mU/mL), with the addition (+) or not (-) of 10 μM ADP, was assessed by measuring ATP release in picomoles (calculated for 10^7 platelets) in control (WT, black bars) and SERCA3$^{-/-}$ (gray bars) platelets. A total of 3 experiments were conducted and presented as mean ± SEM, using 1-way ANOVA followed by Tukey's multiple comparison test; ns, not significant; ***$P < .001$. (C) The expression of the α-granule membrane marker P-selectin following thrombin platelet stimulation was assessed by flow cytometry on control (black bars) or SERCA3$^{-/-}$ (gray bars) platelets. The same experiment was conducted in the presence of apyrase (5 U/mL, noted "+ Apy") or added ADP (10 μM, noted "+ ADP") on control (WT, black bars) or SERCA3$^{-/-}$ (gray bars) platelets. Data presented are the means of 3 separate experiments in duplicates, as means ± SEM, as assessed by 1-way ANOVA followed by Tukey's multiple comparison test; ns, not significant; **$P < .01$.

platelets (presumably leaving SERCA3-dependent Ca^{2+} stores unaffected) but completely inhibited mobilization in SERCA3$^{-/-}$ platelets, indicating complete inhibition of SERCA2b (Figure 6D). Importantly, specific inhibition of SERCA2b did not affect ATP release, contrary to tBHQ-mediated SERCA3 inhibition (Figure 6G). Altogether these results thus demonstrate that catalytically active SERCA3, and not SERCA2b, is involved in dense granule secretion, through its Ca^{2+} pump activity and SERCA3-dependent Ca^{2+} stores.

Ca^{2+} stores are defective in SERCA3$^{-/-}$ platelets

SERCA3 depletion is expected to lead to depletion of SERCA3-dependent Ca^{2+} stores and hence to altered Ca^{2+} mobilization.

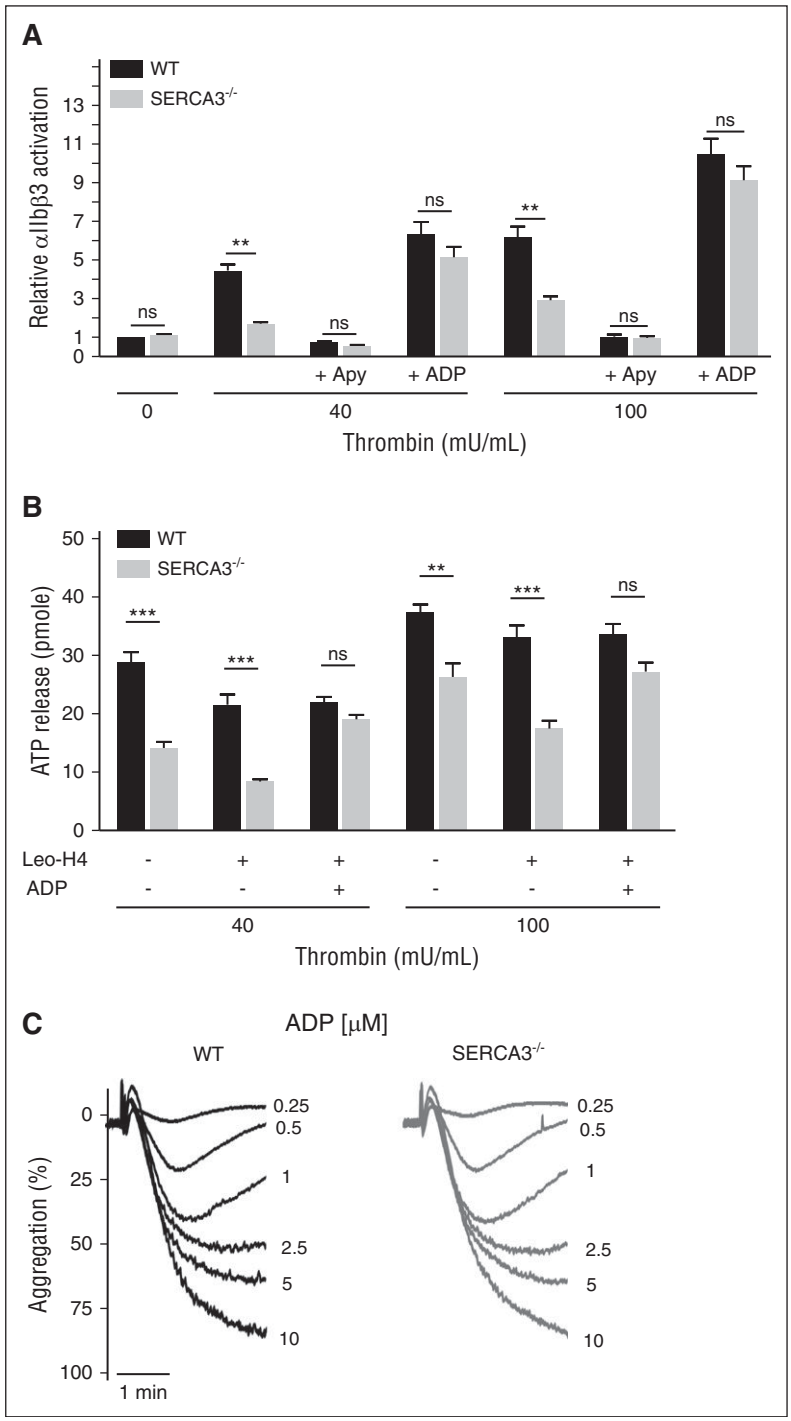

Figure 5. Assessment of $\alpha_{IIb}\beta_3$ activation and engagement in washed platelets from control or SERCA3$^{-/-}$ mice and aggregation to ADP. (A) Quantitation of activated $\alpha_{IIb}\beta_3$ integrin at the surface of washed platelets was assessed by flow cytometry by binding of the specific mAb JON/A to control (black bars) or SERCA3$^{-/-}$ (gray bars) platelets upon activation with thrombin at 40 or 100 mU/mL. The same experiments were conducted in the presence of 5 U/mL apyrase (noted "+ Apy") or after addition of 10 μM ADP ("+ ADP"). Statistical significance was established with 1-way ANOVA followed by Tukey's multiple comparison test; ns, not significant; $^{**}P < .01$. (B) Assessment of the role of $\alpha_{IIb}\beta_3$ engagement in dense granule secretion in SERCA3$^{-/-}$ platelets. Platelets stimulated with either 40 or 100 mU/mL of thrombin were subjected to aggregation, in the absence (-) or the presence (+) of the blocking mAb Leo.H4 (20 μg/mL) specific for mouse $\alpha_{IIb}\beta_3$, as well as in the absence (-) or the presence (+) of 10 μM ADP. Secretion was assessed by ATP measurement in the supernatant. Using WT as control, statistical significance was established with 1-way ANOVA followed by Tukey's multiple comparison test; ns, not significant; $^{**}P < .01$; $^{***}P < .001$. (C) Aggregation to ADP was assessed at 0.25, 0.5, 1, 2.5, 5, and 10 μM in control (WT) or SERCA3$^{-/-}$ platelet-rich plasma.

Platelets were subjected to ionomycin, which permeabilizes inner membranes and empties Ca^{2+} stores, and to Tg at high concentration (1 μM) to prevent Ca^{2+} store reuptake by both SERCA3 and SERCA2b (supplemental Figure 4B). SERCA3$^{-/-}$ platelets exhibited a weaker cytosolic Ca^{2+} release signal than control platelets (0.65 relative ratio assessed by areas under the curves) consistent with partially depleted Ca^{2+} stores in SERCA3$^{-/-}$ platelets. Conversely, Ca^{2+} reuptake was assessed in control and SERCA3$^{-/-}$ platelets by Ca^{2+} mobilization triggered by thrombin, followed after 3 minutes of stimulation (allowing Ca^{2+} store refilling) by Tg (1 μM, inhibiting both SERCAs) to let stored Ca^{2+} "leak" into the cytosol (supplemental Figure 5C). Tg triggered significantly less Ca^{2+} release in SERCA3$^{-/-}$ platelets than in control platelets, consistent with less efficient Ca^{2+} reuptake in SERCA3$^{-/-}$ platelets than in controls, underlining the functional relevance of SERCA3. Both the lower levels of Ca^{2+} store release and the low Ca^{2+} store reuptake in SERCA3$^{-/-}$ platelets strongly suggest that SERCA3-dependent Ca^{2+} stores are involved, at least in part, in dense granule secretion.

Discussion

We have analyzed SERCA3$^{-/-}$ mice and found a significant prolonged bleeding time and defective thrombosis in vivo. Functional assessment

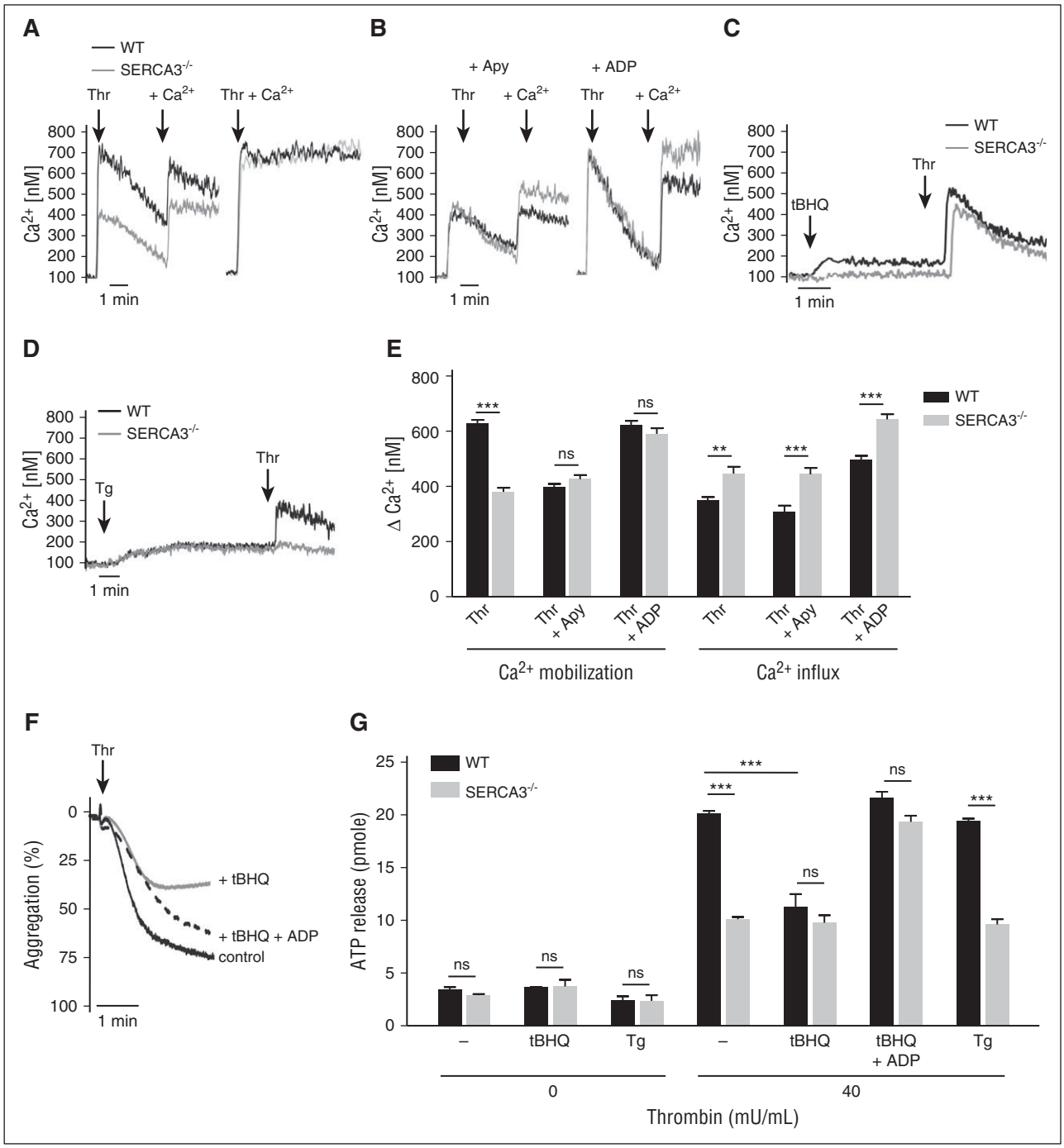

Figure 6. Effect of SERCA3 deletion or pharmacological inhibition on Ca^{2+} mobilization, Ca^{2+} influx, aggregation, and secretion in washed platelets. (A) Ca^{2+} mobilization was assessed in unstirred control (WT, black tracings) and SERCA3$^{-/-}$ (gray tracings) platelets preincubated with the cytosolic Ca^{2+} fluorescent probe Oregon Green BAPTA-AM after stimulation with 40 mU/mL thrombin ("Thr") by flow cytometry in conditions of no external Ca^{2+} (1 mM EGTA). Ca^{2+} influx was assessed after 4 minutes by addition of 1 mM $CaCl_2$ ("Ca^{2+}"). Global Ca^{2+} signaling was also assessed by addition of 1 mM Ca^{2+} together with thrombin ("Thr + Ca^{2+}") (right tracing). Data are expressed as nM Ca^{2+}, as calculated from calibration experiments (see supplemental Methods). (B) Ca^{2+} mobilization was assessed in the same conditions as in panel A, but in the presence of apyrase (5 U/mL) ("+ Apy") or ADP (1 μM) ("+ ADP"). (C) Ca^{2+} mobilization by 40 mU/mL thrombin was assessed after preincubation with the SERCA3-specific inhibitor tBHQ (C; 10 μM) or with Tg (D) at a concentration affecting only SERCA2b (200 nM; see supplemental Figure 5A). (E) Maximal Ca^{2+} mobilization and Ca^{2+} influx from experiments in panel A (stimulation with 40 mU/mL thrombin in the presence of 100 μM EGTA and Ca^{2+} influx after $CaCl_2$ [300 μM] addition) and in panel B (same as in panel A, but in the presence of 5 U/mL apyrase [Thr + Apy] or of 10 μM ADP [Thr + ADP]). Values were calculated after subtraction of unstimulated Ca^{2+} level (ΔCa^{2+} nM). Data presented are means ± SEM, n = 3, using 1-way ANOVA followed by Tukey's multiple comparison test: ns, not significant; $^{**}P < .01$; $^{***}P < .001$. (F) Washed control platelets were preincubated with dimethyl sulfoxide (control) or tBHQ 10 μM (tBHQ) or tBHQ and ADP (10 μM each) for 4 minutes prior to addition of 40 mU/mL thrombin (Thr). (G) Washed control (WT, black bars) or SERCA3$^{-/-}$ (gray bars) platelets were preincubated with either buffer alone "-", tBHQ (10 μM), or Tg (200 nM), and then either buffer ("0"), thrombin 40 mU/mL, or thrombin and 10 μM ADP ("+ ADP") and incubated further for 3 minutes. ATP secretion was then measured in supernatants. Data presented are means ± SEM, n = 3, using 1-way ANOVA followed by Tukey's multiple comparison test: ns, not significant; $^{***}P < .001$.

of SERCA3$^{-/-}$ platelets in vitro has confirmed a defect in adhesion, thrombus formation over collagen, and aggregation elicited by either collagen or thrombin. This indicated that platelets were directly affected by SERCA3 ablation, and that the defect was independent of the stimulus pathway. Most importantly, we found that the defect could be tracked down to a markedly reduced secretion as assessed by ATP measurement and, thus, presumably reduced dense granule exocytosis. Importantly all affected functions in platelet SERCA3$^{-/-}$, including adhesion under flow, aggregation, and secretion, were reversed by exogenous ADP, adding more support to the idea that ablation of SERCA3 leads to an ADP secretion defect. Experiments conducted with 5HT showed that (1) this weak agonist also stored in dense granules is defective to the same extent as ATP, confirming that the defect lies in the release mechanism of dense granules; (2) like ATP, it reaches normal secretion when ADP is added to thrombin; but (3) unlike ADP, it is unable to restore normal aggregation or secretion of SERCA3$^{-/-}$ platelets upon thrombin stimulation. This strengthens the hypothesis that SERCA3 depletion does affect release of a fraction of dense granules, and that this release is specifically dependent upon ADP costimulation, and not costimulation by just any weak agonist.

In addition, this SERCA3-dependent secretion is independent of $\alpha_{IIb}\beta_3$ engagement and only dependent on primary platelet activation. Importantly, aggregation to ADP of SERCA3$^{-/-}$ platelets was normal indicating that ADP-dependent activation pathways of platelets were not altered by SERCA3 ablation. Our results indicate also that SERCA3 ablation does not affect dense granules, as evidenced by normal mepacrine content, normal serotonin content, or electron microscopy imaging. It follows that SERCA3 ablation is responsible for alteration of dense granule secretory rather than storage pathways.

Importantly, pharmacological inhibition of SERCA3 but not of SERCA2b recapitulated the ADP secretory defect of SERCA3 genetic ablation, clearly showing a specific role for SERCA3 in secretion. Moreover, this demonstrates that SERCA3 catalytic activity is required for secretion, pointing to SERCA3-dependent Ca^{2+} storage and/or signaling as involved in secretion regulation. Of note, when platelets were maximally stimulated with 2 U/mL thrombin, SERCA3$^{-/-}$ platelets still exhibited a significant differential secretion compared with controls, whether assessed by ATP or 5HT release (supplemental Figure 3B-C, respectively), only compensated for by added ADP. This secretion resistance to strong stimulation argues in favor of a pool of dense granules present but not releasable in SERCA3-deleted platelets. This would thus be consistent with 2 physically and/or functionally separate ADP secretory pathways, possibly corresponding to distinct populations of dense granules and/or to different exocytosis pathways, 1 involving SERCA3 (and its Ca^{2+} stores) and not the other. An attractive hypothesis could be that this subpopulation of dense granules corresponds to SERCA3-dependent Ca^{2+}-stores, explaining the link between ADP release and SERCA3. However, we found no colocalization between SERCA3 and dense granules by confocal microscopy (data not shown): we conclude that SERCA3-dependent Ca^{2+} stores are distinct from dense granules but regulate exocytosis of a subpopulation of dense granules, for example proximal to the plasma membrane, allowing early release of ADP.

We noted that α-granule secretion, in absence of $\alpha_{IIb}\beta_3$ engagement, is almost completely dependent on ADP release. This is consistent with an earlier report showing that dense granules are mobilized earlier than α-granules[36] and with 2 recent reports showing that mouse models of Hermansky-Pudlak syndrome, which are defective in dense granules, exhibit, upon low agonist stimulation or laser-induced injury in vivo, a defect in α-granule (and lysosome) secretion secondary to the lack of ADP secretion.[37,38] Moreover, their observations of an autocrine ADP secretion[39] are consistent with our contention that ADP secretion (here SERCA3-dependent) reinforces platelet activation by other agonists.

Interestingly, there was an increased level of SOCE in SERCA3$^{-/-}$ platelets, apparently compensating for the low level of Ca^{2+} mobilization (such that the overall Ca^{2+} cytosolic rise upon agonist stimulation in the presence of external Ca^{2+} was normal). This compensating SOCE is consistent with the low levels of Ca^{2+} stores in SERCA3$^{-/-}$ platelets, known to induce recruitment of STIM1 and STIM2 by Orai-1.[40] Of note, this sustained SOCE is not modulated by ADP scavenging or addition, strengthening the idea that it is only driven by Ca^{2+} store depletion, and not via an ADP-dependent pathway. Thus, SOCE appears as a compensatory mechanism in the context of SERCA3 ablation (or inhibition), possibly explaining the limited hemostasis impact on SERCA3$^{-/-}$ mice. Interestingly, Harper et al have shown that NC(K)X Ca^{2+} exchangers drive initial SOCE upon Tg-induced Ca^{2+} stores depletion, triggering dense granule secretion, which potentiated activation through ADP, ATP, and 5HT pathways.[41] Although this observation points to a link between Ca^{2+} regulation and an autocrine platelet activation amplification, it clearly acts in a different manner because it involves NC(K)X and SOCE, not being specific for ADP.

Importantly, tBHQ-mediated SERCA3 inhibition in human platelets leads to defective aggregation, ATP secretion, and $\alpha_{IIb}\beta_3$ activation (Z.E., R.B., M.B., and J.-P.R., unpublished data, December 20, 2015). Thus, SERCA3 plays the same role in human and mouse platelets.

Finally, SERCA3 depletion or inhibition appears to lead to defective SERCA3-dependent Ca^{2+} storing. This conclusion stems from several convergent observations: First, mobilization of Ca^{2+} from intracellular compartments was clearly affected in SERCA3$^{-/-}$ platelets, independent of the agonist used. Second, SERCA3$^{-/-}$ platelets exhibit stored Ca^{2+} levels lower than control platelets, as evidenced by experiments assessing release of total Ca^{2+} stores by ionomycin and Tg (supplemental Figure 4B). Third, blockade by the SERCA3-specific pharmacological inhibitor tBHQ (leading to Ca^{2+} "leakage" from SERCA3-dependent Ca^{2+} stores), in conditions (10 μM) where it did elicit Ca^{2+} release in the cytosol of control but not of SERCA3$^{-/-}$ platelets, reproduced the defect in Ca^{2+} mobilization, as well as in secretion. This effect was SERCA3-specific because it was not observed with 200 nM Tg, specific for SERCA2b. One can thus conclude that a Ca^{2+} storage pool dependent on SERCA3, and not on SERCA2b, seems to be required for a release of ADP, itself seemingly important to full platelet activation in conditions of low agonist concentration.

In conclusion, our data provide evidence that platelet activation seems to involve a release of ADP through a secretory pathway under the control of SERCA3-dependent Ca^{2+} stores, independently from $\alpha_{IIb}\beta_3$ integrin engagement. The link between SERCA3-dependent Ca^{2+} stores and SERCA3-dependent ADP stores remains to be established.

Acknowledgments

The authors thank P. Gilon and G. E. Shull for providing the SERCA3$^{-/-}$ mice; Emilie Namur for setting up the Oregon Green fluorescence-Ca^{2+} standard curves; and Christelle Repérant for help with platelet preparation and flow cytometry. The authors also thank the CeCILE-SFR/Centre Commun d'Imagerie de Lyon-Est–Structure Fédérative de Recherche (France) for expert technical assistance in electron microscopy studies.

Z.E. is a PhD candidate at Université Paris-Sud, and this work is submitted in partial fulfillment of the requirement for a PhD.

This work was supported in part by INSERM and Université Paris-Sud, as well as a fellowship from the Ministère de

l'Education Nationale, de l'Enseignement Supérieur et de la Recherche (Z.E.).

Authorship

Contribution: Z.E., F.A., E.B., J.-C.B., R.B., and M.B. performed experiments; Z.E., R.B., M.B., and J.-P.R. analyzed results; R.B., F.A., M.B., and J.-P.R. designed experiments; J.-P.R. wrote the manuscript; and Z.E., F.A., N.P., R.B., M.B., and J.-P.R. critically edited the manuscript.

Conflict-of-interest disclosure: The authors declare no competing financial interests.

Correspondence: Jean-Philippe Rosa, INSERM U1176, Hôpital Bicêtre, 82 rue du Général Leclerc, 94276 Le Kremlin Bicêtre Cedex, France; e-mail: jean-philippe.rosa@inserm.fr.

References

1. Brini M, Carafoli E. Calcium pumps in health and disease. *Physiol Rev.* 2009;89(4):1341-1378.
2. Enouf J, Bredoux R, Papp B, et al. Human platelets express the SERCA2-b isoform of Ca (2+)-transport ATPase. *Biochem J.* 1992;286(1): 135-140.
3. Papp B, Enyedi A, Pászty K, et al. Simultaneous presence of two distinct endoplasmic-reticulum-type calcium-pump isoforms in human cells. Characterization by radio-immunoblotting and inhibition by 2,5-di-(t-butyl)-1,4-benzohydroquinone. *Biochem J.* 1992; 288(1):297-302.
4. Bobe R, Bredoux R, Corvazier E, et al. Sarco/endoplasmic reticulum Ca^{2+}ATPase (SERCA) isoforms: 1970-1998: 5 proteins; 1998-2005: 14 proteins. *Curr Top Biochem Res.* 2005;7:1-16.
5. Brini M, Calì T, Ottolini D, Carafoli E. Calcium pumps: why so many? *Compr Physiol.* 2012;2(2): 1045-1060.
6. Toyoshima C, Nomura H. Structural changes in the calcium pump accompanying the dissociation of calcium. *Nature.* 2002;418(6898):605-611.
7. Lytton J, Westlin M, Burk SE, Shull GE, MacLennan DH. Functional comparisons between isoforms of the sarcoplasmic or endoplasmic reticulum family of calcium pumps. *J Biol Chem.* 1992;267(20):14483-14489.
8. Carrion R Jr, Ro YT, Patterson JL. Purification, identification, and biochemical characterization of a host-encoded cysteine protease that cleaves a leishmaniavirus gag-pol polyprotein. *J Virol.* 2003; 77(19):10448-10455.
9. Walsh EP, Lamont DJ, Beattie KA, Stark MJ. Novel interactions of *Saccharomyces cerevisiae* type 1 protein phosphatase identified by single-step affinity purification and mass spectrometry. *Biochemistry.* 2002;41(7):2409-2420.
10. Burge SM, Wilkinson JD. Darier-White disease: a review of the clinical features in 163 patients. *J Am Acad Dermatol.* 1992;27(1):40-50.
11. Dhitavat J, Cobbold C, Leslie N, Burge S, Hovnanian A. Impaired trafficking of the desmoplakins in cultured Darier's disease keratinocytes. *J Invest Dermatol.* 2003;121(6): 1349-1355.
12. Shimizu H, Tan Kinoshita MT, Suzuki H. Darier's disease with esophageal carcinoma. *Eur J Dermatol.* 2000;10(6):470-472.
13. Korošec B, Glavač D, Rott T, Ravnik-Glavač M. Alterations in the ATP2A2 gene in correlation with colon and lung cancer. *Cancer Genet Cytogenet.* 2006;171(2):105-111.
14. Korošec B, Glavač D, Volavšek M, Ravnik-Glavač M. ATP2A3 gene is involved in cancer susceptibility. *Cancer Genet Cytogenet.* 2009; 188(2):88-94.
15. Brouland JP, Gélébart P, Kovàcs T, Enouf J, Grossmann J, Papp B. The loss of sarco/endoplasmic reticulum calcium transport ATPase 3 expression is an early event during the multistep process of colon carcinogenesis. *Am J Pathol.* 2005;167(1):233-242.
16. Varadi A, Lebel L, Hashim Y, Mehta Z, Ashcroft SJ, Turner R. Sequence variants of the sarco (endo)plasmic reticulum Ca(2+)-transport ATPase 3 gene (SERCA3) in Caucasian type II diabetic patients (UK Prospective Diabetes Study 48). *Diabetologia.* 1999;42(10):1240-1243.
17. Ji Y, Lalli MJ, Babu GJ, et al. Disruption of a single copy of the SERCA2 gene results in altered Ca2+ homeostasis and cardiomyocyte function. *J Biol Chem.* 2000;275(48):38073-38080.
18. Liu LH, Boivin GP, Prasad V, Periasamy M, Shull GE. Squamous cell tumors in mice heterozygous for a null allele of Atp2a2, encoding the sarco (endo)plasmic reticulum Ca2+-ATPase isoform 2 Ca2+ pump. *J Biol Chem.* 2001;276(29): 26737-26740.
19. Liu LH, Paul RJ, Sutliff RL, et al. Defective endothelium-dependent relaxation of vascular smooth muscle and endothelial cell Ca2+ signaling in mice lacking sarco(endo)plasmic reticulum Ca2+-ATPase isoform 3. *J Biol Chem.* 1997;272(48):30538-30545.
20. Iguchi N, Ohkuri T, Slack JP, Zhong P, Huang L. Sarco/endoplasmic reticulum Ca2+-ATPases (SERCA) contribute to GPCR-mediated taste perception. *PLoS One.* 2011;6(8):e23165.
21. Arredouani A, Guiot Y, Jonas JC, et al. SERCA3 ablation does not impair insulin secretion but suggests distinct roles of different sarcoendoplasmic reticulum Ca(2+) pumps for Ca(2+) homeostasis in pancreatic beta-cells. *Diabetes.* 2002;51(11):3245-3253.
22. Beauvois MC, Arredouani A, Jonas JC, et al. Atypical Ca2+-induced Ca2+ release from a sarco-endoplasmic reticulum Ca2+-ATPase 3-dependent Ca2+ pool in mouse pancreatic beta-cells. *J Physiol.* 2004;559(1):141-156.
23. Beauvois MC, Merezak C, Jonas JC, Ravier MA, Henquin JC, Gilon P. Glucose-induced mixed [Ca2+]c oscillations in mouse beta-cells are controlled by the membrane potential and the SERCA3 Ca2+-ATPase of the endoplasmic reticulum. *Am J Physiol Cell Physiol.* 2006;290(6): C1503-C1511.
24. Kovàcs T, Berger G, Corvazier E, et al. Immunolocalization of the multi-sarco/endoplasmic reticulum Ca2+ ATPase system in human platelets. *Br J Haematol.* 1997;97(1): 192-203.
25. López JJ, Redondo PC, Salido GM, Pariente JA, Rosado JA. Two distinct Ca2+ compartments show differential sensitivity to thrombin, ADP and vasopressin in human platelets. *Cell Signal.* 2006; 18(3):373-381.
26. López JJ, Jardín I, Bobe R, et al. STIM1 regulates acidic Ca2+ store refilling by interaction with SERCA3 in human platelets. *Biochem Pharmacol.* 2008;75(11):2157-2164.
27. Wuytack F, Eggermont JA, Raeymaekers L, Plessers L, Casteels R. Antibodies against the non-muscle isoform of the endoplasmic reticulum Ca2(+)-transport ATPase. *Biochem J.* 1989; 264(3):765-769.
28. Martin V, Bredoux R, Corvazier E, Papp B, Enouf J. Platelet Ca(2+)ATPases: a plural, species-specific, and multiple hypertension-regulated expression system. *Hypertension.* 2000;35(1): 91-102.
29. Adam F, Kauskot A, Nurden P, et al. Platelet JNK1 is involved in secretion and thrombus formation. *Blood.* 2010;115(20):4083-4092.
30. Denis C, Methia N, Frenette PS, et al. A mouse model of severe von Willebrand disease: defects in hemostasis and thrombosis. *Proc Natl Acad Sci USA.* 1998;95(16):9524-9529.
31. Wall JE, Buijs-Wilts M, Arnold JT, et al. A flow cytometric assay using mepacrine for study of uptake and release of platelet dense granule contents. *Br J Haematol.* 1995;89(2):380-385.
32. Bergmeier W, Schulte V, Brockhoff G, Bier U, Zirngibl H, Nieswandt B. Flow cytometric detection of activated mouse integrin alphaIIbbeta3 with a novel monoclonal antibody. *Cytometry.* 2002;48(2):80-86.
33. Sarratt KL, Chen H, Zutter MM, Santoro SA, Hammer DA, Kahn ML. GPVI and alpha2beta1 play independent critical roles during platelet adhesion and aggregate formation to collagen under flow. *Blood.* 2005;106(4):1268-1277.
34. Bobe R, Bredoux R, Corvazier E, et al. How many Ca(2)+ATPase isoforms are expressed in a cell type? A growing family of membrane proteins illustrated by studies in platelets. *Platelets.* 2005; 16(3-4):133-150.
35. Varga-Szabo D, Braun A, Nieswandt B. Calcium signaling in platelets. *J Thromb Haemost.* 2009; 7(7):1057-1066.
36. Jonnalagadda D, Izu LT, Whiteheart SW. Platelet secretion is kinetically heterogeneous in an agonist-responsive manner. *Blood.* 2012;120(26): 5209-5216.
37. Meng R, Wu J, Harper DC, et al. Defective release of α granule and lysosome contents from platelets in mouse Hermansky-Pudlak syndrome models. *Blood.* 2015;125(10):1623-1632.
38. Sharda A, Kim SH, Jasuja R, et al. Defective PDI release from platelets and endothelial cells impairs thrombus formation in Hermansky-Pudlak syndrome. *Blood.* 2015;125(10):1633-1642.
39. Storrie B. Defective platelet autocrine signaling in HPS. *Blood.* 2015;125(10):1515-1516.
40. Zbidi H, Jardin I, Woodard GE, et al. STIM1 and STIM2 are located in the acidic Ca2+ stores and associates with Orai1 upon depletion of the acidic stores in human platelets. *J Biol Chem.* 2011; 286(14):12257-12270.
41. Harper AG, Mason MJ, Sage SO. A key role for dense granule secretion in potentiation of the Ca2+ signal arising from store-operated calcium entry in human platelets. *Cell Calcium.* 2009; 45(5):413-420.

2016 128: 1129-1138
doi:10.1182/blood-2015-10-678383 originally published online June 14, 2016

Full activation of mouse platelets requires ADP secretion regulated by SERCA3 ATPase–dependent calcium stores

Ziane Elaïb, Frédéric Adam, Eliane Berrou, Jean-Claude Bordet, Nicolas Prévost, Régis Bobe, Marijke Bryckaert and Jean-Philippe Rosa

Blood (print ISSN 0006-4971, online ISSN 1528-0020), is published weekly by the American Society of Hematology, 2021 L St, NW, Suite 900, Washington DC 20036.

Supplemental Methods

Electron microscopy

Standard electron microscopy (EM) for platelet morphology of WT and SERCA3$^{-/-}$ mice was performed according to the standard procedure, as previously described.[1,2]

Blood collection and mouse platelet preparation

Blood was collected and platelets isolated exactly as previously described.[1]

Platelet aggregation

Platelet aggregation was carried out with washed platelets induced by G protein-coupled receptor (GPCR) agonists (ADP, thrombin, and PAR4-AP) and collagen in the presence or absence of apyrase (5U/mL). Light transmission was measured through the stirred suspension of platelets ($2.5x10^8$ platelets/mL) during 3 minutes using a Chronolog aggregometer (Chrono-Log Corporation, USA).[1]

Flow cytometry

Washed platelets (3×10^8/mL) were stimulated by thrombin for 10 minutes at 37°C without stirring. Then, platelets were incubated with phycoerythrin (PE)-conjugated JON/A antibody or fluorescein isothiocyanate (FITC)-labeled rat anti-mouse CD62P (P-selectin) mAb (Wug.E9) and directly analyzed on an Accuri C6 flow cytometer (BD Biosciences; Le Pont de Claix, France).

Platelet dense granule secretion

Dense granule secretion was quantified by assessment of ATP release after platelet aggregation using an ATP determination kit (Molecular Probes, Saint Aubrin, France), as previously described.[1]

Western blotting

Western blotting of washed platelets (2.5 x 10^8/mL; 300 μL) was conducted as previously published.[1] 14-3-3ζ was used as normalization standard because it is much less variable than GAPDH or actin.[3] Images of the chemiluminescent signal were captured using a G BOX Chemi XT16 Image System and quantified using Gene Tools version 4.0.0.0 (Syngene, Cambridge, UK).

Calibration methods for intracellular [Ca^{2+}] assessment.

The following calibration method was used to assess the intracellular free [Ca^{2+}] using BAPTA Oregon green probe, based on the equation (1) of Tsien and Pozzan[4] for a non-ratio-metric dye that establishes a proportional relationship between [Ca^{2+}] and fluorescence signal intensity.

$$[Ca^{2+}] = Kd \times (f - f_{min})/(f_{max} - f) \qquad (1)$$

where f is the intensity of the fluorescence signal, f_{max} is the fluorescence signal in saturated free [Ca^{2+}], meaning the measured fluorescence when ionomycin was added to the medium in presence of 2mM free extracellular Ca^{2+} and f_{min} is the fluorescence signal at zero free [Ca^{2+}], measured after a subsequent addition of EGTA (10mM). Kd is the dissociation constant of BAPTA Oregon-green for Ca^{2+} and was estimated to 206 ± 5 nM in the cuvette by Maravall et al.,[5] and corrected up 30% for the intracellular environment.[6]

Additionally, as the intensity level of f_{max} and f_{min} is dependent on the amount of probe loaded in platelets, further experiments were conducted in order to determine the relationship between f_{min} and f_{max} compared with the basal fluorescence level. The graphs presented below clearly show that the level of f_{min} and f_{max} is linearly correlated to the basal level of fluorescence. Therefore, we used the indicated equations to calculate f_{max} and f_{min} when these values were not measured during the experiments.

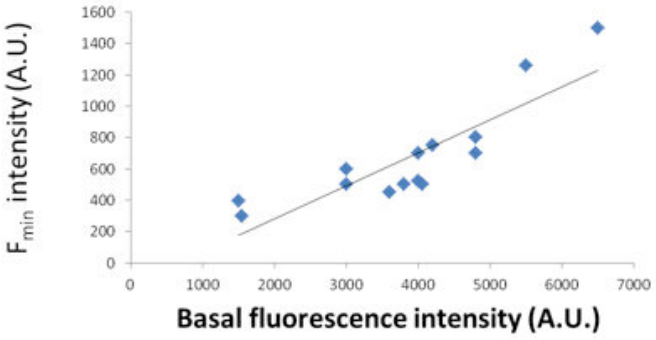

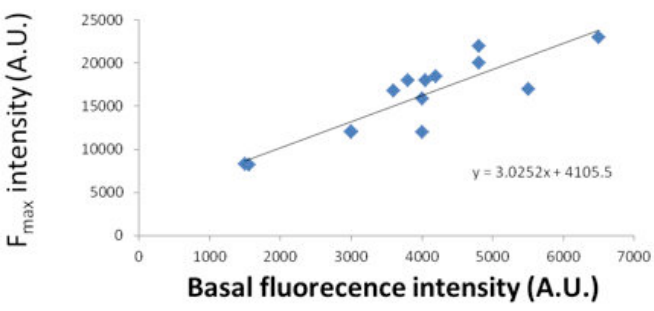

Assessment of dense granule content in platelets by mepacrine fluorescence.

Washed platelets (7.5 x 10^7/mL) or platelet rich plasma (diluted in phosphate buffer at 7.5 x 10^7 platelets/mL) were incubated with 125μM mepacrine for 30 minutes at room temperature.[7] Fluorescence intensity was determined using an Accuri C6 flow cytometer (BD Biosciences; Le Pont de Claix, France).

Legends to supplemental Figures.

Figure S1

Quantitation of platelet surface receptors of control and SERCA3$^{-/-}$ platelets by flow cytometry. Platelet surface receptors of control (WT) and SERCA3$^{-/-}$ platelets were quantitated by flow cytometry using antibodies specific for (A) GPVI, the collagen receptor, (B) the GPIbα subunit of the GPIb-IX-V receptor for VWF, (C) the α_2 subunit of the $\alpha_2\beta_1$ integrin, a receptor for collagen, (D) the α_{IIb} subunit of the $\alpha_{IIb}\beta_3$ integrin, receptor for fibrinogen. Data presented are the means ± SEM of 3 experiments. Statistical significance was assessed using the Student's *t* test.

Figure S2

Aggregation, secretion, $\alpha_{IIb}\beta_3$ activation and P-selectin expression of control and SERCA3$^{-/-}$ platelets stimulated with PAR4-AP. (A) Washed platelets from control (WT, black) or SERCA3$^{-/-}$ (gray) mice were subjected to aggregation with 40μM or 100μM PAR4-AP, an agonist of the PAR4 thrombin receptor. (B) Washed platelets from control (WT, black) or SERCA3$^{-/-}$ (gray) platelets were preincubated with apyrase (Apy) (5U/mL), prior to induction of aggregation with 40μM or 100μM PAR4-AP. All aggregation tracings are representative of 3 experiments. (C) ATP secretion from (WT, black bars or SERCA3$^{-/-}$, white bars) platelets aggregated in (A) was quantitated by luminescence (see Methods) in the supernatants from 10^7 platelets. ATP is expressed as pmoles. Data are expressed as

means ± SEM, n=3, using the 1-way ANOVA followed by Tukey's multiple comparison test; ***P<0.001. (D) The amount of activated $\alpha_{IIb}\beta_3$ integrin was assessed by flow cytometry by binding of the specific monoclonal antibody JON/A to control (WT, closed squares) or SERCA3$^{-/-}$ (open squares) platelets upon activation with PAR4-AP at different concentrations. Data are expressed as means ± SEM, n=3, using the 1-way ANOVA followed by Tukey's multiple comparison test; *P<0.05, **P<0.01. (E) The expression of P-selectin following PAR4-AP stimulation of platelets was assessed by flow cytometry on control (WT, closed squares) or SERCA3$^{-/-}$ (open squares) platelets. Data are expressed as means ± SEM, n=3, using the 1-way ANOVA followed by Tukey's multiple comparison test; *P<0.05, **P<0.01.

Figure S3

Assessment of dense granule content and of maximal ATP or 5HT secretion in control and SERCA3$^{-/-}$ platelets. (A) Dense granules were assessed by staining of platelets with the dense granule-specific fluorescent reporter mepacrine, and fluorescence assessed by flow cytometry (see supplemental Methods). Means ± SEM are presented for 3 experiments on a total of 8 control (WT, closed circles) and 9 SERCA3$^{-/-}$ (open circles) mice, using the Student's *t* test. (B) Washed platelets from control (WT, black bars) or SERCA3$^{-/-}$ (white bars) were stimulated with 2 U/mL of thrombin under stirring conditions for 5 minutes to allow for maximal secretion. Platelets were pelleted and ATP secretion was assessed by luminescence (see supplemental Methods) in the supernatants from 10^7 platelets. ATP is expressed as pmoles. Data are expressed as means ± SEM, n=3, using the 1-way ANOVA followed by Tukey's multiple comparison test; ns, not significant; ***P<0.001. (C) Washed platelets from control (WT, white) or SERCA3$^{-/-}$ (black) mice were stimulated with either buffer ("0"), thrombin (0.040 or 2 U/ml), in absence or presence of 10μM ADP ("+ADP) for 3 minutes under stirring, centrifuged and 5HT assessed in the supernatant (see Methods). 5HT was also assessed in total platelet lysate ("Plt lysate"). Data are expressed as means ± SEM, n=3, using the 1-way ANOVA followed by Tukey's multiple comparison test; ns, not significant; ***P<0.001. (D) Washed platelets (control, WT, black and

SERCA3$^{-/-}$, SERCA3, gray) were subjected to aggregation in the presence of 5HT alone at 1, 5 and 10μM. This is representative of 3 independent experiments. (E) Washed platelets from wild-type (WT, black tracings) or SERCA3$^{-/-}$ (SERCA3, gray tracings) were subjected to aggregation upon 40mU/mL thrombin stimulation for 3 minutes in the presence of serotonin (5HT) at 0, 1, 5 or 10μM. This result is representative of 3 independent experiments. (F) Washed control (black) or SERCA3$^{-/-}$ (gray) platelets were subjected to thrombin stimulation at 0 or 40 mU/mL in the absence (-) or presence (+) of 10μM 5HT, and ATP release assessed as pmoles. Data are expressed as means ± SEM, n=3, using the one way ANOVA followed by Tukey's multiple comparison test; ns, not significant; ***P<0.001.

Figure S4

Assessment of Ca^{2+} mobilization, Ca^{2+} entry or total Ca^{2+} store release in washed control, SERCA3$^{-/-}$ or tBHQ-treated platelets. (A) Washed control (black) or SERCA3$^{-/-}$ (gray) platelets pre-incubated with Oregon-Green BAPTA-AM were stimulated with 100mU/mL of thrombin for 3 minutes in the absence of extracellular Ca^{2+} (EGTA 100μM) to assess Ca^{2+} mobilization from internal stores, followed by addition of 1 mM Ca^{2+} in the buffer to measure Ca^{2+} influx. (B) Ca^{2+} store release was assessed in washed control (black) or SERCA3$^{-/-}$ (grey) platelets loaded with Oregon-Green BAPTA-AM by addition of ionomycin (50nM) to release Ca^{2+} from internal stores, and Tg (1μM) to block both SERCA2b and SERCA3 in order to prevent Ca^{2+} re-uptake in stores. (C) Washed control (black) or SERCA3$^{-/-}$ (gray) platelets were preincubated with Oregon Green BAPTA-AM, and either ethanol (i) or 5 (ii), 10 (iii) or 15μM (iv) tBHQ in the presence of EGTA (100μM), for 4 minutes, prior to stimulation with 40 mU/mL of thrombin in absence of stirring. Note that 10μM tBHQ triggers spontaneous Ca^{2+} mobilization in WT platelets and not in SERCA3$^{-/-}$ platelets, while both exhibit comparable Ca^{2+} mobilization at 15μM tBHQ.

Figure S5

Ca^{2+} mobilization, store release and re-uptake in washed control or SERCA3$^{-/-}$ platelets. (A) Ca^{2+} mobilization dose-response of thapsigargin (Tg) in control and SERCA3$^{-/-}$ platelets. Platelets from either control (WT) or SERCA3$^{-/-}$ mice were washed, loaded with Oregon Green BAPTA-AM and incubated in the presence of EGTA (100μM) with either DMSO, or Tg at 200nM, 500nM, or 1 μM. Ca^{2+}-induced Oregon Green BAPTA-AM fluorescence was detected by flow cytometry, and quantitated as indicated in supplemental Methods. The experiment presented is representative of three. (B) Washed control (black) or SERCA3$^{-/-}$ (gray) platelets were challenged with Tg at 200 or 300nM, comparatively to its solvent, DMSO, for 8 minutes before stimulation with 40mU/mL thrombin. Note the absence of Ca^{2+} mobilization in SERCA3$^{-/-}$ platelets while still significant in WT platelets at 200nM Tg, (but no more at 300nM Tg), indicating full blockade of SERCA2b but not of SERCA3 at this Tg concentration.

(C) Ca^{2+} re-uptake was assessed in washed platelets stimulated with 40 mU/mL of thrombin for 3 minutes before addition of the inhibitor Tg (1 μM) to prevent Ca^{2+} re-uptake by SERCA2b and SERCA3, in the absence or the presence of extracellular Ca^{2+} (EGTA 100μM).

Supplemental References

1. Adam F, Kauskot A, Nurden P, et al. Platelet JNK1 is involved in secretion and thrombus formation. *Blood*. 2010;115(20):4083-4092.
2. Nurden P, Chretien F, Poujol C, Winckler J, Borel-Derlon A, Nurden A. Platelet ultrastructural abnormalities in three patients with type 2B von Willebrand disease. *Br J Haematol*. 2000;110(3):704-714.
3. Baumgartner R, Umlauf E, Veitinger M, et al. Identification and validation of platelet low biological variation proteins, superior to GAPDH, actin and tubulin, as tools in clinical proteomics. *J Proteomics*. 2013;94:540-551.
4. Tsien R, Pozzan T. Measurement of cytosolic free Ca2+ with quin2. *Methods Enzymol*. 1989;172:230-262.
5. Maravall M, Mainen ZF, Sabatini BL, Svoboda K. Estimating intracellular calcium concentrations and buffering without wavelength ratioing. *Biophys J*. 2000;78(5):2655-2667.
6. Minta A, Kao JP, Tsien RY. Fluorescent indicators for cytosolic calcium based on rhodamine and fluorescein chromophores. *J Biol Chem*. 1989;264(14):8171-8178.
7. Wall JE, Buijs-Wilts M, Arnold JT, et al. A flow cytometric assay using mepacrine for study of uptake and release of platelet dense granule contents. *Br J Haematol*. 1995;89(2):380-385.

Figure S1

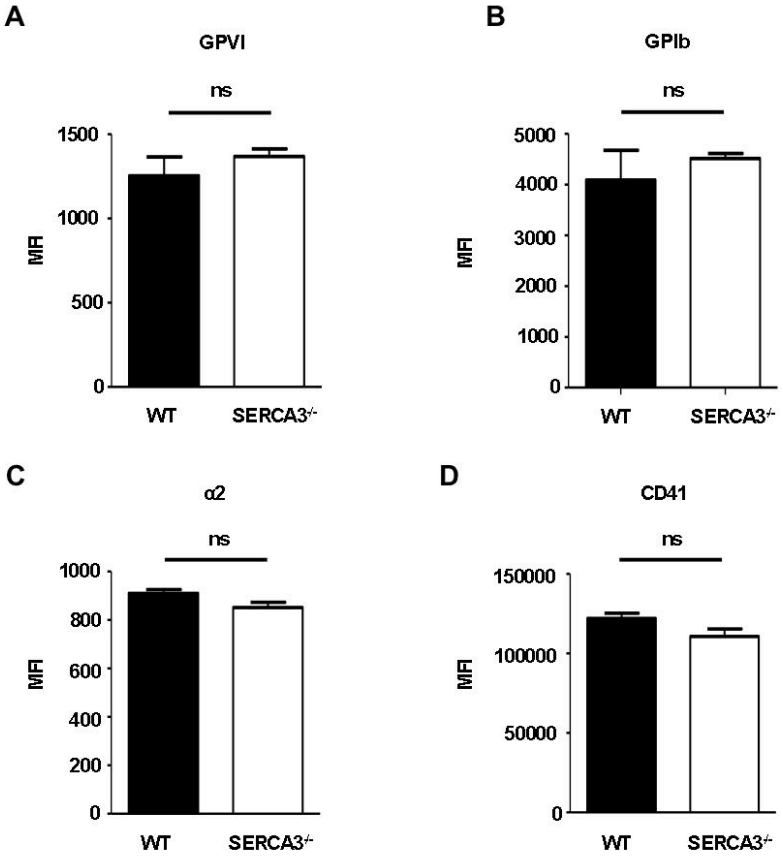
A
GPVI
ns
1500
1000
500
0
MFI
WT
SERCA3-/-
B
GPIb
ns
5000
4000
3000
2000
1000
0
MFI
WT
SERCA3-/-
C
α2
ns
1000
800
600
400
200
0
MFI
WT
SERCA3-/-
D
CD41
ns
150000
100000
50000
0
MFI
WT
SERCA3-/-

Figure S2

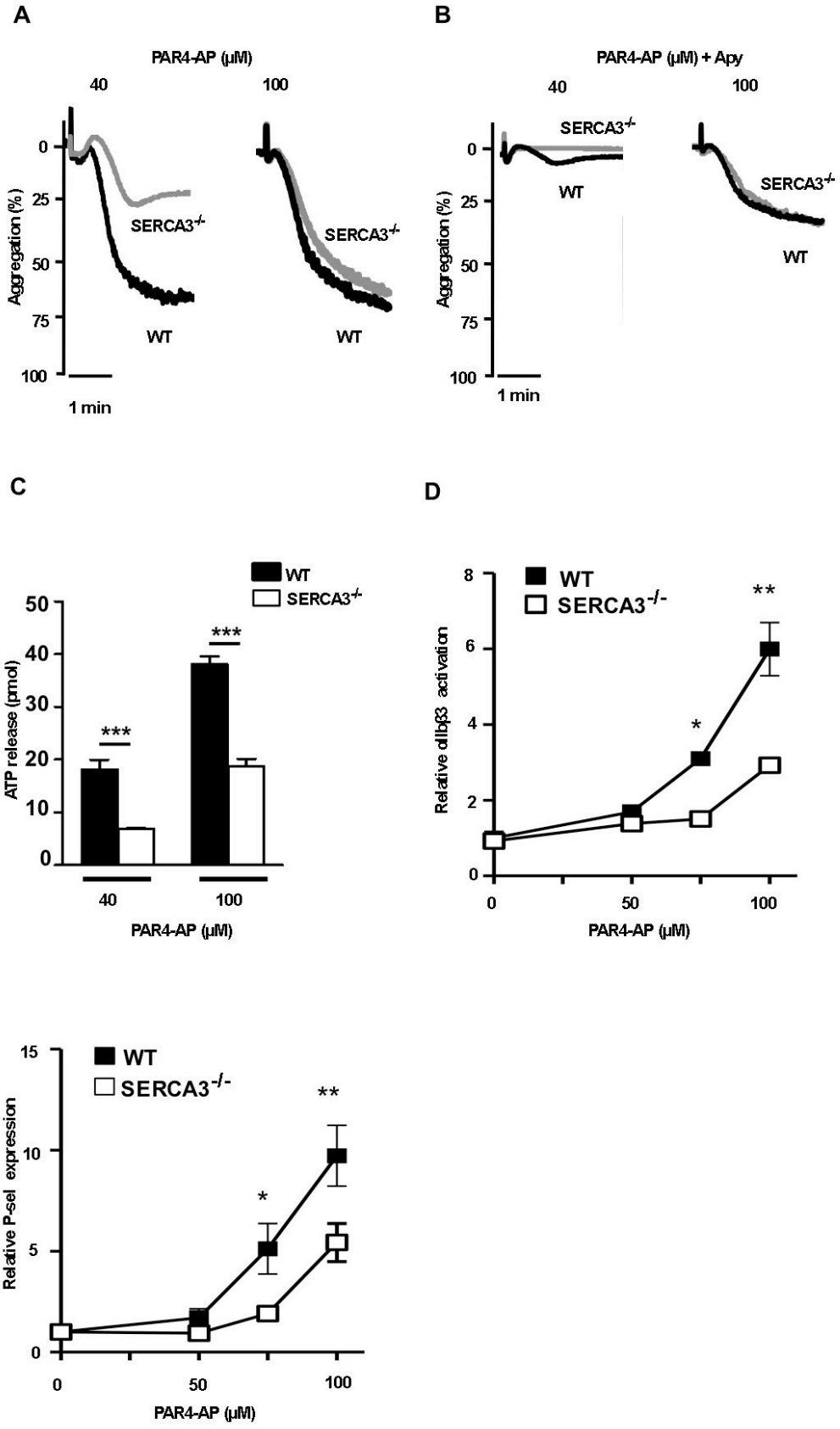
A
PAR4-AP (μM)
40
100
0
25
50
75
100
Aggregation (%)
SERCA3-/-
WT
1 min
B
PAR4-AP (μM) + Apy
C
WT
SERCA3-/-
ATP release (pmol)
***
PAR4-AP (μM)
D
Relative dIIb3 activation
*
**
E
Relative P-sel expression

Figure S3

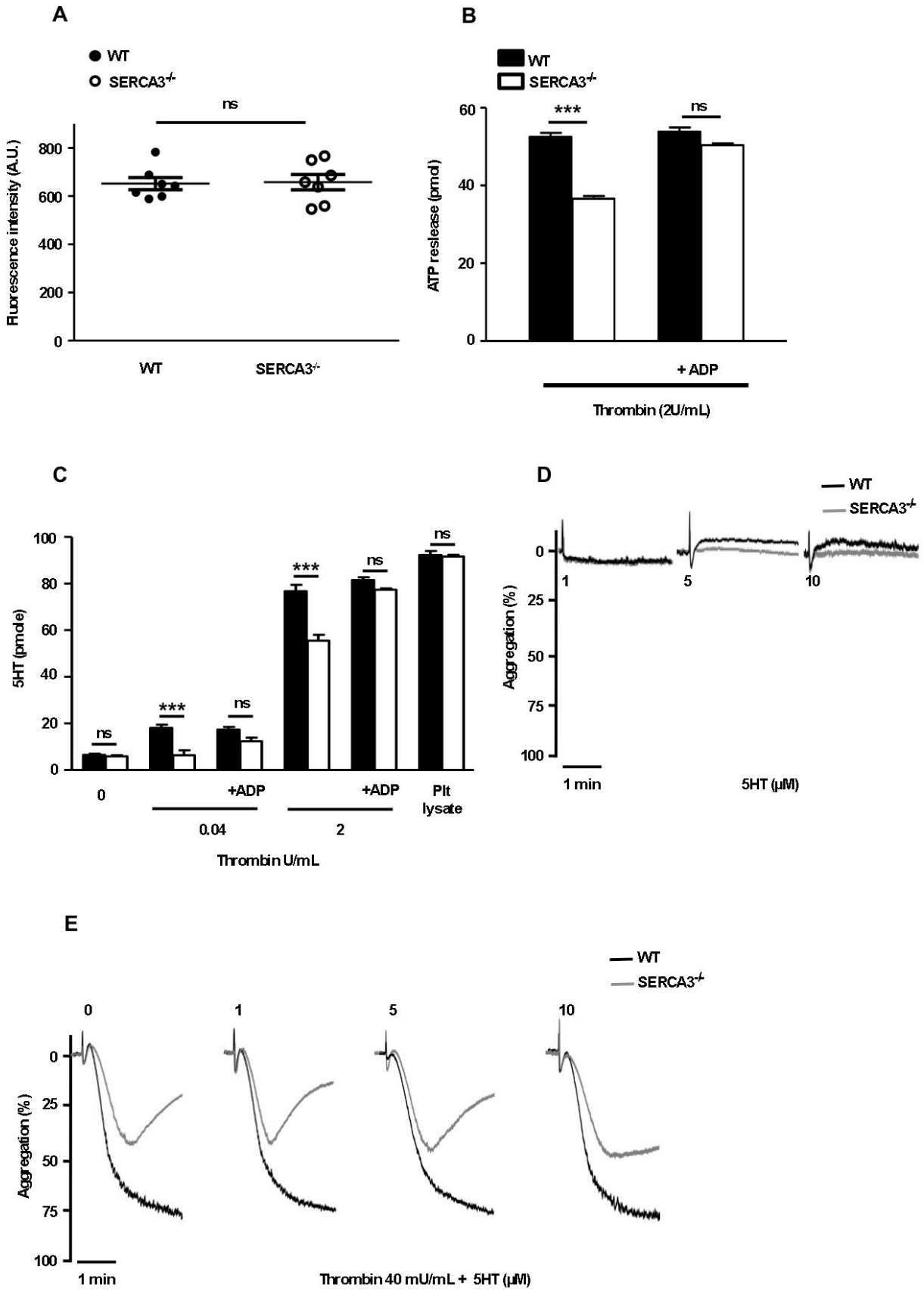
A
WT
SERCA3-/-
ns
Fluorescence intensity (A.U.)
800
600
400
200
0
WT
SERCA3-/-
B
WT
SERCA3-/-
***
ns
ATP release (pmol)
60
40
20
0
+ ADP
Thrombin (2U/mL)
C
5HT (pmole)
100
80
60
40
20
0
ns
***
ns
***
ns
ns
0
+ADP
+ADP
Plt lysate
0.04
2
Thrombin U/mL
D
WT
SERCA3-/-
Aggregation (%)
0
25
50
75
100
1
5
10
1 min
5HT (µM)
E
WT
SERCA3-/-
0
1
5
10
Aggregation (%)
0
25
50
75
100
1 min
Thrombin 40 mU/mL + 5HT (µM)

Figure S3

F

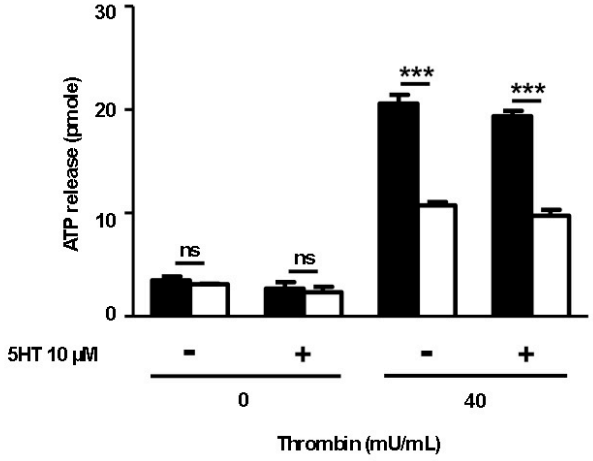

Figure S4

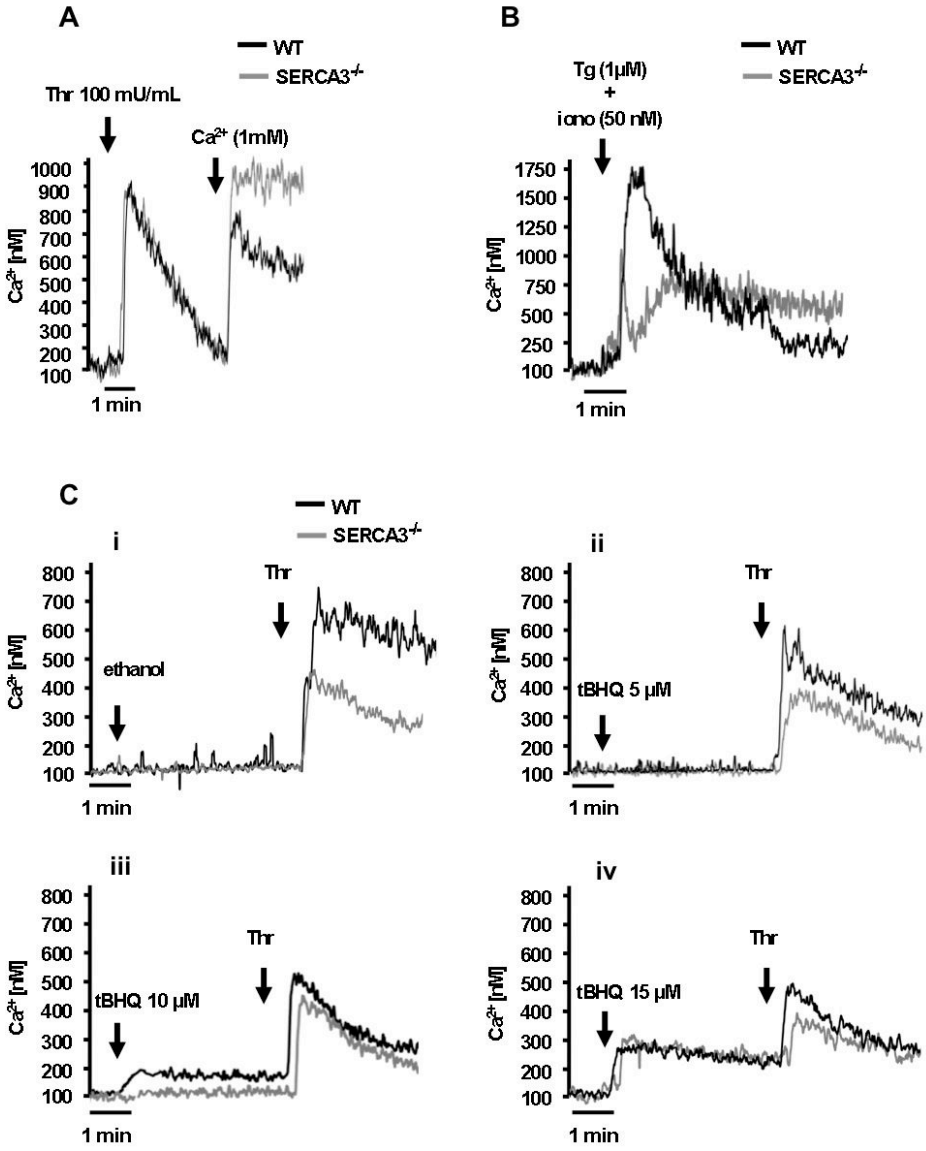
A
WT
SERCA3-/-
Thr 100 mU/mL
Ca2+ (1mM)
Ca2+ [nM]
1 min
B
WT
SERCA3-/-
Tg (1µM)
+
iono (50 nM)
Ca2+ [nM]
1 min
C
WT
SERCA3-/-
i
Thr
ethanol
Ca2+ [nM]
1 min
ii
Thr
tBHQ 5 µM
Ca2+ [nM]
1 min
iii
Thr
tBHQ 10 µM
Ca2+ [nM]
1 min
iv
Thr
tBHQ 15 µM
Ca2+ [nM]
1 min

Figure S5

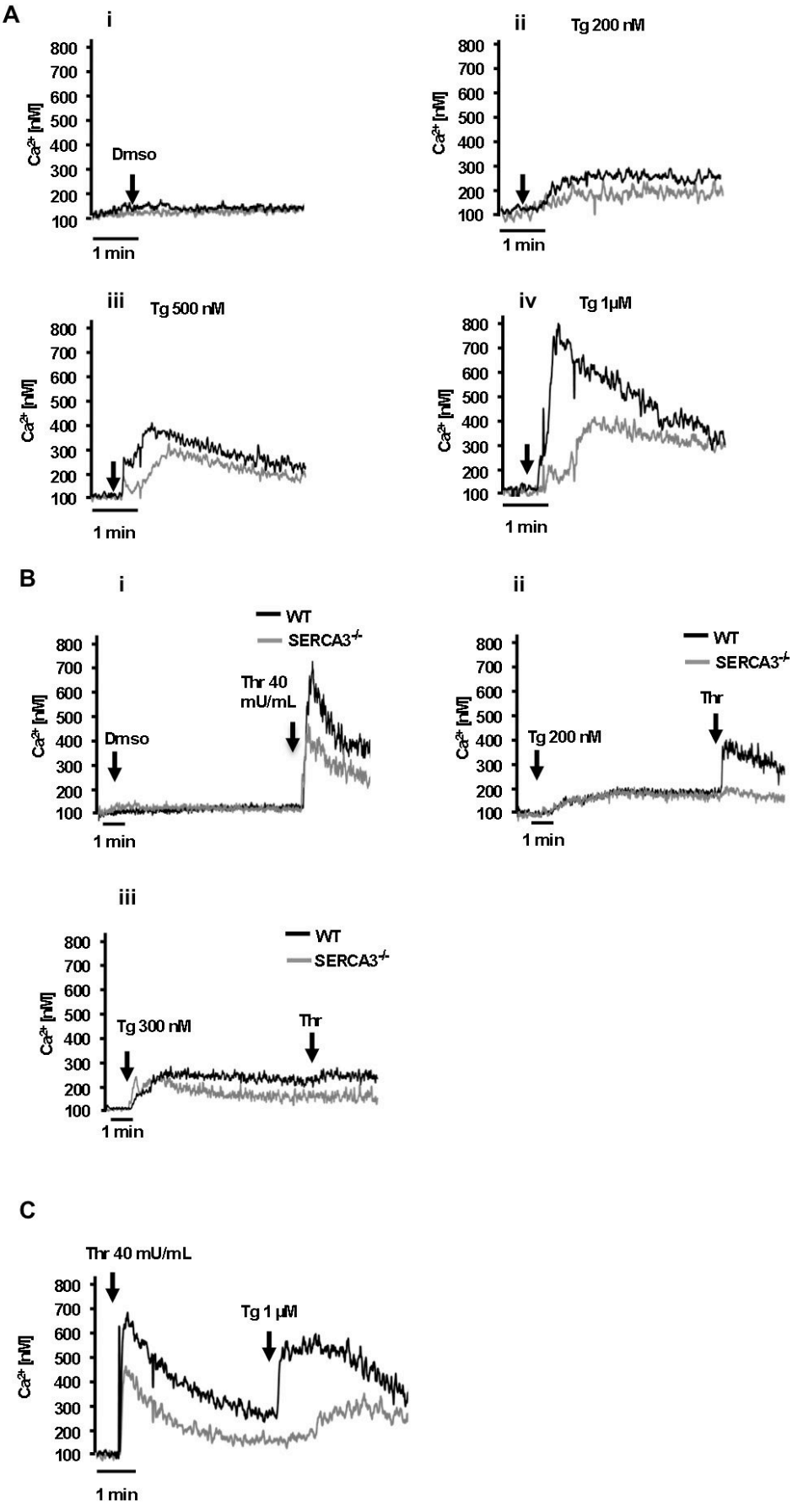
A
i
ii
Tg 200 nM
iii
Tg 500 nM
iv
Tg 1µM
Dmso
1 min
Ca2+ [nM]
B
i
ii
iii
WT
SERCA3-/-
Thr 40 mU/mL
Thr
Tg 200 nM
Tg 300 nM
C
Thr 40 mU/mL
Tg 1 µM

Article II

Rôle de SERCA3 dans les fonctions plaquettaires chez l'homme

Nos résultats précédents ont montré que SERCA3 joue un rôle important dans les fonctions plaquettaires chez la souris, en contrôlant une sécrétion d'ADP primaire nécessaire à l'activation plaquettaire complète.

Nous avons voulu vérifier si le rôle de SERCA3 était similaire dans les plaquettes humaines. En prétraitant les plaquettes de sujets normaux avec du tBHQ, l'inhibiteur préférentiel de SERCA3, nous avons observé une diminution de la mobilisation calcique, de l'agrégation et de la sécrétion granulaire dense (donc d'ADP). De plus l'addition d'ADP exogène au premier activateur court-circuite l'inhibition par le tBHQ. Ces résultats suggèrent l'existence d'une voie de signalisation dépendante de SERCA3 conduisant à une sécrétion primaire d'ADP, importante aussi bien dans les plaquettes humaines que murines.

Par ailleurs l'exploration d'une pathologie, l'obésité morbide, nous a permis d'observer une diminution de l'expression de SERCA3 corrélée à une diminution des fonctions plaquettaires *in vitro* (agrégation, activation d' $\alpha_{IIb}\beta_3$, mobilisation calcique et surtout sécrétion granulaire dense). De plus, l'ADP exogène additionné au premier activateur permet de restaurer ces fonctions plaquettaires.

Nous pensons que la diminution de l'expression de SERCA3 pourrait être un mécanisme adaptatif limitant l'activation plaquettaire dans un environnement pro thrombotique. En effet, un an après un by-pass gastrique et un fort amaigrissement, les mêmes patients retrouvent une expression normale de SERCA3 et une activité plaquettaire similaire à la population témoin.

Ces résultats confirment que SERCA3 joue un rôle important dans les fonctions plaquettaires chez l'homme en contrôlant la sécrétion d'ADP et que le contrôle de l'expression de SERCA3 peut être régulé dans des conditions physio-pathologiques pour abaisser le niveau d'activation plaquettaire. Ce travail a fait l'objet d'un article ci-joint en voie de soumission.

REDUCED PLATELET SERCA3 EXPRESSION AND SUBSEQUENT PLATELET INHIBITION IN SEVERE OBESITY ARE REVERSIBLE AFTER WEIGHT LOSS

Short title

Platelet SERCA3 is reversibly decreased in obesity

Authorship

Ziane Elaïb,[1*] Jose Javier Lopez,[1*] Muriel Coupaye,[2,3] Kevin Zuber,[4] Yann Becker,[1] Aurélie Kondratieff,[1] Christelle Repérant,[1] Marion Pépin,[1] Laurence Salomon,[4] France Teillet,[6,7] Simon Msika,[5,6] Dominique de Prost,[6,7] Rosa Jean-Philippe, [1] Régis Bobe,[1**] & Alain Stépanian,[6,8,9**]

[1] INSERM Unité Mixte de Recherche–Santé 1176, Université Paris-Sud, Université Paris-Saclay, Le Kremlin-Bicêtre, France

[2] Service des Explorations Fonctionnelles, Hôpital Louis Mourier, Assistance Publique – Hôpitaux de Paris, Colombes, France

[3] Centre Intégré Nord Francilien de prise en charge de l'Obésité (CINFO), Paris, France

[4] Département de Biostatistiques, Santé publique et Information médicale, Fondation Rotschild, Paris, France

[5] Service de Chirurgie Digestive, Hôpital Louis Mourier, Assistance Publique – Hôpitaux de Paris, Colombes, France

[6] Université Paris Diderot, Sorbonne Paris Cité, Paris, France

[7] Service d'Hématologie et Transfusion, Hôpital Louis Mourier, Assistance Publique – Hôpitaux de Paris, Colombes, France

[8] Service d'Hématologie biologique, Hôpital Lariboisière, Assistance Publique – Hôpitaux de Paris, Paris, France

[9] EA3518, Institut Universitaire d'Hématologie, Hôpital Saint Louis, Paris-Diderot, Paris, France

* These authors contributed equally to this work.

** These authors are joint senior authors on this work.

Corresponding author

Alain STEPANIAN

Hôpital Lariboisière

Service d'Hématologie biologique

2 rue Ambroise Paré

75010 Paris – France

alain.stepanian@aphp.fr

Phone: + 33 1 49 95 89 47

Fax: + 33 1 49 95 64 03

Word counts for text and abstract, figure/table count and reference count

Text: 3785 words (tout sans Kévin); abstract: 249 words; figure/table: 1487 words; reference: 32 references, 779 words.

Scientific category chosen during submission

Key Points

- Severe obesity is associated with decreased platelet aggregation, calcium mobilization and secretion, due to decreased SERCA3 expression. (138)
- After weight loss, platelet SERCA3 expression is upregulated and platelet aggregation, activation and calcium mobilization are restored. (135)

Abstract

In obese patients, platelet activity is described as increased, however it is associated with a reduced sensitivity to antiplatelet agents. These effects are associated to platelet dysfunctions and were attributed to perturbation in calcium homeostasis. The aim of our study was to explore these dysfunctions before and after weight loss. We conducted a monocentric patient/control study. Patients were women with body mass index (BMI) $\geq$ 35 kg/m^2, without hypertension, diabetes, dyslipidemia, cancer, sepsis or inflammation and controls were women with BMI >18.5 and < 25 kg/m^2, with the same exclusion criteria. Patients and controls were matched for age ± 3 years. Each pair of subjects has been seen twice: at inclusion and 1 year after gastric bypass surgery in patient.

We included 40 obese patients and 40 control subjects; 36 obese patients were analyzed after weight loss. We observed reduced sensitivity to agonists and lower calcium response of platelets from patients with severe obesity in conjunction with a decreased expression of platelet Sarco/Endoplasmic Reticulum Ca^{2+}ATPase (SERCA3). In obese patients, all abnormalities were independent from metabolic syndrome and normalized after weight loss. Finally, pharmacological inhibition of SERCA3 activity in control platelets resulted to similar defects than in obese patients; these defects were dependent on ADP secretion. ADP addition to agonist was able to compensate SERCA3 deficiency and restore normal calcium mobilization, aggregation and secretion in platelets from obese patients. This is the first report of a human pathophysiological condition, associated with a platelet SERCA3 deficiency. In obese, these dysfunctions are reversible and normalized after weight loss.

Introduction

Obesity is an abnormal accumulation of body fat that may impair health and subsequently constitutes a major cardiovascular risk factor.[1] It has reached epidemic proportions in the world and has more than doubled since 1980, according to the World Health Organization.[2,3] In 2014, more than 1.9 billion adults, 18 years and older, were overweight. Of these, over 600 million were obese. Body mass index (BMI) is a simple index of weight-for-height that is commonly used to classify overweight and obesity in adults. Obesity is defined as a BMI value $\geq$ 30 kg/m^2 and the risk of comorbidities is considered to be severe when BMI $\geq$ 35 kg/m^2 (WHO, 2000). Indeed, a high BMI is associated to myocardial infarction,[4,5] stroke[6,7] and venous thromboembolism (deep vein thrombosis and pulmonary embolism) risk.[8,9] In addition to the metabolic changes associated to obesity, modifications of hemostasis participate to the mechanisms of thrombosis in obesity.[10] More precisely, modifications in platelet functions, such as hyper-reactivity or reduced sensitivity to the physiological and pharmacological antiplatelet agents have been reported in obesity.[11,12] The increased platelet activation is notably reported when associated to type 2 diabetes mellitus or to metabolic syndrome.[12]

Platelet functions can indeed be modulated by several factors associated to these later conditions, such as low-grade pro-inflammatory state, insulin resistance, variations of leptin and adiponectin levels, oxidative stress or endothelial dysfunction.[11,12] Moreover, insulin decreases the sensitivity of circulating platelets to agonists.[13] Such dysfunctions could result from Ca^{2+} intracellular signaling in platelets. Sarco-endoplasmic reticulum calcium (Ca^{2+}) adenosine triphosphatases (ATPase) (SERCA) pump Ca^{2+} into intracellular stores and participate to the intracellular signaling in platelets.[14] In a mouse model, we recently showed that absence or inhibition of SERCA3 in platelet resulted in defects in thrombus formation, platelet aggregation and ADP secretion.[15] The aim of our study was to explore i) the platelet functions (aggregation, activation and secretion) and platelet calcium mobilization in obese patients; ii) the impact of weight loss on these parameters. We thus compared platelet functions between obese patients and lean control subjects, and performed a second comparison after weight loss in obese patients, i.e. one year after a Roux-en-Y Gastric Bypass (RYGB) Surgery.

Patients and Methods

Patients and Study design

All subjects were recruited in the Functional Exploration Department of Louis Mourier University Hospital (AP-HP, Colombes, France) between September 2011 and July 2014. Considering the large predominance of women in our patients, we decided to perform this study in women only. Inclusion criteria for obese patients (P) were: age ≥ 18 and ≤ 60 years old; female gender; body mass index (BMI) ≥ 35 kg/m^2; without weight variation > 5 kg in the last 3 months; patient scheduled for a RYGB Surgery. Exclusion criteria were: use of any antiplatelet therapy during one month before inclusion; type 1 or type 2 diabetes, or patient with diabetes therapy; arterial hypertension, or patient with antihypertensive treatment; patient with malignant disease, sepsis or inflammatory disease; medical history with coronary or cerebrovascular ischemic events; ongoing pregnancy. Control subjects (C) were healthy volunteers recruited among the medical and paramedical staff of our institution with following inclusion criteria: age ≥ 18 and ≤ 60 years old; female gender; BMI > 18.5 and < 25 kg/m^2; without weight variation > 5 kg in the last 3 months. Non-inclusion criteria were the same as for Patients. Patients and controls were matched for age ± 3 years.

Obese patients and matched control subjects were evaluated and compared a first time at inclusion. They were evaluated and compared a second time one year after RYGB Surgery in obese patients, with the same clinical and laboratory investigations.

The study protocol was approved by the ethics committee of Saint-Louis University Hospital, Paris (France) (Institutional Review Board; Agreement of US Department of Health and Human Services N° IRB 00003835; 2011/04NICB). In our study, each patients and controls gave informed written consent. The study were registered in clinical trials registry (NCT00632671). All authors had access to primary clinical trial data.

Anthropometry and Blood pressure determination

Height and weight were measured with standard methods for patients and controls. Two brachial cuff blood pressure recordings were obtained at 5-min intervals and the mean value was entered. An obese-cuff was used when necessary. Smoking was defined as cigarette use within the previous 30 days. Metabolic syndrome was defined according to the International Diabetes Federation (IDF) criteria: waist circumference > 80 cm plus at least two of the following abnormalities: fasting glycaemia ≥ 5.5 mmol/L or previously diagnosed type 2 diabetes, systolic/diastolic blood pressure ≥ 130/85 mmHg or antihypertensive medication,

triglycerides ≥ 1.7 mmol/L or lipid-lowering therapy, high density lipoprotein (HDL)-cholesterol < 1.30 mmol/L or lipid-lowering therapy.[16]

Blood sampling

Written informed consent was obtained from each woman before enrolment and blood sampling. Venous blood was collected after an overnight fast in 1:10 final volume of 0.129 M tri-sodium citrate, 15% K_3EDTA, sodium heparin or Acid Citrate Dextrose (ACD) containing tubes (Vacutainer, Becton-Dickinson, France) from a peripheral vein using a 21-gauge needle. For platelet function explorations, platelet-rich plasma was obtained from ACD blood within 4 hours after sampling. Platelet-poor plasma was obtained from citrated blood by double-centrifugation at 2500 g for 20 minutes, and aliquoted samples were stored at −80°C before being tested. Measurement of total, LDL- and HDL-cholesterol, triglycerides, fasting glucose, blood glycated hemoglobin, insulin, fibrinogen, platelet count, mean platelet volume and high-sensitivity C-reactive protein (hs-CRP) were performed using standard methods.

Materials

Antibodies: for SERCA3, the Pan-SERCA3 monoclonal antibody, PL/IM430 was used,[17] anti-14-3-3 ζ polyclonal antibody was purchased from Santa Cruz Biotechnology (Heidelberg, Germany). Goat anti-rabbit/mouse IgG conjugated with peroxidase were purchased from Jackson ImmunoResearch (West Grove, PA). PAC-1–FITC antibody was purchased from BD Biosciences (Le pont de Claix, France). ADP was purchased from Kordia (Leiden, Netherland). Majority of other laboratory chemicals including were purchased from Sigma-Aldrich (St. Quentin Fallavier, France).

Washed platelet preparation

Samples from obese patients and control subjects were always processed in parallel. Venous blood was collected in 10% (vol/vol) ACD-A buffer (75 mM trisodium citrate, 44 mM citric acid, 136 mM glucose, pH 6) and PPACK (80 μM) to prevent coagulation. Platelet-rich plasma (PRP) was obtained by centrifugation (120 g for 15 minutes at 20°C). Platelets were isolated from PRP by centrifugation (730 g for 12 minutes at 20°C) and washed in the presence of apyrase (100 mU/mL) and prostaglandin E1 (1 μM) to minimize platelet activation. Platelets were suspended in wash buffer (103 mM NaCl, 5 mM KCl, 1 mM $MgCl_2$, 5 mM Glucose, 36 mM citric acid, pH 6.5) and suspension was centrifuged (730 g for 12 minutes at 20°C). Platelets were re-suspended again in wash buffer and centrifuged again for

12 minutes at 730 g. Platelets were adjusted to similar levels (3 x 10^8 platelet/mL) in Tyrode-HEPES buffer (137 mM NaCl, 2 mM KCl, 0.3 mM NaH_2PO_4, 5.5 mM glucose, 5 mM N-2-hydroxyethylpiperazine-N′-2-ethanesulfonic acid, 12 mM $NaHCO_3$, 2 mM $CaCl_2$, pH 7.3). Platelet count was controlled before assays using hemocytometer.

Platelet aggregation

Platelet aggregation was carried out with washed platelets induced by G protein-coupled receptor (GPCR) agonist thrombin. Light transmission was measured through the stirred suspension of platelets (2.5 x 10^8 platelets/mL) for 3 minutes using a Chronolog aggregometer (Chrono-Log Corporation, USA). Dose/response curves were obtained in response to thrombin concentrations from 30 to 200 mU/mL. Half maximal effective concentration (EC_{50}) was defined as the thrombin concentration needed to induce a 50% aggregation response. EC_{50} were compared between obese patients and control subjects as histograms of normalized values to each matched control subject.

Flow Cytometry

Washed platelets (3 x 10^8/mL) were stimulated by thrombin for 10 minutes at 37°C without stirring. Then, Flow cytometry, using Accuri C6 flow cytometer (BD Biosciences; Le Pont de Claix, France), was performed to detect the activation markers on platelet surface including P-selectin expression and PAC-1 binding; the results were expressed as the mean fluorescence.

Measurement of intracellular calcium

Unstirred platelets (3 x 10^7 platelets/mL) were loaded with the Ca^{2+}-sensitive dye Oregon Green 488 BAPTA 1-AM (1 mM) for 45 minutes at 20°C. Ca^{2+} mobilization from intracellular stores induced by thrombin was analyzed in Ca^{2+} free medium and in the presence of 100 µM EGTA using an Accuri C6 flow cytometer. Changes in Ca^{2+} signal intensity were calculated as the ratios of fluorescence of activated over non-activated platelets and the area below the curve for 2 minutes after agonist addition was chosen as an indicator of the calcium response. Results are expressed as areas under the curves (2 min), compared between obese patients and control subjects, or for each patient, as percentage of the value obtained for the matched control. Three minutes after agonist stimulation, 300 µM of $CaCl_2$ were added to evaluate calcium influx from extracellular medium (results expressed as the same).

Immunoblotting

Washed platelet pellet from obese and control subjects were lyzed with RIPA buffer in presence of protease-phosphatase inhibitor (Thermo Scientific, USA). The lysis products were processed for SDS PAGE and immunoblotted for SERCA3 expression using PL/IM430 antibody. Expression of 14-3-3 ζ was used as internal control of protein loading.

Platelet dense granule secretion

Dense granule secretion was quantified as ATP release assessed after platelet aggregation using an ATP determination kit (Molecular Probes, Saint Aubrin, France), as previously described.[18]

Statistical analysis

Experimental values were presented as mean ± standard error of mean (SEM) or standard deviation (SD). Shapiro-Wilk tests and graphical methods such as examining the histograms and QQ-Plots were used to assess normality. For variables that were normal, t-tests (paired and unpaired) were used, whereas for variables that were not normal Paired Wilcoxon tests and Mann-Whitney tests were used and a p-value less than 0.05 was considered to be statistically significant.

Results

Study population

We included 40 obese patients and 40 matched control subjects. Eight obese patients could not be evaluated a second time. Six patients were lost to follow-up and 2 patients became pregnant. We thus evaluated 32 obese patients a second time, 528 ± 137 days (mean ± standard deviation, 388 to 963 days) after the time of inclusion, and 486 ± 128 days after RYGB surgery. Of the 32 matched control subjects, 26 were evaluated a second time (6 lost to follow-up). Table 1 shows general demographic, medical and metabolic characteristics of both groups at baseline (inclusion) and at second evaluation. During the mean follow-up, the obese patients lost weight (37.5 ± 8.7 kg; mean ± standard deviation, 24.4 to 59.2 kg); 24/32 patients (75%) had a BMI < 35 kg/m^2 and 15/32 patients (47%) < 30 kg/m^2 after weight loss. This was associated with subsequent normalization of metabolic characteristics such as blood lipids or carbohydrate metabolism, and inflammation markers (Table 1).

Platelet aggregation is decreased in severe obese patients and restored after weight loss

Firstly, platelets from obese patients were tested for aggregation. Figure 1A displays a typical platelet aggregation traces in response to thrombin, compared between platelets from obese patients (P1) and from control subjects (C1) at inclusion. Figure 1B displays typical dose/response obtained in response to thrombin concentrations from 30 to 200 mU/mL. We observed that the subsequent thrombin concentration EC_{50} was significantly higher for platelets from obese patients than control subjects (1.66 ± 0.3-fold increase, p=0.001) (Figure 1C). Interestingly, after weight loss, obese patients displayed similar response to thrombin stimulation when compared to control subjects tested in parallel (1.10 ± 0.01-fold increase for obese (P2) compared to control (C2), p=0.40) (Figure 1D).

Platelet activation is decreased in severe obese patients and restored after weight loss

To confirm that decreased platelet aggregation in obese patients was not due to desensitization during platelet purification steps, we measured platelet P-selectin expression in all subjects. P-selectin expression was similar in platelets from obese patients and control subjects at inclusion and at second evaluation, i.e. after weight loss in obese patients (Figure 2A). Similarly, in basal condition no difference binding of PAC-1 to $\alpha_{IIb}\beta_3$ was observed between both groups at inclusion (Figures 2B and 2C). Interestingly, we observed a significant lower $\alpha_{IIb}\beta_3$ activation in response to thrombin (50 mU/mL and 100 mU/mL) for platelet from obese patients at inclusion (P1) (p=0.02 and p=0.003, respectively) (Figure 2B), while PAC-1 binding was similar after weight loss (P2) when compared to control subjects during follow-up (C2) (p=0.11 and p=0.37, respectively at 50 and 100 mU/mL thrombin) (Figure 2C). These results suggest that the defect in platelet activation observed in severe obese patients is not due to desensitization of platelets along their preparation, but illustrates a decrease in platelet function.

Calcium mobilization is decreased in severe obese patients and restored after weight loss

As calcium signal plays an important role in platelet signaling pathways involved upstream of integrin activation, calcium mobilization from intracellular stores in platelet was analyzed. Figures 3A displays typical decreased in calcium mobilization in response to thrombin (100 mU/mL) in platelets from obese patients (P1) when compared to control subjects (C1) at inclusion and restored after weight loss (P2). Calcium mobilization measured as area under the curve (AUC) is significantly lower in platelets from obese patients and reached 77 ± 5.2 % of the control response ($p<10^{-4}$) (Figure 3C). The calcium mobilization was restored in obese

patients after weight loss to 95 ± 4 % of the control response (p=0.20) (Figure 3C). The decrease in calcium mobilization was associated with a weak decrease in calcium influx from extracellular medium that was slightly lower in platelets from obese patients when compared to control subjects (92 ± 12 % of the control response, p=0.23) (Figures 3D & 3E). No difference was observed in calcium influx after weight loss.

Severe obesity is associated with a low expression of SERCA3 that is upregulated after weight loss.

SERCA3 expression in platelets from severe obese patients is significantly decreased when compared to platelets from matched control subjects (Figure 4). Total SERCA3 expression analysis was performed in platelet lysates from obese patients at inclusion and after weight loss (P1 and P2, respectively) and compared to matched control subjects at inclusion and after follow-up (C1 and C2, respectively); protein levels were assessed by 14-3-3 ζ expression (Figure 4A) and results are displayed as normalized ratio intensity for SERCA3 over 14-3-3 ζ expression (Figure 4B). In platelets from obese patients, SERCA3 expression significantly decreased to 47 ± 7 % of control platelets (p <10^{-4}). In contrast, when a similar exploration was made using the same subject after weight loss, the level of SERCA3 expression was increased up to 160 ± 30 % of control (p=0.22) (Figures 4A and 4B). These results suggest that SERCA3 expression can be reversibly modulated by pathological conditions. They were also confirmed by the lower effect of SERCA3 inhibitor tBHQ on calcium leak from SERCA3 dependent store in obese patients' platelets: calcium leak is significantly decreased to 64 ± 6 % of the control response at inclusion and restored to 107 ± 6 % after weight loss (p<10^{-3} and p=0.98, respectively) (Figure 4C).

Inhibition of SERCA3 activity inhibits ADP dependent platelet activation.

To further confirm that platelet defects were due to the decrease in SERCA3 expression, SERCA3 activity was inhibited by tBHQ (10 µM) in platelets from control subjects. SERCA3 inhibition results in a decrease of human platelet aggregation, secretion and calcium mobilization in response to thrombin (Figures 5A, 5B and 5C, respectively). Ethanol 0.01% or tBHQ (5 µM) pretreated platelets displayed normal calcium mobilization. Addition of ADP to thrombin stimulation restored aggregation, secretion and calcium mobilization, suggesting that, similarly to what was previously described in mouse platelet, inhibition of SERCA3 in human platelets leads to ADP dependent decrease activation.

Platelet secretion is decreased in obese patients and restored after weight loss

Finally, we investigated in 5 obese patients (P1) for platelet secretion and role of ADP and compared to matched control subjects (C1). Our results confirmed that platelet secretion was also affected in platelets from obese patients (Figure 6A); the level of secretion in these platelets was similar to that of platelets from control subjects after SERCA3 inhibition using tBHQ. Figure 6A also shows that ADP addition to thrombin could restore normal secretion in platelets from obese patients or from control subjects, pretreated or not with tBHQ. Moreover, ADP addition was also able to restore platelet aggregation and calcium mobilization in platelets from obese subjects (Figures 6B and 6C). Moreover, in obese patients or control subjects, platelet aggregation was restored by ADP addition on platelets pretreated or not with tBHQ (Figures 6B). And finally, while SERCA3 inhibition using tBHQ decrease calcium mobilization in response to thrombin in control platelets to the level observed in platelets from obese subjects, exogenous ADP did also restore calcium mobilization in platelets from obese Patients (Figures 6C).

Influence of metabolic syndrome

Among obese patients, 18 patients over 40 had metabolic syndrome (MS). As expected, none of them had MS after RYGB surgery. At inclusion, we did not observe any significant difference between obese patients with or without MS in the thrombin concentration EC_{50} for platelet aggregation (p=0.19), PAC-1 binding using 100 mU/mL thrombin (p=0.37), Ca^{2+} mobilization AUC (p=0.68) or SERCA3 expression (p=0.82) (data not shown).

Discussion

To our knowledge, this is the first report of acquired platelet SERCA3 deficiency in a human pathological context. In our study, we demonstrate that aggregation, activation, calcium mobilization, ATP secretion and SERCA3 expression are significantly decreased in platelets from severe obese patients, when compared to non-obese control subjects and independently from metabolic syndrome. These dysfunctions are all restored when the patients lose weight, after a gastric bypass. Moreover, our results show that thrombin-induced platelet aggregation, ATP release and calcium mobilization in severe obese patients are restored after ADP addition.

Obesity is associated to both systemic inflammatory and prothrombotic states, which are likely to contribute to its cardiovascular consequences.[19] These conditions are both known to be associated to platelet activation, making platelets likely to play a central role in arterial thrombosis and vascular inflammation in obesity. Indeed, in obesity, platelet functions are described as altered and platelets display lower response to antiplatelet agents in the same time.[11,12,20,21] Platelet hyperreactivity description is mainly based on increased mean platelet volume, platelet count, soluble P-selectin, urinary 11-dehydro-TXB_2 (the major enzymatic metabolite of TXA_2), soluble CD40L, or platelet microparticles; [11,12,22] these reports also often refer to type 2 diabetes mellitus or to metabolic syndrome. Dellas *et al* performed aggregation tests on platelets from obese patients and compared the results to those obtained in lean controls.[23] They observed that platelets from obese donors exhibited a more pronounced aggregatory response to ADP stimulation compared to platelets from normal-weight control subjects. In opposite, our results show that in severe obese patients, platelets are less actives when compared to platelets from lean patients treated in the same conditions at the same time. This discrepancy might be explained by our experimental conditions, with washed platelets whereas Dellas *et al* used PRP diluted with homologous platelet-poor plasma (PPP). When we compared them to control subjects, platelets from obese patients displayed the same level of surface P-selectin expression, but demonstrated coherently decreased thrombin-induced aggregation, αIIbβ3 activation, calcium mobilization and secretion. Furthermore, we could observe that the level in SERCA3 expression was also reduced in severe obesity. Lower SERCA3 expression in platelets exhibits a lower level of Ca^{2+} in SERCA3 controlled stores as revealed by the blockade by the SERCA3 specific pharmacological inhibitor tBHQ that leads to Ca^{2+} leakage from SERCA3 dependent stores. Interestingly, these results are in agreement with the recent data obtained with SERCA3 deficient mice or after SERCA3 activity inhibition using tBHQ.[14] In mouse model, our group found that SERCA3 was

specifically targeting distinct Ca^{2+} stores, whose mobilization leads to a primary secretion of granules that could be specific dense granules as they contain ATP, ADP and serotonin.[14] Likewise, we have observed that extracellular ADP addition was able to restore normal platelet activity bypassing the inhibition due to lower SERCA3 activity. Thus, we can propose that similarly to what was described in mice, human platelet SERCA3 is controlling a specific Ca^{2+} store whose mobilization participates to a primary ADP secretion that synergizes with the main signaling pathways such as IP3 dependent signaling.

Importantly, our results show that the decrease of SERCA3 expression appears to be reversible, since weight loss after gastric bypass, restores SERCA3 expression and platelet functions. To our knowledge, this is the first reported human pathophysiological condition with associated platelet SERCA3 decreased expression. Variations in the SERCA3 gene (*ATP2A3*) have been previously reported in type 2 diabetes mellitus patients, but the effect of these variations on the expression of SERCA3 in pancreatic islets beta-cells is not known.[24] In our studied patients, as the decreased platelet SERCA3 expression is restored after weight loss, we can hypothesize that several acquired mechanisms might potentially regulated platelet SERCA3 expression. Endoplasmic reticulum (ER) stress has been shown to have an important role in the development of insulin resistance and diabetes in obesity.[25] Interestingly, in a mouse model, Fu *et al* have demonstrated that in the liver, obesity-induced alterations in ER fatty acid and lipid composition result in the inhibition of SERCA2b activity and ER stress.[26] Moreover, they showed that this ER stress is reversible and can be restored by correcting the obesity-induced alteration of ER phospholipid composition, or by *in vivo* hepatic SERCA overexpression and is associated to glucose homeostasis improvement. Based on these data, we can hypothesize that similar mechanisms could exist with human obesity-induced alterations in megakaryocytes ER and subsequent SERCA3 inhibition in platelets. Other studies also suggest that obesity-induced alterations in the milieu could modulate SERCA expression or activity: in a mouse model, obesity is associated with modification by oxidation of SERCA2a in cardiomyocytes.[27] Moreover, recent studies indicated that inflammation can affect cellular maturation of stem-like megakaryocyte progenitors. [28] Indeed, Haas *et al.,* described that inflammatory state results in subsequent rapid and efficiently production of platelets. This maturation process seems to allow both maturation and proliferation. Interestingly, it has been showed that SERCA3 expression is a late event during megakaryocyte maturation [29] and it is also well established that cell proliferation is associated to decreased expression of SERCA3 or SERCA2 in different cell lines.[30,31] In the context of inflammatory state such as severe obesity, Hass *et al* findings could explain several

observations: slight increase in platelet count and increased mean platelet volume often described in obese patients,[32] accelerated platelet turn-over which can explain resistance to antiplatelet agents in obesity [33] and of course, the decreased expression of SERCA3 we observe in our study.

In conclusion, our study shows that in platelets from severe obese patients, SERCA3 expression is decreased when compared to lean control subjects, with subsequent diminished calcium mobilization and associated platelet hyporeactivity. These changes are acquired, as they are restored after weight loss, but their pathophysiological significance is a new question to elucidate. An attractive hypothesis could be that this decrease in SERCA3 expression is a physiological response allowing lower platelet activability in order to limit spontaneous platelets activation in a context of pathological and prothrombotic conditions such as morbid obesity. Moreover, platelet SERCA3 decreased expression may have a clinical impact, as it can constitute a new key explaining the different response of obese patients to antiplatelet drugs.

Acknowledgments

Authors sincerely thank Corinne Garnier for excellent logistic support in patients' enrollment and follow-up scheduling, Maryse Lamotte and Brigitte Martel for taking care of the samples. They also greatly acknowledge the patients and controls who agreed to participate to the study. This work was supported by Grant CRC 10018 (Contrat de Recherche Clinique) from Assistance Publique–Hôpitaux de Paris.

Authorship Contributions

Contribution: A.S., R.B., D.P. and L.S. conceived and designed the study; M.C., F.T., D.P. and A.S. performed the inclusion and follow-up of patients; S.M. performed gastric bypass; A.S. performed clinical data collection; experiments were conceived by R.B. J.P.R. J.J.L. and Z.E. and performed by Z.E., J.J.L., A.K., Y.B., C.R., M.P. and R.B; results were analyzed by K.Z., R.B., A.S. and L.S.; A.S. and R.B. wrote the manuscript; Z.E., D.P., J.P.R., L.S., K.Z., A.S. and R.B. critically edited the manuscript.

Conflict of Interest Disclosures

The authors declared no conflict of interest.

References

1. Van Gaal LF, Mertens IL, De Block CE. Mechanisms linking obesity with cardiovascular disease. *Nature*. 2006;444(7121):875-80.

2. World Health Organization Fact Sheet N311. Obesity and overweight. 2013

3. WHO. Obesity: preventing and managing the global epidemic. Report of a WHO Consultation. WHO Technical Report Series 894. Geneva: World Health Organization, 2000.

4. Wolk R, Berger P, Lennon RJ, Brilakis ES, Somers VK. Body mass index: a risk factor for unstable angina and myocardial infarction in patients with angiographically confirmed coronary artery disease. *Circulation*. 2003;108:2206–2211.

5. Yusuf S, Hawken S, Ounpuu S, *et al*. Obesity and the risk of myocardial infarction in 27 000 participants from 52 countries: a case-control study. *Lancet*. 2005;366:1640–1649.

6. Rexrode KM, Hennekens CH, Willett WC, *et al*. A prospective study of body mass index, weight change, and risk of stroke in women. JAMA. 1997;27:1539–1545.

7. Suk SH, Sacco RL, Boden-Albala B, *et al*. Abdominal obesity and risk of ischemic stroke: the Northern Manhattan Stroke Study. *Stroke*. 2003;34:1586–1592.

8. Stein PD, Beemath A, Olson RE. Obesity as a risk factor in venous thromboembolism. *Am J Med*. 2005;118:978–980.

9. Parkin L, Sweetland S, Balkwill A, *et al*. Body mass index, surgery, and risk of venous thromboembolism in middle-aged women: a cohort study. *Circulation*. 2012;125:1897–1904.

10. Blokhin IO, Lentz SR. Mechanisms of thrombosis in obesity. Curr Opin Hematol. 2013 Sep;20(5):437-444.

11. Anfossi G, Russo I, Trovati M. Platelet dysfunction in central obesity. *Nutr Metab Cardiovasc Dis*. 2009;19(6):440-449.

12. Santilli F, Vazzana N, Liani R, Guagnano MT, Davì G. Platelet activation in obesity and metabolic syndrome. *Obes Rev*. 2012;13(1):27-42.

13. Santilli F, Simeone P, Liani R, Davì G. Platelets and diabetes mellitus. Prostaglandins Other Lipid Mediat. 2015;120:28-39.

14. Brini M, Carafoli E. Calcium pumps in health and disease. *Physiol Rev*. 2009;89:1341-1378.

15. Elaïb Z, Adam F, Berrou E *et al*. Full activation of mouse platelets requires ADP secretion regulated by SERCA3 ATPase-dependent calcium stores. *Blood*. 2016 Aug 25;128(8):1129-1138.

16. Alberti K, Zimmet P, Shaw J. The metabolic syndrome—a new worldwide definition. *Lancet.* 2005;366:1059-1062.

17. Kovàcs T, Corvazier E, Papp B *et al*. Controlled proteolysis of Ca(2+)-ATPases in human platelet and non-muscle cell membrane vesicles. Evidence for a multi-sarco/endoplasmic reticulum Ca(2+)-ATPase system. *J Biol Chem*. 1994;269(8):6177-6184.

18. Adam F, Khatib AM, Lopez JJ *et al*. Apelin: an antithrombotic factor that inhibits platelet function. *Blood*. 2016;127:908-920.

19. Sowers JR. Obesity as a cardiovascular risk factor. *Am J Med*. 2003;115 Suppl 8A:37S-41S.

20. Beavers CJ, Heron P, Smyth SS, Bain JA, Macaulay TE. Obesity and Antiplatelets-Does One Size Fit All? *Thromb Res*. 2015;136:712-716.

21. Angiolillo DJ, Fernández-Ortiz A, Bernardo E *et al*. Platelet aggregation according to body mass index in patients undergoing coronary stenting: should clopidogrel loading-dose be weight adjusted? *J Invasive Cardiol*. 2004;16(4):169-174.

22. Stepanian A, Bourguignat L, Hennou S *et al*. Microparticle increase in severe obesity: not related to metabolic syndrome and unchanged after massive weight loss. *Obesity* (Silver Spring). 2013;21(11):2236-2243.

23. Dellas C, Schäfer K, Rohm I, Lankeit M, Ellrott T, Faustin V. Absence of leptin resistance in platelets from morbidly obese individuals may contribute to the increased thrombosis risk in obesity. *Thromb Haemost* 2008;100:1123–1129.

24. Varadi A, Lebel L, Hashim Y, Mehta Z, Ashcroft SJ, Turner R. Sequence variants of the sarco(endo)plasmic reticulum Ca(2+)-transport ATPase 3 gene (SERCA3) in Caucasian type II diabetic patients (UK Prospective Diabetes Study 48). *Diabetologia*. 1999;42(10):1240-1243.

25. Hotamisligil GS. Endoplasmic reticulum stress and the inflammatory basis of metabolic disease. *Cell*. 2010;140:900–917.

26. Fu S, Yang L, Li P *et al*. Aberrant lipid metabolism disrupts calcium homeostasis causing liver endoplasmic reticulum stress in obesity. *Nature*. 2011;473(7348):528-531.

27. Li SY, Yang X, Ceylan-Isik AF, Du M, Sreejayan N, Ren J. Cardiac contractile dysfunction in Lep/Lep obesity is accompanied by NADPH oxidase activation, oxidative modification of sarco(endo)plasmic reticulum Ca2+-ATPase and myosin heavy chain isozyme switch. *Diabetologia*. 2006;49(6):1434-1446.

28. Haas S, Hansson J, Klimmeck D *et al*. Inflammation-Induced Emergency Megakaryopoiesis Driven by Hematopoietic Stem Cell-like Megakaryocyte Progenitors. *Cell Stem Cell*. 2015;17(4):422-434.

29. Nurden P, Debili N, Vainchenker W *et al.* Impaired megakaryocytopoiesis in type 2B von Willebrand disease with severe thrombocytopenia. *Blood* 2006, 108(8):2587-2595.

30. Mountian I, Manolopoulos VG, De Smedt H, Parys JB, Missiaen L, Wuytack F. Expression patterns of sarco/endoplasmic reticulum Ca(2+)-ATPase and inositol 1,4,5-

trisphosphate receptor isoforms in vascular endothelial cells. *Cell Calcium*. 1999;25(5):371-380.

31. Lipskaia L, Hulot JS, Lompré AM. Role of sarco/endoplasmic reticulum calcium content and calcium ATPase activity in the control of cell growth and proliferation. *Pflugers Arch*. 2009;457(3):673-685.

32. Raoux L, Moszkowicz D, Vychnevskaia K *et al*. Effect of Bariatric Surgery-Induced Weight Loss on Platelet Count and Mean Platelet Volume: a 12-Month Follow-Up Study. *Obes Surg*. 2017;27(2):387-393.

33. Angiolillo DJ, Fernandez-Ortiz A, Bernardo E *et al*. Variability in individual responsiveness to clopidogrel: clinical implications, management, and future perspectives. *J Am Coll Cardiol*. 2007;49(14):1505-1516.

Tables

Table 1. Demographic, medical and metabolic characteristics of the study population. All subjects are women. Data during follow-up were obtained *circa* one year after Gastric Bypass Surgery in obese patients and subsequently in control subjects, when possible.

	Baseline			Follow-up		
	Control subjects	Obese patients	*p*	Control subjects	Obese patients	*p*
	(n = 40)	(n = 40)		(n = 26)	(n = 32)	
Age (years)	35 [29 ; 42]	32.5 [27.6 ; 41.3]				
BMI (kg/m^2)	21 [20.0 ; 23.2]	42.6 [39.3 ; 47.5]	$< 10^{-4}$	21.2 [20 ; 22.3]	30 [25 ; 33.7]	$< 10^{-4}$
Waist circumference (cm)	73 [70 ; 78]	112 [108 ; 117]	$< 10^{-4}$	73.5 [69 ; 77]	88 [78 ; 92.5]	$< 10^{-4}$
Waist to hip ratio	0.78 [0.73 ; 0.80]	0.90 [0.82 ; 0.95]	$< 10^{-4}$	0.77 [0.74 ; 0.81]	0.80 [0.77 ; 0.84]	0.02
Blood pressure (mm Hg)						
- Systolic	120 [110 ; 120]	128 [121 ; 133]	$< 10^{-4}$	110 [110 ; 120]	120 [110 ; 122]	0.06
- Diastolic	80 [70 ; 80]	71 [66 ; 78]	0.004	80 [70 ; 80]	68 [61.5 ; 72]	0.0002
Blood lipids (mmol/L)						
- Total cholesterol	4.9 [4.4 ; 5.5]	5.1 [4.4 ; 5.8]	0.23	4.9 [4.6 ; 5.3]	4.3 [3.7 ; 4.6]	$< 10^{-3}$
- LDL-cholesterol	2.9 [2.3 ; 3.4]	3.3 [2.9 ; 3.9]	0.005	2.9 [2.5 ; 3.2]	1.5 [1.3 ; 1.7]	10^{-3}
- HDL-cholesterol	1.6 [1.4 ; 1.8]	1.2 [1.1 ; 1.3]	$< 10^{-4}$	1.7 [1.5 ; 1.9]	2.4 [2 ; 2.75]	0.0503
- Triglycerides	0.6 [0.4 ; 0.7]	1.1 [0.80 ; 1.39]	$< 10^{-4}$	0.6 [0.5 ; 0.6]	0.67 [0.50 ; 0.86]	0.17
Blood glucose (mmol/L)	4.7 [4.5 ; 4.9]	5.3 [4.9 ; 5.7]	$< 10^{-4}$	4.8 [4.4 ;5]	4.7 [4.4 ; 4.8]	0.20
Blood insulin (mIU/L)	6 [4.4 ; 9.2]	15.9 [10.2 ; 25.4]	$< 10^{-3}$	6.2 [5.3 ; 11.3]	6.5 [4.5 ; 9.1]	0.54
Blood glycated hemoglobin (%)	5.5 [5.3 ; 5.6]	5.8 [5.6 ; 6]	$< 10^{-4}$	5.2 [5.1 ; 5.4]	5.3 [5.2 ; 5.4]	0.71
Platelets (Giga/L)	231 [207 ; 263]	283 [257 ; 314]	10^{-4}	243 [193 ; 284]	261 [224 ; 300]	0.17
MPV (fL)	10.7 [10 ; 11.6]	10.9 [10.2 ; 11.3]	0.80	10.7 [7.8 ; 11.6]	10.9 [10.2 ; 11.3]	0.64
C-reactive protein (mg/L)	2 [1.5 ; 2]	13 [6 ; 18]	$< 10^{-4}$	2 [2 ; 2.8]	2 [2 ; 2]	0.10
Fibrinogen (g/L)	2.81 [2.48 ; 3.03]	3.97 [3.63 ; 4.33]	$< 10^{-4}$	2.8 [2.5 ; 3.3]	3.19 [2.73 ; 3.58]	0.02

Data are presented as number (%) or median and range between 25th and 75th percentiles. BMI: body mass index, MPV: mean platelet volume.

Figure Legends

Figure 1. Severe obesity is associated to a decreased platelet aggregation that is reversible after weight loss.

(**Fig. 1A**) Typical platelet aggregation curves in response to thrombin, observed between control (C1, black line) and obese patients (P1, gray line) at inclusion. Washed platelets were stimulated with 100 mU/mL of thrombin and recorded for aggregation for 4 min (the bar below tracings correspond to a time duration of 1 min). Aggregation intensities are expressed as percent of light transmitted, 100% corresponding to buffer alone. Note the lower aggregation rate of patient platelets. (**Fig. 1B**) Typical dose/response curve obtained in response to thrombin concentrations from 0.03 to 0.2 U/mL in control subjects (C1) and obese patients (P1) at inclusion. Percentages of aggregation were reported to determine the concentration necessary to induce 50% of aggregation (EC_{50}). (**Fig. 1C and 1D**) For each patient, thrombin EC_{50} was normalized to matched control. The figures display mean normalized EC_{50} (error bard represent standard error of mean) at the time of inclusion (n=18) (**Fig. 1C**) and after weight loss in obese patients (P2) compared to control subjects at second evaluation (C2) (n=30) (**Fig. 1D**). *** p=0.001; ns, non-significant (Wilcoxon's t test).

Figure 2. Obesity is associated to a decrease in platelet activation which is normalized after weight loss.

(**Fig. 2A**) Mean levels of basal P-Selectin expression (% positive cells ± SEM) of washed platelets from control subjects (C1, C2) or obese patients (P1, P2) analyzed using flow cytometry. Similarly, in control subjects (black square) and obese patients (white square), platelet activation was assessed by PAC-1 binding (% of fluorescence) in absence of calcium (EDTA), or after incubation with indicated concentration of thrombin. Each Value is displayed as percent of fluorescence compared to the level of fluorescence measured in control platelets in response to thrombin 100 mU/mL, taken as 100%. This analysis was performed at inclusion (n=18) (**Fig. 2B**) and after weight loss in obese patients (n=22) (**Fig. 2C**). *p=0.002; **p=0.003; ns, non-significant (Wilcoxon's test).

Figure 3. Severe obesity is associated to a decrease in calcium mobilization to thrombin that is normalized after weight loss.

(**Fig. 3A**) Ca^{2+} mobilization was assessed in unstirred control (C1, black tracings) and obese patients (P1, gray tracings) platelets after stimulation with 100 mU/mL thrombin by flow cytometry in absence of external Ca^{2+} (100 µM EGTA) using the cytosolic Ca^{2+} fluorescent

probe Oregon-Green-BAPTA-AM. Typical curves obtained at inclusion and after weight loss in obese patients are displayed on the left and right panels, respectively. Ca^{2+} mobilization measurements (area under the curve (AUC) for 2 min) of control subjects and obese patients, at inclusion (C1 and P1 respectively, n=35) and after weight loss in obese patients (C2 and P2 respectively, n=31) are presented either as dot plots of all measurements (**Fig. 3B**) or as the percentage of the value obtained for the matched control (**Fig. 3C**). Three minutes after thrombin stimulation, extracellular Ca^{2+} (300 µM) was added to compare Ca^{2+} influx and similarly, Ca^{2+} influx measurement (AUC for 2 min) of control subjects and obese patients, at inclusion (C1 and P1 respectively, n=31) and after weight loss in obese patients (C2 and P2 respectively, n=27) are presented either as dot plots of all measurements (**Fig. 3D**) or as the percentage of the value obtained for the matched control (**Fig. 3E**). Figures 3B and 3D: **** $p<10^{-4}$; ns, non-significant (Mann-Whitney's test, with obese patients and control subjects compared as matched pairs). Figures 3C and 3E: ns, non-significant (Wilcoxon's test).

Figure 4. Severe obesity is associated to low expression of SERCA3 that is upregulated after weight loss.

(**Fig. 4A**) SERCA3 expression analyzes were performed using pan SERCA3 PL/IM430 antibody in platelet lysates in control subjects (C1) and obese patients (P1) at inclusion and after weight loss in patients (P2) – i.e. one year after Roux-en-Y Bypass surgery –and concomitant controls follow-up (C2). (**Fig. 4B**) Protein levels were assessed by 14-3-3□ expression and results are displayed as normalized ratio intensity for SERCA3 over 14-3-3□ expression. (**Fig. 4C**) SERCA3 dependent Ca^{2+} store content was depleted using SERCA3 inhibitor tBHQ (10 µM) and calcium increase in cytosol was measured by flow cytometry using the cytosolic Ca^{2+} fluorescent probe Oregon-Green-BAPTA-AM. Ca^{2+} leak due to SERCA3 inhibition in platelets from control subjects and obese patients at inclusion (C1 and P1 respectively, n=25) and after weight loss in obese patients (C2 and P2 respectively, n=25) are presented as the percentage of the value obtained for the matched control. **** $p<10^{-4}$; ns, non-significant (Wilcoxon's test).

Figure 5. Inhibition of SERCA3 activity inhibits ADP dependent platelet activation.

(**Fig. 5A**) Washed control platelets were or not pretreated with tBHQ (10 µM) for 8 min (SERCA3 specific pharmacological inhibitor) before stimulation with 40 mU/mL of thrombin in presence or not of ADP (10 µM) and recorded for aggregation for 4 min (the bar below

tracings correspond to a time of 1 min). (**Fig. 5B**) Secretion of control or tBHQ pretreated platelets stimulated with either 40 mU/mL of thrombin, 10 µM of ADP or combination of both were assessed by ATP measurement in the supernatant. Results are expressed as mean ± SEM (n=6). Typical Ca^{2+} mobilization curves, observed in unstirred control platelets in response to 5 µM tBHQ or 0.01% EtOH followed by stimulation with 40 mU/mL of thrombin (**Fig. 5C**) or in response to 10 µM tBHQ followed by stimulation with 40 mU/mL of thrombin in presence or in absence of 10 µM ADP (**Fig. 5D**). Ca^{2+} mobilizations in patients were compared as area under the curve (**Fig. 5E**). Results are expressed as mean ± SEM (n=3).

Figure 6. Severe obesity is associated to decreased platelet secretion that is normalized by ADP addition.

(**Fig. 6A**) Secretion was assessed by ATP measurement in the supernatant of control (C1, black square) or obese patients (P1, white square) platelets pretreated or not with 10 µM tBHQ (SERCA3 specific pharmacological inhibitor) and stimulated with 40 mU/mL of thrombin in combination or not of 10 µM ADP. (**Fig. 6B**) Washed control (C1, black tracings) or obese patients (P1, gray tracings) platelet were or not pretreated with tBHQ (10 µM) for 8 min before stimulation with 40 mU/mL of thrombin in presence or not of ADP (10 µM) and recorded for aggregation for 3 min (the bar below tracings corresponds to a time of 1min). (**Fig. 6C**) Typical Ca^{2+} mobilization curves, observed in control subjects (C1, black tracings) or obese patients (P1, gray tracings) platelets in response to 40 mU/mL of thrombin in presence or in absence of 10 µM ADP. Results are expressed as mean ± SEM (n=5). ***p*=0.008; ns, non-significant (Wilcoxon's test).

Figure 1

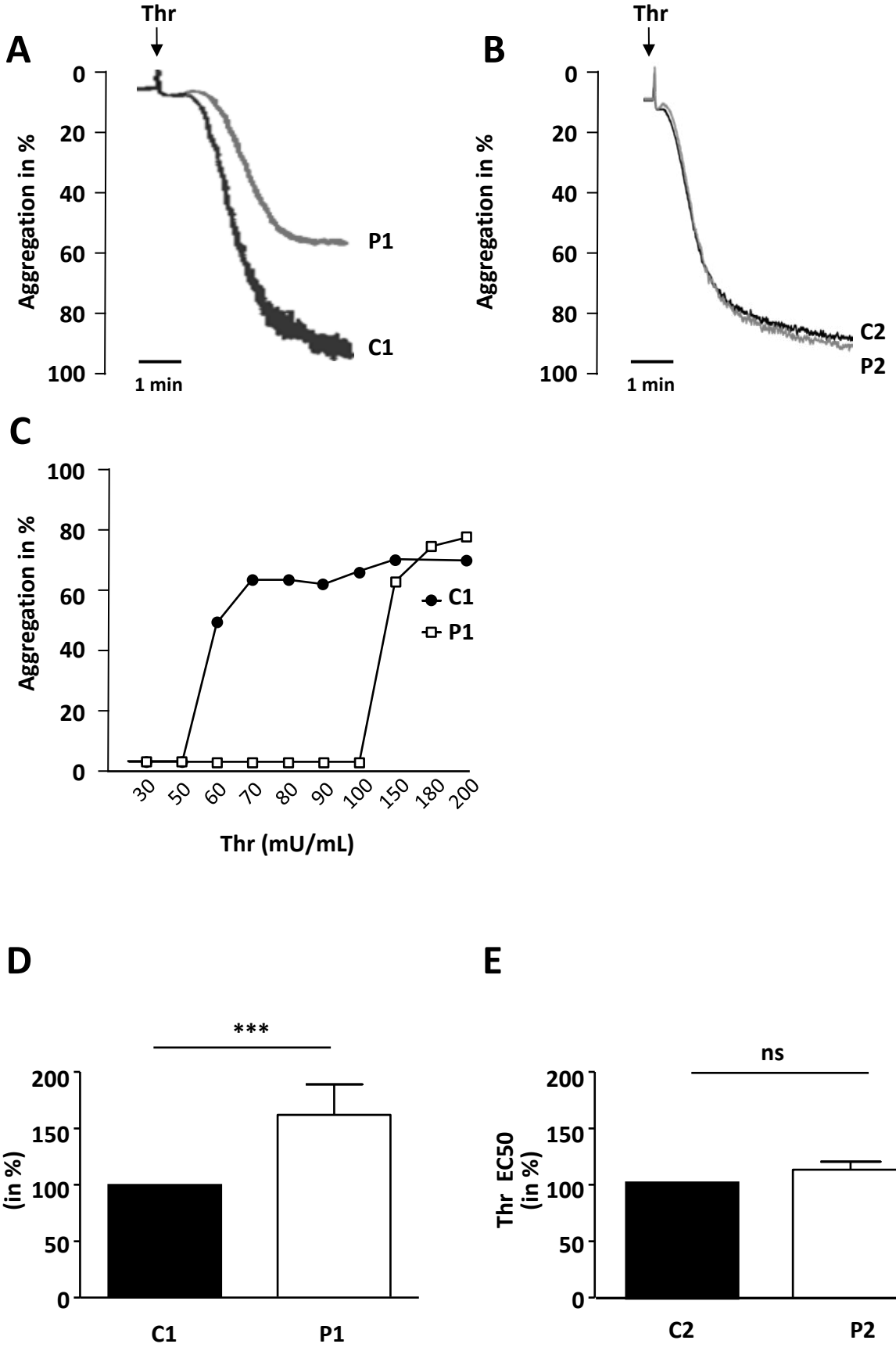
A
Thr
Aggregation in %
0
20
40
60
80
100
P1
C1
1 min
B
Thr
Aggregation in %
0
20
40
60
80
100
C2
P2
1 min
C
Aggregation in %
100
80
60
40
20
0
C1
P1
30
50
60
70
80
90
100
150
180
200
Thr (mU/mL)
D
***
Thr EC50 (in %)
200
150
100
50
0
C1
P1
E
ns
Thr EC50 (in %)
200
150
100
50
0
C2
P2

Figure 2

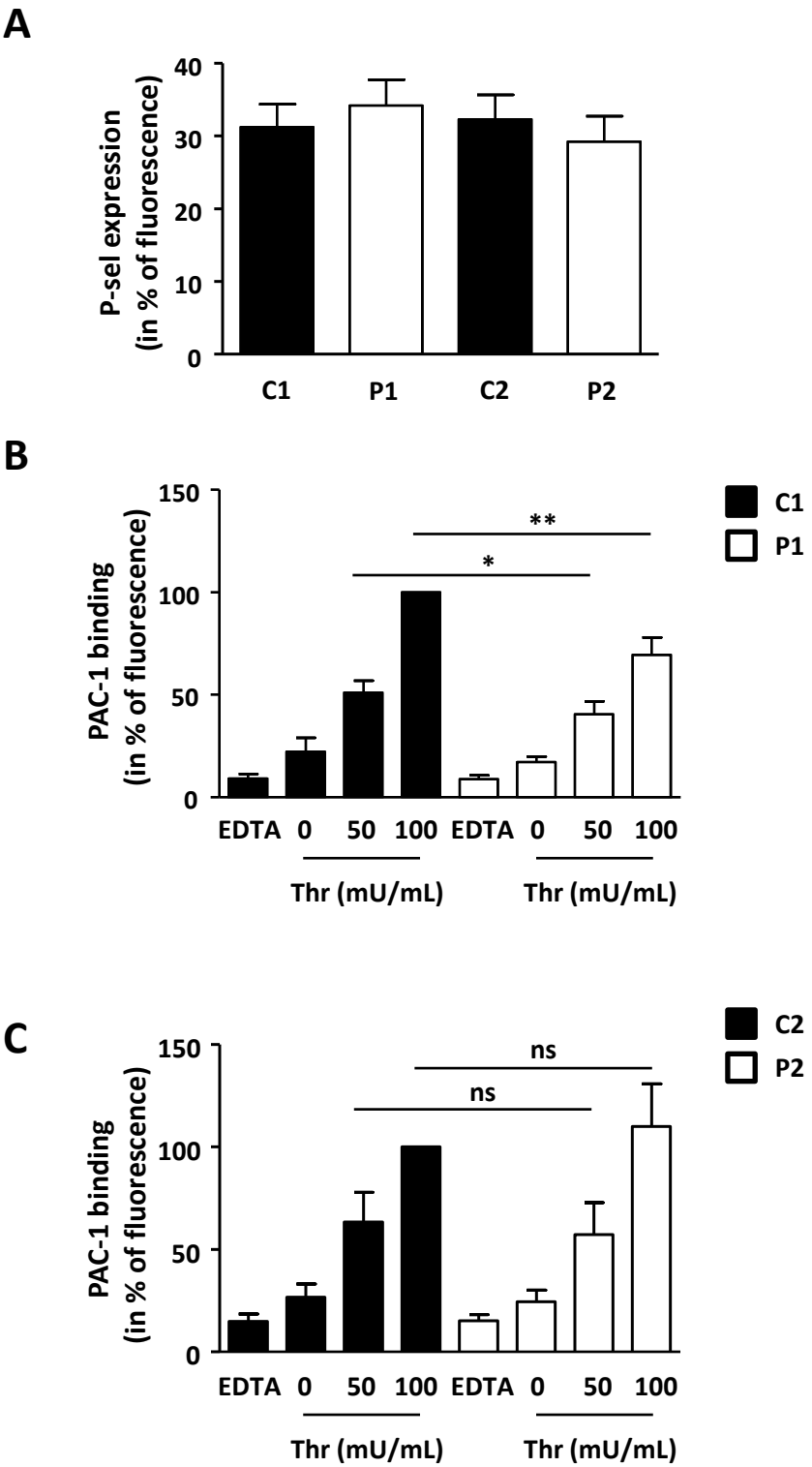
A
P-sel expression (in % of fluorescence)
40
30
20
10
0
C1
P1
C2
P2
B
PAC-1 binding (in % of fluorescence)
150
100
50
0
**
*
C1
P1
EDTA 0 50 100 EDTA 0 50 100
Thr (mU/mL)
Thr (mU/mL)
C
PAC-1 binding (in % of fluorescence)
150
100
50
0
ns
ns
C2
P2
EDTA 0 50 100 EDTA 0 50 100
Thr (mU/mL)
Thr (mU/mL)

Figure 3

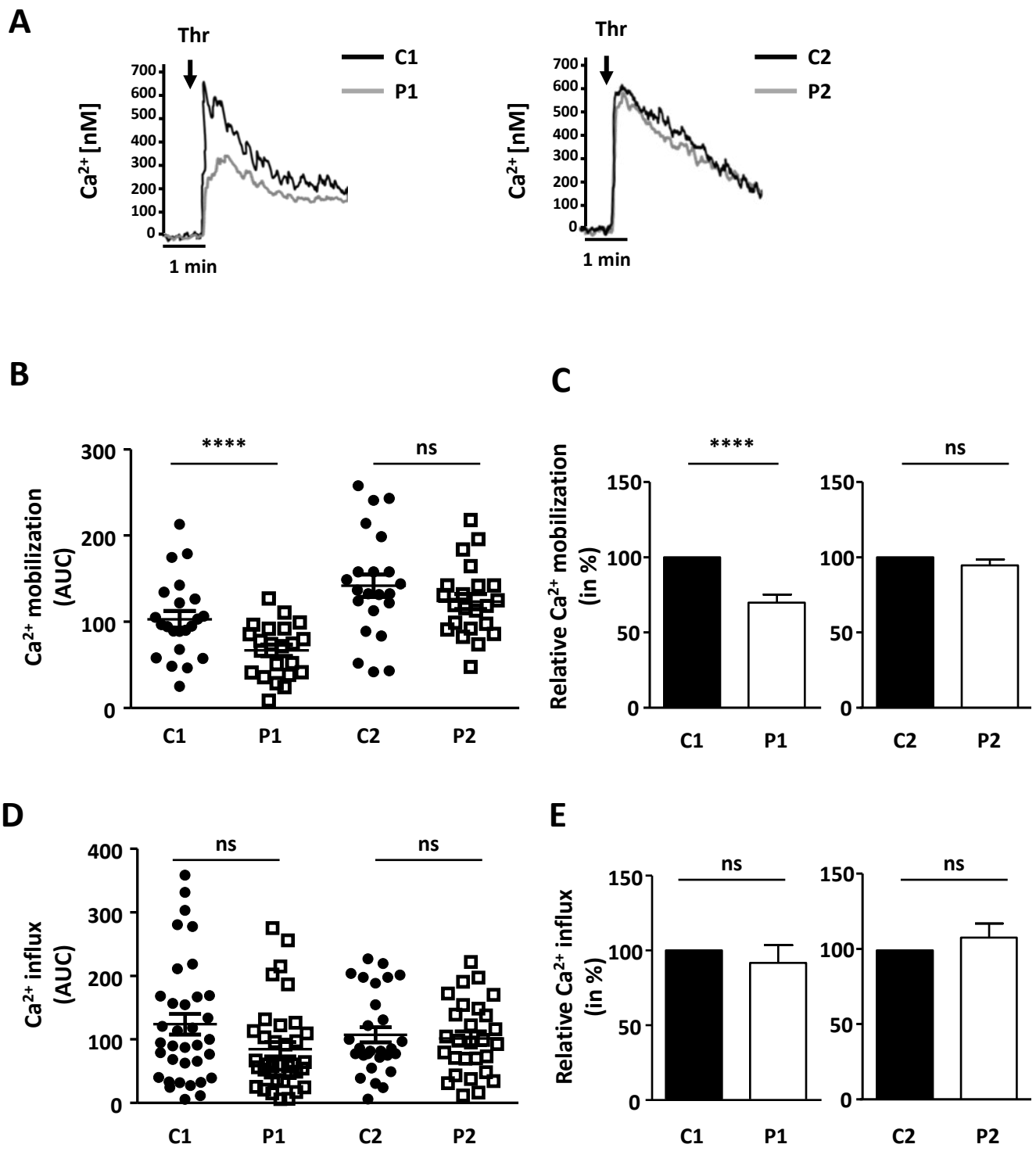
A
Thr
C1
P1
Ca2+ [nM]
700
600
500
400
300
200
100
0
1 min
Thr
C2
P2
Ca2+ [nM]
700
600
500
400
300
200
100
0
1 min
B
****
ns
Ca2+ mobilization (AUC)
300
200
100
0
C1
P1
C2
P2
C
****
ns
Relative Ca2+ mobilization (in %)
150
100
50
0
C1
P1
150
100
50
0
C2
P2
D
ns
ns
Ca2+ influx (AUC)
400
300
200
100
0
C1
P1
C2
P2
E
ns
ns
Relative Ca2+ influx (in %)
150
100
50
0
C1
P1
150
100
50
0
C2
P2

Figure 4

A

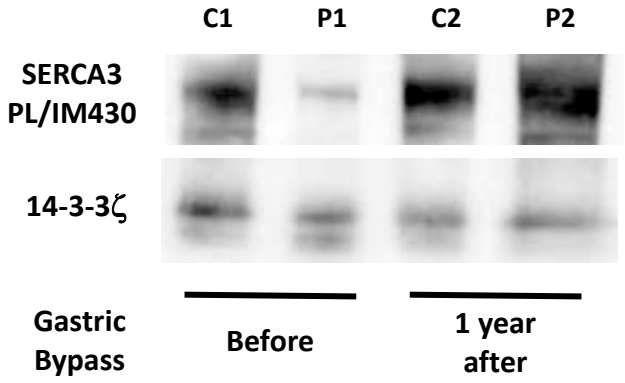
C1
P1
C2
P2
SERCA3
PL/IM430
14-3-3ζ
Gastric
Bypass
Before
1 year
after

B

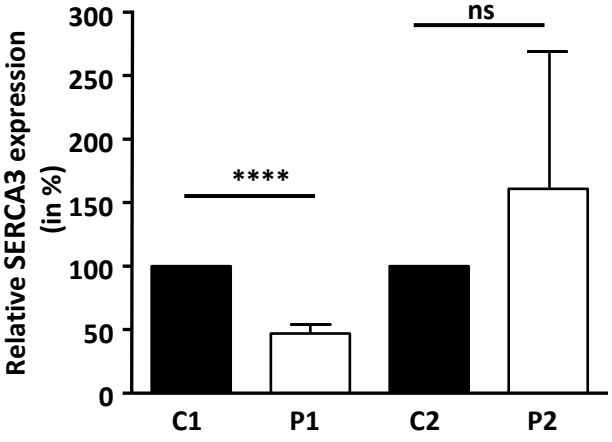
Relative SERCA3 expression
(in %)
300
250
200
150
100
50
0
****
ns
C1
P1
C2
P2

C

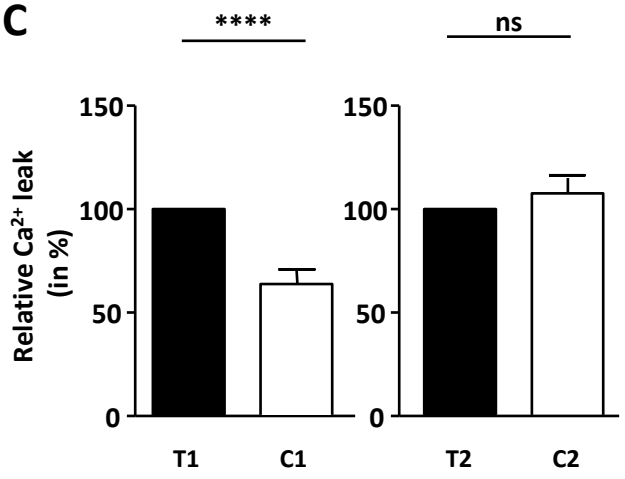
Relative Ca2+ leak
(in %)
150
100
50
0
****
ns
T1
C1
T2
C2

Figure 5

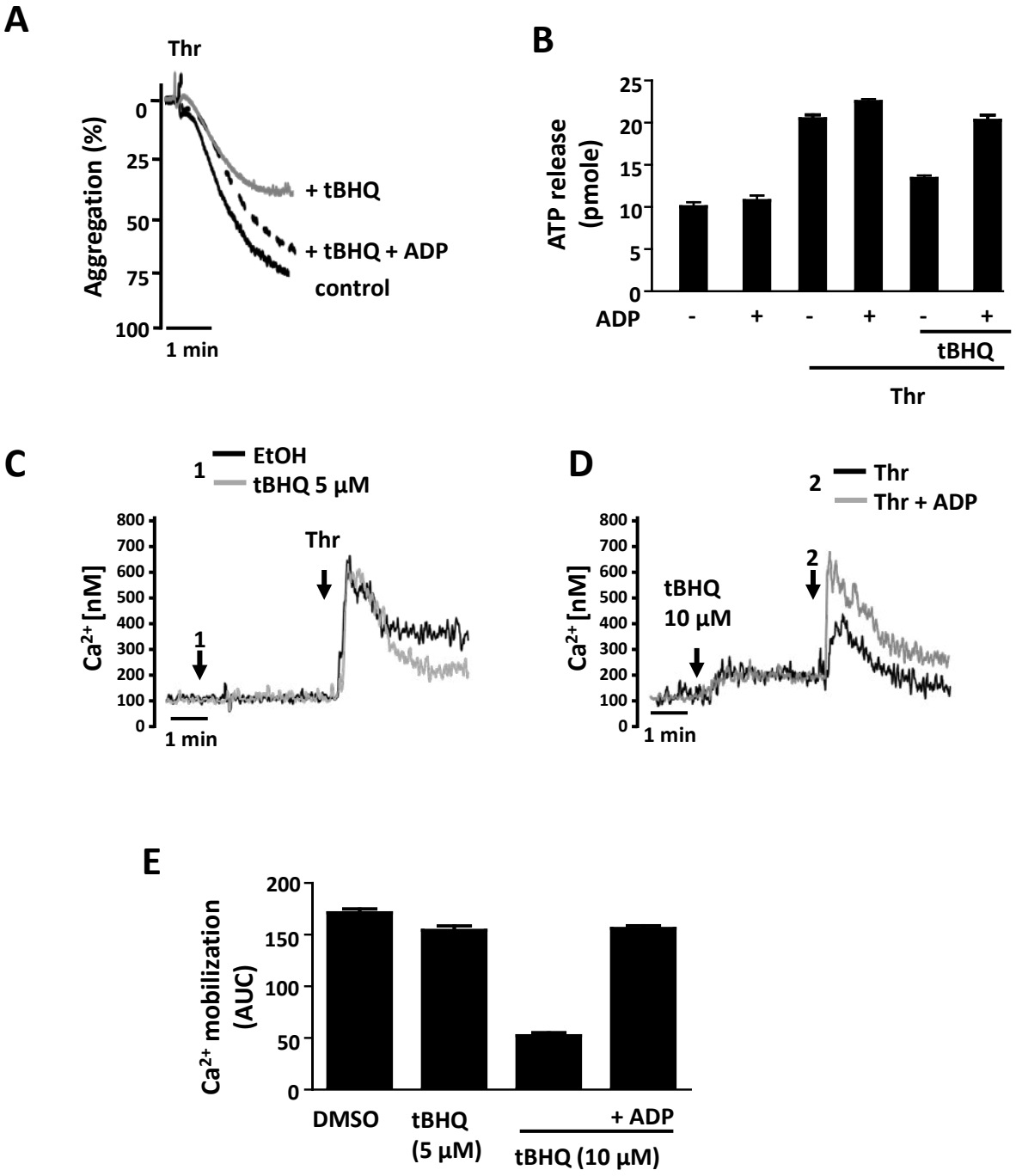
A
Thr
Aggregation (%)
0
25
50
75
100
+ tBHQ
+ tBHQ + ADP
control
1 min
B
ATP release (pmole)
25
20
15
10
5
0
ADP
-
+
-
+
-
+
tBHQ
Thr
C
1
EtOH
tBHQ 5 µM
Ca2+ [nM]
800
700
600
500
400
300
200
100
0
Thr
1
1 min
D
2
Thr
Thr + ADP
tBHQ
10 µM
2
1 min
E
Ca2+ mobilization (AUC)
200
150
100
50
0
DMSO
tBHQ (5 µM)
+ ADP
tBHQ (10 µM)

Figure 6

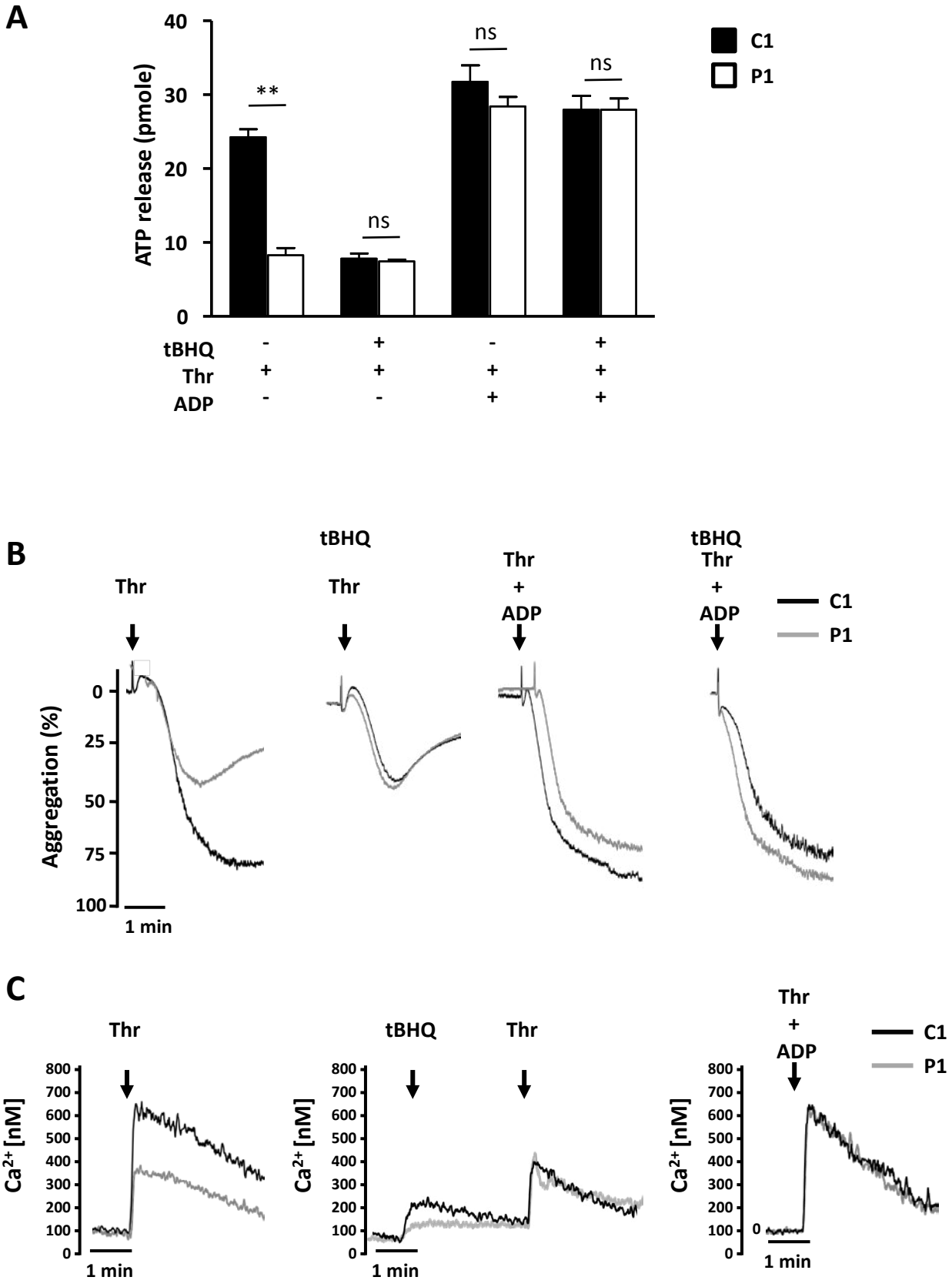
A
ATP release (pmole)
40
30
20
10
0
**
ns
ns
ns
C1
P1
tBHQ - + - +
Thr + + + +
ADP - - + +
B
Thr
tBHQ
Thr
Thr + ADP
tBHQ Thr + ADP
C1
P1
Aggregation (%)
0
25
50
75
100
1 min
C
Thr
tBHQ
Thr
Thr + ADP
C1
P1
Ca2+ [nM]
800
700
600
500
400
300
200
100
0
1 min

Article III

La sécrétion initiale d'ADP plaquettaire dépend de SERCA3 et du NAADP

Dans les travaux précédents, nous avons montré que les souris SERCA3$^{-/-}$ présentaient un défaut de l'hémostase et une résistance a la thrombose dû à un déficit de sécrétion granulaire dense, entrainant une diminution des fonctions plaquettaires. Nous avons postulé que SERCA3 contrôlait de façon spécifique une voie de sécrétion initiale d'ADP capable d'agir en synergie avec un faible stimulus de la plaquette (thrombine ou collagène à faibles concentrations), aboutissant à un renforcement de la sécrétion et de l'agrégation.

J'ai cherché à comprendre quel était le lien entre sécrétion (supposée rapide, mais non démontrée) et SERCA3. En me basant sur les études anciennes de localisation par microscopie électronique, et aussi de l'imagerie confocale (voir figure19) montrant une localisation périphérique de SERCA3 (248), j'ai pensé que les réserves calciques SERCA3 était proches de la membrane plasmique, et j'ai exploité une sonde calcique fluorescente ratiométrique, FURA2-NearMem-AM (Fura-2-NM), qui mesure spécifiquement le Ca^{2+} cytosolique juxta-membranaire: j'ai découvert, à l'aide des plaquettes SERCA3$^{-/-}$ que Fura-2-NM détectait uniquement le Ca^{2+} mobilisé à partir des réserves SERCA3, et pas des réserves SERCA2b. J'ai émis l'hypothèse que la voie de sécrétion initiale d'ADP devait *a priori* être indépendante de l'ADP lui-même et c'est effectivement ce que j'ai pu observer. Pour approfondir la caractérisation de la voie de mobilisation dépendante SERCA3, j'ai analysé les seconds messagers impliqués dans la mobilisation calcique, l'inositol tris-phosphate (IP3), le plus connu (et qui libère le Ca^{2+} à partir des réserves dépendantes de SERCA2b) et l'acide nicotinique dinucléotide phosphate (NAADP). De façon très intéressante, la mobilisation SERCA3 semble ne pas être activée par IP3. En effet, nous avons trouvé, que l'inhibition pharmacologique de la production d'IP3 avec le U73122 affecte uniquement les réserves SERCA2b et pas les réserves SERCA3. Surtout, j'ai pu montrer en utilisant soit l'antagoniste de la voie NAADP (Ned19) soit son mimétique, le NAADP-AM, que les réserves SERCA3 étaient mobilisables par le NAADP.

Je me suis également attaché à mesurer directement la sécrétion d'ADP (et non pas d'ATP, utilisé jusque-là, mais non impliqué fonctionnellement). J'ai ensuite analysé la cinétique de sécrétion d'ADP et d'ATP, et montré qu'elle était détectable dès 5 secondes après stimulation par la thrombine (40 mU/mL), mais absente dans les plaquettes SERCA3$^{-/-}$, ou après inhibition

de SERCA3 par tBHQ, mais n'était pas inhibée par TG. Ces résultats démontrent directement l'existence d'une sécrétion rapide (moins de 5 secondes) dépendante de SERCA3. Cette sécrétion initiale s'est avérée sensible au NED19 et insensible à l'inhibition de la production de l'IP3, suggérant fortement une voie rapide de sécrétion d'ADP contrôlée par NAADP et SERCA3.

Mais la mobilisation calcique n'est pas suffisante pour activer des plaquettes, il faut en général une activation de signalisation, notamment des PKCs, opérée par le diacylglycérol, en plus de Ca^{2+}.

Les expériences menées avec le NAADP-AM montrent que la mobilisation de Ca^{2+} induite par le NAADP seul n'induisait pas la sécrétion d'ATP. Mais, en présence d'OAG, un analogue du DAG, la sécrétion a été induite par NAADP-AM ce qui suggère que la sécrétion primaire d'ADP dépend à la fois de la mobilisation du Ca^{2+} depuis les réserves SERCA3 par NAADP, mais aussi du DAG libéré par PLCs.

En conclusion, nous avons mis en évidence une nouvelle voie de signalisation indispensable pour l'activation complète des plaquettes. Cette voie de signalisation implique la mobilisation des réserves contrôlées par SERCA3 de façon indépendante de l'IP3 mais dépendante du NAADP et spécifiquement engagée dans la libération précoce d'ADP lors de l'activation plaquettaire. C'est l'objet de mon 3ème manuscrit, ci-joint et en préparation.

NAADP mediates primary SERCA3-dependent ADP secretion in platelets.

NAADP mediates SERCA3-dependent Ca^{2+} signaling and the primary ADP secretion of platelets.

Ziane Elaïb,[1] Miao Feng,[1] Marijke Bryckaert,[1] Jean-Philippe Rosa[1¶] and Régis Bobe [1¶]

Affiliations

[1]INSERM UMR_S 1176; Univ. Paris-Sud ; Université Paris-Saclay, France.

¶ J.-P.R. and R.B. equally contributed to this work

Abstract: 241 words; Text : 4000 words; 6 figures; 1 table; XX references

Correspondence: Jean-Philippe Rosa, M.D. PhD

INSERM U1176, Hôpital Bicêtre, 82 rue du Général Leclerc, 94276 Le Kremlin Bicêtre Cedex, France.

Email: jean-philippe.rosa@inserm.fr

Tel: +33 149595636; Fax: +33 146719472

Running title: NAADP and SERCA3-dependent activation pathway.

Key Points: Early SERCA3-dependent ADP secretion pathway is elicited by NAADP and not IP3.

Abstract 246

We have recently demonstrated that weak platelet stimulation requiring ADP secretion is dependent upon a signaling pathway specifically involving calcium (Ca^{2+}) mobilization from internal stores controlled by the sarco-endoplasmic reticulum Ca^{2+} ATPase type 3 (SERCA3) but not by stores controlled by SERCA2b (Elaib et al, Blood 2016;128(8):1129-1138). This secretory pathway is triggered by agonists such as thrombin or collagen, but not by ADP, and can be by-passed by exogenous ADP. Here, we demonstrate that SERCA3-controlled ADP secretion is detectable as early as 5s following platelet stimulation, SERCA2b-dependent secretion being delayed to 10s. We show that only SERCA3- and not SERCA2b-dependent Ca^{2+} mobilization is detectable by the Ca^{2+} probe Fura-2-NM, which is specific for intracellular Ca^{2+} proximal to peripheral membranes and that SERCA2b and SERCA3-dependent mobilizations were controlled by two distinct pathways. SERCA2b-dependent Ca^{2+} is mobilized by inositol-1,4,5-trisphosphate (IP3) downstream of phospholipase-C (PLC) activation, while SERCA3-dependent Ca^{2+} mobilization and primary dense granule secretion are unaffected by the PLC inhibitor U73122, suggesting that SERCA3 Ca^{2+} stores are not depleted by IP3. In contrast, the second messenger nicotinic acid adenosine dinucleotide phosphate (NAADP) appeared to specifically mobilize SERCA3 (but not SERCA2b)-dependent Ca^{2+} stores, since blocked by the NAADP receptor antagonist Ned-19 or conversely, triggered by exogenous NAADP-AM. Moreover NAADP-AM was able to promote ADP secretion when added 1-Oleoyl-2-acetyl-*sn*-glycerol (OAG), a diacylglycerol analog. We thus conclude that primary platelet ADP secretion is controlled by a SERCA3-dependent signaling pathway regulated by NAADP and not by IP3, driving early dense granule secretion.

Introduction

Among regulatory mechanisms of Ca^{2+} intracellular signaling in platelets, the sarco-endoplasmic Ca^{2+}ATPases (SERCAs) which pump Ca^{2+} into intracellular stores are particularly relevant.[1] SERCAs are encoded by 3 genes, *ATP2A1*, *ATP2A2* and *ATP2A3*, which produce several alternate transcripts and protein isoforms: SERCA1a/b, SERCA2a-c, and SERCA3a-f. They are found in multiple tissues, but platelets exhibit only SERCA2b and SERCA3 isoforms.[2-4] SERCAs maintain a Ca^{2+} concentration gradient between the cytosol (100nM) and the ER (1mM), requiring degradation of ATP[5] into ADP then released into the cytosol.[6]

SERCA enzymes share similar structures with distinct intrinsic activities: higher Ca^{2+} affinity for SERCA2b than for SERCA3 ($K_{1/2}$~ 0.27 µM versus 1 µM) but a lower Ca^{2+} uptake (7 nmol/min/mg of protein versus 21 nmol/min/mg)[7,8] allowing cytosolic Ca^{2+} to be maintained at low levels in the resting cells.[9]

Pathologies and mouse models provide insight into SERCA2b and SERCA3 functions. Mutations in the human *ATP2A2* gene affecting SERCA2, lead to the Darier's syndrome in humans, a dermatological syndrome.[10,11] SERCA mutations are associated with some cancers,[12-14] suggesting involvement in cell differentiation.[15] SERCA3 human mutations seem associated with type II diabetes.[16] Mouse SERCA2 knockouts are not viable at the homozygous state, but heterozygotes exhibit SERCA2a- (defect in heart contractility and relaxation)[17] and SERCA2b-type defects, evocative of the Darier's syndrome.[18] Mouse SERCA3 knockouts exhibit no phenotypic alterations,[19] except for an altered gustatory nerve response.[20] Impaired relaxation of SERCA3$^{-/-}$ aorta rings was reported, with defective relaxation of vascular smooth muscle cells, altered Ca^{2+} signaling and low NO production.[19] *In vitro*, low insulin secretion and altered Ca^{2+} oscillations were reported.[21-23] Altogether these results point to a potential specific role for SERCA3 in Ca^{2+} signal modulation.

Among other differences in platelets is topology, as suggested by immuno-electron microscopy studies: peripheral for SERCA3, more central for SERCA2b.[24] Functional differentiation includes, based on pharmacological studies, the specific association of SERCA3 with acidic Ca^{2+} stores,[25] as well as with,

physically or functionally, STIM1, the Ca^{2+} sensor of store operated Ca^{2+} entry (SOCE) during which SERCA3 achieves Ca^{2+} stores replenishing.[26] We have recently reported that SERCA3-dependent and not SERCA2b-dependent Ca^{2+} stores are involved in a dense granule secretory pathway important for weak agonist platelet stimulation.[27] Here we show that ADP secretion dependent on SERCA3 Ca^{2+} stores is an early secretory pathway triggered within seconds following activation, and is dependent upon the Ca^{2+} mobilization second messenger NAADP, and not inositol-3-phosphate (IP3), which in turn triggers a later secretory pathway dependent on SERCA2b Ca^{2+} stores.

Material and Methods

Material

Fibrillar collagen (equine type I) and adenosine 5'-diphosphate (ADP) were obtained from Kordia (Leiden, The Netherlands). Apyrase (grade VII), rhodamine 6G, bovine thrombin, ferric chloride, indomethacin, the SERCA inhibitors thapsigargin, 2,5-dinucleotide-(tert-butyl)-1,4-benzohydroquinone (tBHQ) and the Phospholipase inhibitors U73122 were obtained from Sigma (St Louis, MO). We purchased d-Phe-Pro-Arg chloromethylketone dihydrochloride (PPACK) from Calbiochem-VWR (Fontenay-sous-Bois, France). Alexa Fluor 488-labeled phalloidin was from Invitrogen (Cergy Pontoise, France). Phycoerythrin (PE)-labeled rat anti-mouse integrin $\alpha_{IIb}\beta_3$ mAb (JON/A), fluorescein isothiocyanate (FITC)-labeled rat anti-mouse CD62P (P-selectin) mAb (Wug.E9) and purified rat anti-mouse integrin $\alpha_{IIb}\beta_3$ mAb (Leo.H4) were from Emfret Analytics (Würzburg, Germany). Oregon Green 488 BAPTA1-AM and Fura2-AM were from was from Molecular Probes (Eugene, OR). Fura2-NearMembrane-AM was from Teflabs (Sunnyvale, CA, USA). The NAADP antagonist Ned-19 was from Tocris (Bristol, UK). ADP kit and NAADP-AM were from Abcam (Cambridge, UK). Polyclonal antibodies specific for SERCA2b[28] and for SERCA3 (N89)[29] were generous gifts from Pr F. Wuytack (Katholieke Universiteit Leuven, Leuven, Belgium). The antibody directed against 14-3-3ζ was obtained from Santa Cruz Biotechnology (Santa Cruz, CA).

SERCA3 knockout mice

The swiss black SERCA3$^{-/-}$ mice originally generated by Dr G.E. Shull (University of Cincinatti, OH)[19] were crossed with C57BL/6 mice and kindly provided by Dr P. Gilon (University of Louvain, Belgium) with the authorization of Dr G.E. Shull. Wild-type litter mate mice were provided as well, and served as controls. Transferred wt/- heterozygous mice were intercrossed and homozygotes were detected by PCR, using published oligonucleotide primers.[19] All experimental procedures were carried out in accordance with the European legislation concerning the use of laboratory animals and approved by the Animal Care and Ethical Committee of Université Paris-Sud (agreement # 00243-02).

Assay of cytosolic calcium by flow cytometry)

Mouse platelets (3 x 10^7 platelets/mL) were loaded with the Ca^{2+}-sensitive dye Oregon Green 488 BAPTA1-AM (1mM) for 45 minutes at 20°C. Ca^{2+} mobilization induced by thrombin was analyzed in Ca^{2+} free medium and in the presence of 0.5mM EGTA using an Accuri C6 flow cytometer. Changes in Ca^{2+} signal intensity were calculated as the ratios of fluorescence of activated over non-activated platelets and the area below the curve for 2 minutes after agonist addition was chosen as an indicator of the Ca^{2+} response.

Assay of cytosolic calcium by video-microscopy.

Mouse platelets (3 x 10^8 platelets/mL) were immobilized onto glass coverslips pre-treated with poly-Lysine (100µg/mL). Platelets were then incubated at room temperature for 30 min with either Fura-2-AM (Fura-2) or Fura-2-NearMembrane-AM (Fura-2-NM) at 100 nM. Then, washed platelets were stimulated with thrombin (40 mU/mL) and fluorescence immediately recorded by epifluorescence microscope (Nikon Eclipse TE2000-U). Excitation wavelengths were 340 and 380 nm for ratio-metric measurements for both probes, and emission fluorescence was captured at 510nm.

Statistical analysis

Statistical significance was evaluated with the Student *t* tests or 1-way ANOVA followed by Tukey pair wise test as indicated, using GraphPad Prism (San Diego, CA).

Results

SERCA3-controlled ADP secretion sets off rapidly and before SERCA2b

Our first observation[27] showed that a SERCA3-dependent dense granule secretion pathway amplifies low agonist platelet stimulation. This pathway most likely involved ADP, based on its suppression by apyrase scavenging, and also since ADP addition to thrombin was able to bypass the absence of SERCA3 in platelets from SERCA3 deficient ($SERCA3^{-/-}$) mice. However SERCA3-dependent ADP secretion is secondary to thrombin activation: we wondered what was the extent of the delay between thrombin activation and ADP co-stimulatory effect (Figure 1A). Interestingly, exogenous ADP restored secretion in $SERCA3^{-/-}$ platelets to the level of wild type (WT) platelets only within the first 5 seconds following thrombin stimulation. After 10, 20 or 30 seconds of thrombin stimulation of $SERCA3^{-/-}$ platelets, no restoration of secretion was obtained by addition of exogenous ADP. Similar results were obtained for Ca^{2+} mobilization, P-selectin expression and αIIbβ3 activation (supplemental Figure 1A-C).

These results suggest that SERCA3 dependent primary ADP secretion most likely occurs within the first 5 seconds following thrombin stimulation. To show evidence of this early secretion, we directly assessed the kinetics of secretion of ADP since directly involved functionally, putatively. After thrombin stimulation, ADP was detected in the supernatant of $SERCA3^{-/-}$ mouse platelets to roughly half the level of WT platelets (Figure 1B), a ratio comparable to ATP (Figure 1C). Importantly, ADP was detectable in WT platelets as early as 5 seconds after thrombin stimulation, while not detected at all in $SERCA3^{-/-}$ platelets (Figure 1D). At 10 seconds, ADP secretion augmented in WT platelets and started rising in $SERCA3^{-/-}$ platelets. After 3 minutes, ADP secretion rose to its maximal level in WT platelets, reaching only half that level in $SERCA3^{-/-}$ platelets. The same kinetics was seen for ATP (Figure 1E; supplemental Figure 2A-B), showing co-secretion of both molecules, favoring the hypothesis of early dense granule secretion. Finally, confirming functional involvement of SERCA3 in early secretion, platelet pretreatment with tBHQ, a SERCA3-specific pharmacological inhibitor, suppressed early secretion at 5 seconds (as assessed by ATP, Fig 1E) of WT platelets which displayed a similar pattern of secretion than $SERCA3^{-/-}$ platelets up to 180s. We concluded that within the 5 seconds following platelet stimulation by thrombin,

ADP and ATP secretion was exclusively dependent on SERCA3 while SERCA3-independent secretion (presumably SERCA2b-dependent) set off at 10 seconds.

Altogether these results are consistent with SERCA3-dependent early ADP secretion taking place early enough to costimulate platelets within the first 5 seconds of thrombin activation.

SERCA3-dependent Ca^{2+} mobilization is proximal to platelet membrane.

Because early ADP secretion is dependent on SERCA3, SERCA3 Ca^{2+} stores mobilization should correlate with ADP secretion kinetics. Because of this time constraint we decided to use the ratiometric fluorescent probe Fura-2 that allows rapid, accurate and quantitative assessment of Ca^{2+} fluxes in the cytosol under videomicroscopy.[30] In addition, because of the likely differential subcellular localization of SERCA3 and SERCA2b,([24,25] and unpublished results) we tested the Fura-2-NearMembrane-AM probe (Fura-2-NM), a derivative of the cytosolic Fura-2-AM probe (Fura-2) but that localizes to the inner leaflet of membranes and selectively detects intracellular Ca^{2+} concentration proximal to membranes.[31] Washed WT platelets pre-loaded with either probe exhibited Ca^{2+} mobilization upon thrombin challenge (Figure 2A-B), though increase in signal intensity appeared weaker using Fura-2-NM versus Fura-2 (Figure 2B). Interestingly, the reduced Ca^{2+} mobilization observed in SERCA3$^{-/-}$ platelets under Fura-2, confirming our earlier results using flow cytometry,[27] was not detected under Fura-2-NM probe (Figure 2B), suggesting that the Fura-2-NM probe does not detect SERCA2b Ca^{2+} stores mobilization. Furthermore, SERCA3 inhibition with tBHQ lowered thrombin-induced Ca^{2+} mobilization of WT platelets to the level of SERCA3$^{-/-}$ platelets (due to the sole SERCA2b mobilization left) using Fura-2 (Figure 2C), that was not detected by Fura-2-NM (Figure 2D). As expected, inhibition of SERCA2b (the only SERCA left in SERCA3$^{-/-}$ platelets) by thapsigargin (200nM, conditions specific for SERCA2b, not affecting SERCA3 function)[27] abolished thrombin-induced Ca^{2+} mobilization in SERCA3$^{-/-}$ but not in WT platelets (because of the SERCA3 Ca^{2+} stores left functional by thapsigargin), as visualized by both Fura-2 and Fura-2-NM (Figure 2E-F). Similar results were obtained using a low concentration of collagen (0.8µg/mL) or PAR-4AP, the agonist peptide for the thrombin receptor (results not shown). Altogether these results establish

that Fura-2-NM specifically detects mobilization of SERCA3 and not SERCA2b Ca^{2+} stores, and thus strengthen the idea of topological differentiation between SERCA3 and SERCA2b Ca^{2+} stores.

Next, we reasoned that SERCA3-dependent mobilization leading to ADP secretion should be independent from ADP itself, since taking place presumably ahead of its secretion. As shown previously,[27] ADP scavenging by apyrase diminishes the overall Ca^{2+} mobilization in WT platelets to the level of SERCA3$^{-/-}$ platelets as confirmed here with Fura-2 (Figure 2G). In contrast, apyrase did not affect SERCA3 Ca^{2+} stores mobilization in WT platelets as detected by Fura-2-NM (Figure 2H). Conversely, exogenous ADP added to thrombin while stimulating mobilization in SERCA3$^{-/-}$ platelets up to the same level than WT platelets under Fura-2 (Figure 2I), did not modify Ca^{2+} mobilization in WT nor in SERCA3$^{-/-}$ platelets as visualized by Fura-2-NM (Figure 2J). These results confirm that the SERCA3-dependent Ca^{2+} mobilization pathway, as specifically visualized by Fura-2-NM, is independent from ADP, and therefore may correspond to the primary SERCA3 Ca^{2+} stores mobilization pathway preceding initial ADP release. Our results also demonstrate that SERCA3 Ca^{2+} stores mobilization contributes to most if not all membrane proximal Ca^{2+} mobilization upon thrombin stimulation, as opposed to SERCA2b Ca^{2+} stores mobilization only detected in the cytosol.

SERCA3-dependent Ca^{2+} mobilization is independent of the second messenger inositol-tris-phosphate but dependent on nicotinic acid adenosine dinucleotide-phosphate.

The differential secretion kinetics between SERCA3$^{-/-}$ and SERCA2b Ca^{2+} stores, along with their apparent different topology ([24]; unpublished), and sensitivity to the Ca^{2+} fluorophore Fura2-NM, suggested that these Ca^{2+} stores may be regulated by distinct signaling pathways. Inositol 1,4,5-tris phosphate (IP3) is the prominent second messenger driving Ca^{2+} mobilization from RE,[32] the recognized SERCA2b-dependent Ca^{2+} storing organelle.[7] To determine whether IP3 mobilized SERCA2b and SERCA3 Ca^{2+} stores, we analyzed Ca^{2+} mobilization in response to thrombin of platelets pre-treated with U73122, a well-characterized specific inhibitor of phospholipase C (PLC).[33] After assessing dose-dependent effects on SERCA3-dependent Ca^{2+} mobilization using SERCA3$^{-/-}$ mice as controls

(supplemental Figure S3A,D), we found that U73122 strongly affected global Ca^{2+} mobilization in WT, and most importantly suppressed Ca^{2+} mobilization in SERCA3$^{-/-}$ platelets, as visualized with Fura-2 (Figure 3B,D). Interestingly however, as visualized with Fura-2-NM, U73122 pretreatment did not affect SERCA3 Ca^{2+} mobilization in WT platelets, while in SERCA3$^{-/-}$ platelets, Ca^{2+} mobilization remained undetected (Figure 3F,H). U73122 pretreatment had no impact on Ca^{2+} mobilization in response to thrombin after SERCA2b inhibition with thapsigargin, or SERCA3 inhibition with tBHQ, as visualized with Fura-2 (supplemental Figure 3E,F). Furthermore, addition of exogenous ADP to thrombin in the presence of U73122, did not affect mobilization in either WT or SERCA3$^{-/-}$ platelets whether visualized by Fura-2 (Figure 3C,D), or Fura-2-NM (Figure 3G,H). Altogether these results are consistent with the primary signaling pathway of ADP secretion not being dependent on IP3.

Two other second messengers, Nicotinic Acid Adenosine Dinucleotide-Phosphate (NAADP) and cyclic Adenosine Dinucleotide-Phosphate ribose (cADPr), are also known to elicit Ca^{2+} mobilization,[34] though the presence and the role of cADPr in platelets is controversial.[35] Interestingly NAADP has been shown to act as second messenger specific for mobilization of Ca^{2+} from acidic stores.[36] SERCA3 has been found associated with acidic stores,[37] and NAADP has been suggested to be the second messenger for platelet SERCA3 Ca^{2+} stores,[25] based on pharmacological studies. To confirm and extend these observations, we used the SERCA3$^{-/-}$ mouse model. In Figure 4A,B as visualized with Fura-2, Ned-19, a well-characterized specific antagonist of NAADP,[38] diminished global Ca^{2+} mobilization in WT platelets to the level of SERCA3$^{-/-}$ platelets. Accordingly, addition of exogenous ADP simultaneously to thrombin abrogated Ned-19 inhibition and restored Ca^{2+} mobilization in both WT and SERCA3$^{-/-}$ platelets as visualized by Fura 2 (Figure 4C,H). To verify that this pathway was independent from IP3, U73122 added to Ned-19 induced total suppression of Ca^{2+} mobilization in both WT and SERCA3$^{-/-}$ platelets as visualized by Fura2 (Fig 4D,H), consistent with ADP triggering IP3 involved in SERCA2b-dependent stores mobilization. Importantly, when visualized with Fura-2-NM, addition of Ned-19 suppressed Ca^{2+} SERCA3 mobilization in WT platelets induced by thrombin (Figure 4E-F,I), and as expected, this effect

was not reversed by exogenous ADP (Figure 4G,I). These results thus strongly suggest that NAADP is the main second messenger mobilizing Ca^{2+} from SERCA3 stores.

Consistent with involvement of NAADP in SERCA3 Ca^{2+} stores mobilization, NAADP-AM in absence of thrombin, while exhibiting mobilization in WT platelets, did not mobilize Ca^{2+} in SERCA3$^{-/-}$ platelets, whether visualized by Fura-2- or Fura-2-NM (Figure 5A,D). Accordingly pre-incubation with Ned-19 prevented NAADP-AM-mediated Ca^{2+} mobilization (Figure 5B,E). Depleting SERCA3 Ca^{2+} stores with the SERCA3 inhibitor tBHQ prevented subsequent mobilization by NAADP-AM (Figure 5C, F), while the SERCA2b-specific inhibitor thapsigargin (Tg, 200 nM) was without effect (Figure 5G?).

Altogether these results are consistent with the mobilisation of SERCA3 Ca^{2+} stores being specifically dependent on the second messenger NAADP, and not IP3.

SERCA3-dependent primary ADP secretion is mediated by NAADP .

In figure 6, secretion kinetics assessed in conditions of NAADP pathway inhibition by Ned-19 after thromgin stimulation was drastically reduced in WT platelets to the level of SERCA3$^{-/-}$ platelets, unaffected throughout secretion kinetics (5s, 10s and 3 min) (6A,B). Consistent with absence of effect on SERCA3 Ca^{2+} mobilization, U73122 did not inhibit early secretion at 5s in WT platelets, while blocking further secretion at later time points (Fig 6A), confirming that the primary secretion in WT platelets is independent from IP3. Likewise, addition of exogenous ADP bypassed Ned-19 inhibition, restoring full secretion in both WT and SERCA3$^{-/-}$ platelets (Figure 6B). These results confirm that intial SERCA3-dependent ADP secretion is mediated via NAADP as second messenger specific for SERCA3 Ca^{2+} stores. Interestingly, NAADP-AM alone was unable to trigger ADP secretion (Figure 6C), most likely because PKCs which regulate secretion require not only Ca^{2+}, but also diacylglycerol from PLC or/and PLD-mediated phospholipids break down.[39] We tested this possibility by addition of 1-Oleoyl-2-acetyl-*sn*-glycerol (OAG), a diacyl-glycerol analog[40] together with NAADP-AM, which triggered secretion in WT, but not in SERCA3$^{-/-}$ platelets (Figure 6C).

Altogether these results are thus consistent with two distinct platelet Ca^{2+} stores controlling secretion differentially: the first, sensitive to tBHQ and Ned-19 is rapid, dependent on SERCA3, independent from ADP and mobilized by NAADP, the other, sensitive to thapsigargin and U73122 is delayed, dependent on SERCA2b and in part on secreted ADP, and is mobilized by IP3 (Figure 7).

Finally, Ned-19 demonstrated a partial inhibitory effect on aggregation of WT and not SERCA3$^{-/-}$platelets (Figure 6D,E). Aggregation of both WT and SERCA3$^{-/-}$ platelets in the presence of Ned-19 was completely restored by exogenous ADP (Figure 6F), consistent with the contention that ADP bypasses the SERCA3/NAADP-dependent pathway. U73122 inhibited low thrombin concentration aggregation of WT platelets, partially and of SERCA3$^{-/-}$ platelets completely (Figure 6G). And, Ned-19 exhibited an additive inhibitory effect with U73122, on both WT and SERCA3$^{-/-}$ platelets (Figure 6H), consistent with involvement of both the NAADP-SERCA3 and the IP3-SERCA2b pathways in aggregation.

Discussion

We have recently reported that mobilization of SERCA3-dependent Ca^{2+} stores specifically controlled partial secretion of dense granules, which appeared important in amplification of platelet activation via ADP dependent pathway, in conditions of low concentration of agonists.[27] We now provide evidence that SERCA3-dependent Ca^{2+} stores mobilization controls a primary ADP secretion, within seconds of agonist platelet stimulation, by direct assessment of the kinetics of ADP secretion. We show that this primary ADP secretion triggers, probably via P_2Y_1 receptors, a secondary wave of ADP secretion, itself dependent on SERCA2b Ca^{2+} stores. Furthermore, we demonstrate that both Ca^{2+} stores were strictly mobilized by distinct second messengers: NAADP for SERCA3-dependent Ca^{2+} stores, and IP3 for SERCA2b-dependent Ca^{2+} stores. The differential mobilization of SERCA3- and SERCA2b-dependent Ca^{2+} was already suggested by earlier studies[25,34,41], based on pharmacological evidence but these lacked a SERCA3-ablated model. The present study definitely confirms that SERCA3 and SERCA2b Ca^{2+} stores are differentially regulated, but more importantly link these pathways to ADP secretion and its autocrine function in platelet activation. Here we show that a functional link between SERCA3 Ca^{2+} stores and rapid initial ADP secretion, important in conditions of low agonist concentrations and this pathway is triggered by NAADP, while a second pathway taking place secondarily is dependent on SERCA2b Ca^{2+} stores mobilized exclusively by IP3 (see Figure 7).

The topological difference between SERCAs could be correlated with the fact that only SERCA3-, but not SERCA2b-, Ca^{2+} store mobilization was visualized with the Fura-2-NM-AM probe (formerly named Fura-2-FFP18), designed to penetrate the cells and to associate with the inner leaflet of the membrane.[31,42] This suggests that SERCA3-dependent Ca^{2+} mobilization occurs preferentially at the plasma membrane, which may appear in contradiction with the idea that SERCAs are located in the ER membrane. However, SERCA3 has been reported to be located at the periphery of the platelet membrane (reference [24], and unpublished) where it participates in the regulation of the Store Operated Calcium Entry (SOCE) through the plasma membrane.[26] It is therefore very likely that SERCA3-dependent Ca^{2+} stores localize to in very close vicinity to the plasma membrane and their mobilization occurs near the plasma membrane, being

specifically visualized by the inner membrane-associated Fura-2-NM, while the cytosolic Fura-2, which exhibits poor accessibility to membrane proximal regions [42] will record Ca^{2+} issued preferentially from SERCA2b-dependent stores, although we show that Ca^{2+} mobilized from SERCA3 stores was also detected with Fura-2.

PLC/IP3 pathway is amplified upon SERCA3 Ca^{2+} stores mobilization. This would be consistent with the notion that SERCA3 Ca^{2+} stores are mobilized first, suggesting then that NAADP is generated prior to IP3. This suggests that CD38, the membrane enzyme that catalyzes the exchange of the nicotinamide group from NADP+ with nicotinic acid to synthesize NAADP[43], acts rapidly upon agonist stimulation, before PLC activation. In a study by Mushtaq et al of platelet functions in a $CD38^{-/-}$ mouse model, the authors reported that NAADP synthesis appeared secondary to IP3 synthesis, based on inhibition of NAADP synthesis by the PLC inhibitor U73122.[34] We believe that different experimental conditions are at the root of this opposite result: these authors used high concentrations of thrombin, 0.5 U/mL, more than 10 times higher than 0.04 U/mL in our study. Also, platelets were subjected to aggregation which adds up activation signals as well as signaling downstream integrin $\alpha_{IIb}\beta_3$, while we focused on initial activation and used unstirred conditions to prevent $\alpha_{IIb}\beta_3$ engagement and subsequent secretion.

Furthermore, we observed that direct mobilization of Ca^{2+} using NAADP-AM was not sufficient to induce the primary ADP secretion or platelet aggregation both requiring another stimulus. When OAG-AM, an analog of DAG, was provided we could observe a stronger mobilization associated with more secretion and aggregation. This result suggests that both Ca^{2+} from SERCA3-dependent stores and DAG are needed to induce initial ADP secretion. It is possible that in physiological conditions most of the DAG is produced by PLC although the fact that U73122 did not block initial ADP secretion suggests the existence of another source of DAG than PLC: PLDs, another class of phospholipases that are also activated by thrombin stimulation are an active source of DAG in platelets,[39] and explain.how the NAADP-SERCA3 pathway leads to active ADP secretion.

One issue raised by this study is related to the nature of dense granules corresponding to the first wave of ADP (and ATP) release upon NAADP/SERCA3-dependent Ca^{2+} store mobilization: since only a fraction

of the total content of granules is released, this brings up the possibility of 2 separate dense granules populations, each associated with one type of SERCA Ca^{2+} stores: according to this hypothesis one subtype of dense granules would be physically and/or functionally associated with SERCA3-dependent Ca^{2+} stores, and would be the only granules able to release their content upon mobilization of SERCA3 stores. The remaining granules would then enter the secretory pathway upon mobilization of the SERCA2b Ca^{2+} stores. Alternatively, the dense granule population would be homogeneous but granules in close proximity to SERCA3 Ca^{2+} stores (possibly near the plasma membrane) would secrete their content upon mobilization of these Ca^{2+} stores. Distinguishing between these two possibilities will require further investigation.

A question raised by our observation is whether our results may be related to the so-called Ca^{2+}-induced Ca^{2+} release (CICR) mechanism where Ca^{2+} released from an intracellular channel can potentiate further Ca^{2+} release from other calcium channels in the vicinity. Such a role for NAADP-mobilized Ca^{2+} has already been proposed in different cell types (ref: Brailoiu Adv Exp Med Biol 2016; Penny Cell calcium 2015). If this was the case, then CICR would occur during the second part of the activation kinetics, where Ca^{2+} release from SERCA3 stores would be responsible for the mobilization of SERCA2b stores Ca^{2+}. However, here it does not appear to be the case since 1°) direct SERCA3-dependent Ca^{2+} mobilization with NAADP-AM alone, which does not lead to the secretion, does not amplify Ca^{2+} mobilization, 2°) exogenous ADP addition was able to bypass the initial Ca^{2+} mobilization defect and was able to restore a complete Ca^{2+} mobilization in both WT and SERCA3$^{-/-}$ platelets.

One of our most relevant findings is that ADP secretion appeared detectable within seconds of agonist stimulation of platelets and in a manner fully dependent on SERCA3 and NAADP pathway, while a secondary ADP secretion pathway follows, dependent on SERCA2b and IP3. The major consequence is that the 2 pathways regulate secretion sequentially. This temporal organization, with NAADP-dependent Ca^{2+} mobilization ahead of other mobilization pathways has already been observed in a number of other cell types, including sea urchin sperm,[44] pancreatic cells,[45] or T-lymphocytes.[46] Though dense granule secretion (or equivalent, such as lysosomes) has not been documented in these cell types and correlated

with Ca^{2+} mobilization differential pathways, our observation may be a general mechanism by which an NAADP-SERCA3 Ca^{2+} mobilization pathway regulates an early secretion of functional relevance to trigger full activation of cells. Future experiments are aimed at addressing this question.

Acknowledgements

This work was supported in part by INSERM and Université Paris-Saclay/Paris-Sud, and a fellowship from the MENSR to Z.E. We thank Dr Gilon and Dr Shull for providing the SERCA3$^{-/-}$ mice. Z.E. is a PhD candidate at Université Paris-Sud and this work is submitted in partial fulfilment of the requirement for the PhD.

Authorship

Contribution: Z.E., M.F., performed experiments; Z.E., R.B., J.-P.R. analyzed results; Z.E., R.B., J.-P.R. designed experiments; J.-P.R. wrote the manuscript; Z.E., M.B., R.B., J.-P.R. critically edited the manuscript.

Disclosure of conflicts-of-interest

The authors declare no conflict-of-interest.

References

1. Brini M, Carafoli E. Calcium pumps in health and disease. *Physiol Rev*. 2009;89(4):1341-1378.
2. Enouf J, Bredoux R, Papp B, et al. Human platelets express the SERCA2-b isoform of Ca(2+)-transport ATPase. *Biochem J*. 1992;286 (Pt 1):135-140.
3. Papp B, Enyedi A, Paszty K, et al. Simultaneous presence of two distinct endoplasmic-reticulum-type calcium-pump isoforms in human cells. Characterization by radio-immunoblotting and inhibition by 2,5-di-(t-butyl)-1,4-benzohydroquinone. *Biochem J*. 1992;288 (Pt 1):297-302.
4. Bobe R, Bredoux R, Corvazier E, et al. How many Ca(2)+ATPase isoforms are expressed in a cell type? A growing family of membrane proteins illustrated by studies in platelets. *Platelets*. 2005;16(3-4):133-150.
5. Brini M, Cali T, Ottolini D, Carafoli E. Calcium pumps: why so many? *Compr Physiol*. 2012;2(2):1045-1060.
6. Toyoshima C, Nomura H. Structural changes in the calcium pump accompanying the dissociation of calcium. *Nature*. 2002;418(6898):605-611.
7. Lytton J, Westlin M, Burk SE, Shull GE, MacLennan DH. Functional comparisons between isoforms of the sarcoplasmic or endoplasmic reticulum family of calcium pumps. *J Biol Chem*. 1992;267(20):14483-14489.
8. Carrion R, Jr., Ro YT, Patterson JL. Purification, identification, and biochemical characterization of a host-encoded cysteine protease that cleaves a leishmaniavirus gag-pol polyprotein. *J Virol*. 2003;77(19):10448-10455.
9. Walsh EP, Lamont DJ, Beattie KA, Stark MJ. Novel interactions of Saccharomyces cerevisiae type 1 protein phosphatase identified by single-step affinity purification and mass spectrometry. *Biochemistry*. 2002;41(7):2409-2420.

10. Burge SM, Wilkinson JD. Darier-White disease: a review of the clinical features in 163 patients. *J Am Acad Dermatol*. 1992;27(1):40-50.
11. Dhitavat J, Cobbold C, Leslie N, Burge S, Hovnanian A. Impaired trafficking of the desmoplakins in cultured Darier's disease keratinocytes. *J Invest Dermatol*. 2003;121(6):1349-1355.
12. Shimizu H, Tan Kinoshita MT, Suzuki H. Darier's disease with esophageal carcinoma. *Eur J Dermatol*. 2000;10(6):470-472.
13. Korosec B, Glavac D, Rott T, Ravnik-Glavac M. Alterations in the ATP2A2 gene in correlation with colon and lung cancer. *Cancer Genet Cytogenet*. 2006;171(2):105-111.
14. Korosec B, Glavac D, Volavsek M, Ravnik-Glavac M. ATP2A3 gene is involved in cancer susceptibility. *Cancer Genet Cytogenet*. 2009;188(2):88-94.
15. Brouland JP, Gelebart P, Kovacs T, Enouf J, Grossmann J, Papp B. The loss of sarco/endoplasmic reticulum calcium transport ATPase 3 expression is an early event during the multistep process of colon carcinogenesis. *Am J Pathol*. 2005;167(1):233-242.
16. Varadi A, Lebel L, Hashim Y, Mehta Z, Ashcroft SJ, Turner R. Sequence variants of the sarco(endo)plasmic reticulum Ca(2+)-transport ATPase 3 gene (SERCA3) in Caucasian type II diabetic patients (UK Prospective Diabetes Study 48). *Diabetologia*. 1999;42(10):1240-1243.
17. Ji Y, Lalli MJ, Babu GJ, et al. Disruption of a single copy of the SERCA2 gene results in altered Ca2+ homeostasis and cardiomyocyte function. *J Biol Chem*. 2000;275(48):38073-38080.
18. Liu LH, Boivin GP, Prasad V, Periasamy M, Shull GE. Squamous cell tumors in mice heterozygous for a null allele of Atp2a2, encoding the sarco(endo)plasmic reticulum Ca2+-ATPase isoform 2 Ca2+ pump. *J Biol Chem*. 2001;276(29):26737-26740.
19. Liu LH, Paul RJ, Sutliff RL, et al. Defective endothelium-dependent relaxation of vascular smooth muscle and endothelial cell Ca2+ signaling in mice lacking sarco(endo)plasmic reticulum Ca2+-ATPase isoform 3. *J Biol Chem*. 1997;272(48):30538-30545.
20. Iguchi N, Ohkuri T, Slack JP, Zhong P, Huang L. Sarco/Endoplasmic reticulum Ca2+-ATPases (SERCA) contribute to GPCR-mediated taste perception. *PLoS One*. 2011;6(8):e23165.
21. Arredouani A, Guiot Y, Jonas JC, et al. SERCA3 ablation does not impair insulin secretion but suggests distinct roles of different sarcoendoplasmic reticulum Ca(2+) pumps for Ca(2+) homeostasis in pancreatic beta-cells. *Diabetes*. 2002;51(11):3245-3253.
22. Beauvois MC, Arredouani A, Jonas JC, et al. Atypical Ca2+-induced Ca2+ release from a sarco-endoplasmic reticulum Ca2+-ATPase 3-dependent Ca2+ pool in mouse pancreatic beta-cells. *J Physiol*. 2004;559(Pt 1):141-156.
23. Beauvois MC, Merezak C, Jonas JC, Ravier MA, Henquin JC, Gilon P. Glucose-induced mixed [Ca2+]c oscillations in mouse beta-cells are controlled by the membrane potential and the SERCA3 Ca2+-ATPase of the endoplasmic reticulum. *Am J Physiol Cell Physiol*. 2006;290(6):C1503-1511.
24. Kovacs T, Berger G, Corvazier E, et al. Immunolocalization of the multi-sarco/endoplasmic reticulum Ca2+ ATPase system in human platelets. *Br J Haematol*. 1997;97(1):192-203.
25. Lopez JJ, Redondo PC, Salido GM, Pariente JA, Rosado JA. Two distinct Ca2+ compartments show differential sensitivity to thrombin, ADP and vasopressin in human platelets. *Cell Signal*. 2006;18(3):373-381.
26. Lopez JJ, Jardin I, Bobe R, et al. STIM1 regulates acidic Ca2+ store refilling by interaction with SERCA3 in human platelets. *Biochem Pharmacol*. 2008;75(11):2157-2164.
27. Elaib Z, Adam F, Berrou E, et al. Full activation of mouse platelets requires ADP secretion regulated by SERCA3 ATPase-dependent calcium stores. *Blood*. 2016;128(8):1129-1138.
28. Wuytack F, Eggermont JA, Raeymaekers L, Plessers L, Casteels R. Antibodies against the non-muscle isoform of the endoplasmic reticulum Ca2(+)-transport ATPase. *Biochem J*. 1989;264(3):765-769.
29. Martin V, Bredoux R, Corvazier E, Papp B, Enouf J. Platelet Ca(2+)ATPases : a plural, species-specific, and multiple hypertension-regulated expression system. *Hypertension*. 2000;35(1 Pt 1):91-102.
30. Erne P, Schachter M, Fabbro D, Miles CM, Sever PS. Calcium transients in human platelets monitored by aequorin, fura-2 and quin-2: effects of protein kinase C activation and inhibition. *Biochem Biophys Res Commun*. 1987;145(1):66-72.

31. Davies EV, Hallett MB. Near membrane Ca2+ changes resulting from store release in neutrophils: detection by FFP-18. *Cell Calcium*. 1996;19(4):355-362.
32. Berridge MJ. The Inositol Trisphosphate/Calcium Signaling Pathway in Health and Disease. *Physiol Rev*. 2016;96(4):1261-1296.
33. Bleasdale JE, Bundy GL, Bunting S, et al. Inhibition of phospholipase C dependent processes by U-73, 122. *Adv Prostaglandin Thromboxane Leukot Res*. 1989;19:590-593.
34. Mushtaq M, Nam TS, Kim UH. Critical role for CD38-mediated Ca2+ signaling in thrombin-induced procoagulant activity of mouse platelets and hemostasis. *J Biol Chem*. 2011;286(15):12952-12958.
35. Ohlmann P, Leray C, Ravanat C, et al. cADP-ribose formation by blood platelets is not responsible for intracellular calcium mobilization. *Biochem J*. 1998;331 (Pt 2):431-436.
36. Galione A. NAADP, a new intracellular messenger that mobilizes Ca2+ from acidic stores. *Biochem Soc Trans*. 2006;34(Pt 5):922-926.
37. Lopez JJ, Camello-Almaraz C, Pariente JA, Salido GM, Rosado JA. Ca2+ accumulation into acidic organelles mediated by Ca2+- and vacuolar H+-ATPases in human platelets. *Biochem J*. 2005;390(Pt 1):243-252.
38. Naylor E, Arredouani A, Vasudevan SR, et al. Identification of a chemical probe for NAADP by virtual screening. *Nat Chem Biol*. 2009;5(4):220-226.
39. Thielmann I, Stegner D, Kraft P, et al. Redundant functions of phospholipases D1 and D2 in platelet alpha-granule release. *J Thromb Haemost*. 2012;10(11):2361-2372.
40. Kaibuchi K, Takai Y, Sawamura M, Hoshijima M, Fujikura T, Nishizuka Y. Synergistic functions of protein phosphorylation and calcium mobilization in platelet activation. *J Biol Chem*. 1983;258(11):6701-6704.
41. Coxon CH, Lewis AM, Sadler AJ, et al. NAADP regulates human platelet function. *Biochem J*. 2012;441(1):435-442.
42. Vorndran C, Minta A, Poenie M. New fluorescent calcium indicators designed for cytosolic retention or measuring calcium near membranes. *Biophys J*. 1995;69(5):2112-2124.
43. Aarhus R, Graeff RM, Dickey DM, Walseth TF, Lee HC. ADP-ribosyl cyclase and CD38 catalyze the synthesis of a calcium-mobilizing metabolite from NADP. *J Biol Chem*. 1995;270(51):30327-30333.
44. Churchill GC, O'Neill JS, Masgrau R, et al. Sperm deliver a new second messenger: NAADP. *Curr Biol*. 2003;13(2):125-128.
45. Yamasaki M, Thomas JM, Churchill GC, et al. Role of NAADP and cADPR in the induction and maintenance of agonist-evoked Ca2+ spiking in mouse pancreatic acinar cells. *Curr Biol*. 2005;15(9):874-878.
46. Gasser A, Bruhn S, Guse AH. Second messenger function of nicotinic acid adenine dinucleotide phosphate revealed by an improved enzymatic cycling assay. *J Biol Chem*. 2006;281(25):16906-16913.

Figure legends

Figure 1. Time-course of costimulation by thrombin and ADP of platelet secretion and comparative secretion of ADP and ATP in WT and SERCA3$^{-/-}$ platelets. WT (black bars) and SERCA3$^{-/-}$ (gray bars) washed platelets in suspension ($3x10^7$ in 300 µL) were stimulated with thrombin (40 mU/mL) and ADP (10µM) added either simultaneously (0s) or after 5, 10, 20 or 30s of thrombin stimulation (A). ATP released in the supernatants was assessed (see Methods) after 3 min stimulation. WT (black bars) and SERCA3$^{-/-}$ (gray bars) washed platelets in suspension ($3x10^7$ in 300 µL) were stimulated with thrombin (40 mU/mL) for 3 min and released ADP (B) or ATP (C) in the supernatants were assessed (see Methods). The kinetics of secretion of ADP (D) and ATP (E) was assessed in the same conditions, but thrombin stimulation was stopped at indicated time points by addition of the thrombin inhibitor D-Phe-Pro-Arg-chloromethylketone (PPACK, 100µM). To demonstrate functional involvement of SERCA3 during secretion, tBHQ (10µM) was preincubated with platelets prior to thrombin stimulation (40 mU/mL) and ATP secretion measured in the supernatant of WT (heavy striped bars) or SERCA3-/- (light striped bars) at, 0, 5, 10 and 180s.

Data presented are means ± SEM, n = 3, using the 1-way ANOVA followed by Tukey's multiple comparison test: ns, not significant, ** P<0.01, *** P <0.001.

Figure 2. **Ca^{2+} mobilization assessed by video-microscopy with the ratio-metric fluorescent Ca^{2+} probes Fura-2-AM and Fura-2-NearMembrane-AM**. Washed platelets immobilized on glass coverslips coated with poly-lysine, were loaded with Fura-2-AM (Fura-2) or Fura-2-NearMembrane-AM (Fura-2-NM), and activated with of thrombin (50 mU/mL). Images were captured using a Nikon 2 Eclipse TE2000-U fluorescence microscope and a captor Black and white CCD (CoolSNAP HQ Photometrics, Tucson, USA) camera at 5s intervals and images captured using the Metamorph program. Images were then quantified using Image J and statistics calculated by GraphPad. Ca^{2+} fluorescence intensities were calculated as Arbtirary Units (AU) using the 340/380 nm excitation fluorescence ratio, the value 1 corresponding to the background level. WT (black tracings), and SERCA3-/- (gray tracings) platelets were

stimulated with thrombin alone, as visualized with Fura-2 (A) or Fura-2-NM (B). To assess SERCA3 functional involvement, platelets were first incubated with tBHQ (10µM) for 4 minutes, or thapsigargin (Tg, 200 nM) for 8 minutes and then challenged with thrombin, and visualized with either Fura-2 (C, E), or Fura-2-NM (D, F) respectively. To assess the role of ADP, platelets were activated with thrombin in the presence of the nucleotide phosphate scavenger apyrase (10 U/m) (G, H), or of ADP (10µM) (I,J). Time scale of recordings is indicated as an horizontal bar representing one minute (1 min).

Figure 3. Role of inositol tris-phosphate in SERCA3 Ca^{2+} store mobilization as assessed with the Phospholipase C inhibitor U73122. WT (black tracings) and SERCA3$^{-/-}$ (gray tracings) platelets were immobilized on poly-lysine glass coverslips and preloaded with Fura-2, and preincubated with DMF in the control experiment (A), or with U73122 (0.75 µM) (B,C) before stimulation with thrombin (A,B) or thrombin and ADP (10µM) (C). Area under curves were then quantitated as arbitrary units (AU) (D): black bars (WT) and gray bars (SERCA3$^{-/-}$); absence (-) or presence (+) of U73122 or ADP are indicated below the graph. Platelets loaded with Fura-2-NM pre-incubated with either DMF (E), or U73122 (F,G), were stimulated with thrombin (E,F) or thrombin and ADP (10µM) (G). Time scale of recordings is indicated as an horizontal bar representing one minute (1 min). Areas under curves were then quantitated as arbitrary units (AU) (H): black bars (WT) and gray bars (SERCA3$^{-/-}$); absence (-) or presence (+) of U73122 or ADP are indicated below the graph.

Data presented are representative of 3 independent experiments and expressed as means ± SEM, using the 1-way ANOVA followed by Tukey's multiple comparison test: *** P <0.001.

Figure 4. Role of NAADP in SERCA3 Ca^{2+} store mobilization. Washed WT (black tracings) or SERCA3$^{-/-}$ (gray tracings) platelets were immobilized on glass coverslips, loaded with either Fura-2 (A-D) or Fura-2-NM (E-G), and pre-incubated with either DMSO (A,E), Ned-19 (100µM) (B-G) or the phospholipase C inhibitor U73122 (0,75µM) (D) and stimulated with thrombin (40 mU/mL).

Fluorescence intensities were calculated as indicated in Methods as ratios to background level (value 1). Time scale of recordings is indicated as an horizontal bar representing one minute (1 min)

Areas under curves were quantitated as arbitrary units as visualized with Fura-2 (H) or Fura-2-NM (I). Black bars are WT platelets, gray bars SERCA3$^{-/-}$ platelets; absence (-) or presence (+) of Ned19, ADP or U73122 are indicated below the graph. Data are representative of 3 to 4 experiments, and expressed as means ± SEM, using the 1-way ANOVA followed by Tukey's multiple comparison test: ns, not significant; *** P <0.001.

Figure 5. Role of NAADP in SERCA3 Ca^{2+} store mobilization. Washed WT (black tracings) or SERCA3$^{-/-}$ (gray tracings) platelets were immobilized on glass coverslips, loaded with Fura-2 (A-C) or Fura-2-NM (D-G), and challenged with NAADP-AM (1µM) alone (A, D), or after preincubation with either Ned-19 (1µM) (B,E)), tBHQ (10µM) (C,F) or Tg (200nM) (G). Data are representative of 3 to 4 experiments. Fluorescence intensities were calculated as indicated in Methods as ratios to background level. Time scale of recordings is indicated as an horizontal bar representing one minute (1 min)

Figure 6. Role of SERCA3, IP3 and NAADP in secretion. Washed WT (black bars) or SERCA3$^{-/-}$ (gray bars) platelets were activated with thrombin (40 mU/mL), then the reaction was stopped by addition of PPACK (100µM) at different time points (5, 10 or 180s), and ATP assessed in supernatants (A). In some experiments, platelets were pretreated with Ned-19 (1µM) or U73122 (0, 75µM?). Restoration of ATP secretion by ADP was assessed in supernatant of WT (black bars) or SERCA3$^{-/-}$ (gray bars) platelets incubated with Ned-19 (B). Secretion induced by NAADP-AM was assessed in absence (-) or presence (+) of OAG (1-Oleoyl-2-acetyl-*sn*-glycerol) an analog of the PKC agonist DAG. Data presented are means ± SEM, n = 3, using the 1-way ANOVA followed by Tukey's multiple comparison test: ns, not significant; *** P <0.001. Washed WT (black tracings) or SERCA3$^{-/-}$ (gray tracings) platelets were subjected to aggregation in a Chronolog Lumiaggregometer (Chrono-Log Corporation, USA -) after activation with

thrombin (40 mU/mL) (D), in the presence of Ned-19 (E), Ned-19 and ADP (10 µM) (F), U73122 (G) or U73122 and Ned-19 (1µM) (H). Arrows indicate the time point of thrombin addition. Time scale of recordings is indicated as an horizontal bar representing one minute (1 min).

Figure 7. Scheme of SERCA3 and NAADPH pathway and ADP secretion. Stimulation of platelets with low agonist concentration (thrombin 40 mU/mL or collagen 0.8 mg/mL) leads to early synthesis of NAADPH by CD38, leading to the early release of Ca2+ stores controlled by SERCA3, which then initiate a rapid wave of ADP secretion within the first 5s following stimulation. This primary ADP secretion reinforces the agonist, costimulation leading to synthesis of IP3, release of Ca2+ stores depending on SERCA2b and secretion of the remaining ADP.

Figure 1

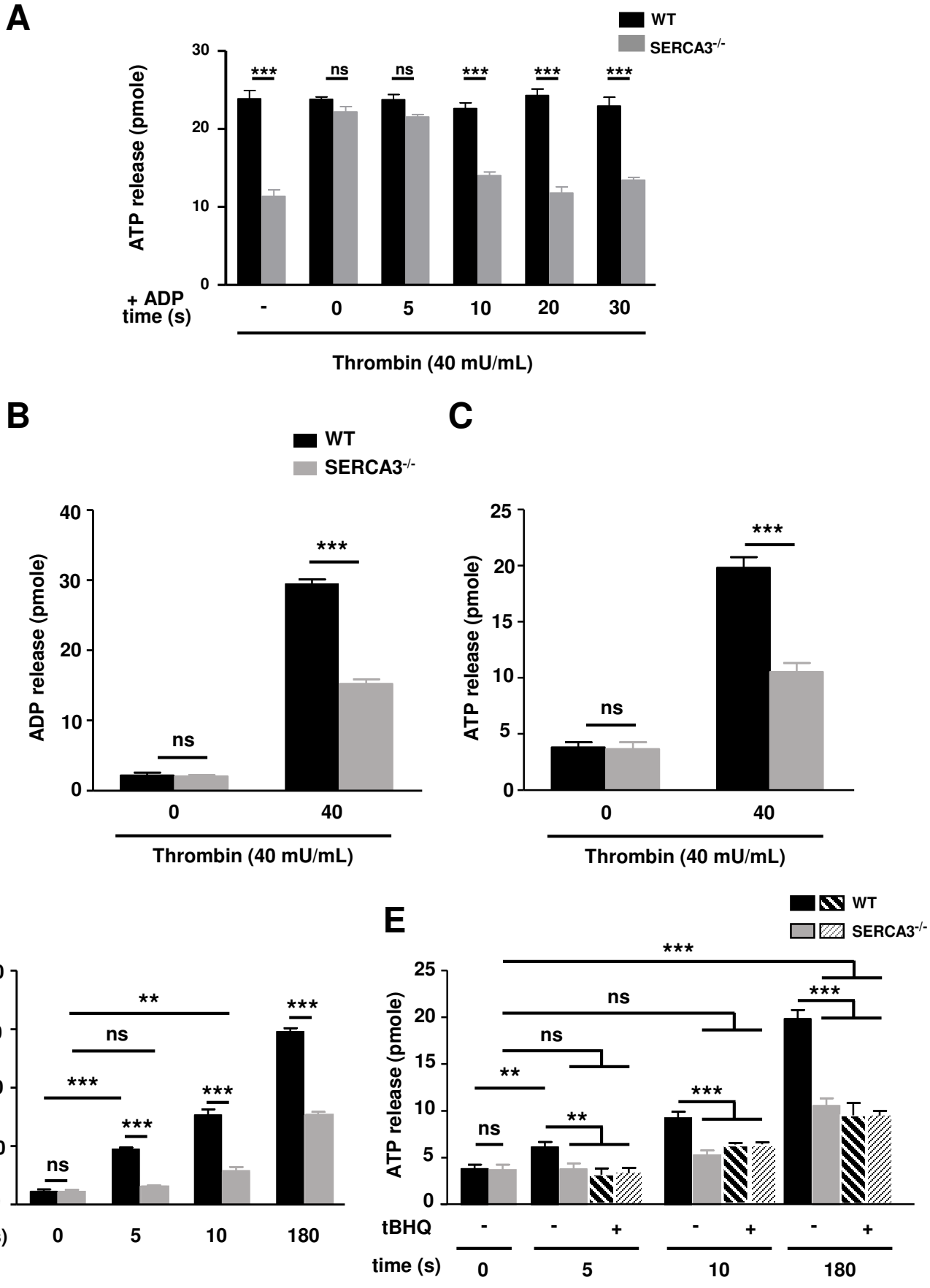
A
WT
SERCA3-/-
ATP release (pmole)
30
20
10
0
***
ns
ns
***
***
***
+ ADP
time (s)
-
0
5
10
20
30
Thrombin (40 mU/mL)
B
WT
SERCA3-/-
ADP release (pmole)
40
30
20
10
0
***
ns
0
40
Thrombin (40 mU/mL)
C
ATP release (pmole)
25
20
15
10
5
0
***
ns
0
40
Thrombin (40 mU/mL)
D
ADP release (pmole)
40
30
20
10
0
**
ns
***
***
***
ns
time (s)
0
5
10
180
E
WT
SERCA3-/-
ATP release (pmole)
25
20
15
10
5
0
***
ns
ns
***
**
**
***
ns
tBHQ
-
-
+
-
+
-
+
time (s)
0
5
10
180

Figure 2

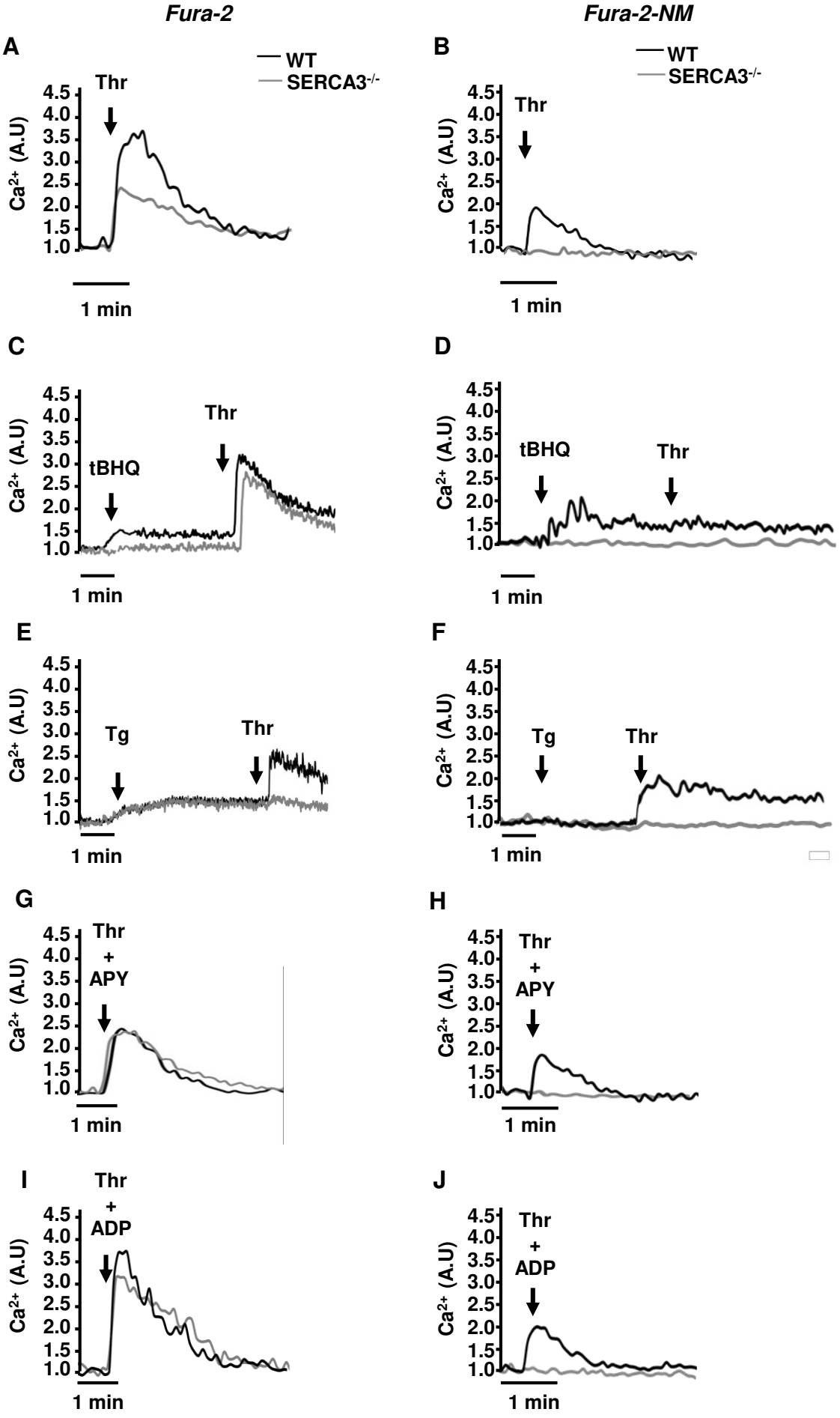
Fura-2
Fura-2-NM
A
B
C
D
E
F
G
H
I
J
WT
SERCA3-/-
Thr
tBHQ
Tg
Thr + APY
Thr + ADP
Ca2+ (A.U)
4.5
4.0
3.5
3.0
2.5
2.0
1.5
1.0
1 min

Figure 3

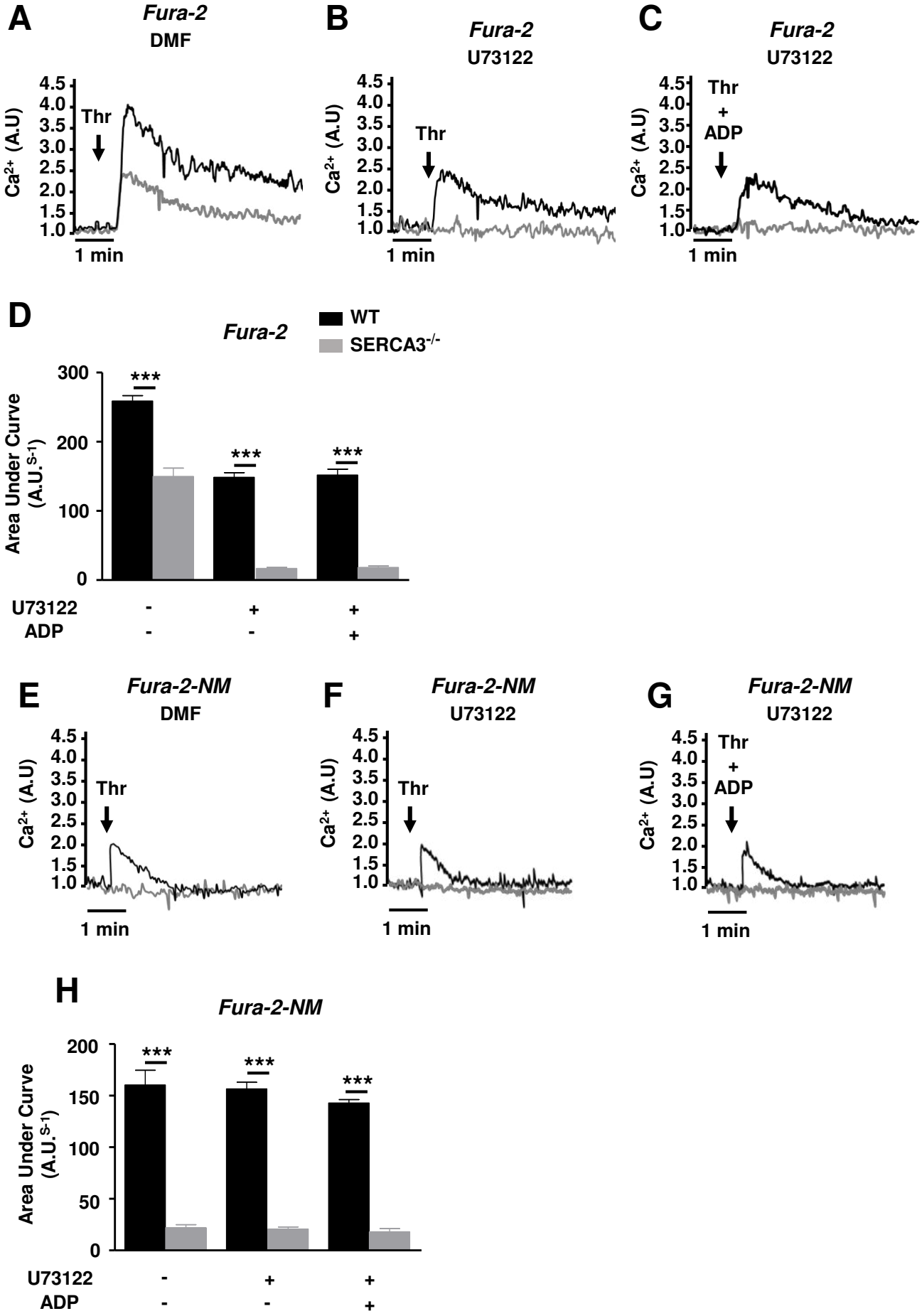
A
Fura-2
DMF
Thr
Ca2+ (A.U)
4.5
4.0
3.5
3.0
2.5
2.0
1.5
1.0
1 min
B
Fura-2
U73122
Thr
Ca2+ (A.U)
1 min
C
Fura-2
U73122
Thr
+
ADP
Ca2+ (A.U)
1 min
D
Fura-2
WT
SERCA3-/-
Area Under Curve
(A.U.S-1)
300
200
100
0
***
***
***
U73122 - + +
ADP - - +
E
Fura-2-NM
DMF
Thr
Ca2+ (A.U)
1 min
F
Fura-2-NM
U73122
Thr
Ca2+ (A.U)
1 min
G
Fura-2-NM
U73122
Thr
+
ADP
Ca2+ (A.U)
1 min
H
Fura-2-NM
Area Under Curve
(A.U.S-1)
200
150
100
50
0
***
***
***
U73122 - + +
ADP - - +

Figure 4

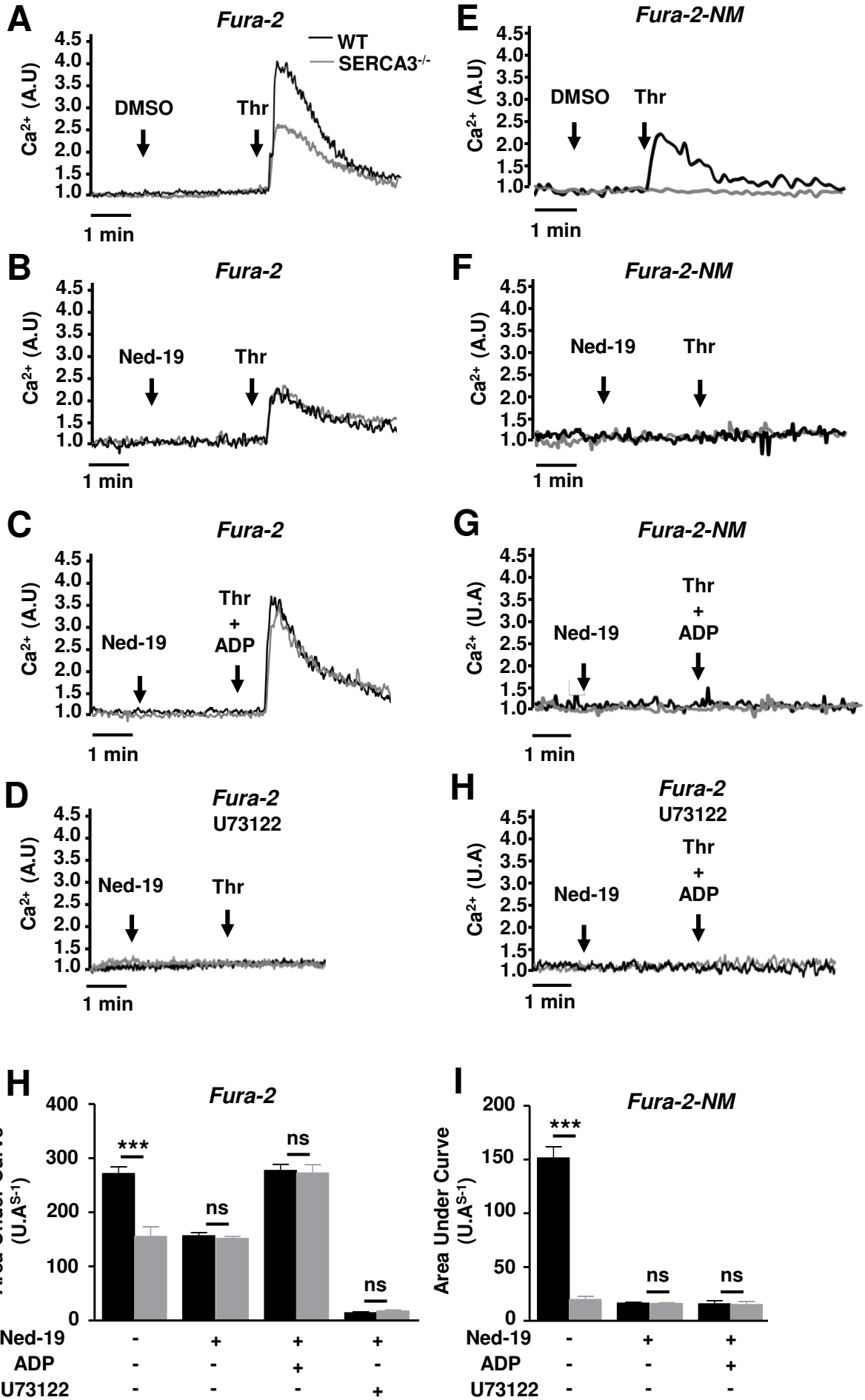
A
Fura-2
WT
SERCA3-/-
Ca2+ (A.U)
DMSO
Thr
1 min
B
Fura-2
Ned-19
Thr
C
Fura-2
Ned-19
Thr + ADP
D
Fura-2
U73122
Ned-19
Thr
E
Fura-2-NM
DMSO
Thr
F
Fura-2-NM
Ned-19
Thr
G
Fura-2-NM
Ca2+ (U.A)
Ned-19
Thr + ADP
H
Fura-2
U73122
Ned-19
Thr + ADP
H
Fura-2
Area Under Curve (U.AS-1)
***
ns
Ned-19
ADP
U73122
I
Fura-2-NM
Area Under Curve (U.AS-1)
***
ns

Figure 5

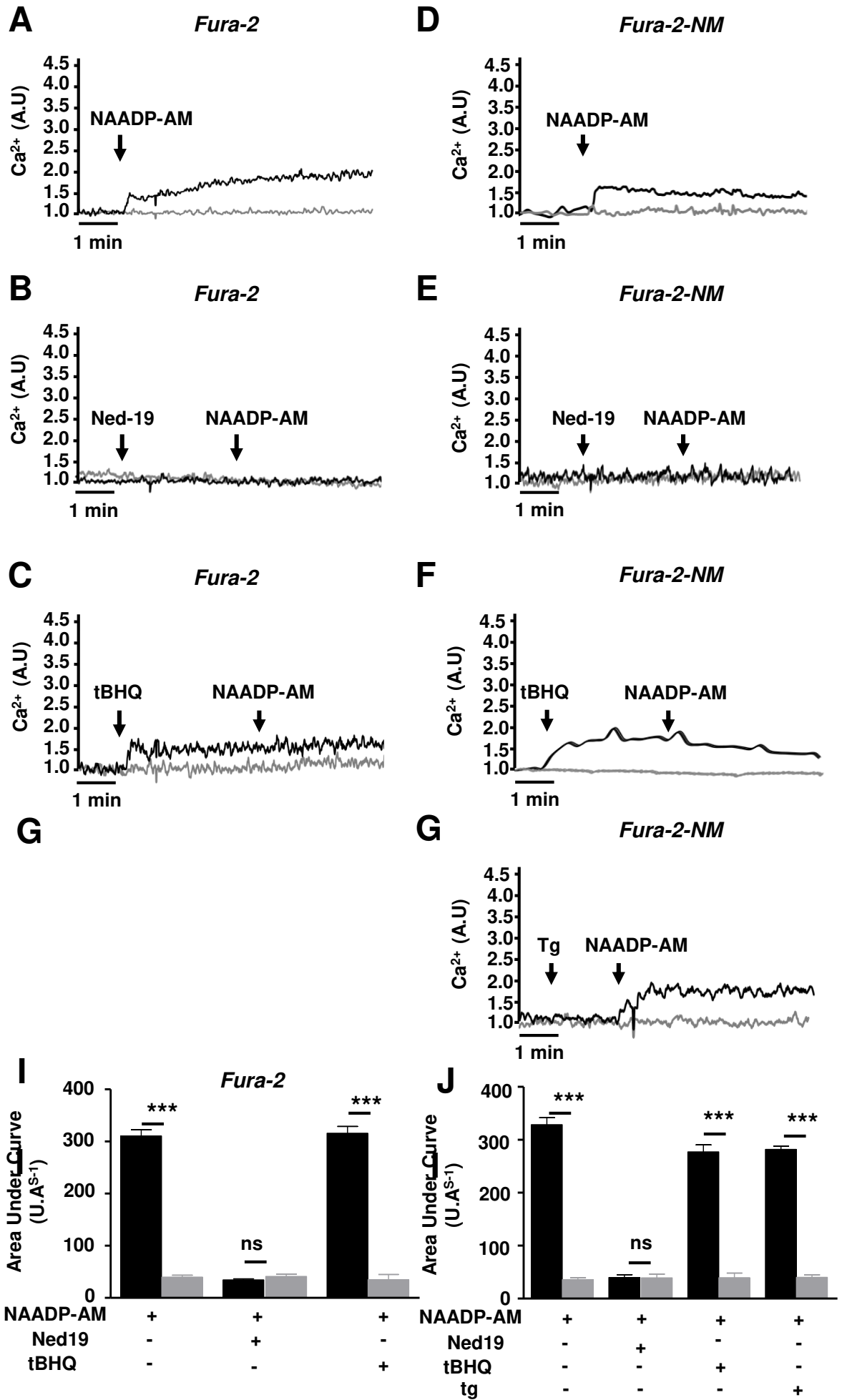
A
Fura-2
NAADP-AM
1 min
D
Fura-2-NM
NAADP-AM
1 min
B
Fura-2
Ned-19
NAADP-AM
1 min
E
Fura-2-NM
Ned-19
NAADP-AM
1 min
C
Fura-2
tBHQ
NAADP-AM
1 min
F
Fura-2-NM
tBHQ
NAADP-AM
1 min
G
G
Fura-2-NM
Tg
NAADP-AM
1 min
Ca2+ (A.U)
I
Fura-2
J
Area Under Curve (U.AS-1)
***
ns
NAADP-AM
Ned19
tBHQ
tg

Figure 6

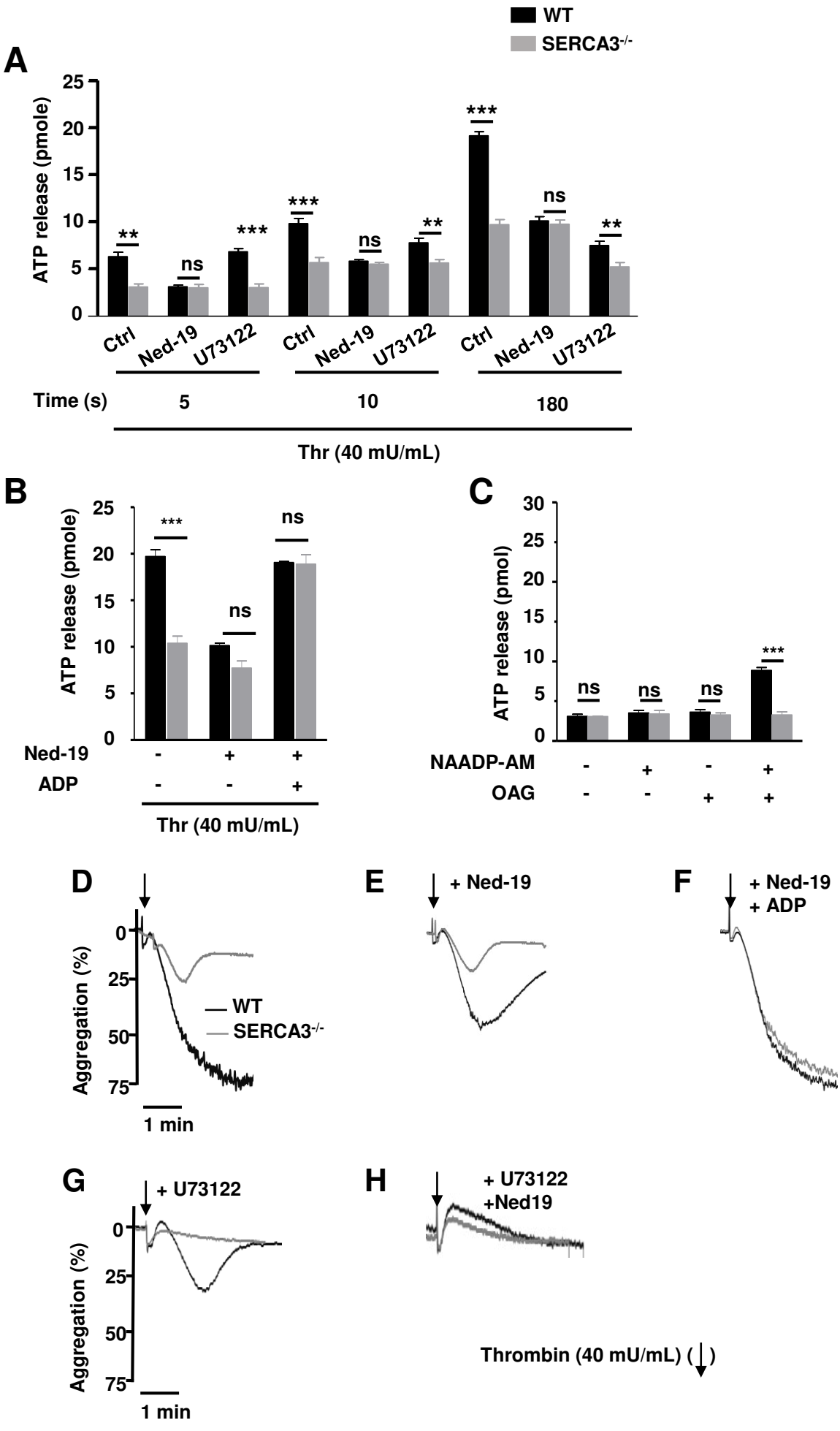
A
WT
SERCA3-/-
ATP release (pmole)
Ctrl
Ned-19
U73122
Time (s)
5
10
180
Thr (40 mU/mL)
B
ATP release (pmole)
Ned-19
ADP
Thr (40 mU/mL)
C
ATP release (pmol)
NAADP-AM
OAG
D
Aggregation (%)
WT
SERCA3-/-
1 min
E
+ Ned-19
F
+ Ned-19
+ ADP
G
+ U73122
Aggregation (%)
1 min
H
+ U73122
+Ned19
Thrombin (40 mU/mL)

Supplemental Figure S1

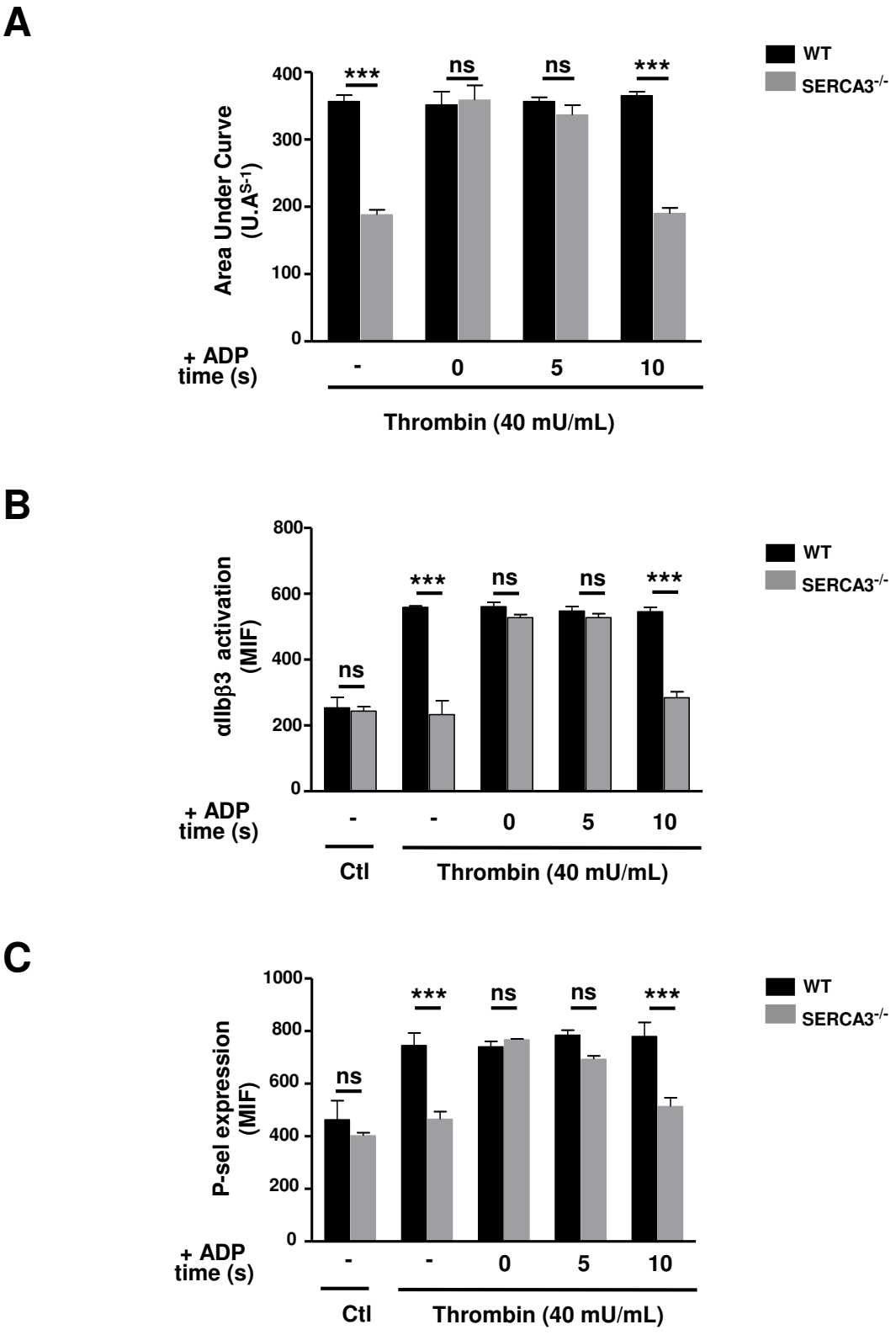

Supplemental Figure S2

A

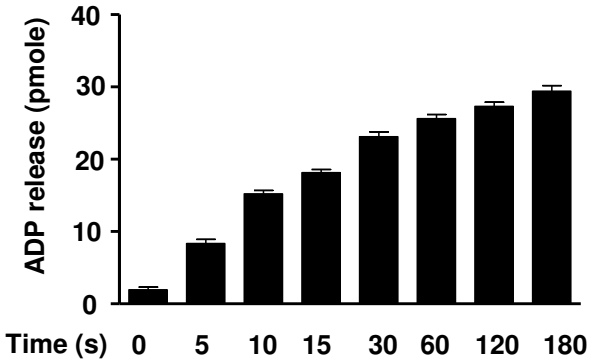

B

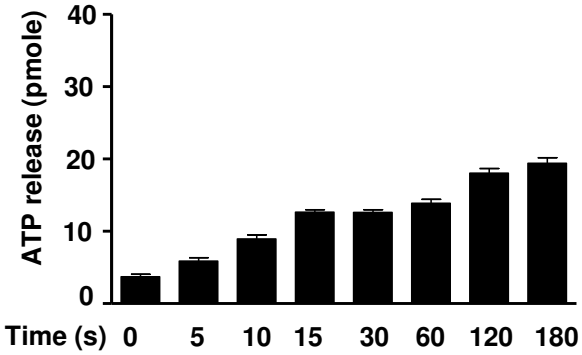

Supplemental Figure S3

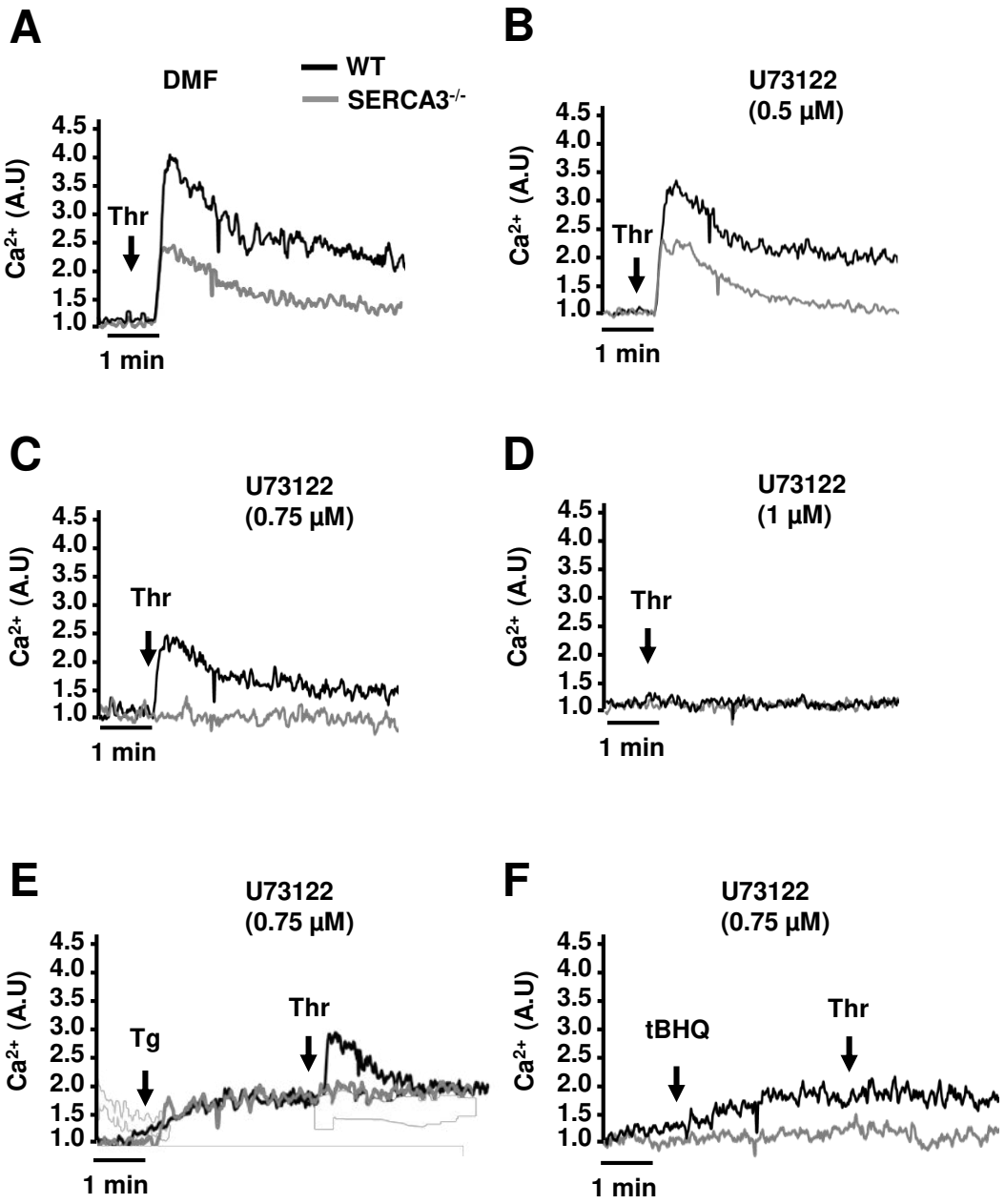

Discussion et perspectives

Les plaquettes jouent un rôle central dans l'hémostase primaire, et leurs fonctions sont dépendantes du signal calcique. Ce signal est composé d'une mobilisation et d'un influx calcique dans le cytosol. C'est dans ce compartiment que le Ca^{2+} joue un rôle important pour l'activation plaquettaire. En effet, après stimulation plaquettaire par la thrombine ou le collagène, il y a activation de la PLC qui produit de l'IP3 qui se lie à son tour sur son récepteur-canal de la membrane du STD pour mobiliser le Ca^{2+}. Ce schéma de signalisation calcique n'a pas évolué depuis presqu'une vingtaine d'années à l'exception de la découverte des SOCS qui permettent l'entrée du Ca^{2+} à partir du milieu extracellulaire et qui sont dépendants des réserves intra-plaquettaires après la mobilisation du Ca^{2+} par l'IP3. Les pompes ATPases calciques SERCA2b et SERCA3 interviennent dans ce schéma puisque globalement elles abaissent le Ca^{2+} cytosolique en le pompant vers des compartiments intracellulaires: soit le STD pour SERCA2b, soit les granules acides pour SERCA3, d'autant plus qu'elles constituent le seul mécanisme d'accumulation à l'intérieur de réserves intraplaquettaires du Ca^{2+}.

La présence d'un grand nombre d'isoformes de SERCA3 dans les plaquettes (6 chez l'homme et 3 chez la souris) suggère que ces pompes sont importantes pour l'activation des plaquettes et contrôlent l'homéostasie calcique. Une des questions qui se pose : pourquoi y a-t-il plusieurs formes de SERCAs (SERCA2 et SERCA3) dans la même cellule. Ont-elles des rôles fonctionnels différents ?

Même si la notion de plusieurs réserves contrôlées par différentes isoformes de SERCAs existe déjà, les études antérieures menées par plusieurs équipes ont suggéré une mobilisation calcique différentielle entre les stocks SERCA3 et SERCA2b après avoir observé par des approches pharmacologiques une association des isoformes de SERCA3 avec les granules acides de type lysosomial et avec les réserves possédant les récepteurs du NAADP (56,58,60,249). Mais ces pistes n'ont pas été réellement approfondies et la notion du rôle spécifique de l'action de SERCA3 dans les plaquettes n'a jamais été définie, probablement en raison de l'absence d'un modèle de souris déficiente en SERCA3. D'où l'intérêt de mon projet qui a été de déterminer si SERCA3 avait un rôle fonctionnel précis et spécifique à l'aide de l'utilisation de ce modèle de souris.

Nous avons commencé à répondre à certaines questions en analysant les fonctions plaquettaires de souris SERCA3$^{-/-}$, et le résultat a été publié (245). Le résultat principal est que les plaquettes SERCA3$^{-/-}$ (mais aussi les plaquettes WT en présence de l'inhibiteur pharmacologique de SERCA3, tBHQ) avaient un déficit de sécrétion d'ADP, responsable d'un défaut d'activation plaquettaire. Par contraste, avec l'inhibiteur pharmacologique de SERCA2 (thapsigargine), la sécrétion des plaquettes de souris sauvages n'était pas affectée. Il apparait donc que le stockage et/ou la signalisation du Ca^{2+} dépendant de SERCA3 sont impliqués dans la régulation de cette sécrétion indépendante de la mobilisation calcique des réserves SERCA2. Ce phénomène n'apparait en particulier qu'à faibles concentrations d'activateurs puisqu'à forte concentration, les fonctions plaquettaires sont normales mais la sécrétion reste diminuée. Néanmoins, l'ajout de l'ADP exogène avec le premier activateur à forte concentration induit la sécrétion complété de l'ATP. Ce résultat montre qu'il n'y a pas de défaut de stockage d'ADP mais plutôt qu'une fraction du stock granulaire est absolument dépendante d'une sécrétion initiale d'ADP lui-même. Mais ce stock serait différent du premier stock lui-même dépendant de SERCA3. La sécrétion des granules alpha a été montrée dépendante de l'ADP sécrété par les granules denses, ce qui est cohérent avec ce qui a été rapporté dans un modèle de souris atteint du syndrome Hermansky-Pudlak, car ces souris ont aussi un défaut de sécrétion des granules alpha dû à l'absence des granules denses.(250) (251).

Il est intéressant de noter que dans les plaquettes SERCA3$^{-/-}$ l'influx calcique est augmenté, ce qui apparemment pourrait compenser le faible niveau de mobilisation du Ca^{2+} (de sorte que l'augmentation globale du Ca^{2+} cytosolique lors de la stimulation plaquettaire en présence de Ca^{2+} externe serait normale). Cette SOCE compensatrice est compatible avec les faibles niveaux de Ca^{2+} dans les réserves, connus pour induire le recrutement de STIM1 par Orai-1 (62). Cette augmentation de l'activation de SOCE n'est pas modulée par la dégradation ou l'addition d'ADP dans le milieu extracellulaire, ce qui renforce l'idée qu'elle est directement induite par la déplétion des réserves SERCA3, et non via une voie dépendante de l'ADP. Ainsi, l'influx calcique apparaît comme un mécanisme compensatoire dans le cas de l'ablation (ou de l'inhibition) de SERCA3, expliquant l'impact limité sur l'hémostase des souris SERCA3$^{-/-}$. Cette conclusion découle de plusieurs observations: premièrement, la mobilisation du Ca^{2+} à partir des compartiments intracellulaires est diminuée dans les plaquettes SERCA3$^{-/-}$. Deuxièmement, les plaquettes SERCA3$^{-/-}$ présentent des niveaux inférieurs de Ca^{2+} stocké par rapport aux plaquettes témoins, comme en témoignent les expériences évaluant la vidange des réserves internes par l'ionomycine et la thapsigargine (1 μM pour bloquer SERCA2b et

SERCA3). Mais il faut remarquer qu'à forte concentration d'activateurs comme pour la thrombine à 100 mU/mL, ou bien quand l'ADP exogène est rajouté au premier activateur à faible dose (thrombine 40mU/mL) il n'y a plus de différence de mobilisation. Ce qui veut dire que c'est l'intensité du signal qui est affaiblie chez les plaquettes SERCA3$^{-/-}$ après stimulation à faibles concentrations d'activateur et cette signalisation mène à la mobilisation des stocks SERCA2. Sachant que les stocks SERCA2 sont dépendants de l'IP3, il se pourrait qu'à forte concentration de thrombine par exemple, le signal est tellement fort qu'il n'a pas besoin d'ADP pour faire mobiliser suffisamment de Ca^{2+} pour une activation normale des plaquettes. Néanmoins la sécrétion d'ADP SERCA3 dépendante reste absente dans ce modèle de souris. Il serait important donc de mesurer directement l'activation des PLC et la production d'IP3.

En plus de la différence fonctionnelle entre SERCA3 et SERCA2, nous avons confirmé leur différence topologique en montrant que SERCA3 a une localisation périphérique et aux extrémités des plaquettes alors que SERCA2 a une localisation plus centrale après visualisation par immunofluorescence (IF) confocale (Figure 19). Ces observations en IF semblent être confirmées par l'utilisation d'une sonde calcique, la sonde Fura-2-NM-AM (anciennement appelée Fura-2-FFP18-AM). Cette sonde a été conçue pour pénétrer à l'intérieur des cellules et s'associer avec le feuillet interne de la membrane (252) (253) et nous avons montré qu'elle ne détectait, en l'absence de Ca^{2+} extracellulaire, que le Ca^{2+} mobilisé depuis les réserves dépendant de SERCA3, suggérant une mobilisation sous-membranaire de ses réserves alors que le Ca^{2+} mobilisé depuis les réserves SERCA2b est uniquement détecté par une sonde cytosolique comme Fura-2. Il semble donc que la mobilisation calcique SERCA3 dépendante se produise près de la membrane plasmique et soit visualisée préférentiellement par le Fura-2-NM associé à la membrane interne, qui ne détecte pas la mobilisation SERCA2. Par contre le Fura-2 cytosolique, qui présenterait une faible accessibilité aux régions proximales, détecterait préférentiellement la mobilisation SERCA2.

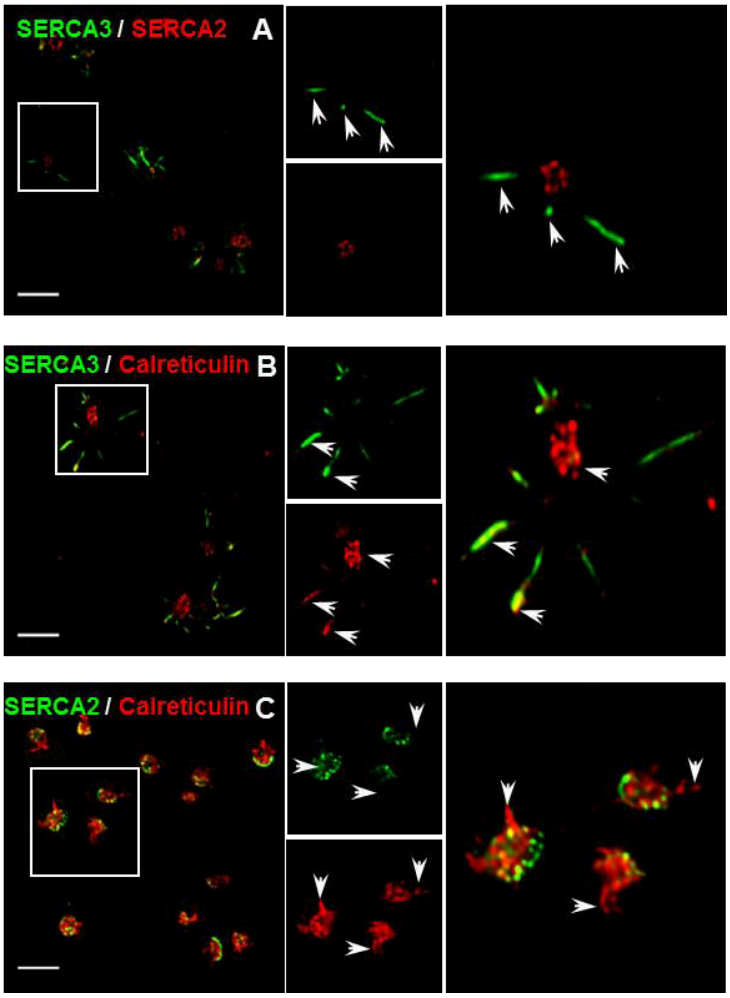

Figure 19 : Distribution de SERCA3 et SERCA2 dans les plaquettes murines. *Immuno-fluorescence confocale après co-maraquage de plaquettes murines C57Bl/6 A) pour SERCA3 (vert) et SERCA2b (rouge) B) SERCA3 (vert) et calréticuline, un marqueur de compartiments calciques (réticulum endoplasmique, granules acides) (rouge) ou C) SERCA2b (vert) et calréticuline (rouge). Les barres représentent 5 µm, objectif x63*

Si les réserves SERCA3 sont proches de la membrane plasmique, elles sont en bonne position pour contrôler une sécrétion rapide. Il reste à savoir si les granules denses dépendants de SERCA3 le sont pour une raison spécifique, par exemple parce qu'associés directement à SERCA3 ou ses réserves, ou bien si c'est un phénomène aléatoire, conséquence de la présence de quelques granules (pour rappel, au total, une dizaine par plaquettes) qui seraient proches de la membrane et donc des réserves SERCA3. Cette question mérite d'être explorée: une des méthodes qui pourrait répondre à cette question est la microscopie en 3D (FIB-SEM) (Focused ion beam / scanning electron *microscope*), ou en fluorescence membranaire avec la technique TIRF (Total Internal Reflection Fluorescence microscopy). Des études biochimiques sur granules purifiés (par exemple par affinité avec billes magnétiques et anti-LAMP2 ou autre

marqueur spécifique de granule dense) pourraient compléter cette observation, en recherchant par exemple la présence de SERCA3 dans la membrane.

Un élément important du projet a été de démontrer que l'observation chez la souris était transposable chez l'Homme. En prétraitant les plaquettes de sujets normaux avec du tBHQ, l'inhibiteur spécifique de SERCA3, nous observons une diminution de leur activation (agrégation, sécrétion et l'activation de $\alpha_{IIb}\beta_3$). L'addition de l'ADP exogène au premier activateur court-circuite l'inhibition par le tBHQ et restaure les fonctions plaquettaires. Ces résultats suggèrent que SERCA3 contrôle chez l'homme une sécrétion primaire d'ADP similaire à celle observée chez la souris. Ces résultats ont été confirmés par une étude cas-contrôle comparant des femmes avec une obésité sévère à des sujets témoins. Nous avons étudié les fonctions plaquettaires d'une cohorte de patientes atteintes d'obésité morbide avec un indice de masse corporelle (IMC) supérieur à 35 kg/m^2. Ces patientes ont subi une opération chirurgicale de by-pass gastrique leur permettant de maigrir et d'atteindre un IMC entre 18.5 et 25 kg/m^2 comme les sujets témoins auxquels elles ont été comparées avant et un an après amaigrissement. Nous avons observé une diminution de l'agrégation plaquettaire en réponse aux différents activateurs et une diminution de la mobilisation calcique chez ces patientes, le tout associé à une diminution de l'expression de SERCA3. Surtout les fonctions plaquettaires et l'expression de SERCA3 se sont normalisées après la perte de poids. De plus, l'addition d'ADP exogène au premier activateur a permis, comme chez la souris, de compenser la diminution de l'expression de SERCA3 et de restaurer la mobilisation, l'agrégation et surtout la sécrétion plaquettaire de ces patientes, alors que les fonctions des plaquettes de sujets témoins sont restées normales. Il s'agit de la première observation physiopathologique humaine liée à une déficience de l'expression de SERCA3 plaquettaire.

La diminution de l'expression de SERCA3 pourrait être un mécanisme protégeant les sujets atteints d'obésité sévère contre le risque pro-thrombotique qui est déjà décrit chez ces personnes. En abaissant le niveau d'expression de SERCA3, le risque d'activation spontanée des plaquettes exposées à des molécules pro-thrombotiques circulantes serait réduit. Cette régulation qui s'opèrerait au niveau de la formation des plaquettes est importante car il a été montré que les sujets atteints d'obésité sévère présentaient une résistance aux inhibiteurs pharmacologiques antiplaquettaires qui pourrait être due à un renouvellement très rapide des plaquettes (254–257). Ce renouvellement accéléré des plaquettes pourrait d'ailleurs expliquer directement la diminution de l'expression de SERCA3 chez les sujets atteints d'obésité morbide. En effet, l'obésité sévère serait comme d'autres syndromes inflammatoires,

consommateur de plaquettes et nécessiterait une production rapide de nouvelles plaquettes. Les travaux de l'équipe d'Essers (258) suggèrent justement qu'en condition inflammatoire, la mégacaryopoïèse pourrait être accélérée en court circuitant la voie classique de maturation. Cette production accrue de mégacaryocytes se ferait sans (ou avec moins d') endomitose, ce qui préserverait les capacités de multiplication des mégacaryocytes. Il est tout-à-fait possible que l'expression de certaines protéines soit perturbée au cours de cette maturation: l'expression de SERCA3 serait maintenue à un niveau faible si cette voie de maturation est abrégée car l'expression de SERCA3 est augmenté au cours de la différentiation cellulaire; réciproquement les cellules prolifératrices perdent l'expression de ces protéines (259) (208) (260) (207).

Nous avons enfin montré que la sécrétion d'ADP contrôlée par SERCA3 s'effectue dans les tout premiers temps de l'activation plaquettaire dès cinq secondes après stimulation. Cette sécrétion rapide est corrélée à un effet de désensibilisation à l'ADP, puisque l'addition d'ADP à des plaquettes $SERCA3^{-/-}$ après leur stimulation à la thrombine ne restaure leur agrégation que durant les premières secondes de stimulation. Cette désensibilisation semble impliquer surtout $P2Y_1$, en accord avec son fonctionnement connu. On peut en déduire donc que la sécrétion rapide d'ADP, SERCA3 dépendante, est compensée par la désensibilisation de $P2Y_1$ limitant donc cette amplification d'activation dans le temps. Il pourrait s'agir donc d'un couplage de deux mécanismes concertés pour réguler l'extension d'activation plaquettaire.

L'étude de la signalisation calcique a révélé un défaut de mobilisation calcique chez les $SERCA3^{-/-}$, mais les sondes utilisées (Oregon Green et Fura2-AM) détectent le Ca^{2+} cytosolique global provenant des réserves SERCA2 et SERCA3 dépendantes. Pour mieux cibler la signalisation calcique SERCA3 dépendante, nous avons utilisé la sonde Fura2NM-AM qui marque le Ca^{2+} uniquement dans la périphérie de la membrane des plaquettes où SERCA3 semble être préférentiellement localisée. Les résultats obtenus avec cette sonde montrent qu'elle ne détecte pas la mobilisation calcique sous-membranaire chez les $SERCA3^{-/-}$ et l'addition, ou la suppression de l'ADP du milieu extracellulaire (par l'apyrase) n'affectent pas cette mobilisation, ce qui signifie que le Ca^{2+} sous-membranaire est mobilisé par SERCA3 et est indépendant de l'ADP. C'est très important car le schéma global qui se dessine est que les réserves SERCA3 contrôlent une sécrétion très rapide d'ADP, donc a priori indépendante de ce nucléotide puisqu'en précédant sa sécrétion. C'est ce que nous avons confirmé, car la sécrétion primaire SERCA3-dépendante est toujours observée même en bloquant les 2 récepteurs d'ADP ($P2Y_1$ et $P2Y_{12}$). À noter que le pendant de cette découverte est que SERCA2b est responsable

de la sécrétion secondaire d'ADP. Une confirmation absolue serait l'analyse de souris SERCA2$^{-/-}$, mais leur létalité in utero rendrait ces expériences difficiles.

Une des questions soulevées au cours de ma thèse est liée à la nature des granules qui sont libérés lors de la première vague de mobilisation dépendante de NAADP et des stocks dépendant de SERCA3. Est-ce des granules denses ?

Comme seule une fraction du contenu total des granules est libérée, il est possible que deux populations distinctes de granules denses existent, chacune associée à un seul type de réserves liées à un type de SERCA. Selon cette hypothèse, un sous-type de granules denses serait associé physiquement et/ou fonctionnellement aux réserves dépendant de SERCA3 et seraient les seuls granules capables de relarguer leur contenu lors de la mobilisation du Ca^{2+} à partir des stocks SERCA3. Les granules restants entreraient alors dans la voie de sécrétion lors de la mobilisation calcique SERCA2b dépendante. Alors comment expliquer qu'en présence d'ADP, les plaquettes sauvage et KO sécrètent les mêmes quantités d'ATP et sérotonine ? Une deuxième hypothèse serait que la population des granules denses serait homogène, mais les granules proches des stocks SERCA3 (éventuellement près de la membrane plasmique) sécrètent leur contenu lors de la mobilisation calcique. Cette hypothèse a l'avantage de pouvoir expliquer qu'en présence d'ADP extracellulaire, la mobilisation est plus forte dans les réserves SERCA2b pour entrainer une sécrétion totale peut être en créant un influx SOCe plus important pour atteindre les régions sous membranaires.

L'observation peut-être la plus significative de nos travaux est que la sécrétion rapide d'ADP contrôlée par SERCA3, est en fait dépendante du NAADP, et non d'IP3, différenciant d'autant la voie SERCA3 de celle de SERCA2b. Bien que la mobilisation des "réserves acides" plaquettaires par le NAADP ait été documentée précédemment (56), son impact fonctionnel n'avait pas été montré. Une des questions relatives à cette observation est comment s'opère la mobilisation par NAADP? Elle a été montrée dépendante d'un récepteur qui reste à identifier, mais surtout implique un canal calcique, Two-Pore Channel ou TPC, dont le sous-type 2 a été montré présent dans les granules denses des cellules Meg-01 (9). Cette observation mérite d'être ré-examinée, car elle impliquerait que le Ca^{2+} mobilisé par NAADP, proviendrait des granules denses, qui pourraient constituer une partie des réserves SERCA3. Cela ferait de la voie SERCA3-NAADP-sécrétion rapide d'ADP, un "module intégré" de sécrétion. Cette hypothèse rejoint celle d'une population hétérogène de granules denses, avec une fraction dépendante de SERCA3. Des expériences futures devraient éclairer cette question, notamment par immuno-électromicroscopie.

Nos travaux suggèrent que les PLCs nécessitent une mobilisation calcique à partir des stocks SERCA3 suivie par une sécrétion d'ADP pour générer pleinement de l'IP3. Cela serait cohérent avec la notion que les stocks SERCA3 sont mobilisés en premier, suggérant alors que NAADP est généré avant IP3. Cela signifie que CD38, l'enzyme membranaire qui catalyse l'échange du groupe nicotinamide de $NADP^+$ avec de l'acide nicotinique pour synthétiser NAADP (261) agit rapidement à la suite de la stimulation par un activateur, avant l'activation de la PLC. Dans une étude de Mushtaq et coll des fonctions plaquettaires dans un modèle de souris $CD38^{-/-}$, les auteurs ont indiqué que la synthèse de NAADP paraissait secondaire à la synthèse d'IP3. Ils se sont basés sur l'inhibition de la synthèse de NAADP par l'inhibiteur de la PLC (U73122) (58). Nous pensons que les différences expérimentales sont à l'origine de ce résultat opposé au nôtre: ces auteurs ont utilisé des concentrations élevées de thrombine, 0.5U/mL, plus de 10 fois supérieures à 0.04 U/mL dans notre étude. De plus, les plaquettes ont été soumises à une agrégation qui additionne les signaux d'activation ainsi que la signalisation outside-in de l'intégrine αIIbβ3, alors que nous nous sommes concentrés sur l'activation initiale et utilisé des conditions non agitées pour prévenir l'engagement αIIbβ3. Enfin, les auteurs montrent que l'utilisation de l'inhibiteur du cADPR (8-Br-cADPR) affecte la mobilisation calcique en réponse à la thrombine dans les plaquettes de souris $CD38^{-/-}$. Mais comme cette molécule inhibe à la fois la production de cADPR et de NAADP, l'existence dans les plaquettes d'une signalisation calcique cADPR dépendante reste à établir. Nous envisageons d'étudier les fonctions plaquettaires et plus particulièrement la sécrétion ainsi que la mobilisation calcique en fura2NM-AM chez les souris déficientes en CD38. L'absence de mobilisation en fura2-NM-AM chez ces souris signifierait que seul le NAADP mobiliserait le Ca^{2+} des réserves SERCA3 dépendantes. L'étude de souris $IP3\text{-}R^{-/-}$ et $TPC2^{-/-}$ en hémostase serait aussi intéressant.

Nos travaux peuvent par ailleurs remettre en cause la notion de CICR (Calcium Induced Calcium Release) qui est un mécanisme expliquant que la mobilisation de Ca^{2+} peut être favorisée par une première libération de Ca^{2+}. (88). En effet, dans les plaquettes, le mécanisme que nous décrivons ressemble à un CICR si l'on fait abstraction de la synergie induite par la sécrétion d'ADP. Le CICR a été décrit dans de nombreux types cellulaires et certains auteurs proposent que la mobilisation du Ca^{2+} par le NAADP joue justement cette fonction. Cependant, cela ne semble pas être le cas, puisque le blocage de l'activité SERCA3 par tBHQ reproduit la suppression de SERCA3 à la fois en termes de mobilisation et de sécrétion ADP. Également, la sécrétion d'ADP est détectable en quelques secondes après la stimulation des plaquettes et

d'une manière entièrement dépendante de SERCA3 et de NAADP, alors qu'une voie de sécrétion ADP secondaire suit, et est dépendante d'IP3 et SERCA2b. Il est donc possible que le mécanisme que nous avons décrit dans la plaquette par lequel une voie SERCA3-NAADP mobilise du Ca^{2+}, ou un mécanisme similaire soit impliqué dans une sécrétion précoce de pertinence fonctionnelle puisse exister dans d'autres types cellulaires pour déclencher leur activation complète. En effet, cette organisation temporelle, avec une mobilisation calcique dépendante du NAADP en amont d'autres voies de mobilisation, a déjà été observée dans un certain nombre de cellules, y compris les spermatozoïdes d'oursins (262) les cellules pancréatiques, (263) ou les lymphocytes T (264), bien que la sécrétion des granules denses (ou équivalent, comme les lysosomes) n'ait pas été documentée dans ces types de cellules et corrélée aux voies différentielles de mobilisation calcique. De plus, aucune corrélation avec un inducteur agissant en synergie n'a été recherchée. Il faudrait donc explorer cette piste d'un rôle général de SERCA3 dans la régulation de sécrétion à effet autocrine amplificateur dans les autres tissus.

L'ensemble de ce travail montre donc l'existence dans les plaquettes murines et humaines d'une voie de sécrétion d'ADP, vraisemblablement granulaire dense, déclenchée dans les secondes suivant l'activation par la thrombine ou le collagène qui entraine la formation de NAADP, qui déclenche une mobilisation calcique spécifique des réserves internes dépendantes de SERCA3. Ce Ca^{2+} mobilisé induit avec le DAG une sécrétion rapide d'ADP d'une fraction des granules denses. L'ADP ainsi libéré active son récepteur P2Y1 qui signalise en synergie avec le premier activateur et déclenche une formation complète d'IP3 par la PLC pour permettre une mobilisation forte du Ca^{2+} des réserves SERCA2b, et entrainer une activation plus soutenue (agrégation et sécrétion du reste des granules denses) (Figure 20).

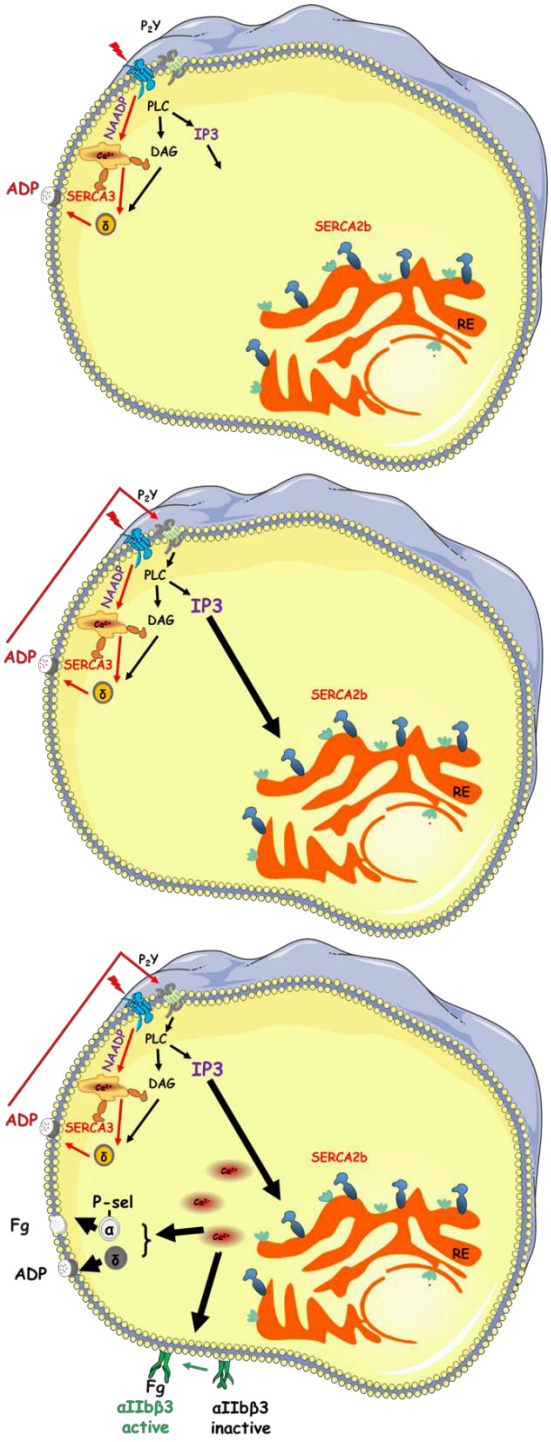

Figure 20 : proposition du modèle d'activation plaquettaire dépendant de SERCA3

A) Apres activation plaquettaire, la production du NAADP mobilise le Ca^{2+} à partir des réserves SERCA3. En parallèle l'activation de la PLC produit l'IP3 et le DAG. Le DAG et le Ca^{2+} vont induire une sécrétion primaire de l'ADP. B) l'ADP secrété se fixe sur son récepteur p_2Y_1 dont l'activation entre en synergie avec le premier activateur pour amplifier la production d'IP3. C) mobilisation soutenue du Ca^{2+} à partir des réserves SERCA2b suivie d'une sécrétion et activation de l'intégrine αIIbβ3 normale

La mise en évidence d'une boucle d'amplification de la réponse plaquettaire directement reliée à cette voie SERCA3 dépendante et passant par une sécrétion d'ADP change la vision de l'activation plaquettaire et fait réfléchir à l'utilisation des antagonistes des récepteurs d'ADP comme le clopidogrel et d'autres thiénopyridines, qui sont déjà utilisés comme antiplaquettaires. L'ADP est connu pour se fixer sur ses récepteurs $P2Y_1$ et $P2Y_{12}$. $P2Y_1$ induit une signalisation menant à l'activation de la PLC alors que le $P2Y_{12}$ induit une signalisation menant à l'activation de la PIK3 pour amplifier l'activation plaquettaire, or nos résultats suggèrent que l'ADP secrété en premier semble agir principalement sur $P2Y_1$ pour amplifier le signal IP3 et laisse imaginer que la seconde vague de sécrétion d'APD qui amplifie l'activation plaquettaire agit via $P2Y_{12}$. Selon les sujets traités, la réponse aux antiagrégants (anti $P2Y_1$ et $P2Y_{12}$) peut avoir des effets secondaires néfastes comme une hémorragie sévère. Nos résultats suggèrent que l'inhibition de la boucle d'amplification dépendant de SERCA3 ne se traduit que par un allongement modéré du temps de saignement. De plus, l'expression des SERCA3 semble pouvoir être physiologiquement régulée sans créer de complications sévères. Le blocage de cette voie de sécrétion d'ADP dépendante de SERCA3 pourrait donc constituer une nouvelle voie thérapeutique permettant une diminution d'un effet thrombotique mais sans aller jusqu'à un effet secondaire sévères.

Références bibliographiques

1. Peters LL, Cheever EM, Ellis HR, Magnani PA, Svenson KL, Smith RV, et al. Large-scale, high-throughput screening for coagulation and hematologic phenotypes in mice*. Physiol Genomics. 2002;11(3):185‑93.

2. Thon JN, Italiano JE. Platelets: production, morphology and ultrastructure. Handb Exp Pharmacol. 2012;(210):3‑22.

3. Eckly A, Rinckel J-Y, Proamer F, Ulas N, Joshi S, Whiteheart SW, et al. Respective contributions of single and compound granule fusion to secretion by activated platelets. Blood. 2016;128(21):2538‑49.

4. Huizing M, Helip-Wooley A, Westbroek W, Gunay-Aygun M, Gahl WA. Disorders of lysosome-related organelle biogenesis: clinical and molecular genetics. Annu Rev Genomics Hum Genet. 2008;9:359‑86.

5. Masliah-Planchon J, Darnige L, Bellucci S. Molecular determinants of platelet delta storage pool deficiencies: an update. Br J Haematol. 2013;160(1):5‑11.

6. Dean GE, Fishkes H, Nelson PJ, Rudnick G. The hydrogen ion-pumping adenosine triphosphatase of platelet dense granule membrane. Differences from F1F0- and phosphoenzyme-type ATPases. J Biol Chem. 1984;259(15):9569‑74.

7. McNicol A, Israels SJ. Platelet dense granules: structure, function and implications for haemostasis. Thromb Res. 1999;95(1):1‑18.

8. Holmsen H, Weiss HJ. Secretable storage pools in platelets. Annu Rev Med. 1979;30:119‑34.

9. Ambrosio AL, Boyle JA, Di Pietro SM. TPC2 mediates new mechanisms of platelet dense granule membrane dynamics through regulation of Ca^{2+} release. Mol Biol Cell. 2015;26(18):3263‑74.

10. Heijnen H, van der Sluijs P. Platelet secretory behaviour: as diverse as the granules … or not? J Thromb Haemost. 2015;13(12):2141‑51.

11. Fitch-Tewfik JL, Flaumenhaft R. Platelet Granule Exocytosis: A Comparison with Chromaffin Cells. Front Endocrinol. 2013;4. Disponible sur: http://www.ncbi.nlm.nih.gov/pmc/articles/PMC3693082/

12. Jonnalagadda D, Izu LT, Whiteheart SW. Platelet secretion is kinetically heterogeneous in an agonist-responsive manner. Blood. 2012;120(26):5209‑16.

13. Golebiewska EM, Poole AW. Platelet secretion: From haemostasis to wound healing and beyond. Blood Rev. 2015;29(3):153‑62.

14. Sehgal S, Storrie B. Evidence that differential packaging of the major platelet granule proteins von Willebrand factor and fibrinogen can support their differential release. J Thromb Haemost JTH. 2007;5(10):2009‑16.

15. Bentfeld-Barker ME, Bainton DF. Identification of primary lysosomes in human megakaryocytes and platelets. Blood. 1982;59(3):472‑81.

16. Södergren AL, Ramström S. Detection of Lysosomal Exocytosis in Platelets by Flow Cytometry. Methods Mol Biol Clifton NJ. 2017;1594:191‑203.

17. Goggs R, Williams CM, Mellor H, Poole AW. Platelet Rho GTPases-a focus on novel players, roles and relationships. Biochem J. 2015;466(3):431‑42.

18. Schwarz UR, Walter U, Eigenthaler M. Taming platelets with cyclic nucleotides. Biochem Pharmacol. 2001;62(9):1153‑61.

19. Walter U, Gambaryan S. cGMP and cGMP-Dependent Protein Kinase in Platelets and Blood Cells. In: Schmidt, Hofmann F, Stasch J-P, éditeurs. cGMP: Generators, Effectors and Therapeutic Implications [Internet]. Springer Berlin Heidelberg; 2009. p. 533‑48. (Handbook of Experimental Pharmacology). Disponible sur: http://link.springer.com/chapter/10.1007/978-3-540-68964-5_23

20. Kaplan ZS, Jackson SP. The role of platelets in atherothrombosis. Hematol Am Soc Hematol Educ Program. 2011;2011:51‑61.

21. George JN. Platelets. The Lancet. 2000;355(9214):1531‑9.

22. Bryckaert M, Rosa J-P, Denis CV, Lenting PJ. Of von Willebrand factor and platelets. Cell Mol Life Sci. 2015;72:307‑26.

23. Boulaftali Y, Hess PR, Kahn ML, Bergmeier W. Platelet ITAM Signaling and Vascular Integrity. Circ Res. 2014;114(7):1174‑84.

24. Ruggeri ZM. Platelet adhesion under flow. Microcirc 1994. 2009;16(1):58‑83.

25. Duvernay MT, Temple KJ, Maeng JG, Blobaum AL, Stauffer SR, Lindsley CW, et al. Contributions of Protease-Activated Receptors PAR1 and PAR4 to Thrombin-Induced GPIIbIIIa Activation in Human Platelets. Mol Pharmacol. 2017;91(1):39‑47.

26. Coughlin SR. Thrombin signalling and protease-activated receptors. Nature. 2000;407(6801):258‑64.

27. Coughlin SR. Protease-activated receptors in hemostasis, thrombosis and vascular biology. J Thromb Haemost JTH. 2005;3(8):1800‑14.

28. Gurbel PA, Kuliopulos A, Tantry US. G-Protein–Coupled Receptors Signaling Pathways in New Antiplatelet Drug Development. Arterioscler Thromb Vasc Biol. 2015;35(3):500‑12.

29. Gachet C. P2 receptors, platelet function and pharmacological implications. Thromb Haemost. 2008;99(3):466‑72.

30. Bhavaraju K, Mayanglambam A, Rao AK, Kunapuli SP. P2Y(12) antagonists as antiplatelet agents - Recent developments. Curr Opin Drug Discov Devel. 2010;13(4):497‑506.

31. Baurand A, Eckly A, Bari N, Léon C, Hechler B, Cazenave JP, et al. Desensitization of the platelet aggregation response to ADP: differential down-regulation of the P2Y1 and P2cyc receptors. Thromb Haemost. 2000;84(3):484-91.

32. Baurand A, Eckly A, Hechler B, Kauffenstein G, Galzi J-L, Cazenave J-P, et al. Differential regulation and relocalization of the platelet P2Y receptors after activation: a way to avoid loss of hemostatic properties? Mol Pharmacol. 2005;67(3):721-33.

33. Ohlmann P, Laugwitz KL, Nürnberg B, Spicher K, Schultz G, Cazenave JP, et al. The human platelet ADP receptor activates Gi2 proteins. Biochem J. 1995;312 (Pt 3):775-9.

34. Stefanini L, Roden RC, Bergmeier W. CalDAG-GEFI is at the nexus of calcium-dependent platelet activation. Blood. 2009;114(12):2506-14.

35. Ambrosio AL, Pietro SMD. Storage pool diseases illuminate platelet dense granule biogenesis. Platelets. 2017;28(2):138-46.

36. Yanachkov IB, Chang H, Yanachkova MI, Dix EJ, Berny-Lang MA, Gremmel T, et al. New Highly Active Antiplatelet Agents with Dual Specificity for Platelet P2Y1 and P2Y12 Adenosine Diphosphate Receptors. Eur J Med Chem. 2016;107:204-18.

37. Félétou M, Vanhoutte PM, Verbeuren TJ. The thromboxane/endoperoxide receptor (TP): the common villain. J Cardiovasc Pharmacol. 2010;55(4):317-32.

38. Li Z, Delaney MK, O'Brien KA, Du X. Signaling during platelet adhesion and activation. Arterioscler Thromb Vasc Biol. 2010;30(12):2341-9.

39. Bergmeier W, Stefanini L. Novel molecules in calcium signaling in platelets. J Thromb Haemost. 2009;7(SUPPL. 1):187-90.

40. Coller BS, Shattil SJ. The GPIIb/IIIa (integrin alphaIIbbeta3) odyssey: a technology-driven saga of a receptor with twists, turns, and even a bend. Blood. 2008;112(8):3011-25.

41. Ringer S. A further Contribution regarding the influence of the different Constituents of the Blood on the Contraction of the Heart. J Physiol. 1883;4(1):29-42.3.

42. Berridge MJ. Elementary and global aspects of calcium signalling. J Physiol. 1997;499 (Pt 2):291-306.

43. Carafoli E, Santella L, Branca D, Brini M. Generation, control, and processing of cellular calcium signals. Crit Rev Biochem Mol Biol. 2001;36(2):107-260.

44. Lipskaia L, Lompré A-M. Alteration in temporal kinetics of Ca_{2+} signaling and control of growth and proliferation. Biol Cell. 2004;96(1):55-68.

45. Williams RJP. The evolution of calcium biochemistry. Biochim Biophys Acta. 2006;1763(11):1139-46.

46. Dong Z, Saikumar P, Weinberg JM, Venkatachalam MA. Calcium in cell injury and death. Annu Rev Pathol. 2006;1:405-34.

47. Alvarez J, Montero M, García-Sancho J. Subcellular Ca(2+) Dynamics. News Physiol Sci Int J Physiol Prod Jointly Int Union Physiol Sci Am Physiol Soc. 1999;14:161-8.

48. Meldolesi J, Pozzan T. The endoplasmic reticulum Ca^{2+} store: a view from the lumen. Trends Biochem Sci. 1998;23(1):10-4.

49. Berridge MJ. Calcium microdomains: organization and function. Cell Calcium. 2006;40(5-6):405-12.

50. Bootman MD, Lipp P, Berridge MJ. The organisation and functions of local Ca(2+) signals. J Cell Sci. 2001;114(Pt 12):2213-22.

51. Gomez-Villafuertes R, Torres B, Barrio J, Savignac M, Gabellini N, Rizzato F, et al. Downstream regulatory element antagonist modulator regulates Ca^{2+} homeostasis and viability in cerebellar neurons. J Neurosci Off J Soc Neurosci. 2005;25(47):10822-30.

52. Voeltz GK, Rolls MM, Rapoport TA. Structural organization of the endoplasmic reticulum. EMBO Rep. 2002;3(10):944-50.

53. Gelebart P, Opas M, Michalak M. Calreticulin, a Ca^{2+}-binding chaperone of the endoplasmic reticulum. Int J Biochem Cell Biol. 2005;37(2):260-6.

54. Collins TJ, Lipp P, Berridge MJ, Bootman MD. Mitochondrial Ca(2+) uptake depends on the spatial and temporal profile of cytosolic Ca(2+) signals. J Biol Chem. 2001;276(28):26411-20.

55. Monteith GR, Blaustein MP. Heterogeneity of mitochondrial matrix free Ca^{2+}: resolution of Ca^{2+} dynamics in individual mitochondria in situ. Am J Physiol. 1999;276(5 Pt 1):C1193-1204.

56. López JJ, Camello-Almaraz C, Pariente JA, Salido GM, Rosado JA. Ca^{2+} accumulation into acidic organelles mediated by Ca^{2+}- and vacuolar H+-ATPases in human platelets. Biochem J. 2005;390(Pt 1):243-52.

57. Cavallini L, Coassin M, Alexandre A. Two classes of agonist-sensitive Ca^{2+} stores in platelets, as identified by their differential sensitivity to 2,5-di-(tert-butyl)-1,4-benzohydroquinone and thapsigargin. Biochem J. 1995;310 (Pt 2):449-52.

58. Mushtaq M, Nam T-S, Kim U-H. Critical role for CD38-mediated Ca^{2+} signaling in thrombin-induced procoagulant activity of mouse platelets and hemostasis. J Biol Chem. 2011;286(15):12952-8.

59. Brass LF, Joseph SK. A role for inositol triphosphate in intracellular Ca^{2+} mobilization and granule secretion in platelets. J Biol Chem. 1985;260(28):15172-9.

60. López JJ, Redondo PC, Salido GM, Pariente JA, Rosado JA. Two distinct Ca^{2+} compartments show differential sensitivity to thrombin, ADP and vasopressin in human platelets. Cell Signal. 2006;18(3):373-81.

61. López JJ, Salido GM, Pariente JA, Rosado JA. Interaction of STIM1 with endogenously expressed human canonical TRP1 upon depletion of intracellular Ca^{2+} stores. J Biol Chem. 2006;281(38):28254-64.

62. Zbidi H, Jardin I, Woodard GE, Lopez JJ, Berna-Erro A, Salido GM, et al. STIM1 and STIM2 are located in the acidic Ca^{2+} stores and associates with Orai1 upon depletion of the acidic stores in human platelets. J Biol Chem. 2011;286(14):12257-70.

63. Tolhurst G, Carter RN, Amisten S, Holdich JP, Erlinge D, Mahaut-Smith MP. Expression profiling and electrophysiological studies suggest a major role for Orai1 in the store-operated Ca^{2+} influx pathway of platelets and megakaryocytes. Platelets. 2008;19(4):308-13.

64. Berna-Erro A, Galan C, Dionisio N, Gomez LJ, Salido GM, Rosado JA. Capacitative and non-capacitative signaling complexes in human platelets. Biochim Biophys Acta. 2012;1823(8):1242-51.

65. Brownlow SL, Sage SO. Transient receptor potential protein subunit assembly and membrane distribution in human platelets. Thromb Haemost. 2005;94(4):839-45.

66. Chami M, Ferrari D, Nicotera P, Paterlini-Bréchot P, Rizzuto R. Caspase-dependent alterations of Ca^{2+} signaling in the induction of apoptosis by hepatitis B virus X protein. J Biol Chem. 2003;278(34):31745-55.

67. Scorrano L, Oakes SA, Opferman JT, Cheng EH, Sorcinelli MD, Pozzan T, et al. BAX and BAK regulation of endoplasmic reticulum Ca^{2+}: a control point for apoptosis. Science. 2003;300(5616):135-9.

68. Tombal B, Denmeade SR, Isaacs JT. Assessment and validation of a microinjection method for kinetic analysis of $[Ca^{2+}]i$ in individual cells undergoing apoptosis. Cell Calcium. 1999;25(1):19-28.

69. Bobe R, Bredoux R, Wuytack F, Quarck R, Kovàcs T, Papp B, et al. The rat platelet 97-kDa Ca^{2+}ATPase isoform is the sarcoendoplasmic reticulum Ca^{2+}ATPase 3 protein. J Biol Chem. 1994;269(2):1417-24.

70. Dean WL, Chen D, Brandt PC, Vanaman TC. Regulation of platelet plasma membrane Ca^{2+}-ATPase by cAMP-dependent and tyrosine phosphorylation. J Biol Chem. 1997;272(24):15113-9.

71. Rosado JA, Saavedra FR, Redondo PC, Hernández-Cruz JM, Salido GM, Pariente JA. Reduced plasma membrane Ca^{2+}-ATPase function in platelets from patients with non-insulin-dependent diabetes mellitus. Haematologica. 2004;89(9):1142-4.

72. Bobe R, Bredoux R, Corvazier E, Lacabaratz-Porret C, Martin V, Kovács T, et al. How many Ca^{2+} ATPase isoforms are expressed in a cell type? A growing family of membrane proteins illustrated by studies in platelets. Platelets. 2005;16(3-4):133-50.

73. Valant PA, Adjei PN, Haynes DH. Rapid Ca^{2+} extrusion via the Na^{+}/Ca^{2+} exchanger of the human platelet. J Membr Biol. 1992;130(1):63-82.

74. Streb H, Bayerdörffer E, Haase W, Irvine RF, Schulz I. Effect of inositol-1,4,5-trisphosphate on isolated subcellular fractions of rat pancreas. J Membr Biol. 1984;81(3):241-53.

75. Nakagawa T, Okano H, Furuichi T, Aruga J, Mikoshiba K. The subtypes of the mouse inositol 1,4,5-trisphosphate receptor are expressed in a tissue-specific and developmentally specific manner. Proc Natl Acad Sci U S A. 1991;88(14):6244-8.

76. Patel S, Churchill GC, Galione A. Coordination of Ca^{2+} signalling by NAADP. Trends Biochem Sci. 2001;26(8):482-9.

77. Patel S, Churchill GC, Sharp T, Galione A. Widespread distribution of binding sites for the novel Ca^{2+}-mobilizing messenger, nicotinic acid adenine dinucleotide phosphate, in the brain. J Biol Chem. 2000;275(47):36495-7.

78. Newton CL, Mignery GA, Südhof TC. Co-expression in vertebrate tissues and cell lines of multiple inositol 1,4,5-trisphosphate (InsP3) receptors with distinct affinities for InsP3. J Biol Chem. 1994;269(46):28613-9.

79. Yoneshima H, Miyawaki A, Michikawa T, Furuichi T, Mikoshiba K. Ca^{2+} differentially regulates the ligand-affinity states of type 1 and type 3 inositol 1,4,5-trisphosphate receptors. Biochem J. 1997;322 (Pt 2):591-6.

80. Matsumoto M, Nagata E. Type 1 inositol 1,4,5-trisphosphate receptor knock-out mice: their phenotypes and their meaning in neuroscience and clinical practice. J Mol Med Berl Ger. 1999;77(5):406-11.

81. Jiang Q-X, Thrower EC, Chester DW, Ehrlich BE, Sigworth FJ. Three-dimensional structure of the type 1 inositol 1,4,5-trisphosphate receptor at 24 A resolution. EMBO J. 2002;21(14):3575-81.

82. Caron AZ, Chaloux B, Arguin G, Guillemette G. Protein kinase C decreases the apparent affinity of the inositol 1,4,5-trisphosphate receptor type 3 in RINm5F cells. Cell Calcium. 2007;42(3):323-31.

83. Carafoli E. The calcium pumping ATPase of the plasma membrane. Annu Rev Physiol. 1991;53:531-47.

84. Bruce JIE, Shuttleworth TJ, Giovannucci DR, Yule DI. Phosphorylation of inositol 1,4,5-trisphosphate receptors in parotid acinar cells. A mechanism for the synergistic effects of cAMP on Ca^{2+} signaling. J Biol Chem. 2002;277(2):1340-8.

85. Toussaint F, Charbel C, Blanchette A, Ledoux J. CaMKII regulates intracellular Ca^{2+} dynamics in native endothelial cells. Cell Calcium. 2015;58(3):275-85.

86. Hajnóczky G, Thomas AP. Minimal requirements for calcium oscillations driven by the IP3 receptor. EMBO J. 1997;16(12):3533.

87. Berridge M, Lipp P, Bootman M. Calcium signalling. Curr Biol CB. 1999;9(5):R157-159.

88. Endo M. Calcium-Induced Calcium Release in Skeletal Muscle. Physiol Rev. 2009;89(4):1153-76.

89. Berridge MJ. Inositol trisphosphate and calcium signalling. Nature. 1993;361(6410):315-25.

90. Berridge MJ, Bootman MD, Roderick HL. Calcium signalling: dynamics, homeostasis and remodelling. Nat Rev Mol Cell Biol. 2003;4(7):517-29.

91. Thrower EC, Hagar RE, Ehrlich BE. Regulation of Ins(1,4,5)P3 receptor isoforms by endogenous modulators. Trends Pharmacol Sci. 2001;22(11):580-6.

92. Varga-Szabo D, Braun A, Nieswandt B. Calcium signaling in platelets. J Thromb Haemost JTH. 2009;7(7):1057-66.

93. El-Daher SS, Patel Y, Siddiqua A, Hassock S, Edmunds S, Maddison B, et al. Distinct localization and function of (1,4,5)IP(3) receptor subtypes and the (1,3,4,5)IP(4) receptor GAP1(IP4BP) in highly purified human platelet membranes. Blood. 2000;95(11):3412-22.

94. Lee HC, Walseth TF, Bratt GT, Hayes RN, Clapper DL. Structural determination of a cyclic metabolite of NAD+ with intracellular Ca^{2+}-mobilizing activity. J Biol Chem. 1989;264(3):1608-15.

95. Lee HC, Aarhus R. A derivative of NADP mobilizes calcium stores insensitive to inositol trisphosphate and cyclic ADP-ribose. J Biol Chem. 1995;270(5):2152-7.

96. Chini EN, Chini CCS, Kato I, Takasawa S, Okamoto H. CD38 is the major enzyme responsible for synthesis of nicotinic acid-adenine dinucleotide phosphate in mammalian tissues. Biochem J. 2002;362(Pt 1):125-30.

97. Rah S-Y, Park K-H, Nam T-S, Kim S-J, Kim H, Im M-J, et al. Association of CD38 with nonmuscle myosin heavy chain IIA and Lck is essential for the internalization and activation of CD38. J Biol Chem. 2007;282(8):5653-60.

98. Brailoiu E, Hoard JL, Filipeanu CM, Brailoiu GC, Dun SL, Patel S, et al. Nicotinic acid adenine dinucleotide phosphate potentiates neurite outgrowth. J Biol Chem. 2005;280(7):5646-50.

99. Kinnear NP, Boittin F-X, Thomas JM, Galione A, Evans AM. Lysosome-sarcoplasmic reticulum junctions. A trigger zone for calcium signaling by nicotinic acid adenine dinucleotide phosphate and endothelin-1. J Biol Chem. 2004;279(52):54319-26.

100. Cancela JM, Churchill GC, Galione A. Coordination of agonist-induced Ca^{2+}-signalling patterns by NAADP in pancreatic acinar cells. Nature. 1999;398(6722):74-6.

101. Boittin F-X, Galione A, Evans AM. Nicotinic acid adenine dinucleotide phosphate mediates Ca^{2+} signals and contraction in arterial smooth muscle via a two-pool mechanism. Circ Res. 2002;91(12):1168-75.

102. Galione A, Churchill GC. Interactions between calcium release pathways: multiple messengers and multiple stores. Cell Calcium. 2002;32(5-6):343-54.

103. Churchill GC, Galione A. NAADP induces Ca^{2+} oscillations via a two-pool mechanism by priming IP3- and cADPR-sensitive Ca^{2+} stores. EMBO J. 2001;20(11):2666-71.

104. Sánchez-Tusie AA, Vasudevan SR, Churchill GC, Nishigaki T, Treviño CL. Characterization of NAADP-mediated calcium signaling in human spermatozoa. Biochem Biophys Res Commun. 2014;443(2):531-6.

105. Parkesh R, Lewis AM, Aley PK, Arredouani A, Rossi S, Tavares R, et al. Cell-permeant NAADP: a novel chemical tool enabling the study of Ca^{2+} signalling in intact cells. Cell Calcium. 2008;43(6):531-8.

106. Naylor E, Arredouani A, Vasudevan SR, Lewis AM, Parkesh R, Mizote A, et al. Identification of a chemical probe for NAADP by virtual screening. Nat Chem Biol. 2009;5(4):220-6.

107. Churchill GC, Okada Y, Thomas JM, Genazzani AA, Patel S, Galione A. NAADP mobilizes Ca(2+) from reserve granules, lysosome-related organelles, in sea urchin eggs. Cell. 2002;111(5):703-8.

108. Bak J, White P, Timár G, Missiaen L, Genazzani AA, Galione A. Nicotinic acid adenine dinucleotide phosphate triggers Ca^{2+} release from brain microsomes. Curr Biol CB. 1999;9(14):751-4.

109. Yamasaki M, Masgrau R, Morgan AJ, Churchill GC, Patel S, Ashcroft SJH, et al. Organelle selection determines agonist-specific Ca^{2+} signals in pancreatic acinar and beta cells. J Biol Chem. 2004;279(8):7234-40.

110. Mitchell KJ, Lai FA, Rutter GA. Ryanodine receptor type I and nicotinic acid adenine dinucleotide phosphate receptors mediate Ca^{2+} release from insulin-containing vesicles in living pancreatic beta-cells (MIN6). J Biol Chem. 2003;278(13):11057-64.

111. Pereira GJS, Hirata H, Fimia GM, do Carmo LG, Bincoletto C, Han SW, et al. Nicotinic acid adenine dinucleotide phosphate (NAADP) regulates autophagy in cultured astrocytes. J Biol Chem. 2011;286(32):27875-81.

112. Jardín I, López JJ, Pariente JA, Salido GM, Rosado JA. Intracellular calcium release from human platelets: different messengers for multiple stores. Trends Cardiovasc Med. 2008;18(2):57-61.

113. Dammermann W, Guse AH. Functional ryanodine receptor expression is required for NAADP-mediated local Ca^{2+} signaling in T-lymphocytes. J Biol Chem. 2005;280(22):21394-9.

114. Langhorst MF, Schwarzmann N, Guse AH. Ca^{2+} release via ryanodine receptors and Ca^{2+} entry: major mechanisms in NAADP-mediated Ca^{2+} signaling in T-lymphocytes. Cell Signal. 2004;16(11):1283-9.

115. Brailoiu E, Churamani D, Cai X, Schrlau MG, Brailoiu GC, Gao X, et al. Essential requirement for two-pore channel 1 in NAADP-mediated calcium signaling. J Cell Biol. 2009;186(2):201-9.

116. Zong X, Schieder M, Cuny H, Fenske S, Gruner C, Rötzer K, et al. The two-pore channel TPCN2 mediates NAADP-dependent Ca^{2+}-release from lysosomal stores. Pflugers Arch. 2009;458(5):891-9.

117. Brailoiu E, Hooper R, Cai X, Brailoiu GC, Keebler MV, Dun NJ, et al. An ancestral deuterostome family of two-pore channels mediates nicotinic acid adenine dinucleotide phosphate-dependent calcium release from acidic organelles. J Biol Chem. 2010;285(5):2897-901.

118. Morgan AJ, Galione A. Two-pore channels (TPCs): current controversies. BioEssays News Rev Mol Cell Dev Biol. 2014;36(2):173-83.

119. Dionisio N, Albarrán L, López JJ, Berna-Erro A, Salido GM, Bobe R, et al. Acidic NAADP-releasable Ca^{2+} compartments in the megakaryoblastic cell line MEG01. Biochim Biophys Acta. 2011;1813(8):1483-94.

120. López JJ, Dionisio N, Berna-Erro A, Galán C, Salido GM, Rosado JA. Two-pore channel 2 (TPC2) modulates store-operated Ca(2+) entry. Biochim Biophys Acta. 2012;

121. Mahaut-Smith MP, Jones S, Evans RJ. The P2X1 receptor and platelet function. Purinergic Signal. 2011;7(3):341-56.

122. Rolf MG, Brearley CA, Mahaut-Smith MP. Platelet shape change evoked by selective activation of P2X1 purinoceptors with alpha,beta-methylene ATP. Thromb Haemost. 2001;85(2):303-8.

123. den Dekker E, Molin DG, Breikers G, van Oerle R, Akkerman JW, van Eys GJ, et al. Expression of transient receptor potential mRNA isoforms and Ca(2+) influx in differentiating human stem cells and platelets. Biochim Biophys Acta. 2001;1539(3):243-55.

124. Hassock SR, Zhu MX, Trost C, Flockerzi V, Authi KS. Expression and role of TRPC proteins in human platelets: evidence that TRPC6 forms the store-independent calcium entry channel. Blood. 2002;100(8):2801-11.

125. Paez Espinosa EV, Murad JP, Ting HJ, Khasawneh FT. Mouse transient receptor potential channel 6: role in hemostasis and thrombogenesis. Biochem Biophys Res Commun. 2012;417(2):853-6.

126. Jones S, Evans RJ, Mahaut-Smith MP. Ca^{2+} influx through P2X1 receptors amplifies P2Y1 receptor-evoked Ca^{2+} signaling and ADP-evoked platelet aggregation. Mol Pharmacol. 2014;86(3):243-51.

127. Vial C, Rolf MG, Mahaut-Smith MP, Evans RJ. A study of P2X1 receptor function in murine megakaryocytes and human platelets reveals synergy with P2Y receptors. Br J Pharmacol. 2002;135(2):363-72.

128. Harper MT, Mason MJ, Sage SO, Harper AGS. Phorbol ester-evoked Ca^{2+} signaling in human platelets is via autocrine activation of P(2X1) receptors, not a novel non-capacitative Ca^{2+} entry. J Thromb Haemost JTH. 2010;8(7):1604-13.

129. Hechler B, Lenain N, Marchese P, Vial C, Heim V, Freund M, et al. A role of the fast ATP-gated P2X1 cation channel in thrombosis of small arteries in vivo. J Exp Med. 2003;198(4):661-7.

130. Rosado JA, Sage SO. Activation of store-mediated calcium entry by secretion-like coupling between the inositol 1,4,5-trisphosphate receptor type II and human transient receptor potential (hTrp1) channels in human platelets. Biochem J. 2001;356(Pt 1):191-8.

131. Jardín I, Redondo PC, Salido GM, Rosado JA. Phosphatidylinositol 4,5-bisphosphate enhances store-operated calcium entry through hTRPC6 channel in human platelets. Biochim Biophys Acta. 2008;1783(1):84-97.

132. Ramanathan G, Gupta S, Thielmann I, Pleines I, Varga-Szabo D, May F, et al. Defective diacylglycerol-induced Ca^{2+} entry but normal agonist-induced activation responses in TRPC6-deficient mouse platelets. J Thromb Haemost JTH. 2012;10(3):419-29.

133. Berg LP, Shamsher MK, El-Daher SS, Kakkar VV, Authi KS. Expression of human TRPC genes in the megakaryocytic cell lines MEG01, DAMI and HEL. FEBS Lett. 1997;403(1):83-6.

134. Vemana HP, Karim ZA, Conlon C, Khasawneh FT. A critical role for the transient receptor potential channel type 6 in human platelet activation. PloS One. 2015;10(4):e0125764.

135. Yu Y, Keller SH, Remillard CV, Safrina O, Nicholson A, Zhang SL, et al. A Functional Single-Nucleotide Polymorphism in the TRPC6 Gene Promoter Associated With Idiopathic Pulmonary Arterial Hypertension. Circulation. 2009;119(17):2313.

136. Varga-Szabo D, Authi KS, Braun A, Bender M, Ambily A, Hassock SR, et al. Store-operated Ca^{2+} entry in platelets occurs independently of transient receptor potential (TRP) C1. Pflugers Arch. 2008;457(2):377-87.

137. Jardin I, Ben Amor N, Bartegi A, Pariente JA, Salido GM, Rosado JA. Differential involvement of thrombin receptors in Ca^{2+} release from two different intracellular stores in human platelets. Biochem J. 2007;401(1):167-74.

138. Grosse J, Braun A, Varga-Szabo D, Beyersdorf N, Schneider B, Zeitlmann L, et al. An EF hand mutation in Stim1 causes premature platelet activation and bleeding in mice. J Clin Invest. 2007;117(11):3540-50.

139. Spassova MA, Soboloff J, He L-P, Xu W, Dziadek MA, Gill DL. STIM1 has a plasma membrane role in the activation of store-operated Ca^{2+} channels. Proc Natl Acad Sci U S A. 2006;103(11):4040-5.

140. Roos J, DiGregorio PJ, Yeromin AV, Ohlsen K, Lioudyno M, Zhang S, et al. STIM1, an essential and conserved component of store-operated Ca^{2+} channel function. J Cell Biol. 2005;169(3):435-45.

141. Gilio K, van Kruchten R, Braun A, Berna-Erro A, Feijge MAH, Stegner D, et al. Roles of platelet STIM1 and Orai1 in glycoprotein VI- and thrombin-dependent procoagulant activity and thrombus formation. J Biol Chem. 2010;285(31):23629-38.

142. Nakamura L, Sandrock-Lang K, Speckmann C, Vraetz T, Bührlen M, Ehl S, et al. Platelet secretion defect in a patient with stromal interaction molecule 1 deficiency. Blood. 2013;122(22):3696-8.

143. Ahmad F, Boulaftali Y, Greene TK, Ouellette TD, Poncz M, Feske S, et al. Relative contributions of stromal interaction molecule 1 and CalDAG-GEFI to calcium-dependent platelet activation and thrombosis. J Thromb Haemost JTH. 2011;9(10):2077-86.

144. Misceo D, Holmgren A, Louch WE, Holme PA, Mizobuchi M, Morales RJ, et al. A dominant STIM1 mutation causes Stormorken syndrome. Hum Mutat. 2014;35(5):556-64.

145. Morin G, Bruechle NO, Singh AR, Knopp C, Jedraszak G, Elbracht M, et al. Gain-of-Function Mutation in STIM1 (P.R304W) Is Associated with Stormorken Syndrome. Hum Mutat. 2014;35(10):1221-32.

146. Markello T, Chen D, Kwan JY, Horkayne-Szakaly I, Morrison A, Simakova O, et al. York platelet syndrome is a CRAC channelopathy due to gain-of-function mutations in STIM1. Mol Genet Metab. 2015;114(3):474-82.

147. Nesin V, Wiley G, Kousi M, Ong E-C, Lehmann T, Nicholl DJ, et al. Activating mutations in STIM1 and ORAI1 cause overlapping syndromes of tubular myopathy and congenital miosis. Proc Natl Acad Sci U S A. 2014;111(11):4197-202.

148. McCarl C-A, Picard C, Khalil S, Kawasaki T, Röther J, Papolos A, et al. ORAI1 deficiency and lack of store-operated Ca^{2+} entry cause immunodeficiency, myopathy, and ectodermal dysplasia. J Allergy Clin Immunol. 2009;124(6):1311-1318.e7.

149. Braun A, Varga-Szabo D, Kleinschnitz C, Pleines I, Bender M, Austinat M, et al. Orai1 (CRACM1) is the platelet SOC channel and essential for pathological thrombus formation. Blood. 2009;113(9):2056-63.

150. Braun A, Varga-Szabo D, Kleinschnitz C, Pleines I, Bender M, Austinat M, et al. Orai1 (CRACM1) is the platelet SOC channel and essential for pathological thrombus formation. Blood. 2009;113(9):2056-63.

151. Bergmeier W, Oh-Hora M, McCarl C-A, Roden RC, Bray PF, Feske S. R93W mutation in Orai1 causes impaired calcium influx in platelets. Blood. 2009;113(3):675-8.

152. van Kruchten R, Braun A, Feijge MAH, Kuijpers MJE, Rivera-Galdos R, Kraft P, et al. Antithrombotic potential of blockers of store-operated calcium channels in platelets. Arterioscler Thromb Vasc Biol. 2012;32(7):1717-23.

153. Blaustein MP, Lederer WJ. Sodium/calcium exchange: its physiological implications. Physiol Rev. 1999;79(3):763-854.

154. Rosado JA, Sage SO. Regulation of plasma membrane Ca^{2+}-ATPase by small GTPases and phosphoinositides in human platelets. J Biol Chem. 2000;275(26):19529-35.

155. Martin V, Bredoux R, Corvazier E, Papp B, Enouf J. Platelet Ca(2+)ATPases : a plural, species-specific, and multiple hypertension-regulated expression system. Hypertens Dallas Tex 1979. 2000;35(1 Pt 1):91-102.

156. Oceandy D, Cartwright EJ, Emerson M, Prehar S, Baudoin FM, Zi M, et al. Neuronal nitric oxide synthase signaling in the heart is regulated by the sarcolemmal calcium pump 4b. Circulation. 2007;115(4):483-92.

157. Dean WL, Whiteheart SW. Plasma membrane Ca(2+)-ATPase (PMCA) translocates to filopodia during platelet activation. Thromb Haemost. 2004;91(2):325-33.

158. Jones S, Solomon A, Sanz-Rosa D, Moore C, Holbrook L, Cartwright EJ, et al. The plasma membrane calcium ATPase modulates calcium homeostasis, intracellular signaling events and function in platelets. J Thromb Haemost. 2010;8(12):2766-74.

159. Ebashi F, Ebashi S. Removal of calcium and relaxation in actomyosin systems. Nature. 1962;194:378-9.

160. Hasselbach W, Makinose M. [The calcium pump of the « relaxing granules » of muscle and its dependence on ATP-splitting]. Biochem Z. 1961;333:518-28.

161. Brini M, Calì T, Ottolini D, Carafoli E. Calcium pumps: why so many? Compr Physiol. 2012;2(2):1045-60.

162. Brandl CJ, deLeon S, Martin DR, MacLennan DH. Adult forms of the Ca^{2+} ATPase of sarcoplasmic reticulum. Expression in developing skeletal muscle. J Biol Chem. 1987;262(8):3768-74.

163. Dode L, Andersen JP, Leslie N, Dhitavat J, Vilsen B, Hovnanian A. Dissection of the Functional Differences between Sarco(endo)plasmic Reticulum Ca^{2+}-ATPase (SERCA) 1 and 2 Isoforms and Characterization of Darier Disease (SERCA2) Mutants by Steady-state and Transient Kinetic Analyses. J Biol Chem. 2003;278(48):47877-89.

164. Lytton J, Westlin M, Burk SE, Shull GE, MacLennan DH. Functional comparisons between isoforms of the sarcoplasmic or endoplasmic reticulum family of calcium pumps. J Biol Chem. 1992;267(20):14483-9.

165. Stammers AN, Susser SE, Hamm NC, Hlynsky MW, Kimber DE, Kehler DS, et al. The regulation of sarco(endo)plasmic reticulum calcium-ATPases (SERCA). Can J Physiol Pharmacol. 2015;93(10):843-54.

166. Callen DF, Baker E, Lane S, Nancarrow J, Thompson A, Whitmore SA, et al. Regional mapping of the Batten disease locus (CLN3) to human chromosome 16p12. Am J Hum Genet. 1991;49(6):1372-7.

167. Zhang Y, Fujii J, Phillips MS, Chen HS, Karpati G, Yee WC, et al. Characterization of cDNA and genomic DNA encoding SERCA1, the Ca^{2+}-ATPase of human fast-twitch skeletal muscle sarcoplasmic reticulum, and its elimination as a candidate gene for Brody disease. Genomics. 1995;30(3):415-24.

168. Toyoshima C, Nakasako M, Nomura H, Ogawa H. Crystal structure of the calcium pump of sarcoplasmic reticulum at 2.6 A resolution. Nature. 2000;405(6787):647-55.

169. MacLennan DH, Brandl CJ, Korczak B, Green NM. Amino-acid sequence of a Ca^{2+} Mg^{2+}-dependent ATPase from rabbit muscle sarcoplasmic reticulum, deduced from its complementary DNA sequence. Nature. 1985;316(6030):696-700.

170. Maruyama K, MacLennan DH. Mutation of aspartic acid-351, lysine-352, and lysine-515 alters the Ca^{2+} transport activity of the Ca^{2+}-ATPase expressed in COS-1 cells. Proc Natl Acad Sci U S A. 1988;85(10):3314-8.

171. Odermatt A, Taschner PE, Khanna VK, Busch HF, Karpati G, Jablecki CK, et al. Mutations in the gene-encoding SERCA1, the fast-twitch skeletal muscle sarcoplasmic reticulum Ca^{2+} ATPase, are associated with Brody disease. Nat Genet. 1996;14(2):191-4.

172. MacLennan DH. Ca^{2+} signalling and muscle disease. Eur J Biochem. 2000;267(17):5291-7.

173. Brandl CJ, Green NM, Korczak B, MacLennan DH. Two Ca^{2+} ATPase genes: homologies and mechanistic implications of deduced amino acid sequences. Cell. 1986;44(4):597-607.

174. Gélébart P, Martin V, Enouf J, Papp B. Identification of a new SERCA2 splice variant regulated during monocytic differentiation. Biochem Biophys Res Commun. 2003;303(2):676-84.

175. Bayle D, Weeks D, Sachs G. The membrane topology of the rat sarcoplasmic and endoplasmic reticulum calcium ATPases by in vitro translation scanning. J Biol Chem. 1995;270(43):25678-84.

176. Lipskaia L, Keuylian Z, Blirando K, Mougenot N, Jacquet A, Rouxel C, et al. Expression of sarco (endo) plasmic reticulum calcium ATPase (SERCA) system in normal mouse cardiovascular tissues, heart failure and atherosclerosis. Biochim Biophys Acta. 2014;1843(11):2705-18.

177. Lompré AM, Anger M, Levitsky D. Sarco(endo)plasmic reticulum calcium pumps in the cardiovascular system: function and gene expression. J Mol Cell Cardiol. 1994;26(9):1109-21.

178. Magnier C, Papp B, Corvazier E, Bredoux R, Wuytack F, Eggermont J, et al. Regulation of sarco-endoplasmic reticulum Ca^{2+}-ATPases during platelet-derived growth factor-induced smooth muscle cell proliferation. J Biol Chem. 1992;267(22):15808-15.

179. Campbell AM, Wuytack F, Fambrough DM. Differential distribution of the alternative forms of the sarcoplasmic/endoplasmic reticulum Ca^{2+}-ATPase, SERCA2b and SERCA2a, in the avian brain. Brain Res. 1993;605(1):67-76.

180. Lee MG, Xu X, Zeng W, Diaz J, Kuo TH, Wuytack F, et al. Polarized expression of Ca^{2+} pumps in pancreatic and salivary gland cells. Role in initiation and propagation of $[Ca^{2+}]i$ waves. J Biol Chem. 1997;272(25):15771-6.

181. Gunteski-Hamblin AM, Greeb J, Shull GE. A novel Ca^{2+} pump expressed in brain, kidney, and stomach is encoded by an alternative transcript of the slow-twitch muscle sarcoplasmic reticulum Ca-ATPase gene. Identification of cDNAs encoding Ca^{2+} and other cation-transporting ATPases using an oligonucleotide probe derived from the ATP-binding site. J Biol Chem. 1988;263(29):15032-40.

182. Vangheluwe P, Schuermans M, Raeymaekers L, Wuytack F. Tight interplay between the Ca^{2+} affinity of the cardiac SERCA2 Ca^{2+} pump and the SERCA2 expression level. Cell Calcium. 2007;42(3):281-9.

183. Wuytack F, Raeymaekers L, Missiaen L. Molecular physiology of the SERCA and SPCA pumps. Cell Calcium. 2002;32(5-6):279-305.

184. Dally S, Bredoux R, Corvazier E, Andersen JP, Clausen JD, Dode L, et al. Ca^{2+}-ATPases in non-failing and failing heart: evidence for a novel cardiac sarco/endoplasmic reticulum Ca^{2+}-ATPase 2 isoform (SERCA2c). Biochem J. 2006;395(2):249-58.

185. Ahn W, Lee MG, Kim KH, Muallem S. Multiple effects of SERCA2b mutations associated with Darier's disease. J Biol Chem. 2003;278(23):20795-801.

186. Hovnanian A. Darier's disease: from dyskeratosis to endoplasmic reticulum calcium ATPase deficiency. Biochem Biophys Res Commun. 2004;322(4):1237-44.

187. Dhitavat J, Dode L, Leslie N, Sakuntabhai A, Lorette G, Hovnanian A. Mutations in the sarcoplasmic/endoplasmic reticulum Ca^{2+} ATPase isoform cause Darier's disease. J Invest Dermatol. 2003;121(3):486-9.

188. Hovnanian A. SERCA pumps and human diseases. Subcell Biochem. 2007;45:337-63.

189. Shull GE. Gene knockout studies of Ca^{2+}-transporting ATPases. Eur J Biochem. 2000;267(17):5284-90.

190. Periasamy M, Reed TD, Liu LH, Ji Y, Loukianov E, Paul RJ, et al. Impaired cardiac performance in heterozygous mice with a null mutation in the sarco(endo)plasmic reticulum Ca^{2+}-ATPase isoform 2 (SERCA2) gene. J Biol Chem. 1999;274(4):2556-62.

191. Ji Y, Lalli MJ, Babu GJ, Xu Y, Kirkpatrick DL, Liu LH, et al. Disruption of a Single Copy of the SERCA2 Gene Results in Altered Ca^{2+} Homeostasis and Cardiomyocyte Function. J Biol Chem. 2000;275(48):38073-80.

192. Bobe R, Hadri L, Lopez JJ, Sassi Y, Atassi F, Karakikes I, et al. SERCA2a controls the mode of agonist-induced intracellular Ca^{2+} signal, transcription factor NFAT and proliferation in human vascular smooth muscle cells. J Mol Cell Cardiol. 2011;50(4):621-33.

193. Burk SE, Lytton J, MacLennan DH, Shull GE. cDNA cloning, functional expression, and mRNA tissue distribution of a third organellar Ca^{2+} pump. J Biol Chem. 1989;264(31):18561-8.

194. Wuytack F, Papp B, Verboomen H, Raeymaekers L, Dode L, Bobe R, et al. A sarco/endoplasmic reticulum Ca^{2+}-ATPase 3-type Ca^{2+} pump is expressed in platelets, in lymphoid cells, and in mast cells. J Biol Chem. 1994;269(2):1410-6.

195. Dode L, Wuytack F, Kools PF, Baba-Aissa F, Raeymaekers L, Briké F, et al. cDNA cloning, expression and chromosomal localization of the human sarco/endoplasmic reticulum Ca(2+)-ATPase 3 gene. Biochem J. 1996;318 (Pt 2):689-99.

196. Dode L, De Greef C, Mountian I, Attard M, Town MM, Casteels R, et al. Structure of the human sarco/endoplasmic reticulum Ca^{2+}-ATPase 3 gene. Promoter analysis and alternative splicing of the SERCA3 pre-mRNA. J Biol Chem. 1998;273(22):13982-94.

197. Bobe R, Bredoux R, Corvazier E, Andersen JP, Clausen JD, Dode L, et al. Identification, expression, function, and localization of a novel (sixth) isoform of the human sarco/endoplasmic reticulum Ca^{2+} ATPase 3 gene. J Biol Chem. 2004;279(23):24297-306.

198. Wuytack F, Dode L, Baba-Aissa F, Raeymaekers L. The SERCA3-type of organellar Ca^{2+} pumps. Biosci Rep. 1995;15(5):299-306.

199. Martin V, Bredoux R, Corvazier E, Van Gorp R, Kovacs T, Gelebart P, et al. Three novel sarco/endoplasmic reticulum Ca^{2+}-ATPase (SERCA) 3 isoforms. Expression, regulation, and function of the membranes of the SERCA3 family. J Biol Chem. 2002;277(27):24442-52.

200. Mekahli D, Bultynck G, Parys JB, De Smedt H, Missiaen L. Endoplasmic-Reticulum Calcium Depletion and Disease. Cold Spring Harb Perspect Biol [Internet]. 2011;3(6). Disponible sur: http://www.ncbi.nlm.nih.gov/pmc/articles/PMC3098671/

201. Gélébart P, Kovács T, Brouland J-P, van Gorp R, Grossmann J, Rivard N, et al. Expression of endomembrane calcium pumps in colon and gastric cancer cells. Induction of SERCA3 expression during differentiation. J Biol Chem. 2002;277(29):26310-20.

202. Liu LH, Paul RJ, Sutliff RL, Miller ML, Lorenz JN, Pun RY, et al. Defective endothelium-dependent relaxation of vascular smooth muscle and endothelial cell Ca^{2+} signaling in mice lacking sarco(endo)plasmic reticulum Ca^{2+}-ATPase isoform 3. J Biol Chem. 1997;272(48):30538-45.

203. Iguchi N, Ohkuri T, Slack JP, Zhong P, Huang L. Sarco/Endoplasmic reticulum Ca^{2+}-ATPases (SERCA) contribute to GPCR-mediated taste perception. PloS One. 2011;6(8):e23165.

204. Kao J, Fortner CN, Liu LH, Shull GE, Paul RJ. Ablation of the SERCA3 gene alters epithelium-dependent relaxation in mouse tracheal smooth muscle. Am J Physiol. 1999;277(2 Pt 1):L264-270.

205. Paltauf-Doburzynska J, Posch K, Paltauf G, Graier WF. Stealth ryanodine-sensitive Ca^{2+} release contributes to activity of capacitative Ca^{2+} entry and nitric oxide synthase in bovine endothelial cells. J Physiol. 1998;513(Pt 2):369-79.

206. Korosec B, Glavac D, Volavsek M, Ravnik-Glavac M. ATP2A3 gene is involved in cancer susceptibility. Cancer Genet Cytogenet. 2009;188(2):88-94.

207. Brouland J-P, Gélébart P, Kovàcs T, Enouf J, Grossmann J, Papp B. The Loss of Sarco/Endoplasmic Reticulum Calcium Transport ATPase 3 Expression Is an Early Event during the Multistep Process of Colon Carcinogenesis. Am J Pathol. 2005;167(1):233-42.

208. Ait-Ghezali L, Arbabian A, Jeibmann A, Hasselblatt M, Hallaert GG, Van den Broecke C, et al. Loss of endoplasmic reticulum calcium pump expression in choroid plexus tumours. Neuropathol Appl Neurobiol. 2014;40(6):726-35.

209. Varadi A, Lebel L, Hashim Y, Mehta Z, Ashcroft SJ, Turner R. Sequence variants of the sarco(endo)plasmic reticulum Ca(2+)-transport ATPase 3 gene (SERCA3) in Caucasian type II diabetic patients (UK Prospective Diabetes Study 48). Diabetologia. 1999;42(10):1240-3.

210. Arredouani A, Guiot Y, Jonas J-C, Liu LH, Nenquin M, Pertusa JA, et al. SERCA3 ablation does not impair insulin secretion but suggests distinct roles of different sarcoendoplasmic reticulum Ca^{2+} pumps for Ca^{2+} homeostasis in pancreatic beta-cells. Diabetes. 2002;51(11):3245-53.

211. Beauvois MC, Arredouani A, Jonas J-C, Rolland J-F, Schuit F, Henquin J-C, et al. Atypical Ca^{2+}-induced Ca^{2+} release from a sarco-endoplasmic reticulum Ca^{2+}-ATPase 3-dependent Ca^{2+} pool in mouse pancreatic beta-cells. J Physiol. 2004;559(Pt 1):141-56.

212. Beauvois MC, Merezak C, Jonas J-C, Ravier MA, Henquin J-C, Gilon P. Glucose-induced mixed $[Ca^{2+}]c$ oscillations in mouse beta-cells are controlled by the membrane potential and the SERCA3 Ca^{2+}-ATPase of the endoplasmic reticulum. Am J Physiol Cell Physiol. 2006;290(6):C1503-1511.

213. Zarain-Herzberg A, García-Rivas G, Estrada-Avilés R. Regulation of SERCA pumps expression in diabetes. Cell Calcium. 2014;56(5):302-10.

214. Sørensen TL-M, Clausen JD, Jensen A-ML, Vilsen B, Møller JV, Andersen JP, et al. Localization of a K+ -binding site involved in dephosphorylation of the sarcoplasmic reticulum Ca^{2+} -ATPase. J Biol Chem. 2004;279(45):46355-8.

215. Das A, Rui H, Nakamoto R, Roux B. Conformational Transitions and Alternating-Access Mechanism in the Sarcoplasmic Reticulum Calcium Pump. J Mol Biol. 2017;429(5):647-66.

216. Makinose M. Possible functional states of the enzyme of the sarcoplasmic calcium pump. FEBS Lett. 1973;37(2):140-3.

217. Clausen JD, McIntosh DB, Vilsen B, Woolley DG, Andersen JP. Importance of conserved N-domain residues Thr441, Glu442, Lys515, Arg560, and Leu562 of sarcoplasmic reticulum Ca^{2+}-ATPase for MgATP binding and subsequent catalytic steps. Plasticity of the nucleotide-binding site. J Biol Chem. 2003;278(22):20245-58.

218. Stokes DL, Delavoie F, Rice WJ, Champeil P, McIntosh DB, Lacapère J-J. Structural studies of a stabilized phosphoenzyme intermediate of Ca^{2+}-ATPase. J Biol Chem. 2005;280(18):18063-72.

219. Toyoshima C, Inesi G. Structural basis of ion pumping by Ca^{2+}-ATPase of the sarcoplasmic reticulum. Annu Rev Biochem. 2004;73:269-92.

220. Toyoshima C. Structural aspects of ion pumping by Ca^{2+}-ATPase of sarcoplasmic reticulum. Arch Biochem Biophys. 2008;476(1):3-11.

221. Chandrasekera PC, Kargacin ME, Deans JP, Lytton J. Determination of apparent calcium affinity for endogenously expressed human sarco(endo)plasmic reticulum calcium-ATPase isoform SERCA3. Am J Physiol Cell Physiol. 2009;296(5):C1105-1114.

222. Carrion R, Ro Y-T, Patterson JL. Purification, identification, and biochemical characterization of a host-encoded cysteine protease that cleaves a leishmaniavirus gag-pol polyprotein. J Virol. 2003;77(19):10448-55.

223. Watanabe A, Arai M, Koitabashi N, Niwano K, Ohyama Y, Yamada Y, et al. Mitochondrial transcription factors TFAM and TFB2M regulate Serca2 gene transcription. Cardiovasc Res. 2011;90(1):57-67.

224. Bhupathy P, Babu GJ, Periasamy M. Sarcolipin and phospholamban as regulators of cardiac sarcoplasmic reticulum Ca^{2+} ATPase. J Mol Cell Cardiol. 2007;42(5):903-11.

225. Negash S, Yao Q, Sun H, Li J, Bigelow DJ, Squier TC. Phospholamban remains associated with the Ca^{2+}- and Mg^{2+}-dependent ATPase following phosphorylation by cAMP-dependent protein kinase. Biochem J. 2000;351(Pt 1):195-205.

226. Periasamy M, Bhupathy P, Babu GJ. Regulation of sarcoplasmic reticulum Ca^{2+} ATPase pump expression and its relevance to cardiac muscle physiology and pathology. Cardiovasc Res. 2008;77(2):265-73.

227. Kadambi VJ, Ponniah S, Harrer JM, Hoit BD, Dorn GW, Walsh RA, et al. Cardiac-specific overexpression of phospholamban alters calcium kinetics and resultant cardiomyocyte mechanics in transgenic mice. J Clin Invest. 1996;97(2):533-9.

228. Luo W, Grupp IL, Harrer J, Ponniah S, Grupp G, Duffy JJ, et al. Targeted ablation of the phospholamban gene is associated with markedly enhanced myocardial contractility and loss of beta-agonist stimulation. Circ Res. 1994;75(3):401-9.

229. Bhupathy P, Babu GJ, Ito M, Periasamy M. Threonine-5 at the N-terminus can modulate sarcolipin function in cardiac myocytes. J Mol Cell Cardiol. 2009;47(5):723-9.

230. Odermatt A, Becker S, Khanna VK, Kurzydlowski K, Leisner E, Pette D, et al. Sarcolipin regulates the activity of SERCA1, the fast-twitch skeletal muscle sarcoplasmic reticulum Ca^{2+}-ATPase. J Biol Chem. 1998;273(20):12360-9.

231. John LM, Lechleiter JD, Camacho P. Differential modulation of SERCA2 isoforms by calreticulin. J Cell Biol. 1998;142(4):963-73.

232. Roderick HL, Lechleiter JD, Camacho P. Cytosolic phosphorylation of calnexin controls intracellular Ca(2+) oscillations via an interaction with SERCA2b. J Cell Biol. 2000;149(6):1235-48.

233. Szász I, Sarkadi B, Schubert A, Gárdos G. Effects of lanthanum on calcium-dependent phenomena in human red cells. Biochim Biophys Acta. 1978;512(2):331-40.

234. Thastrup O, Cullen PJ, Drøbak BK, Hanley MR, Dawson AP. Thapsigargin, a tumor promoter, discharges intracellular Ca^{2+} stores by specific inhibition of the endoplasmic reticulum Ca^{2+}-ATPase. Proc Natl Acad Sci U S A. 1990;87(7):2466-70.

235. Seidler NW, Jona I, Vegh M, Martonosi A. Cyclopiazonic acid is a specific inhibitor of the Ca^{2+}-ATPase of sarcoplasmic reticulum. J Biol Chem. 1989;264(30):17816-23.

236. Oldershaw KA, Taylor CW. 2,5-Di-(tert-butyl)-1,4-benzohydroquinone mobilizes inositol 1,4,5-trisphosphate-sensitive and -insensitive Ca^{2+} stores. FEBS Lett. 1990;274(1-2):214-6.

237. Sagara Y, Inesi G. Inhibition of the sarcoplasmic reticulum Ca^{2+} transport ATPase by thapsigargin at subnanomolar concentrations. J Biol Chem. 1991;266(21):13503-6.

238. Yu M, Zhong L, Rishi AK, Khadeer M, Inesi G, Hussain A, et al. Specific substitutions at amino acid 256 of the sarcoplasmic/endoplasmic reticulum Ca^{2+} transport ATPase mediate resistance to thapsigargin in thapsigargin-resistant hamster cells. J Biol Chem. 1998;273(6):3542-6.

239. Toyoshima C, Nomura H. Structural changes in the calcium pump accompanying the dissociation of calcium. Nature. 2002;418(6898):605-11.

240. Ma H, Zhong L, Inesi G, Fortea I, Soler F, Fernandez-Belda F. Overlapping effects of S3 stalk segment mutations on the affinity of Ca^{2+}-ATPase (SERCA) for thapsigargin and cyclopiazonic acid. Biochemistry (Mosc). 1999;38(47):15522-7.

241. Moncoq K, Trieber CA, Young HS. The molecular basis for cyclopiazonic acid inhibition of the sarcoplasmic reticulum calcium pump. J Biol Chem. 2007;282(13):9748-57.

242. Takahashi M, Kondou Y, Toyoshima C. Interdomain communication in calcium pump as revealed in the crystal structures with transmembrane inhibitors. Proc Natl Acad Sci U S A. 2007;104(14):5800-5.

243. Laursen M, Bublitz M, Moncoq K, Olesen C, Møller JV, Young HS, et al. Cyclopiazonic acid is complexed to a divalent metal ion when bound to the sarcoplasmic reticulum Ca^{2+}-ATPase. J Biol Chem. 2009;284(20):13513-8.

244. Lytton J, Zarain-Herzberg A, Periasamy M, MacLennan DH. Molecular cloning of the mammalian smooth muscle sarco(endo)plasmic reticulum Ca^{2+}-ATPase. J Biol Chem. 1989;264(12):7059-65.

245. Elaïb Z, Adam F, Berrou E, Bordet J-C, Prévost N, Bobe R, et al. Full activation of mouse platelets requires ADP secretion regulated by SERCA3 ATPase-dependent calcium stores. Blood. 2016;128(8):1129-38.

246. Laursen M, Bublitz M, Moncoq K, Olesen C, Møller JV, Young HS, et al. Cyclopiazonic acid is complexed to a divalent metal ion when bound to the sarcoplasmic reticulum Ca^{2+}-ATPase. J Biol Chem. 2009;284(20):13513-8.

247. Papp B, Enyedi A, Kovács T, Sarkadi B, Wuytack F, Thastrup O, et al. Demonstration of two forms of calcium pumps by thapsigargin inhibition and radioimmunoblotting in platelet membrane vesicles. J Biol Chem. 1991;266(22):14593-6.

248. Kovàcs T, Berger G, Corvazier E, Pàszty K, Brown A, Bobe R, et al. Immunolocalization of the multi-sarco/endoplasmic reticulum Ca^{2+} ATPase system in human platelets. Br J Haematol. 1997;97(1):192-203.

249. Coxon CH, Lewis AM, Sadler AJ, Vasudevan SR, Thomas A, Dundas KA, et al. NAADP regulates human platelet function. Biochem J. 2012;441(1):435-42.

250. Meng R, Wu J, Harper DC, Wang Y, Kowalska MA, Abrams CS, et al. Defective release of α granule and lysosome contents from platelets in mouse Hermansky-Pudlak syndrome models. Blood. 2015;125(10):1623-32.

251. Sharda A, Kim SH, Jasuja R, Gopal S, Flaumenhaft R, Furie BC, et al. Defective PDI release from platelets and endothelial cells impairs thrombus formation in Hermansky-Pudlak syndrome. Blood. 2015;125(10):1633-42.

252. Vorndran C, Minta A, Poenie M. New fluorescent calcium indicators designed for cytosolic retention or measuring calcium near membranes. Biophys J. 1995;69(5):2112-24.

253. Davies EV, Hallett MB. Near membrane Ca^{2+} changes resulting from store release in neutrophils: detection by FFP-18. Cell Calcium. 1996;19(4):355-62.

254. Anfossi G, Russo I, Trovati M. Platelet dysfunction in central obesity. Nutr Metab Cardiovasc Dis NMCD. 2009;19(6):440-9.

255. Beavers CJ, Heron P, Smyth SS, Bain JA, Macaulay TE. Obesity and Antiplatelets-Does One Size Fit All? Thromb Res. 2015;136(4):712-6.

256. Santilli F, Vazzana N, Liani R, Guagnano MT, Davì G. Platelet activation in obesity and metabolic syndrome. Obes Rev Off J Int Assoc Study Obes. 2012;13(1):27-42.

257. Angiolillo DJ, Fernández-Ortiz A, Bernardo E, Barrera Ramírez C, Sabaté M, Fernandez C, et al. Platelet aggregation according to body mass index in patients undergoing

coronary stenting: should clopidogrel loading-dose be weight adjusted? J Invasive Cardiol. 2004;16(4):169-74.

258. Haas S, Hansson J, Klimmeck D, Loeffler D, Velten L, Uckelmann H, et al. Inflammation-Induced Emergency Megakaryopoiesis Driven by Hematopoietic Stem Cell-like Megakaryocyte Progenitors. Cell Stem Cell. 2015;17(4):422-34.

259. Mountian I, Manolopoulos VG, De Smedt H, Parys JB, Missiaen L, Wuytack F. Expression patterns of sarco/endoplasmic reticulum Ca^{2+}-ATPase and inositol 1,4,5-trisphosphate receptor isoforms in vascular endothelial cells. Cell Calcium. 1999;25(5):371-80.

260. Lipskaia L, Hulot J-S, Lompré A-M. Role of sarco/endoplasmic reticulum calcium content and calcium ATPase activity in the control of cell growth and proliferation. Pflugers Arch. 2009;457(3):673-85.

261. Aarhus R, Graeff RM, Dickey DM, Walseth TF, Lee HC. ADP-ribosyl cyclase and CD38 catalyze the synthesis of a calcium-mobilizing metabolite from NADP. J Biol Chem. 1995;270(51):30327-33.

262. Churchill GC, O'Neill JS, Masgrau R, Patel S, Thomas JM, Genazzani AA, et al. Sperm deliver a new second messenger: NAADP. Curr Biol CB. 2003;13(2):125-8.

263. Yamasaki M, Thomas JM, Churchill GC, Garnham C, Lewis AM, Cancela J-M, et al. Role of NAADP and cADPR in the induction and maintenance of agonist-evoked Ca^{2+} spiking in mouse pancreatic acinar cells. Curr Biol CB. 2005;15(9):874-8.

264. Gasser A, Bruhn S, Guse AH. Second messenger function of nicotinic acid adenine dinucleotide phosphate revealed by an improved enzymatic cycling assay. J Biol Chem. 2006;281(25):16906-13.

Annexes :

Biochimica et Biophysica Acta 1843 (2014) 2705–2718

Contents lists available at ScienceDirect

Biochimica et Biophysica Acta

journal homepage: www.elsevier.com/locate/bbamcr

Expression of sarco (endo) plasmic reticulum calcium ATPase (SERCA) system in normal mouse cardiovascular tissues, heart failure and atherosclerosis

Larissa Lipskaia [a,b,c], Zela Keuylian [d,e,1], Karl Blirando [d,1], Nathalie Mougenot [f], Adeline Jacquet [f], Clotilde Rouxel [d], Haifa Sghairi [g,h], Ziane Elaib [g,h], Regis Blaise [d], Serge Adnot [b,c], Roger J. Hajjar [a], Elie R. Chemaly [a,i], Isabelle Limon [d], Regis Bobe [g,h,*]

[a] Mount Sinai School of Medicine, Cardiovascular Research Center, NY, USA
[b] Inserm, U955, Equipe 8, Créteil, France
[c] Université Paris-Est, Faculté de médecine, Créteil, France
[d] Sorbonne Universités, UPMC Univ Paris 06, CNRS, UMR 8256 B2A, IBPS, F-75005, Paris, France
[e] INSERM U1155, Tenon Hospital, Paris, France
[f] PECMV, IFR14, Paris 6, France
[g] INSERM U770, Le Kremlin-Bicetre, France
[h] Université Paris-sud, Le Kremlin-Bicetre, France
[i] Department of Biomedical Engineering, University of Virginia, School of Medicine, Charlottesville, VA, USA

ARTICLE INFO

Article history:
Received 6 May 2014
Received in revised form 29 July 2014
Accepted 1 August 2014
Available online 7 August 2014

Keywords:
Ca^{2+}ATPase
SERCA
Calcium signaling
Cardiovascular
Heart
Smooth muscle cells

ABSTRACT

The sarco(endo)plasmic reticulum Ca^{2+}ATPases (SERCA) system, a key regulator of calcium cycling and signaling, is composed of several isoforms. We aimed to characterize the expression of SERCA isoforms in mouse cardiovascular tissues and their modulation in cardiovascular pathologies (heart failure and/or atherosclerosis).

Five isoforms (SERCA2a, 2b, 3a, 3b and 3c) were detected in the mouse heart and thoracic aorta. Absolute mRNA quantification revealed SERCA2a as the dominant isoform in the heart (~99%). Both SERCA2 isoforms co-localized in cardiomyocytes (CM) longitudinal sarcoplasmic reticulum (SR), SERCA3b was located at the junctional SR. In the aorta, SERCA2a accounted for ~91% of total SERCA and SERCA2b for ~5%. Among SERCA3, SERCA3b was the most expressed (~3.3%), mainly found in vascular smooth muscle cells (VSMC), along with SERCA2a and 2b.

In failing CM, SERCA2a was down-regulated by 2-fold and re-localized from longitudinal to junctional SR. A strong down-regulation of SERCA2a was also observed in atherosclerotic vessels containing mainly synthetic VSMCs. The proportion of both SERCA2b and SERCA3b increased to 9.5% and 8.3%, respectively.

In conclusion: 1) SERCA2a is the major isoform in both cardiac and vascular myocytes; 2) the expression of SERCA2a mRNA is ~30 fold higher in the heart compared to vascular tissues; and 3) nearly half the amount of SERCA2a mRNA is measured in both failing cardiomyocytes and synthetic VSMCs compared to healthy tissues, with a relocation of SERCA2a in failing cardiomyocytes. Thus, SERCA2a is the principal regulator of excitation–contraction coupling in both CMs and contractile VSMCs.

1. Introduction

Ca^{2+} homeostasis plays a pivotal role in cardiovascular contractile function. Among various Ca^{2+} transporters, the calcium pumps sarco/endoplasmic reticulum Ca^{2+}ATPase (SERCA) is the only active Ca^{2+} transporter in the sarcoplasmic reticulum (SR). In muscular cells, SERCA controls the SR Ca^{2+} store that can be mobilized during muscle contraction and it decreases cytosolic Ca^{2+} concentration to allow muscle relaxation. However, Ca^{2+} signaling is complex and several SERCA proteins have been described in human cardiomyocytes [1]. Regulation of their function is a key mechanism controlling not only contractile function, but also protein expression and cellular differentiation through excitation/transcription coupling [2].

The growing family of SERCA is coded by 3 *ATP2A1-3* genes located on different chromosomes, encoding for SERCA1, SERCA2 and SERCA3 isoforms respectively; further diversity is generated by alternative splicing [3]. Isoform expression is also specific to cell-type and developmental stage [3].

* Corresponding author at: INSERM U770, Le Kremlin-Bicetre, France. Tel.: +33 1 49 59 56 40; fax: +33 1 46 71 94 72.
E-mail address: regis.bobe@inserm.fr (R. Bobe).
[1] Both authors contribute equally to the manuscript.

http://dx.doi.org/10.1016/j.bbamcr.2014.08.002
0167-4889/

The SERCA1 gene encodes for 2 spliced mRNA variants (adult (a) and fetal (b)), mostly expressed in fast-twitch skeletal muscle [3].

The SERCA2 gene gives rise to four species (a–d) through alternative splicing of the SERCA2 gene [1]. The so-called "cardiac isoform" SERCA2a, is expressed in cardiac muscle, slow-twitch skeletal muscle and smooth muscle cells, while SERCA2b is a ubiquitous isoform expressed in muscle and non-muscle cells [3]. SERCA2a and SERCA2b are produced by alternative splicing of the SERCA gene and differ only by the replacement of the last 4 amino acids of SERCA2a by an additional 49 amino acids in SERCA2b, possibly coding for an additional trans-membrane loop in the SR [4].

SERCA3 has various 3′-end spliced variants encoding the common SERCA3a isoform [5], in addition to species-specific isoforms, including 5 human (SERCA3b-f) [5–7], 2 mouse (SERCA3b-c) [8] and 1 rat (SERCA3b/c) proteins [9]. SERCA3 isoforms are mostly expressed in non-muscle cells, especially in endothelial and hematopoietic cells, with minor expression in muscle cells [3].

At least 14 different SERCA mRNA variants have been identified with their corresponding proteins. Some of these isoforms are specific to humans; to date, SERCA2c, SERCA2d, SERCA3d, SERCA3e and SERCA3f [1].

As all the members of the SERCA family share the same efficiency (transport of two Ca^{2+} ions per ATP), SERCA isoforms functionally differ only by their affinity for Ca^{2+} ($2b > 2a = 1 > 2c > 3$) and their Ca^{2+} transport turn-over rates, SERCA2b having the lowest transport capacity among all SERCA isoforms [3,10–12]. In-vitro functional characterization of the main muscular SERCA isoforms clearly indicated that SERCA2a displays a lower affinity for Ca^{2+} but has a higher turnover rate compared to SERCA2b. SERCA3 isoforms are characterized by an even lower Ca^{2+} affinity but a rapid turnover rate [13].

Several SERCA isoforms have been described in the cardiovascular system (reviewed in [14]), particularly in human cardiomyocytes [1]. At least 6 SERCA isoforms: SERCA2a, 2b, 2c and SERCA3a, 3d and 3f have been described in human cardiomyocytes with distinct intracellular localization [1]. Of note, in the mouse and human adult heart, SERCA2a was described as the major cardiac isoform, while SERCA2b appeared as the minor one [1,15].

In vascular smooth muscle cells from the rat thoracic aorta, SERCA2a and SERCA2b mRNA were shown to account respectively for 30% and 70% of total SERCA2 mRNA [16], and expression of other isoforms was not reported. It is well established that SERCA2a is down-regulated during pathologic cardiac hypertrophy and heart failure, and its down-regulation is associated with impaired calcium cycling, as previously reviewed in detail [17]). A similar down-regulation of SERCA2a was observed during vascular proliferative remodeling (reviewed in [18,19]). Restoration of SERCA2a expression by gene transfer improves various features of heart failure in preclinical models and in phase 1 and phase 2 clinical trials [20,21]. It also prevents VSMC proliferation in animal models of restenosis after vascular injury [18]. Altogether, present studies demonstrate that the physiological role of SERCA2a in muscle cells is to regulate "contractile" calcium cycling.

The physiological roles of other isoforms detected in the heart (SERCA2b, SERCA2c and various SERCA3 family members (3a, 3d and 3f)) remain unclear [1,11,22]. Reduced SERCA expression and activity are recognized as a major event in cardiomyocyte hypertrophy and vascular proliferative remodeling. However, the existence of a physiological and pathophysiological interplay between various SERCA isoforms, potentially forming a system, has not been investigated. Therefore, we aimed to characterize the expression and the cellular localization of the SERCA isoform system in normal mouse cardiomyocytes, vascular smooth muscle and endothelial cells (referred to respectively as CM, VSMC, EC) and in mouse models of heart failure and atherosclerosis.

2. Material and methods

2.1. Animal models

2.1.1. Model of heart failure

Eight week old C57BL/6 male mice were purchased from Janvier (CERJ, Saint Berthevin, France). Animals were housed at 5 per cage under controlled environmental conditions, with 12 h light:dark cycle at 22 °C of controlled temperature, food and water ad libitum. Animal experiments were conducted in agreement with our institutional guidelines for the use of animals in research.

Mice were anesthetized by intraperitoneal injection of pentobarbital sodium (50 mg/kg), intubated, and mechanically ventilated with 100% oxygen via a positive pressure respirator (Minivent type 845, Hugo Sachs, Elektronik-Harvard Apparatus, Germany). The ventilation rate was 170 strokes per minute, and the tidal volume was 200 μl. Body temperature was maintained at 37 °C. A left thoracotomy was performed in the fourth intercostal space to induce left ventricular infarction (myocardial infarction, MI) by ligation of the left anterior descending coronary with an 8-0 Prolene, or for a sham operation (Sham). The chest was closed in layers. Myocardial ischemia was confirmed by the occurrence of regional blanching.

Echocardiographic examination was performed under isoflurane sedation, using the echocardiography-Doppler (General Electric Medical systems Co, Vivid 7 Dimension/Vivid 7 PRO) with a probe emitting ultrasounds with 9–14 MHz frequency. Two-dimensional images and M-mode measurements were used to quantify left ventricular dimension and function. At least three sets of measures were obtained from three different cardiac cycles. Echocardiography was performed at 1 month and 6 months after MI. At 6 months, the animals were sacrificed and the heart was removed for morphometric analysis and tissue sampling.

2.1.2. Model of atherosclerosis

$ApoE^{-/-}$ mice were purchased from Charles River. Mice were housed under a 12-hour light/12-hour dark cycle (relative humidity: 55–60%; temperature: 22 °C) and were given standard chow and water ad libitum. At 48 weeks of age, male mice were sacrificed by a lethal dose of pentobarbital (intra-peritoneal injection) and heart tissues with attached aortic roots and aortas were collected. Aortas were immediately dissected, snap frozen in RNA later (Ambion) and stored at −80 °C for subsequent RNA extraction. Heart tissues were fixed in 4% formalin for 1 h then soaked in 20% glucose overnight. Tissues were frozen and stored at −80 °C.

2.2. Ultrasound biomicroscopy of atherosclerosis lesions in the brachiocephalic arteries

Images were acquired of the brachiocephalic artery every 3 weeks in mice starting from 30 weeks of age up to 48 weeks. Prior to ultrasound examination, all mice were anesthetized with 3% isoflurane gas and maintained lightly anesthetized with an isoflurane dose of 1.5% during analysis (Minerve Veterinary Equipment, France). The hair of the anterior chest wall was removed and ultrasound transmission gel was applied liberally before scanning. Ultrasound examinations were performed using the Ultrasound Biomicroscope (VEVO 2100, Visualsonics, Toronto) with a 40 MHz probe (MS550D). The Ultrasound Biomicroscope allows real time in vivo observations at high resolution (90 and 40 μM lateral and axial resolution, respectively) using a high frequency transducer (40 MHz). Real time visualization was assessed at 60 images/s. Images were taken in B-mode, or 2 dimensional mode. The probe was positioned in a right parasternal and longitudinal long- and short-axis view at the level of the ascending aorta. More specifically, the location transducer was at the lower 1/3rd of the chest; the direction of the transducer was posterior and leftward, 70° with the coronal plane; the orientation of the imaging plane was parallel to the central axis of

the mouse's body. Proximal and distal plaque areas were defined respectively as the plaque close to the aortic root and the plaque close to the bifurcation of the left subclavian artery. The long axis view in B-mode was used to the bifurcation of the left subclavian artery. The long axis view in B-mode was used to measure the total atherosclerotic plaque surface (mm^2); lesions visualized in the superior and inferior portion of the brachiocephalic artery were outlined and measured by VEVO2100 software. The image chosen from each ultrasonographic sequence corresponds to the one representing the largest detected atherosclerotic plaque for all mice.

2.3. RNA extraction of aortas

Tissues were thawed and homogenized in an Ultrathurax mechanical homogenizer. mRNA was extracted using the standard Trizol protocol (Life Technologies) until phase separation. RNA precipitation was performed using the RNeasy Midi Kit (Qiagen) according to the manufacturer's instructions, in order to optimize RNA collection and reduce the risk of contamination by organic solvents. RNA quality was determined by agarose gel electrophoresis with ethidium bromide; the 18S and 28S RNA bands were visualized under UV light.

2.4. Histological analysis

Cardiac fibrosis was determined by Sirius red staining by using a Picrosirius Red Stain Kit (Polysciences Inc.). Cryosections were fixed in Bouin's solution (1 h, 56 °C), then stained with Sirius red. Collagen fibers in the heart stained a red color and the cardiac fibrotic area was evaluated using ImageJ software. Cardiac fibrosis was quantified including the infarct scar. The size of cardiomyocytes was evaluated on cross sections using Wheat germ agglutinin (WGA) Alexa Fluor® 488 conjugate (Invitrogen).

2.5. Real-time quantitative reverse transcription–polymerase chain reaction (RT-PCR) assays

Relative gene expression was determined using two-step quantitative real-time PCR. Total RNA was isolated with TRIzol reagent (Invitrogen) followed by a cleanup step as described in the RNeasy Isolation kit (Qiagen) with on-column DNase I treatment to eliminate contaminating genomic DNA with RNase-free DNase Set (Qiagen). After annealing oligodT (1 μM) to template RNAs (0.5 μg) at 70 °C for 5 min, primer extension was initiated by adding the RT-MMLV enzyme plus 0.5 mM dNTP, 1U RNAsin and 10 mM dithiothreitol (DTT), and carried out for 45 min at 37 °C. Quantitative PCR was performed using the Light Cycler LC480 (Roche Diagnostics). The PCR mix included 5 μl of each reverse transcriptase (diluted 1:25) and 300 nM of each primer in 1 × Light Cycler DNA SYBR Green 1 Master Mix. The forward and reverse primer sequences for complementary DNA (cDNA) of mouse genes (Table 1) were designed with Primer Express software according to European Molecular Biology Laboratory accession numbers.

PCRs were performed using the following thermal settings: denaturation and enzyme activation at 95 °C for 5 min, followed by 40 cycles of 95 °C (10 s), 60 °C (15 s), and 72 °C (15 s). Post-amplification dissociation curves were performed to verify the presence of a single amplification product and the absence of primer dimers. Controls and water blanks were included in each run; they were negative in all cases. Relative expression of a target gene (SERCA) was standardized by a non-regulated reference gene (GAPDH or calsequestrin). Real-time quantitative PCR data represent the amount of each target messenger RNA (mRNA) relative to the amount of GAPDH gene mRNA or cardiac calsequestrin gene mRNA, estimated in the logarithmic phase of the PCR. Each specific cDNA amplicon was purified and serial dilutions of determined concentration were used to determine the fit coefficients of the relative standard curve. Absolute quantification of SERCA mRNA was performed by interpolation of its PCR signal (Cq) into this standard curve using the Livak-Schmittgen equation: Quantity $= 10^{(Cq - b) / m}$, where b is the y-intercept and m is the slope of the linear regression [23].

2.6. Protein analysis

Immunoblots were performed according to a standard protocol. Immunolabelings were performed on acetone-fixed sections according to a standard protocol. The following SERCA primary antibodies were used: anti-SERCA2a and anti-SERCA2b were from affinity Bioreagent, the anti-SERCA2c was directed against the corresponding human peptide (YLEPVLSSEL) that is mostly preserved in the potential mice SERCA2c terminal part (YLEQPVLSLEP) and was produced by Eurogentec. The anti-SERCA3a (C90) was raised against the rat sequence LSRHHVDEKKDLK that is nearly similar to the mice sequence LSRNHMDEKKDLK, anti-SERCA3b was specifically raised against the mice peptide TGKKGPEVNPNPGSRGES, and the anti-SERCA3c was directed against the human C-Terminal peptide of SERCA3c; HTGLASLKK that is also very close to the C-terminal part of the mice SERCA3c: HTGLASWKKRT. [1,7]. The other primary antibodies used were purchased from Santa Cruz Biotechnology: anti-glyceraldehyde 3-phosphate dehydrogenase (GAPDH) (sc-47424), anti-calsequestrine (sc-28274) and anti-desmin (sc-271677) and anti-PECAM (sc-1506).

2.7. Confocal immunofluorescence microscopy

Immunostaining was performed using the described upper primary antibodies and secondary antibodies conjugated to Alexa-546 or Alexa-488. Slides were examined with a Leica TCS4D confocal scanning laser microscope equipped with a 25 mW argon laser and a 1 mW helium-neon laser, using a Plan Apochromat 63× objective (NA 1.40, oil immersion). Green fluorescence was observed with a 505–550 nm band-pass emission filter under 488 nm laser illumination.

Table 1
The forward and reverse primer sequences for complementary DNA (cDNA) of mouse genes.

	Forward	Reverse
SERCA2a	CTCCATCTGCTTGTCCAT	GCGGTTACTCCAGTATTG
SERCA2b	CTCCATCTGCTTGTCCAT	GGCTGCACACACTCTTTAC
SERCA2c	CTCCATCTGCTTGTCCAT	CTAAGGCTCTAAGTCGAGAA
SERCA3	GGGGTGGTGCTTCAGATGTCTCTGC	GGGGACCCTCCTGTGCTGGCTGGCC
SERCA3a	GGGGTGGTGCTTCAGATGTCTCTGC	CCTTTTTTTCATCCATGTGATTCC
SERCA3b	GGGGTGGTGCTTCAGATGTCTCTGC	CCTTTTTTTCCGGTGTGGTATGG
SERCA3c	GGGGTGGTGCTTCAGATGTCTCTGC	TTTTCCAAGAAGCCAACCCGG
GAPDH	ACA CAT TGG GGG TAG GAA CA	AAC TTT GGC ATT GTG GAA
Calsequestrine	CCT TTG AGC GCA TCG AG	GAT GTA AGG CTG GAA GTG T
E-selectin	AGG GCT TTA GCT TGC AT	CGT CAA GGC TTG GAC ATT
MHC	GGC TTC ATT TGT TCC TTC CA	GGA GCG TCC ATT TCT TCT TC
SM22	TAT GGC AGC AGT GCA GAG	CTT TCT TCA TAA ACC AGT TGG GA
Smoothelin	TCT CAA CAG CGA GAA GC T GA	TGG TCA ACT CCT CGA CAT CA

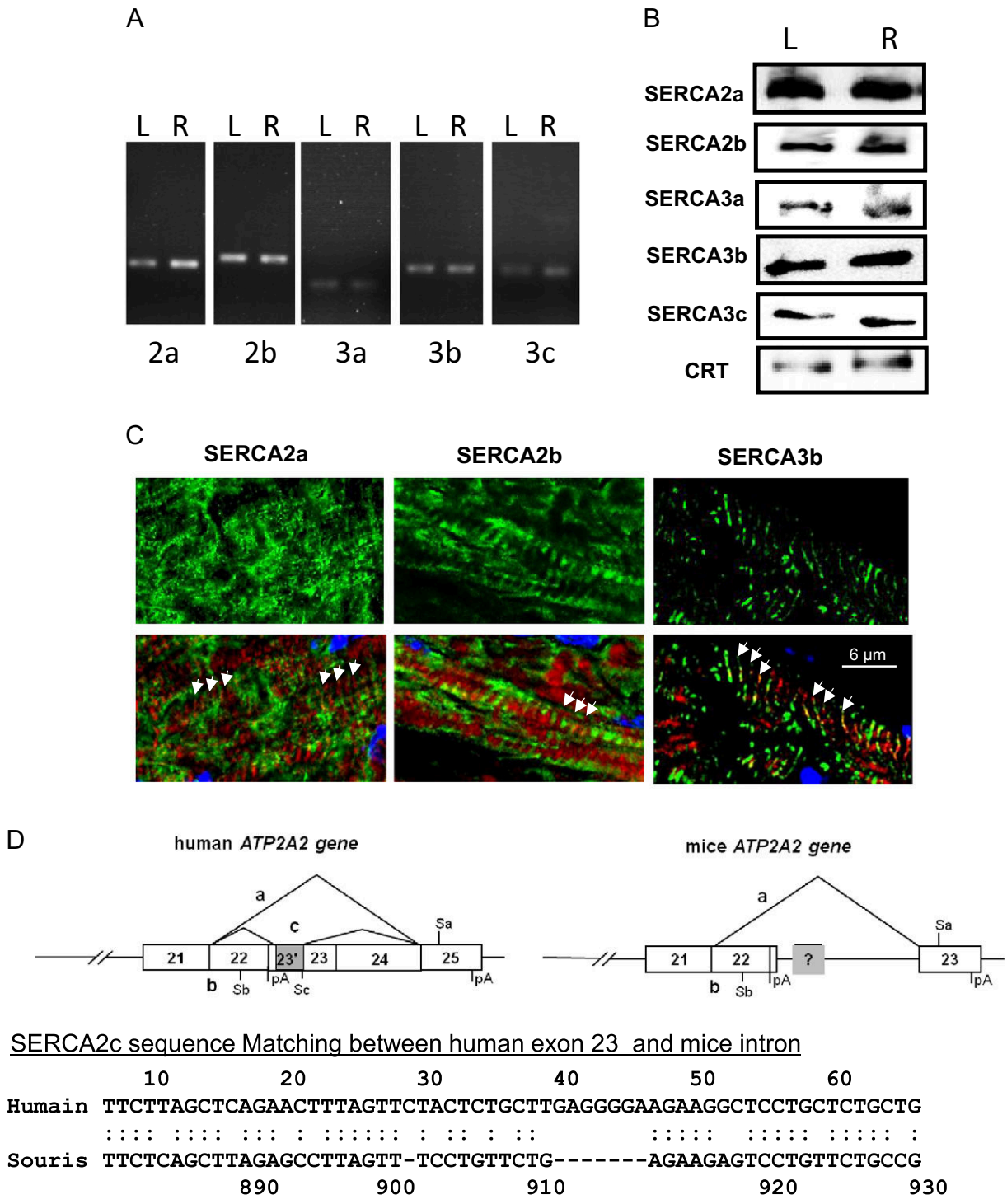

Fig. 1. Endogenous expression of SERCA 2 & 3 isoform mRNA and proteins in normal mouse heart. Expression of the different SERCA isoforms was assessed either by RT-PCR (**A**) or by immunodetection (**B**) in left (L) or right (R) ventricle. The amount of protein loads in each well was controlled using detection of calreticulin (CRT) as indicated in methods. **C**. Localization of the three major SERCA isoforms (green) within the cardiomyocytes (longitudinal sections from left ventricle). Confocal immunofluorescence. Red—F-actin, phalloidin staining. Arrows indicate the position of I-band. **D.** Schematic representation of human and mice ATP2A2 gene and comparison between human cDNA exon 23 with the hypothetical mice analog.

Red fluorescence was observed with a 560 nm long-pass emission filter under 543 nm laser illumination. Pinholes were set at 1.0 airy units. Stacks of images were collected every 0.4 µm along the z-axis. All settings were kept constant to allow comparison. For double immunofluorescence, dual excitation using the multitrack mode (images taken sequentially) was achieved using the argon and He/Ne lasers.

2.8. Statistical analysis

All quantitative data are presented as mean of at least 3 independent experiments ± SEM. One-way ANOVA tests were performed for comparisons between multiple groups. Statistical comparisons of 2 groups were done by an unpaired Student's *t*-test. Differences were considered significant for $P < 0.05$.

3. Results

3.1. Identification of SERCA isoforms expressed in normal mouse cardiovascular tissues

The SERCA system of the mouse heart was first characterized in normal C57-BL/6 mice by RT-PCR and western blot (Fig. 1A & B). RT-PCR analysis revealed the expression of at least 5 SERCA isoforms in the left and right ventricles: 2a, 2b, 3a, 3b and 3c (Fig. 1A). No SERCA2c mRNA was found in mice, while a corresponding sequence displaying 66.7% of similarity for a score 96, was identified in the mouse SERCA2 gene (Fig. 1D). Expression of these isoforms in the heart at the protein level was also confirmed by immunoblot analysis (Fig. 1B). Absolute quantitative real-time PCR shows SERCA2a to be the major cardiac isoform (~99.9%) whereas the ubiquitous SERCA2b represents less than 0.1% of total SERCA mRNA (Table 2). SERCA3 transcript variants were all expressed at very low levels compared to SERCA2a and SERCA2b. As shown in immunofluorescent images (Fig. 1C), i) SERCA2a was located in the longitudinal reticulum of cardiomyocytes, in opposite phase to the position of the I-band (F-actin) indicated by phalloidin staining; ii) SERCA2b demonstrated sub-compartmental localization and a uniform distribution similar to SERCA2a. In contrast, the third cardiac isoform SERCA3b co-localized with the I-bands (Fig. 1C), suggesting an expression preferentially in the junctional reticulum, near Z-band and traversal tubules. No specific localization for minor SERCA isoforms (SERCA3a and 3c) was clearly observed in cardiomyocytes, suggesting that these isoforms are more specific to vascular cells.

The same isoforms were identified by RT-PCR analysis in WT mouse aorta, but their relative expressions were different compared to the heart (Table 2). SERCA2a appeared, once again, as the major isoform in the normal aorta, but its expression is much lower than in the heart (~30 pg/μg of RNA in aorta vs ~920 pg/μg of RNA in the heart). Although SERCA2b expression was 0.86 and 1.6 pg/1 μg of total RNA in the heart and aorta respectively, the percentage of SERCA2a still represented more than 90% of total SERCA, and that of SERCA2b isoform ~5%. Expression of SERCA3b is higher in the aorta than in heart, respectively 1.01 ± 0.21 pg/μg RNA and 0.19 ± 0.07 pg/μg RNA. The percentage of SERCA3b (3.3%) is similar to that of SERCA2b while the last two other SERCA3 isoforms remained poorly express in the aorta.

3.2. Localization of SERCA isoforms expressed in normal murine cardiovascular tissues.

Confocal immunofluorescence confirmed distinct distribution of SERCA isoforms within cardiomyocytes and vascular cells (Fig. 2). As expected, SERCA2a was abundantly expressed in cardiomyocytes; in the coronary arteries, SERCA2a expression was barely detectable in vascular smooth muscle cells (VSMC) but substantial in endothelial cells (EC). Interestingly, in aorta samples, expression of SERCA2a, detected by immunofluorescence, was found in both vascular smooth muscle and endothelial cells (Fig. 3). The ubiquitous SERCA2b isoform was expressed at similar levels in every cell type (cardiomyocytes, VSMC and EC) (Figs. 2 & 3), whereas SERCA3a isoform seemed restricted to EC. Of note, low expression of SERCA3a was also detected in aortic VSMC (Fig. 3). In contrast, the SERCA3b isoform was strongly expressed in VSMC and hardly in EC (Figs. 2 & 3). Finally, SERCA3c isoform expression was faint in every cardiovascular cell type. Remarkably, in EC, ubiquitous isoform SERCA2b and SERCA3b were located in the basal part of the cell, whereas SERCA2a and SERCA3a were positioned in the luminal part (Fig. 2), supporting the functional association of SERCA2a and SERCA3a required for NO synthesis [19,24].

3.3. Alteration of expression and/or subcellular localization of SERCA isoforms in cardiomyocytes during heart failure

The heart failure model used was myocardial infarction (MI) induced by ligation of the left coronary artery in 2 month old C57BL6 mice. Progressive remodeling was evidenced by left ventricular (LV) dilation and deterioration of LV function at 1 and 6 months after infarction (Fig. 4A & Table 3). Six months after MI induction, heart weight and heart weight/body weight or heart weight/tibia length ratios were increased (Table 4). Furthermore, histological examination revealed an increase of the size of LV cardiomyocytes in MI mice (Fig. 4B) and fibrosis in the scarred area of the myocardial infarction (Fig. 4C).

In order to quantify mRNA expression, we first determined the rate of amplification for each cDNA (Supplementary data Fig. 1S). Next, we assessed SERCA isoform expression in the mouse model of heart failure using real-time RT-PCR analysis and confocal immunofluorescence microscopy (Fig. 5 & Table 2). Since a high level of fibrosis was observed in MI hearts, leading to a higher proportion of non-cardiomyocyte cells, we used the ubiquitous GAPDH gene and cardiomyocyte specific cardiac calsequestrin gene (CSQ) as reference gene since they have been shown to be stable in the course of hypertrophic remodeling [25]. As expected, the relative expression of SERCA2a transcripts was significantly decreased in failing hearts regardless of the reference gene used (Fig. 5A & B), whereas that of SERCA2b remained unchanged. Concerning the other SERCA isoform transcript expressions, a similar decrease of expression was observed for SERCA3b and 3c in failing hearts, while no significant differences were obtained for SERCA3a (Fig. 5C & D). These results were further confirmed for SERCA2 (a and b) isoforms at the protein level by western blot (Fig. 5E–G).

Cellular localization of SERCA isoforms within failing cardiomyocytes was assessed by confocal microscopy immunofluorescence (Fig. 5H). In sham cardiomyocytes, SERCA2a and SERCA2b demonstrated a similar

Table 2
Absolute quantification of different SERCA variants mRNA in normal and diseased cardiovascular tissues.

SERCA (pg/1 μg RNA)	Control heart ($n = 22$)	Failing heart ($n = 23$)	(Multiple comparison test) $P < 0.05$	WT aorta ($n = 9$)	ApoE ($^{-/-}$) aorta ($n = 8$)	(Multiple comparison test) $P < 0.05$
SERCA2a	919.4 ± 143.5	436.01 ± 61.6	***	27.90 ± 6.64	13.77 ± 0.81	*
SERCA2b	0.86 ± 0.17	0.64 ± 0.11	ns	1.59 ± 0.19	1.61 ± 0.20	ns
SERCA3a	0.003 ± 0.001	0.002 ± 0.0002	ns	0.016 ± 0.003	00.070 ± 0.025	*
SERCA3b	0.193 ± 0.08	0.028 ± 0.003	*	1.01 ± 0.21	1.42 ± 0.15	ns
SERCA3c	0.014 ± 0.005	0.003 ± 0.001	ns	0.11 ± 0.01	0.12 ± 0.01	ns

SERCA (%)	Control heart ($n = 22$)	Failing heart ($n = 23$)	WT aorta ($n = 9$)	ApoE ($^{-/-}$) aorta ($n = 8$)
SERCA2a	99.89	99.84	91.07	81.15
SERCA2b	0.093	0.146	5.19	9.47
SERCA3a	<0.001	<0.001	0.05	0.41
SERCA3b	0.021	0.006	3.30	8.28
SERCA3c	0.001	<0.001	0.38	0.69

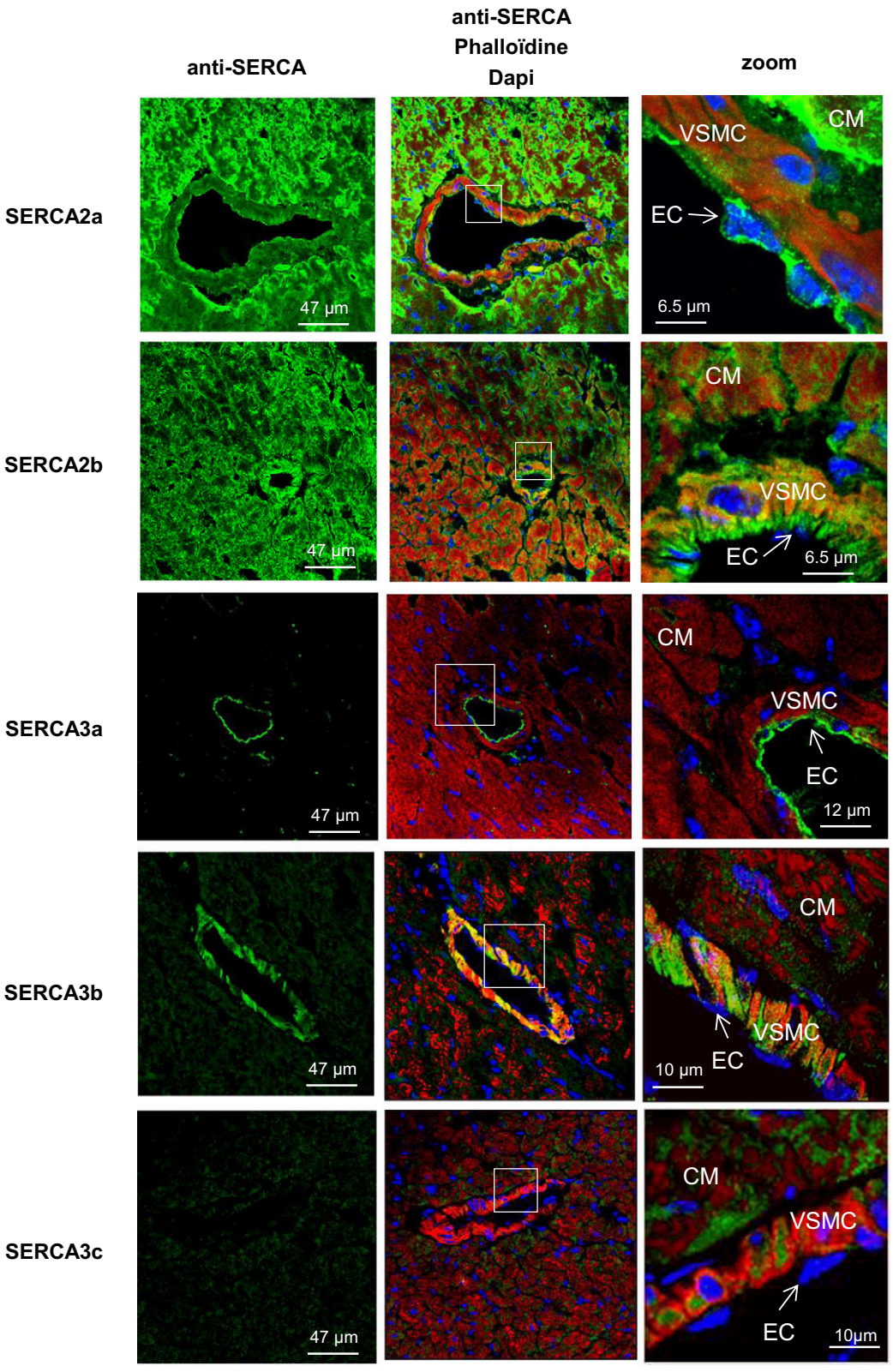

Fig. 2. Expression of SERCA isoforms in cardiovascular tissues and cells. **A.** Localization of SERCA isoforms in the left ventricle of normal mice by cell type. Confocal immunofluorescence microscopy with SERCA-specific antibodies (green) of left ventricle sections from normal mice. Red—F-actin, phalloidin. Nuclei were stained with Dapi (blue). Abbreviations: CM—cardiomyocytes; VSMC—vascular smooth muscle cells; EC—endothelial cells.

subcompartmental localization in the longitudinal reticulum, in opposite phase with the position of the Z-line, delineated by desmin staining (Fig. 5H). In marked contrast, both of these SERCA2 isoforms were co-localized with the Z-line area in failing cardiomyocytes, suggesting a re-localization of these two proteins from the longitudinal to the junctional reticulum.

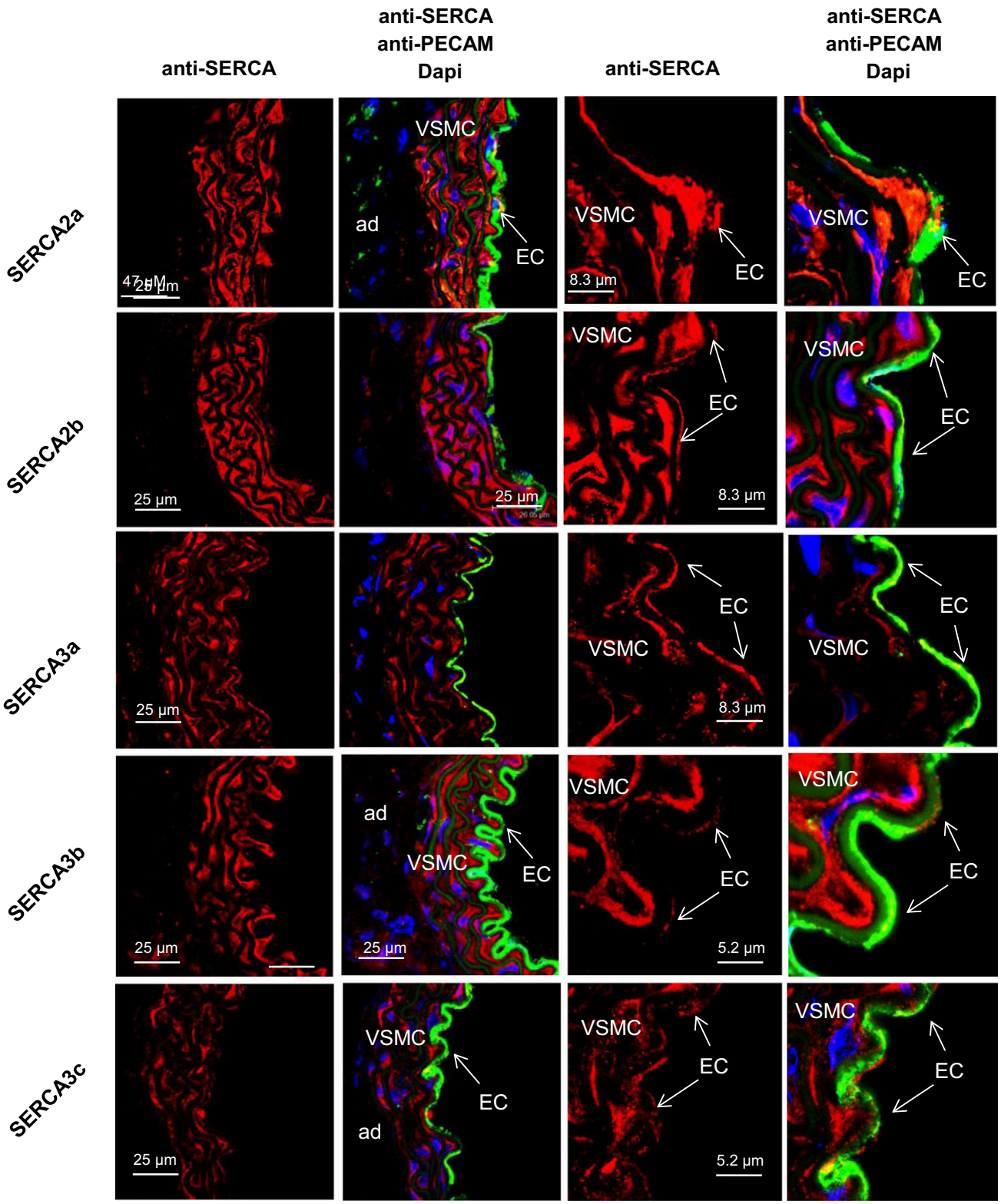

Fig. 3. Cell-specific expression of SERCA isoforms in normal mouse thoracic aorta. Confocal immunofluorescence with SERCA specific antibodies (red) of aorta sections from normal mice. Green—immunofluorescence with PECAM, a marker of endothelial cells. Nuclei were stained with Dapi (blue). Abbreviations: CM—cardiomyocytes; VSMC—vascular smooth muscle cells; EC—endothelial cells.

3.4. Alteration of expression and/or subcellular localisation of SERCA isoforms in vessels during atherosclerosis

We used hypercholesterolemic apolipoprotein$^{-/-}$ mice (ApoE$^{-/-}$) as a model of vascular remodeling (Fig. 6). Lesion development in the brachiocephalic artery of ApoE$^{-/-}$ mice was visualized by high-resolution ultrasound biomicroscopy. Plaque size significantly increased beginning at 42 weeks of age and continued to increase until the end of the study (Fig. 6A). Lesion surface area was greatest at 200 μm from the appearance of the first aortic valve cusp and

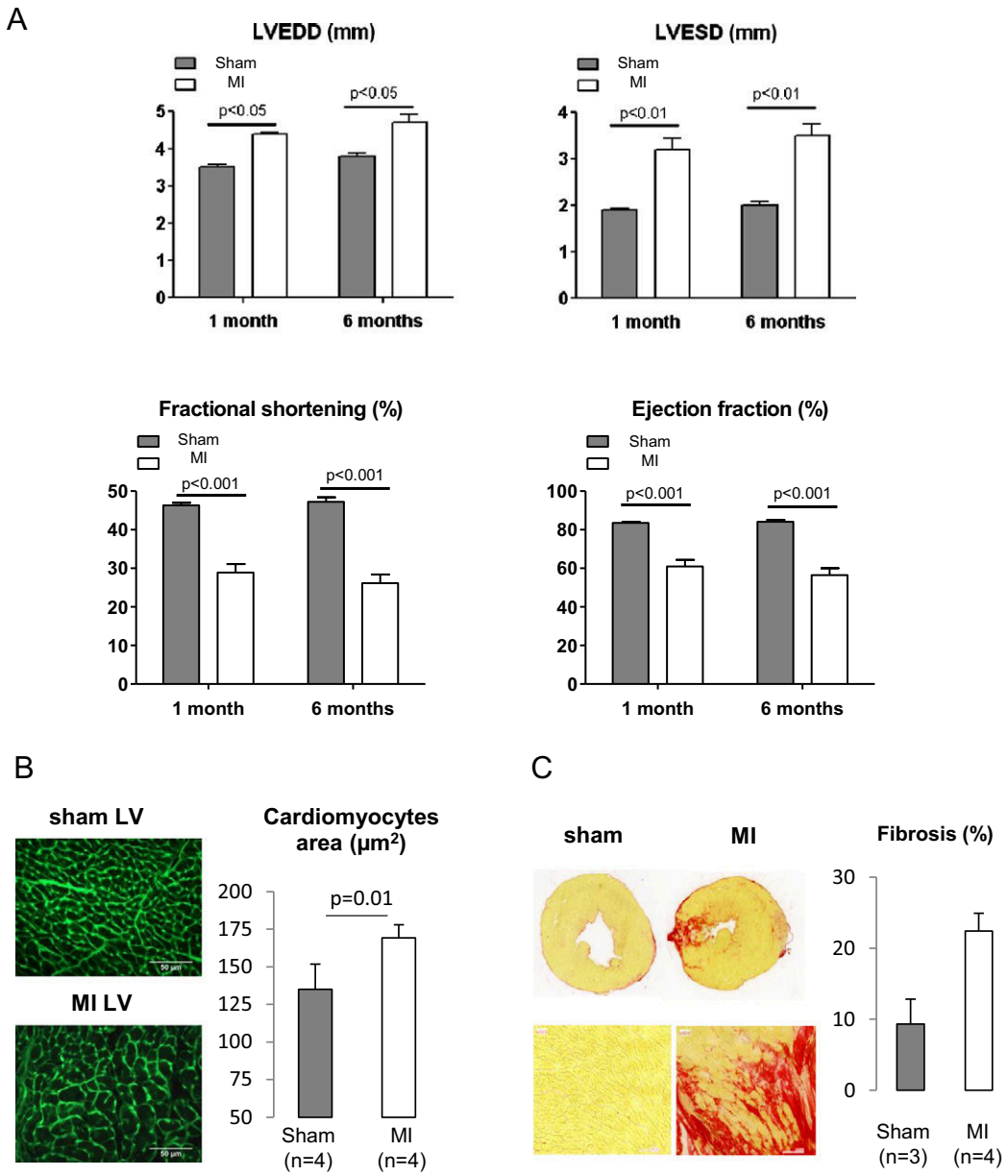

Fig. 4. Assessment of LV function, cardiomyocytes hypertrophy and myocardial fibrosis in MI hearts. **A.** Assessment of LV function using transthoracic echocardiography in sham operated and MI mice, 1 and 6 months after surgery. LVEDD: left ventricle end diastolic diameter; LVESD: left ventricle end systolic diameter. **B.** Analysis of cardiomyocytes sizes in sham and MI left ventricles. Left panel: Germ agglutinin staining. Right panel: Mean cardiomyocytes area in 4 sham- and 4 MI-operated animals. 250 individual measurements from 5 sections were performed for each animal. **C.** Sirius red staining of heart cross sections. Left panel: Representative image. Right panel: Relative quantification of fibrosis. Zone of infarction is included in the quantification.

Table 3
Assessment of cardiac function by transthoracic echography in sham operated and MI mice, 1 and 6 months after surgery.

	1 month after surgery			6 months after surgery		
	Sham operated ($n = 7$) Mean ± SD	MI ($n = 16$) Mean ± SD	p (t-test)	Sham operated ($n = 7$) Mean ± SD	MI ($n = 15$) Mean ± SD	p (t-test)
HR (b/min)	512.4 ± 9.7	483.0 ± 16.1	p = ns	531.2 ± 15.9	493.5 ± 15.9	p = ns
IVSDT (mm)	0.61 ± 0.01	0.51 ± 0.01	$p < 0.01$	0.67 ± 0.04	0.61 ± 0.02	p = ns
IVSST (mm)	1.04 ± 0.02	0.86 ± 0.04	$p < 0.05$	1.21 ± 0.004	0.92 ± 0.03	$p < 0.01$
PWDT (mm)	0.82 ± 0.03	0.61 ± 0.02	$p < 0.01$	0.90 ± 0.03	0.71 ± 0.03	$p < 0.01$
PWST (mm)	1.20 ± 0.05	0.95 ± 0.07	$p < 0.01$	1.35 ± 0.05	1.03 ± 0.05	$p < 0.01$
H/R (IVSDT + PWDT) / LVEDD	4.07 ± 0.14	2.65 ± 0.13	$p < 0.01$	4.10 ± 0.24	2.92 ± 0.18	$p < 0.01$

The following parameters were measured: IVSDT: interventricular septum diastolic thickness; IVSST: interventricular septum systolic thickness; LVEDD: left ventricle end diastolic diameter; LVESD: left ventricle end systolic diameter; PWDT; posterior wall diastolic thickness; PWST: posterior wall systolic thickness; EDV: end diastolic volume; ESV: end systolic volume; EF: ejection fraction; FR: fractional shortening; Ejct vol: ejection volume; HR: heart rate; h/r = (IVSDT + PWDT)/LVEDD.

Table 4
Morphometric analysis of sham operated and MI mice, 6 months after surgery.

	Sham operated ($n = 7$) Mean ± SD	MI ($n = 15$) Mean ± SD	p (t-test)
Body weight (g)	30.86 ± 0.34	30.67 ± 0.41	ns
Heart weight (mg)	155.30 ± 2.76	197.7 ± 11.21	$p < 0.001$
Tibia length (cm)	1.78 ± 0.02	1.79 ± 0.02	ns
Heart/body weight	5.04 ± 0.08	6.45 ± 0.37	$p < 0.001$
Heart/tibia length	87.01 ± 1.63	110.05 ± 5.977	$p < 0.001$

smallest at 800 μm, corresponding to the emergence of the aorta (Fig. 6B).

Given that the development of atherosclerotic lesions is associated with the trans-differentiation of VSMC from a contractile towards synthetic/proliferating/inflammatory phenotype [18,26], we first analyzed the expression of markers of phenotype and inflammation (Fig. 7A). The expressions of smooth muscle myosin heavy chain alpha (α-MHC), SM22 alpha (SM22) and smoothelin, all markers of contractile smooth muscle, were significantly decreased in thoracic aortas from ApoE$^{-/-}$ mice with atherosclerotic plaques (Fig. 7A). In contrast, the expression of E-selectin, a cell adhesion molecule expressed only in endothelial cells activated by cytokines and known to play an important role in the recruitment of these cells to inflammatory sites, was significantly increased in atherosclerotic vessels (Fig. 7A), confirming the phenotypic transition of VSMCs in thoracic aorta from ApoE$^{-/-}$ mice.

Pathological vascular remodeling in ApoE$^{-/-}$ mice was associated with a 2 fold decrease of the major isoform SERCA2a (Fig. 7B & Table 2). Furthermore, SERCA2b, SERCA3b and SERCA3c expressions were also decreased in atherosclerotic vessels (Fig. 7B & C; Table 2). Remarkably, the expression of SERCA3a isoform augmented 8 fold even if its percentage only reached 0.4% in ApoE$^{-/-}$ mice aorta (Fig. 7C; Table 2).

Histological analysis confirmed the presence of atherosclerotic lesions on aortic roots of all ApoE$^{-/-}$ animals; no lesions were observed in control mice (Fig. 6). The media area of aortic root atherosclerotic lesions, defined by elastin layers (Fig. 7D), was severely damaged and contained a large area composed of crowded elastic fibers lacking VSMC. Abundant neointima, defined as a layer within the internal elastic lamina (IEL) and lumen, was clearly identified in aortic roots from ApoE$^{-/-}$ animals. SERCA2a was expressed in both VSMC and EC of aortic roots (Fig. 7D), in agreement with our observations in coronary vessels and in the aorta (Fig. 2 & 3). As expected, SERCA3a expression was highest in the EC layer (Fig. 8D). SERCA2a expression was dramatically decreased in both neointima and media of atherosclerotic lesions in ApoE$^{-/-}$ mice. Nevertheless, SERCA2a was still detected in the luminal part of atherosclerotic vessels suggesting its expression in ECs. Furthermore, SERCA3a was abundantly expressed in the luminal part of the atherosclerotic vessels suggesting an enlargement of the endothelial cell layer. Large and round SERCA3a positive cells were also visualized in the neointima.

4. Discussion

We demonstrated the simultaneous expression of several SERCA isoforms with differential calcium affinity and pump activity in mouse cardiomyocytes, VSMC and endothelial cells and their dynamic variation and reorganization in disease states.

4.1. In mouse cardiomyocytes

The SERCA system is composed of at least 4 isoforms: SERCA 2a, 2b, 3b and 3c each with a specific intracellular location, as illustrated in Fig. 8A. In human heart, we previously described at least 6 SERCA isoforms: SERCA2a, 2b, 2c and SERCA3a, 3d and 3f [1,22].

We, and others [1,15], using relative mRNA quantification, have identified SERCA2a as the major cardiac isoform and SERCA2b as a minor cardiac isoform. Here, we observed a global reduction of both SERCA2 and SERCA3 expression in our pathological model. We also report that even though SERCA2a is down-regulated during pathologic cardiac hypertrophy and heart failure, its relative expression remains largely predominant. Observation from previous works from transgenic mice clearly suggested that the level of SERCA2a expression is critical. Wuytack et al. have produced transgenic mice in which SERCA2a was replaced by SERCA2b, resulting in cardiac dysfunction and hypertrophy [27], showing that the high Ca^{2+} affinity SERCA2b isoforms appeared to be an inadequate substitute for SERCA2a. The total level of SERCA2 was lower in SERCA2a-deficient mice in an initial study, but further overexpression of SERCA2b in these cardiomyocytes led to increased SR calcium transport and enhanced mechanical function (contractility and relaxation), without preventing cardiac hypertrophy [15] or fibrosis [4]. Althought, a spontaneous two-fold increase in cardiac phospholamban expression might counteract a possible effect of SERCA2b [27]. Interestingly, SERCA2b/WT heterozygous mice in which the natural SERCA2a isoform is the major isoform do not present hypertrophy, confirming that SERCA2a is necessary and most likely sufficient.

Reduced SERCA2a activity and SR Ca^{2+} uptake lead to abnormal Ca^{2+} handling in failing cardiomyocytes including an increase in diastolic Ca^{2+}, abnormally long time course of Ca^{2+} transients, and decrease in SR Ca^{2+} release [28]. Furthermore, reduction of SERCA2a expression by RNA silencing in cardiac myocytes resulted in increased expression of transient receptor potential channels (TRPC) and activation of the calcium/calcineurin-dependent complex [29]. These Ca^{2+}-dependent signaling pathways initiate and sustain hypertrophic growth and remodeling, which often progress to heart failure [20,28]. By lowering cytosolic Ca^{2+}, SERCA2a expression inhibits calcineurin activity and associated hypertrophic and apoptotic signaling pathways [30].

Similarly to what was described in human cardiomyocytes, both SERCA2a and SERCA2b proteins were targeted to the same subcellular regions (longitudinal SR) [1,4,31]. In the normal condition, SERCA2 proteins were found in opposite phase to the position of the I-band, in the SR wrapping myofilaments. This is consistent with the SR being the source of large Ca^{2+} mobilization into the cytosol, during cardiac excitation–contraction coupling, essential to produce a rapid increase in cytosolic [Ca^{2+}] responsible for activation of the myofilaments to be translated into a proper twitch contraction. The rate of the rise of cytosolic Ca^{2+} depends on the triggering and gating of the RyR and the amount of Ca^{2+} available in SR for release [32].

We have found that in cardiomyocytes from failing hearts, SERCA2 proteins relocated to the Z-line (Fig. 8B). The Z line is closer to extracellular exchange area (T-tubule) and contains LTCC and RyR channels. The LTCCs and RyR form couplons at the interface between the sarcolemma and the junctional SR. A defective coupling of Ca^{2+} influx via LTCC, preventing the activation of RyR, has been implicated in a reduced SR Ca^{2+} release in heart failure. Both functional changes in LTCC properties and structural re-organization of this L-type channel within T-tubules could be involved [33]. Relocation of SERCA2 to the Z-line in hypertrophied myocytes might be associated to T-tubule disorganization shown to coincide with myocardial dysfunction and calcium transient abnormalities in hypertensive rats [34] and suggest a compensation of defective LTCC/RyR coupling by rising available SR Ca^{2+} content.

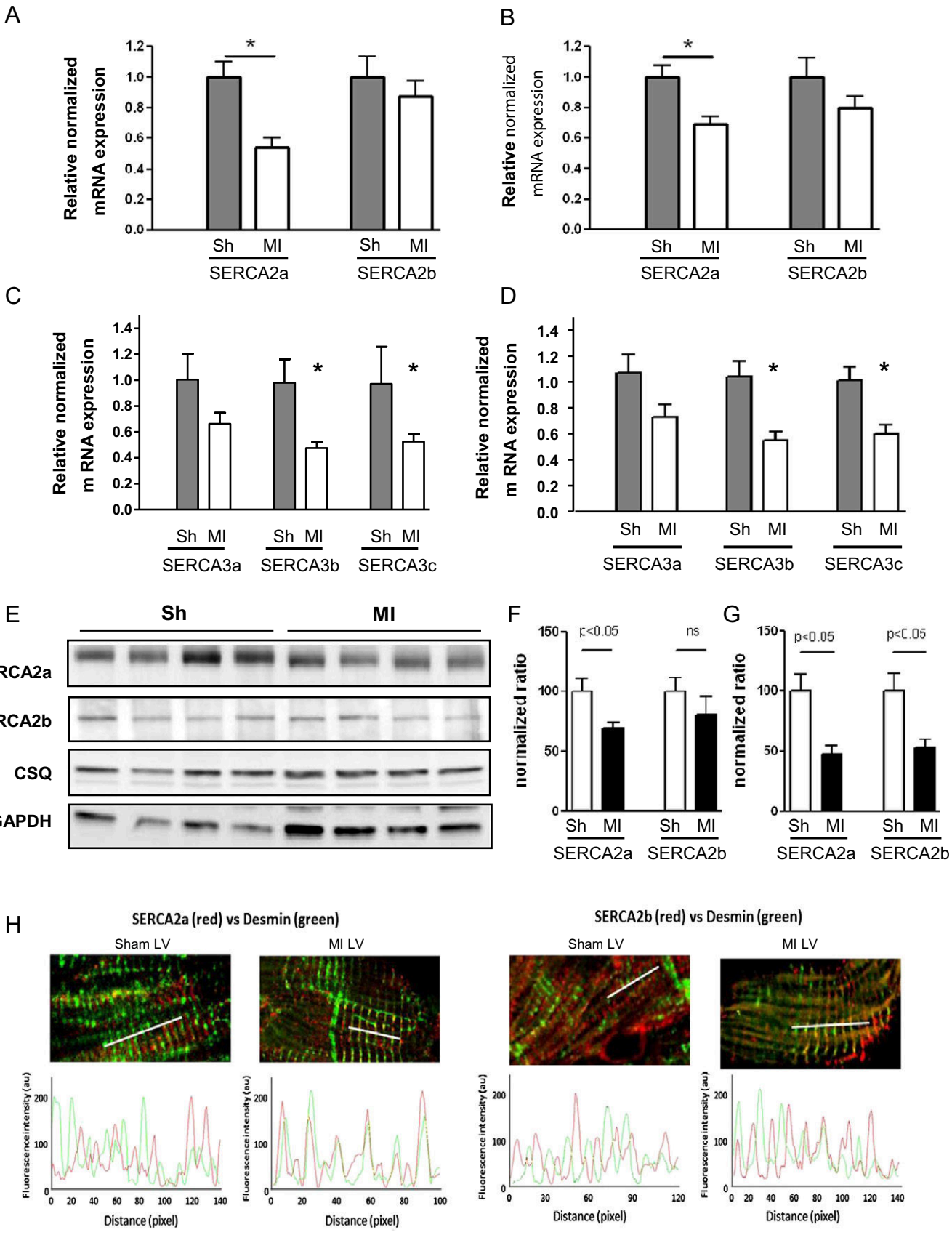

Fig. 5. Alteration of SERCA isoform expression in the failing heart. Relative expression of SERCA 2a and 2b variants in sham- ($n = 9$) and MI- ($n = 20$) operated animals normalized on calsequestrin (CSQ) (**A**) and GAPDH (**B**). Relative expression of SERCA 3a, 3b and 3c variants in sham- ($n = 12$) and MI- ($n = 20$) operated animals normalized on calsequestrin (CSQ) (**C**) and GAPDH (**D**). **E.** Immunoblot analysis (left panel) and bar-graph representing normalized relative quantification of SERCA2a and SERCA2b expression in sham-operated and MI animals. **F.** Localization of SERCA2a and SERCA2b within cardiomyocytes from sham (left panel) and MI (right panel) mouse hearts. **Upper panel:** Confocal microscopy immunofluorescence with a-SERCA (red) and a-desmin (green) antibodies on transverse sections. **Lower panel:** Analysis of SERCA and desmin colocalization in normal and failing cardiomyocytes.

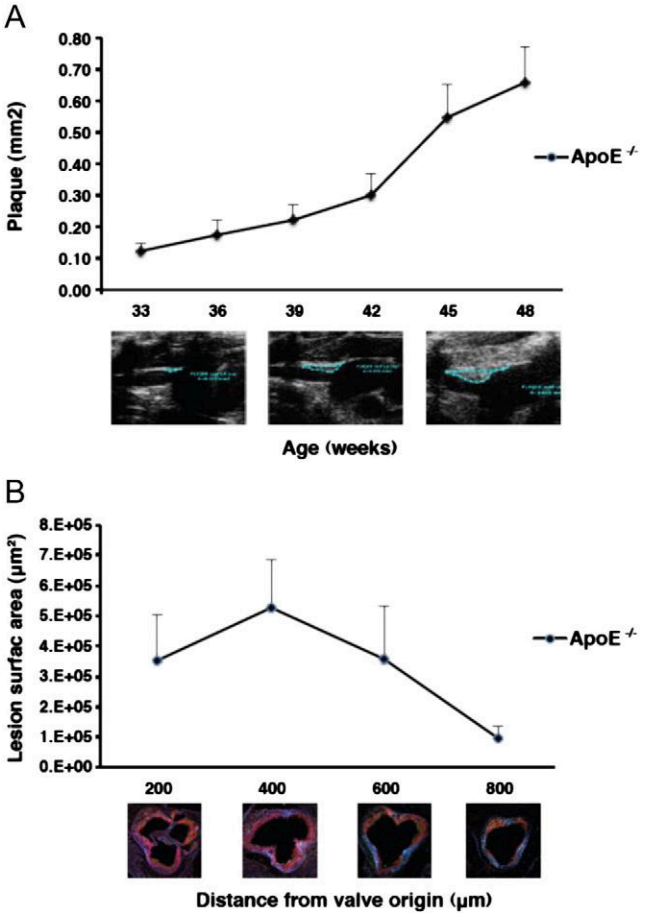

Fig. 6. Atherosclerotic plaques in aged ApoE ($^{-/-}$) mice. **A.** Lesion development in the brachiocephalic artery of ApoE KO mice visualized by high-resolution ultrasound biomicroscopy (UBM). Lesion size (y axis, mm^2) was measured for every mouse at all time points examined. The study began at 33 weeks of age and images were taken every 3 weeks until the end of the study at 48 weeks of age. The ultrasound images underneath the graph represent plaque development at 33, 39 and 48 weeks of age. The atherosclerotic plaques are contoured in white lines. Plaque surface area was calculated by the VEVO software. **B.** Quantification of atherosclerotic lesion surface area in the aortic roots of ApoE KO mice. Lipid content was quantified on aortic root cryosections from 48 week old mice stained with oil red O and analyzed under polarized light. The distance from the valve origin represents 200, 400, 600, and 800 μm from the appearance of the first aortic valve cusp; 800 μm is the emergence of the aorta (800 μm). $n = 6$.

Remarkably, relocation of SERCA2 from the SR wrapping myofilaments might result in slow rise Ca^{2+} influx across the sarcolemma ensuing in inefficient contraction.

The mouse SERCA system expressed in the heart is also distinct from the human one, as no SERCA2c mRNA was found in mice. While the role played by SERCA2C in human heart remained to be clarified, its specific localization to longitudinal SR and intercalated discs in close proximity to the sarcolemma, an area that could display relatively high calcium concentration, was in agreement with its lower apparent affinity for Ca^{2+}. Such localization was not observed for SERCA expressed in mouse cardiomyocyte. But it is possible that some function associated to SERCA2c in human heart could be done by SERCA3b which also share similar affinity for Ca^{2+}.

Among SERCA3 isoforms, only SERCA3b was clearly identified in mouse cardiomyocytes by its specific location at the junctional SR, near the T-tubules, which corresponds to the localization of SERCA3a in human cardiomyocytes [1]. It is tempting to imagine that this area is more adapted to the SERCA3 protein as it can be richer in Ca^{2+} (due to its interaction with the extracellular medium), considering that SERCA3 works at a higher Ca^{2+} concentration than SERCA2 isoforms.

Limited data are available on human failing cardiac tissue, in which only a significant increase in SERCA3f was recently demonstrated, in addition to the well-established decrease in SERCA2a [1]. While the SR regulates excitation–contraction coupling due to its special ability to store calcium, the role of the ER in protein synthesis and processing and the disruption of such processes in pathologic situations (known as ER stress) is of growing importance in cardiomyocyte and in heart failure [1]. In this regard, an interesting connection can be made between 1) the increased expression of SERCA3f in human heart failure with a parallel increase in ER stress markers [22], and 2) the ability of SERCA3f to induce ER stress and apoptosis in HEK-293 cells [35]. SERCA3f and SERCA3b share the same C-terminal end and SERCA3b was also able to induce ER stress in human cells. However, it is not clear whether SERCA3b can be seen as an equivalent of SERCA3f in mice, as it is down-regulated in heart failure while SERCA3f expression was described to increase.

4.2. In vascular smooth muscle cells

The SERCA system is composed of at least 4 isoforms: SERCA 2a, 2b, 3b and 3c. As opposed to previous studies [16], SERCA2a was identified as a major isoform in both contractile and synthetic VSMC using the method of absolute mRNA quantification. Technical differences may account for the different results. This finding is novel but not surprising taking into account that synthetic VSMCs are able to produce tonic contraction (rev. [18,19]). In VSMCs, oscillatory type of Ca^{2+} transients triggers phasic contraction, typical of coronary and low resistance arteries highly expressing SERCA2a. Tonic contractions observed in large arteries and veins are driven by the steady-state increase in cytosolic Ca^{2+}, observed also in synthetic VSMC (rev. [18,19]). Several observations support the evidence that the calcium response shape appears to be dependent on SERCA2a expression: 1) blocking SERCA activity also strongly inhibits the Ca^{2+} oscillations, demonstrating that they are caused by release of Ca^{2+} from the SR [36–38]; 2) trans-differentiation of VSMC towards synthetic phenotype is associated with a loss of both Ca^{2+} oscillations and SERCA2a expression (this paper and [39,40]; and 3) SERCA2a gene transfer to synthetic cultured VSMC modifies the agonist-induced calcium transient from steady-state to oscillatory mode [41]. Importantly, restoring SERCA2a expression by gene transfer in synthetic cultured VSMC also inhibits Ca^{2+} dependent activation of transcription factor NFAT required for proliferation and migration of VSMC [30,41,42].

We also report a relatively high expression of the SERCA3b isoform in mouse VSMC, similar to one of the ubiquitous SERCA2b isoform. In humans, SERCA3b have been found highly expressed in the lung, kidney and pancreas; however its cellular localization and specific function have not yet been investigated [19]. The fact that SERCA3b expression appears to be important in normal VSMC and its specific localization in cardiomyocytes at the junctional SR near T tubules suggests that it could be involved in interaction with extracellular Ca^{2+} influx.

4.3. In endothelial cells

The SERCA system is composed of at least 5 isoforms: SERCA2a, 2b, 3a as well as the slightly expressed 3b and 3c. First, we have detected a strong expression of SERCA3a in EC, confirming previous observations describing SERCA3a as a major endothelial-specific isoform [43]. Second, according to immunolabeling data, SERCA2a appears to be a major isoform co-expressed with SERCA3a in the luminal part of EC. This latter observation is consistent with the described role of SERCA3a and SERCA2a in EC related to the regulation of NO synthesis from L-arginine by the nitric oxide synthase (eNOS, endothelial nitric oxide synthase) (rev in [19,44]). Several observations support the cooperative action of SERCA2a and SERCA3a in the control of NO production

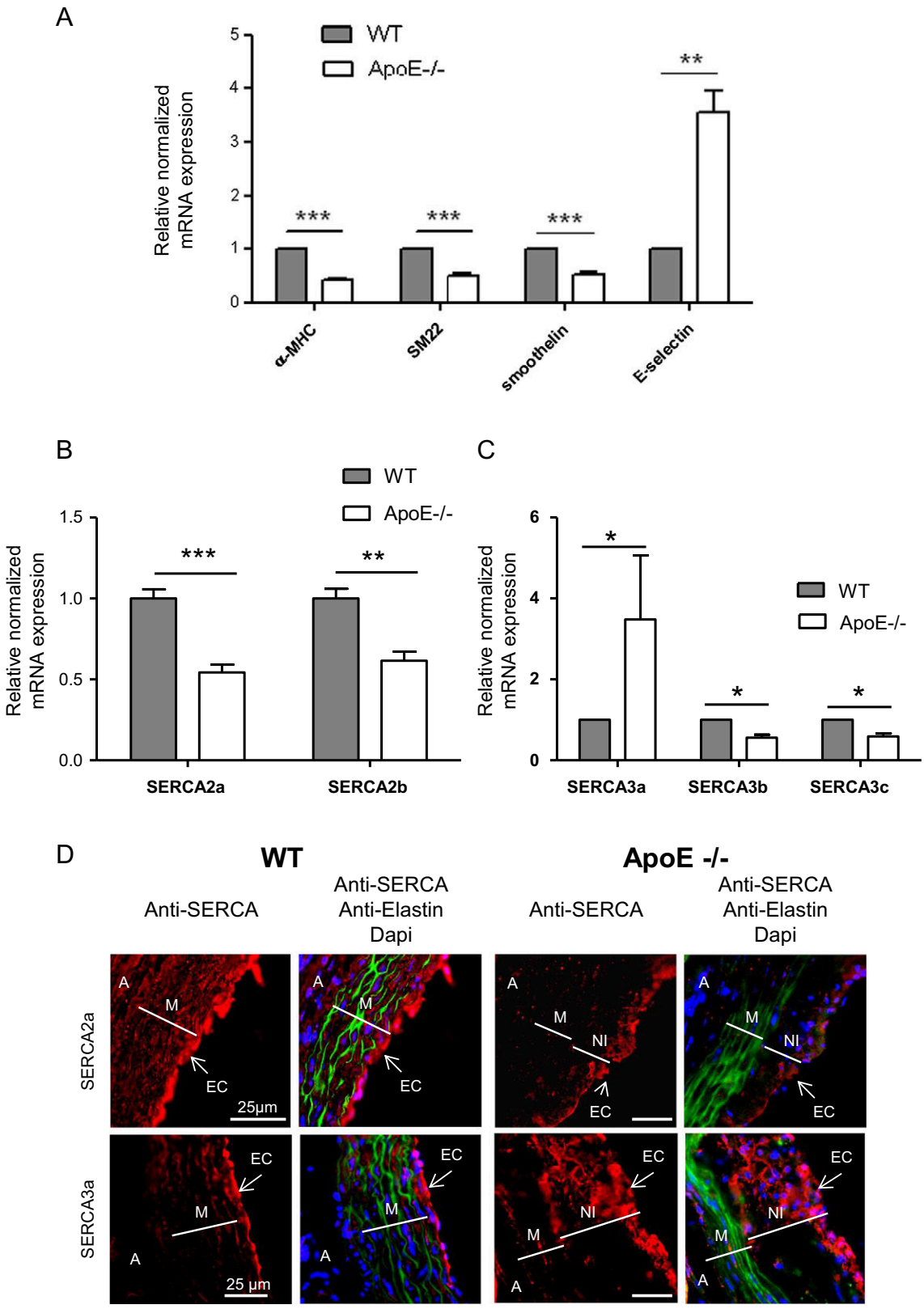

Fig. 7. Alteration of SERCA isoforms expression in atherosclerotic vessels. **A.** Real-time RT-PCR analysis of makers of contractile VSMC and inflammation in WT ($n = 7$) and MI ($n = 4$) animals. **B & C.** Real-time RT-PCR analysis of SERCA2 and SERCA3 family members expression in WT ($n = 7$) and MI ($n = 4$) animals. **D**. Immunofluorescence with SERCA specific antibodies (red) of aorta root sections from normal and ApoE$^{-/-}$ mice. Green—elastin autofluorescence. Nuclei were stained with Dapi (blue). Abbreviations: A—adventitia, M—media, NI—neointima, and EC—endothelial cells.

in EC: 1) ablation of SERCA3 genes results in defective nitric oxide (NO) synthesis [45]; 2) SERCA2a and SERCA3a colocalize with eNOS and caveolin in sub-plasma membrane reticulum in EC [19,24]; and 3) overexpression of SERCA2a in human EC, resulting in increased ER Ca^{2+} storage and mobilization, also enhances eNOS activity and cGMP production [24].

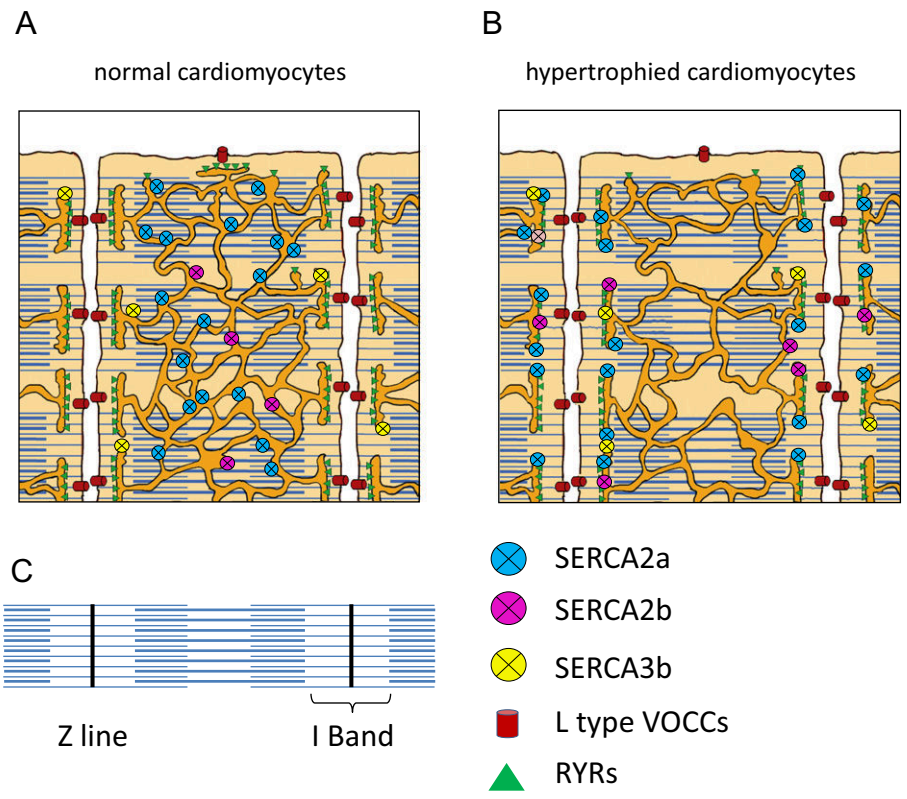

Fig. 8. Schematic localization of SERCA isoforms in normal and hypertrophied cardiomyocytes. Schematic representations of the structure of normal (Panel A) and failing (Panel B) cardiac myocytes illustrate the relative position of the SERCA isoforms on the SR network that wrap around the myofibrils. Panel C shows the topology of a myofibril.

We report an increase in SERCA3a expression in atherosclerotic vessels, together with a modification of the pattern of expression. The increase in SERCA3a expression might compensate the decrease of SERCA2a. However, the SERCA3a expression appears more diffuse at the atherosclerosis site compared to its normal localization. Given the fact that SERCA3a is preferentially expressed by endothelial cells and blood cells [46,47], it is interesting to suggest that SERCA3a expression indicates the infiltration of endothelial cells precursors or monocytes in the neointima of atherosclerotic vessels, as it is described (intimal hyperplasia in murine models [48].

5. Conclusions

The simultaneous expression of several SERCA isoforms in cardiovascular cells enlightens possible functions for each of the SERCA isoforms, given the specific expression and localization. Data obtained in a particular set of pathological conditions revealed specific regulation of SERCA isoforms, suggesting that not only the variety, but also the combination of SERCA isoforms achieves tight regulation of cellular functions. We have identified SERCA2a as the major isoform in both cardiac and vascular myocytes, in normal and pathological conditions. The expression of SERCA2a mRNA is ~30 fold higher in the heart compared to vascular tissues, in conformity with highest impact of contractile function in cardiomyocyte physiology. Notably, nearly half the amount of SERCA2a mRNA is measured in both failing cardiomyocytes and synthetic VSMCs compared to healthy tissues. Our study shows that the SERCA2a isoform is the principal regulator of excitation–contraction coupling in both CMs and contractile VSMCs and supports a dynamic and integrated regulation of the SERCA isoform system. The roles of previously unexplored isoforms, along with the dynamic interactions between isoforms, deserve further studies.

Supplementary data to this article can be found online at http://dx.doi.org/10.1016/j.bbamcr.2014.08.002.

Acknowledgements

This study was supported by grants from the INSERM, Ministère de la Recherche, DHU Ageing Thorax-Vessels-Blood (A-TVB), ANR Grant 11 BSV1 034 01, Association Française contre les Myopathies (AFM 14048, AFM 16442), and Fondation Cœur-poumon. Dr Hajjar was supported by NIH grants R01 HL117505, HL093183, and P50 HL112324.

References

[1] S. Dally, E. Corvazier, R. Bredoux, R. Bobe, J. Enouf, Multiple and diverse coexpression, location, and regulation of additional SERCA2 and SERCA3 isoforms in nonfailing and failing human heart, J. Mol. Cell. Cardiol. 48 (2010) 633–644.
[2] T. Seidler, G. Hasenfuss, L.S. Maier, Targeting altered calcium physiology in the heart: translational approaches to excitation, contraction, and transcription, Physiology (Bethesda) 22 (2007) 328–334.
[3] M. Periasamy, A. Kalyanasundaram, SERCA pump isoforms: their role in calcium transport and disease, Muscle Nerve 35 (2007) 430–442.
[4] A.L. Greene, M.J. Lalli, Y. Ji, G.J. Babu, I. Grupp, M. Sussman, M. Periasamy, Overexpression of SERCA2b in the heart leads to an increase in sarcoplasmic reticulum calcium transport function and increased cardiac contractility, J. Biol. Chem. 275 (2000) 24722–24727.
[5] F. Wuytack, B. Papp, H. Verboomen, L. Raeymaekers, L. Dode, R. Bobe, J. Enouf, S. Bokkala, K.S. Authi, R. Casteels, A sarco/endoplasmic reticulum Ca^{2+}ATPase 3-type Ca^{2+} pump is expressed in platelets, in lymphoid cells, and in mast cells, J. Biol. Chem. 269 (1994) 1410–1416.
[6] V. Martin, R. Bredoux, E. Corvazier, R. Van Gorp, T. Kovacs, P. Gelebart, J. Enouf, Three novel sarco/endoplasmic reticulum Ca^{2+}ATPase (SERCA) 3 isoforms. Expression, regulation, and function of the membres of the SERCA3 family, J. Biol. Chem. 277 (2002) 24442–24452.
[7] R. Bobe, R. Bredoux, E. Corvazier, J.P. Andersen, J.D. Clausen, L. Dode, T. Kovacs, J. Enouf, Identification, expression, function, and localization of a novel (sixth) isoform of the human sarco/endoplasmic reticulum Ca^{2+}ATPase 3 gene, J. Biol. Chem. 279 (2004) 24297–24306.
[8] P.D. Borge Jr., B.A. Wolf, Insulin receptor substrate 1 regulation of sarco-endoplasmic reticulum calcium ATPase 3 in insulin-secreting beta-cells, J. Biol. Chem. 278 (2003) 11359–11368.
[9] V. Martin, R. Bredoux, E. Corvazier, B. Papp, J. Enouf, Platelet Ca^{2+}ATPases: a plural, species-specific, and multiple hypertension-regulated expression system, Hypertension 35 (2000) 91–102.

[10] H. Verboomen, F. Wuytack, H.D. Smedt, B. Himpens, R. Casteels, Functional difference between SERCA2a and SERCA2b Ca^{2+} pumps and their modulation by phospholamban, Biochem. J. 286 (1992) 591–596.
[11] S. Dally, R. Bredoux, E. Corvazier, J.P. Andersen, J.D. Clausen, L. Dode, M. Fanchaouy, P. Gelebart, V. Monceau, F. Del Monte, J.K. Gwathmey, R. Hajjar, C. Chaabane, R. Bobe, A. Raies, J. Enouf, Ca^{2+}ATPases in non-failing and failing heart: evidence for a novel cardiac sarco/endoplasmic reticulum Ca^{2+}ATPase 2 isoform (SERCA2c), Biochem. J. 395 (2006) 249–258.
[12] J. Lytton, M. Westlin, S.E. Burk, G.E. Shull, D.H. MacLennan, Functional comparisons between isoforms of the sarcoplasmic or endoplasmic reticulum family of calcium pumps, J. Biol. Chem. 267 (1992) 14483–14489.
[13] S.L. Dodd, T.J. Koesterer, Clenbuterol attenuates muscle atrophy and dysfunction in hindlimb-suspended rats, Aviat. Space Environ. Med. 73 (2002) 635–639.
[14] E.R. Chemaly, R. Bobe, S. Adnot, R.J. Hajjar, L. Lipskaia, Sarco (Endo) plasmic Reticulum Calcium ATPases (SERCA) isoforms in the normal and diseased cardiac, vascular and skeletal muscle systems, J. Cardiovasc. Dis. Diagn. 1 (2013) 6.
[15] P. Vangheluwe, M. Schuermans, L. Raeymaekers, F. Wuytack, Tight interplay between the Ca^{2+} affinity of the cardiac SERCA2 Ca^{2+} pump and the SERCA2 expression level, Cell Calcium 42 (2007) 281–289.
[16] D.O. Levitsky, M. Clergue, F. Lambert, M.V. Souponitskaya, T.H. Le Jemtel, Y. Lecarpentier, A.M. Lompre, Sarcoplasmic reticulum calcium transport and Ca(2+)-ATPase gene expression in thoracic and abdominal aortas of normotensive and spontaneously hypertensive rats, J. Biol. Chem. 268 (1993) 8325–8331.
[17] A.M. Lompre, R.J. Hajjar, S.E. Harding, E.G. Kranias, M.J. Lohse, A.R. Marks, Ca^{2+} cycling and new therapeutic approaches for heart failure, Circulation 121 (2010) 822–830.
[18] L. Lipskaia, I. Limon, R. Bobe, H. R, Calcium cycling in synthetic and contractile phasic or tonic vascular smooth muscle cells, in: S.H. InTech (Ed.), Current Basic and Pathological Approaches to the Function of Muscle Cells and Tissues—From Molecules to Humans, 2012.
[19] L. Lipskaia, L. Hadri, P. Le Prince, B. Esposito, F. Atassi, L. Liang, M. Glorian, I. Limon, A.M. Lompre, S. Lehoux, R.J. Hajjar, SERCA2a gene transfer prevents intimal proliferation in an organ culture of human internal mammary artery, Gene Ther. 20 (2013) 396–406.
[20] L. Lipskaia, E.R. Chemaly, L. Hadri, A.M. Lompre, R.J. Hajjar, Sarcoplasmic reticulum Ca(2+) ATPase as a therapeutic target for heart failure, Expert. Opin. Biol. Ther. 10 (2010) 29–41.
[21] V. Kairouz, L. Lipskaia, R.J. Hajjar, E.R. Chemaly, Molecular targets in heart failure gene therapy: current controversies and translational perspectives, Ann. N. Y. Acad. Sci. 1254 (2012) 42–50.
[22] S. Dally, V. Monceau, E. Corvazier, R. Bredoux, A. Raies, R. Bobe, F. del Monte, J. Enouf, Compartmentalized expression of three novel sarco/endoplasmic reticulum Ca^{2+}ATPase 3 isoforms including the switch to ER stress, SERCA3f, in non-failing and failing human heart, Cell Calcium 45 (2009) 144–154.
[23] K.J. Livak, T.D. Schmittgen, Analysis of relative gene expression data using real-time quantitative PCR and the 2(−Delta Delta C(T)) Method, Methods 25 (2001) 402–408.
[24] L. Hadri, R. Bobe, Y. Kawase, D. Ladage, K. Ishikawa, F. Atassi, D. Lebeche, E.G. Kranias, J.A. Leopold, A.M. Lompre, L. Lipskaia, R.J. Hajjar, SERCA2a gene transfer enhances eNOS expression and activity in endothelial cells, Mol. Ther. 18 (2010) 1284–1292.
[25] N.R. DiPaola, W.E. Sweet, L.B. Stull, G.S. Francis, C. Schomisch Moravec, Beta-adrenergic receptors and calcium cycling proteins in non-failing, hypertrophied and failing human hearts: transition from hypertrophy to failure, J. Mol. Cell. Cardiol. 33 (2001) 1283–1295.
[26] L. Lipskaia, L. Hadri, J.J. Lopez, R.J. Hajjar, R. Bobe, Benefit of SERCA2a gene transfer to vascular endothelial and smooth muscle cells: a new aspect in therapy of cardiovascular diseases, Curr. Vasc. Pharmacol. 11 (2013) 465–479.
[27] M. Ver Heyen, S. Heymans, G. Antoons, T. Reed, M. Periasamy, B. Awede, J. Lebacq, P. Vangheluwe, M. Dewerchin, D. Collen, K. Sipido, P. Carmeliet, F. Wuytack, Replacement of the muscle-specific sarcoplasmic reticulum Ca(2+)-ATPase isoform SERCA2a by the nonmuscle SERCA2b homologue causes mild concentric hypertrophy and impairs contraction-relaxation of the heart, Circ. Res. 89 (2001) 838–846.
[28] A.R. Marks, Calcium cycling proteins and heart failure: mechanisms and therapeutics, J. Clin. Invest. 123 (2013) 46–52.
[29] M. Seth, C. Sumbilla, S.P. Mullen, D. Lewis, M.G. Klein, A. Hussain, J. Soboloff, D.L. Gill, G. Inesi, Sarco(endo)plasmic reticulum Ca^{2+}ATPase (SERCA) gene silencing and remodeling of the Ca^{2+} signaling mechanism in cardiac myocytes, Proc. Natl. Acad. Sci. U. S. A. 101 (2004) 16683–16688.
[30] L. Lipskaia, F. del Monte, T. Capiod, S. Yacoubi, L. Hadri, M. Hours, R.J. Hajjar, A.M. Lompre, Sarco/endoplasmic reticulum Ca^{2+}-ATPase gene transfer reduces vascular smooth muscle cell proliferation and neointima formation in the rat, Circ. Res. 97 (2005) 488–495.
[31] P. Vangheluwe, W.E. Louch, M. Ver Heyen, K. Sipido, L. Raeymaekers, F. Wuytack, Ca^{2+} transport ATPase isoforms SERCA2a and SERCA2b are targeted to the same sites in the murine heart, Cell Calcium 34 (2003) 457–464.
[32] D.M. Bers, Cardiac excitation–contraction coupling, Nature 415 (2002) 198–205.
[33] V. Bito, F.R. Heinzel, L. Biesmans, G. Antoons, K.R. Sipido, Crosstalk between L-type Ca^{2+} channels and the sarcoplasmic reticulum: alterations during cardiac remodelling, Cardiovasc. Res. 77 (2008) 315–324.
[34] S.J. Shah, G.L. Aistrup, D.K. Gupta, M.J. O'Toole, A.F. Nahhas, D. Schuster, N. Chirayil, N. Bassi, S. Ramakrishna, L. Beussink, S. Misener, B. Kane, D. Wang, B. Randolph, A. Ito, M. Wu, L. Akintilo, T. Mongkolrattanothai, M. Reddy, M. Kumar, R. Arora, J. Ng, J.A. Wasserstrom, Ultrastructural and cellular basis for the development of abnormal myocardial mechanics during the transition from hypertension to heart failure, Am. J. Physiol. Heart Circ. Physiol. 306 (2014) H88–H100.
[35] C. Chaabane, E. Corvazier, R. Bredoux, S. Dally, A. Raies, A. Villemain, E. Dupuy, J. Enouf, R. Bobe, Sarco/endoplasmic reticulum Ca^{2+} ATPase type 3 isoforms (SERCA3b and SERCA3f): distinct roles in cell adhesion and ER stress, Biochem. Biophys. Res. Commun. 345 (2006) 1377–1385.
[36] I.S. Bartlett, G.J. Crane, T.O. Neild, S.S. Segal, Electrophysiological basis of arteriolar vasomotion in vivo, J. Vasc. Res. 37 (2000) 568–575.
[37] R.E. Haddock, C.E. Hill, Differential activation of ion channels by inositol 1,4,5-trisphosphate (IP3)- and ryanodine-sensitive calcium stores in rat basilar artery vasomotion, J. Physiol. 545 (2002) 615–627.
[38] R.E. Haddock, G.D. Hirst, C.E. Hill, Voltage independence of vasomotion in isolated irideal arterioles of the rat, J. Physiol. 540 (2002) 219–229.
[39] L. Lipskaia, M.L. Pourci, C. Delomenie, L. Combettes, D. Goudouneche, J.L. Paul, T. Capiod, A.M. Lompre, Phosphatidylinositol 3-kinase and calcium-activated transcription pathways are required for VLDL-induced smooth muscle cell proliferation, Circ. Res. 92 (2003) 1115–1122.
[40] O. Vallot, L. Combettes, P. Jourdon, J. Inamo, I. Marty, M. Claret, A.M. Lompre, Intracellular Ca(2+) handling in vascular smooth muscle cells is affected by proliferation, Arterioscler. Thromb. Vasc. Biol. 20 (2000) 1225–1235.
[41] R. Bobe, L. Hadri, J.J. Lopez, Y. Sassi, F. Atassi, I. Karakikes, L. Liang, I. Limon, A.M. Lompre, S.N. Hatem, R.J. Hajjar, L. Lipskaia, SERCA2a controls the mode of agonist-induced intracellular Ca^{2+} signal, transcription factor NFAT and proliferation in human vascular smooth muscle cells, J. Mol. Cell. Cardiol. 50 (2011) 621–633.
[42] E. Merlet, L. Lipskaia, A. Marchand, L. Hadri, N. Mougenot, F. Atassi, L. Liang, S.N. Hatem, R.J. Hajjar, A.M. Lompre, A calcium-sensitive promoter construct for gene therapy, Gene Ther. 20 (2013) 248–254.
[43] I.I. Mountian, F. Baba-Aissa, J.C. Jonas, S. Humbert De, F. Wuytack, J.B. Parys, Expression of Ca(2+) transport genes in platelets and endothelial cells in hypertension, Hypertension 37 (2001) 135–141.
[44] J. Kao, C.N. Fortner, L.H. Liu, G.E. Shull, R.J. Paul, Ablation of the SERCA3 gene alters epithelium-dependent relaxation in mouse tracheal smooth muscle, Am. J. Physiol. 277 (1999) L264–L270.
[45] L.H. Liu, R.J. Paul, R.L. Sutliff, M.L. Miller, J.N. Lorenz, R.Y. Pun, J.J. Duffy, T. Doetschman, Y. Kimura, D.H. MacLennan, J.B. Hoying, G.E. Shull, Defective endothelium-dependent relaxation of vascular smooth muscle and endothelial cell Ca^{2+} signaling in mice lacking sarco(endo)plasmic reticulum Ca^{2+}ATPase isoform 3, J. Biol. Chem. 272 (1997) 30538–30545.
[46] I. Machuca, C. Domenget, P. Jurdic, Identification of avian sarcoplasmic reticulum Ca(2+)-ATPase (SERCA3) as a novel 1,25(OH)(2)D(3) target gene in the monocytic lineage, Exp. Cell Res. 250 (1999) 364–375.
[47] T. Kovacs, F. Felfoldi, B. Papp, K. Paszty, R. Bredoux, A. Enyedi, J. Enouf, All three splice variants of the human sarco/endoplasmic reticulum Ca^{2+}ATPase 3 gene are translated to proteins: a study of their co-expression in platelets and lymphoid cells, Biochem. J. 358 (2001) 559–568.
[48] D.Y. Hui, Intimal hyperplasia in murine models, Curr. Drug Targets 9 (2008) 251–260.

Regular Article

PLATELETS AND THROMBOPOIESIS

A new form of macrothrombocytopenia induced by a germ-line mutation in the *PRKACG* gene

Vladimir T. Manchev,[1,2,3] Morgane Hilpert,[1,2,3] Eliane Berrou,[4] Ziane Elaib,[4] Achille Aouba,[5] Siham Boukour,[1,3,4] Sylvie Souquere,[3,6] Gerard Pierron,[3,6] Philippe Rameau,[3,7] Robert Andrews,[8] François Lanza,[9] Regis Bobe,[4] William Vainchenker,[1,3] Jean-Philippe Rosa,[4] Marijke Bryckaert,[4] Najet Debili,[1,3] Remi Favier,[1,10] and Hana Raslova[1,3]

[1]Institut National de la Santé et de la Recherche Médicale, Unité Mixte de Recherche 1009, Université Paris-Sud 11, Equipe Labellisée Ligue Contre le Cancer, Villejuif, France; [2]University Paris Diderot, Paris, France; [3]Gustave Roussy, Villejuif, France; [4]Institut National de la Santé et de la Recherche Médicale, Unité Mixte de Recherche_S 770, Université Paris-Sud 11, Le Kremlin Bicêtre, France; [5]Assistance Publique-Hôpitaux de Paris, Médecine Interne-Immunologie Clinique, Antoine Beclere Hospital, Clamart, France; [6]Centre National de la Recherche Scientifique, Unité Mixte de Recherche 8122, Université Paris-Sud 11, Villejuif, France; [7]Plate Forme Imagerie et Cytomètrie de Flux, Integrated Research Cancer Institute in Villejuif, Villejuif, France; [8]Australian Centre for Blood Diseases, Monash University, Melbourne, Australia; [9]Institut National de la Santé et de la Recherche Médicale, UMR S949, Université de Strasbourg, Etablissement Français du Sang Alsace, Strasbourg Cedex, France; and [10]Assistance Publique-Hôpitaux de Paris, Armand Trousseau Children Hospital, French Reference Center for Platelet Disorders, Haematological Laboratory, Paris, France

Key Points

- We identify a new type of autosomal recessive macrothrombocytopenia associated with a mutation in PRKACG, coding the PKA catalytic subunit.
- The homozygous PRKACG mutation leads to a deep defect in proplatelet formation that was restored by the overexpression of wild-type PRKACG.

Macrothrombocytopenias are the most important subgroup of inherited thrombocytopenias. This subgroup is particularly heterogeneous because the affected genes are involved in various functions such as cell signaling, cytoskeleton organization, and gene expression. Herein we describe the clinical and hematological features of a consanguineous family with a severe autosomal recessive macrothrombocytopenia associated with a thrombocytopathy inducing a bleeding tendency in the homozygous mutated patients. Platelet activation and cytoskeleton reorganization were impaired in these homozygous patients. Exome sequencing identified a c.222C>G mutation (missense p.74Ile>Met) in *PRKACG,* a gene encoding the γ-catalytic subunit of the cyclic adenosine monophosphate-dependent protein kinase, the mutated allele cosegregating with the macrothrombocytopenia. We demonstrate that the p.74Ile>Met PRKACG mutation is associated with a marked defect in proplatelet formation and a low level in filamin A in megakaryocytes (MKs). The defect in proplatelet formation was rescued in vitro by lentiviral vector-mediated overexpression of wild-type PRKACG in patient MKs. We thus conclude that PRKACG is a new central actor in platelet biogenesis and a new gene involved in inherited thrombocytopenia with giant platelets associated with a thrombocytopathy. (*Blood*. 2014;124(16):2554-2563)

Introduction

Inherited thrombocytopenias (ITs) are a heterogeneous group of blood disorders characterized by a reduced platelet count in blood. Some of these diseases are exclusively restricted to megakaryocytes (MKs) and platelets, whereas others also affect other tissues. Functional platelet defects are also often associated, and their severity may lead to a high risk of bleeding. Based on the mean platelet volume, ITs have been classified into 3 subgroups with large, normal, or small platelets.

The most important subgroup of inherited platelet disorders is characterized by low platelet counts and the presence of large and giant platelets, designated as macrothrombocytopenia. This subgroup includes 2 types of thrombocytopenia. The first type is characterized by syndromic features associated with mutations in genes encoding myosin IIA in myosin heavy chain 9 (MYH9)-related disease, filamin-A (FLNa) in FLNa-related thrombocytopenia, friend leukemia integration 1 (FLI1) in Paris-Trousseau syndrome, and ATP-binding cassette sub-familly G member 5 (ABCG5) macrothrombocytopenia associated with sitosterolemia. In contrast, the second type lacks syndromic features and is related to mutations in genes encoding transcription factors such as GATA1 and GFI1B and for cytoskeletal proteins or surface receptors such as tubulin β1, αIIbβ3, and platelet glycoprotein Ib (GPIb)/platelet glycoprotein IX (GPIX).[1,2] Recently, next-generation sequencing methodology led to the identification of the *NBEAL2* gene altered in Gray platelet syndrome[3] and of the *ACTN1* gene affected in congenital macrothrombocytopenia (CMTP).[4]

Here, using exome sequencing, we identified for the first time a c.222C>G mutation in the *PRKACG* gene in a family with a novel form of IT. *PRKACG* encodes the γ isoform of the catalytic subunit

Submitted January 27, 2014; accepted July 9, 2014. Prepublished online as *Blood* First Edition paper, July 24, 2014; DOI 10.1182/blood-2014-01-551820.

V.T.M. and M.H. contributed equally to this work.

R.F. and H.R. contributed equally to this work.

The online version of this article contains a data supplement.

There is an Inside *Blood* Commentary on this article in this issue.

The publication costs of this article were defrayed in part by page charge payment. Therefore, and solely to indicate this fact, this article is hereby marked "advertisement" in accordance with 18 USC section 1734.

(Cγ) of cyclic adenosine monophosphate (cAMP)-dependent protein kinase A (PKA), and the mutation is predicted to lead to a missense p.74Ile>Met substitution. This mutation is responsible for the autosomal recessive IT characterized by defects in proplatelet formation and platelet activation in the homozygous patients, identifying a new mechanism responsible for thrombocytopenia and thrombocytopathy.

Material and methods

Patients

Blood samples from patients and healthy subjects were collected after informed written consent was obtained in accordance with the Declaration of Helsinki. The study was approved by the Ethic Committee of the Institut National de la Santé et de Recherche Médicale Recherche Biomédicale (INSERM RBM) 01-14.

Samples

Venous blood from the patient was collected in 10% (volume to volume) ACD-A buffer (75 mM trisodium citrate, 44 mM citric acid, and 136 mM glucose, pH 4). The platelet-rich plasma was prepared by centrifugation at 80*g* for 10 minutes. Platelets were pelleted by centrifugation at 2100*g* for 10 minutes. Platelets were washed in the presence of apyrase (100 mU/mL) and prostaglandin E1 (1 μM) to minimize platelet activation. The number of platelets from the patient and the control was adjusted to similar levels (2.5×10^8 platelets/mL) in Tyrode's buffer (137 mM NaCl, 2 mM KCl, 0.3 mM NaH_2PO_4, 1 mM $MgCl_2$, 5.5 mM glucose, 5 mM *N*-2-hydroxyethylpiperazine-*N*′-2-ethanesulfonic acid, 12 mM $NaHCO_3$, and 2 mM $CaCl_2$, pH7.3). For western blot analysis of platelets, remaining red blood cells (GPA^+) were depleted using immunomagnetic beads (AutoMACS; Miltenyi Biotec SAS).

Peripheral blood $CD34^+$ cells were separated by double-positive selection using a magnetic cell-sorting system (AutoMACS; Miltenyi Biotec SAS).

Free intracellular calcium concentration measurement

Washed platelets (2.5×10^7 platelets/mL) were loaded with Oregon green 488 BAPTA1-AM (1 μM; Molecular Probes, Eugene, OR) for 45 minutes at 20°C. Platelets were then diluted in Tyrode's buffer to 2.5×10^6 platelets/mL, and the cytosolic Ca^{2+} concentration was analyzed using an Accuri C6 (Becton Dickinson) flow cytometer. First, Ca^{2+} mobilization in response to thrombin was observed in absence of extracellular Ca^{2+} (100 μM EGTA). After 3 minutes, Ca^{2+} influx was induced by adding Ca^{2+} (300 μM) in extracellular medium.

Platelet spreading and F-actin/G-actin quantification

Glass coverslips were precoated with human von Willebrand factor (VWF; 10 μg/mL) in the presence of botrocetin (5 μg/mL) and with fibrinogen (100 μg/mL; HYPHEN BioMed SAS) overnight at 4°C. Then washed platelets (10^7 platelets/mL; 150 μL) were allowed to adhere at room temperature. After 30 minutes, adherent platelets were fixed with 4% paraformaldehyde in 0.1 M piperazine-N,N′bis(2-ethanesulfonic acid), 2 M glycerol, 1 mM EGTA, and 1 mM $MgCl_2$, pH 6.9, for 15 minutes and then permeabilized in the same buffer containing 0.2% Triton X-100 for 5 minutes. Platelets were stained with both Alexa Fluor488-labeled phalloidin and Alexa Fluor594-labeled DNAse I (Molecular Probes) and then visualized under an epifluorescence microscope (Eclipse 600; Nikon France). Cell surfaces and F- and G-actin contents were determined using ImageJ version 1.42k (rsb.info.nih.gov/ij).

Targeted exome sequencing (v5-70 Mb)

Library preparation, capture, sequencing, and variant detection were performed by IntegraGen S.A. (Evry, France). Genomic DNA was extracted with the DNA purification kit (Quiagen), captured using Agilent in-solution enrichment methodology with their biotinylated oligonucleotides probes library (Human All Exon v5-70 Mb; Agilent), followed by paired-end 75-base massively parallel sequencing on Illumina HiSEQ 2000. For detailed explanations of the process, see Gnirke et al.[5] Sequence capture, enrichment, and elution were performed according to the manufacturer's instructions and protocols (SureSelect; Agilent). Briefly, 3 μg of each genomic DNA was fragmented by sonication and purified to yield fragments of 150 to 200 bp. Paired-end adaptor oligonucleotides from Illumina were ligated on repaired, A-tailed DNA fragments and then purified and enriched by 4 to 6 polymerase chain reaction (PCR) cycles. Five hundred nanograms of these purified Libraries was hybridized to the SureSelect oligo probe capture library for 24 hours. After hybridization, washing, and elution, the eluted fraction was PCR-amplified with 10 to 12 cycles, purified, and quantified by quantitative PCR to obtain sufficient DNA template for downstream applications. Each eluted-enriched DNA sample was then sequenced on an Illumina HiSEQ 2000 as paired-end 75-base reads. Image analysis and base calling were performed using Illumina Real Time Analysis Pipeline version 1.12 with default parameters.

The bioinformatics analysis of sequencing data was based on the Illumina pipeline (CASAVA1.8.2). CASAVA performs alignment of the reads to a reference genome (hg19) with the alignment algorithm ELANDv2, and then calls the SNPs based on the allele calls and read depth and detects variants. Only the positions included in the oligonucleotide probe coordinates ±20 bp were conserved. Genetic variation annotation was performed using the IntegraGen in-house pipeline, which consists of gene annotation (RefSeq), detection of known polymorphisms (dbSNP 132; 1000Genome), and mutation characterization (exonic, intronic, silent, or nonsense).

For each position, the exomic frequencies (homo and heterozygous) were determined from the IntegraGen exome database and the exome results provided by HapMap.

The *PRKACG* mutation was validated by Sanger sequencing using forward (5′-ACCGCCATGGGCAACGC-3′) and reverse (5′-GAAAACC CACAGGGGCACAA-3′) primers.

In vitro MK differentiation

Patient or control $CD34^+$ cells were grown in serum-free medium as previously reported.[6] The medium was supplemented with 10 ng/mL thrombopoietin (TPO) (Kirin Brewery) and 25 ng/mL stem cell factor (SCF; Biovitrum AB).

Flow cytometry analysis

MKs were stained with directly coupled monoclonal antibodies anti–CD41-phycoerythrin and anti–CD42a-allophycocyanin (BD Biosciences) for 30 minutes at 4°C. Platelet surface staining of CD41a, CD42a, and CD62P was performed with the PLT Gp/Receptors kit (Biocytex) at room temperature before and after activation by the thrombin receptor agonist peptide (25 μM). For western blot analysis, MKs were sorted according to CD41 and CD42 expression using an Influx flow cytometer equipped with 5 lasers (BD Biosciences).

Ploidy analysis

At day 10 of culture, Hoechst 33342 (10 μg/mL; Sigma-Aldrich) was added in the medium of cultured MKs for 2 hours at 37°C. Cells were then stained with directly coupled monoclonal antibodies: anti–CD41-phycoerythrin and anti-CD42a-allophycocyanin (BD Biosciences) for 30 minutes at 4°C.[7] Ploidy was measured in the $CD41^+CD42^+$ cell population by means of an Influx flow cytometer (BD Biosciences) and calculated as previously described.[7]

Quantification of proplatelets bearing MKs

To evaluate the percentage of MKs forming proplatelets (PPTs) in liquid medium, $CD41^+$ cells were sorted at day 6 of culture and plated in 96-well plates at a concentration of 2000 cells per well in serum-free medium in the presence of TPO (10 ng/mL). MKs displaying PPTs were quantified between

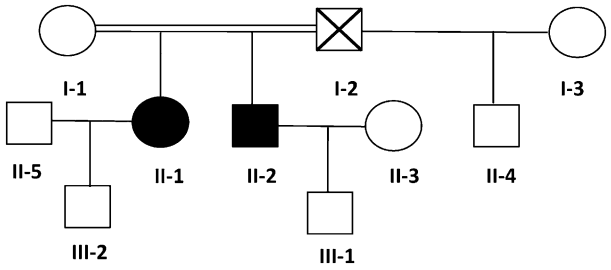

Figure 1. Family tree. Circles, females; squares, males; black filled symbols, affected individuals; white symbols, nonaffected individuals; symbol with a diagonal line, deceased individual; double horizontal line, consanguinity.

day 11 and 13 of culture by enumerating 200 cells per well using an inverted microscope (Carl Zeiss) at a magnification of ×200. MKs displaying PPTs were defined as cells exhibiting ≥1 cytoplasmic process with constriction areas (3 wells were examined for each individual and condition).

Fluorescence microscopy

Fibrinogen (Sigma-Aldrich) was incubated at the concentration of 20 μg/mL on coverslips overnight at 4°C. Primary MKs grown in serum-free medium were plated on coated coverslips for 2 hours at 37°C (5% CO_2 in air). Cells were then fixed in 2% paraformaldehyde for 10 minutes, permeabilized with 0.2% Triton X-100 for 5 minutes, and incubated with monoclonal anti-β tubulin (Sigma-Aldrich) and rabbit anti-VWF antibody (Dako) for 1 hour, followed by incubation with Alexa 555-conjugated goat anti-mouse immunoglobulin G (IgG) and Alexa 633-conjugated goat anti-rabbit IgG (Molecular Probes) for 30 minutes. Finally, slides were mounted using Vectashield with 4,6 diamidino-2-phenylindole (Molecular Probes). The PPT-forming MKs (cells expressing VWF) were examined under a Leica DMI 4000, SPE laser scanning microscope (Leica Microsystems) with a 63×/1.4 numeric aperture oil objective. The diameters of platelet-like structures occurring along PPTs were measured with LAS AF version 2.4.1 software, and images were processed using Adobe Photoshop 6.0 software.

Intraplatelet measurement of cAMP by enzyme-linked immunosorbent assay

Control and patient platelets (10^7) were washed as described in the sample section and centrifuged at 2100*g* for 10 minutes at 4°C. Pellets were then resuspended in 200 μL of lysis buffer for 10 minutes at room temperature; 100 μL of the solution was used for the assay performed in duplicate. Intracellular cAMP was measured with the Amersham cAMP Biotrak Enzyme-immunoassay system (GE Healthcare) using the nonacetylation enzyme immunoassay procedure following the manufacturer's recommendation. Optical density was read at 450 nm on a microplate reader (model 680; Bio-Rad), and results were calculated following the manufacturer's recommendation.

Virus construction and cell transduction

The cDNA of PRKACG was cloned under the promoter EF1α into the bicistronic lentivirus also encoding for the PGK-GFP cassette. The c.222C>G mutation was introduced by directed mutagenesis. Viral particles production and cell transduction were performed, as previously described.[8] Control $CD34^+$ cells (10^6/mL) were prestimulated for 24 hours with TPO, interleukin-3, SCF, and Fms-like tyrosin kinase 3-ligand and transduced with concentrated lentiviral (wild-type or mutated PRKACG) particles for 12 hours at a multiplicity of infection of 10, followed by a second transduction. Cells were then cultured in the presence of TPO and SCF alone. $CD41^+GFP^+$ cells were sorted by flow cytometry (FACS Vantage; BD Biosciences) 6 days after transduction. The $CD41^+GFP^+$ cells were further assessed for the ability to form PPTs or for the diameter of PPT-like structures by immunofluorescence assay.

Western blot assays

MKs were sorted by CD41 and CD42 expression at day 12 of culture, pelleted, and sonicated in 2× Laemli buffer (100 mM Tris-HCl, pH 6.8, 0.05% bromphenol blue, 4% sodium dodecyl sulfate [SDS], and 20% glycerol) supplemented with 100 mM dithiothreitol. Washed unstimulated platelets were lysed in SDS denaturing buffer (50 mM Tris, 100 mM NaCl, 50 mM NaF, 5 mM EDTA, 40 mM β-glycerophosphate, 100 μM phenylarsine oxide, 1% SDS, 5 μg/mL leupeptin, and 10 μg/mL aprotinin, pH 7.4). The proteins were subjected to SDS-polyacrylamide gel electrophoresis and transferred to nitrocellulose. The membranes were incubated with various primary antibodies: affinity-purified rabbit anti–GPIbβ-phospho-Ser^{166} and total rabbit anti-GPIbβ antibodies both previously described,[9] mouse anti–β-actin and anti-HSC70 antibodies (Sigma-Aldrich), mouse anti-PRKACG antibody (Abcam), and rabbit anti-Filamin A antibody (Cell Signaling), followed by horseradish peroxidase-linked secondary antibodies. Protein blots were analyzed using Image Quant LAS 4000 (GE Healthcare), and protein expressions were quantified using ImageQuant TL 8.1 software.

Electron microscopy

Blood (200 μL) was centrifuged at 2100*g* for 10 minutes in Eppendorf microtubes. Plasma was removed, and the pellet was fixed with 1.5% glutaraldehyde (Fluka Chemie) in 0.1 M phosphate-buffered saline, pH 7.2, for 1 hour at room temperature. The platelet disk was cut into small slices and washed 3 times in 1× phosphate-buffered saline. For morphological examination, fixed platelets were postfixed in 1% osmic acid, dehydrated in ethanol, and embedded in Epon by standard methods.[10] Sections were observed with a Technai 12 transmission electron microscope (FEI).

Statistical analyses

Data are presented as means ± standard deviation (SD) or ± standard error of the mean (SEM) as indicated. Statistical significance was determined by a 2-tailed Mann-Whitney test or unpaired Student *t* test with Welch's correction. $P < .05$ was considered statistically significant.

Results

Family description

A severe thrombocytopenia (5×10^9/L) was initially identified after a bleeding episode in 1 21-year-old woman of West Indian origin

Table 1. Clinical characteristics of *PRKACG*-related thrombocytopenia patients

Family member	Age at diagnosis (years)	Current age (years)	Platelet count (×10^9/L)	MPV (fL)	Hemoglobin (g/dL)	Leukocytes (×10^9/L)	Bleeding score	TPO level (ng/L)
I-1		44	210	10.3	11	4.5	NB	35
II-1	4	23	5	ND	9	5	3	23
II-2	2	26	8	ND	12.3	5.6	2	25
II-3		21	229	10.8	12.9	7.1	NB	20
III-1		3	276	10.4	10.4	8	NB	30
III-2		90 d	277	11	17	14	NB	ND

Normal TPO level, <30 ng/L. MPV, mean platelet volume; NB, no bleeding; ND, not done.

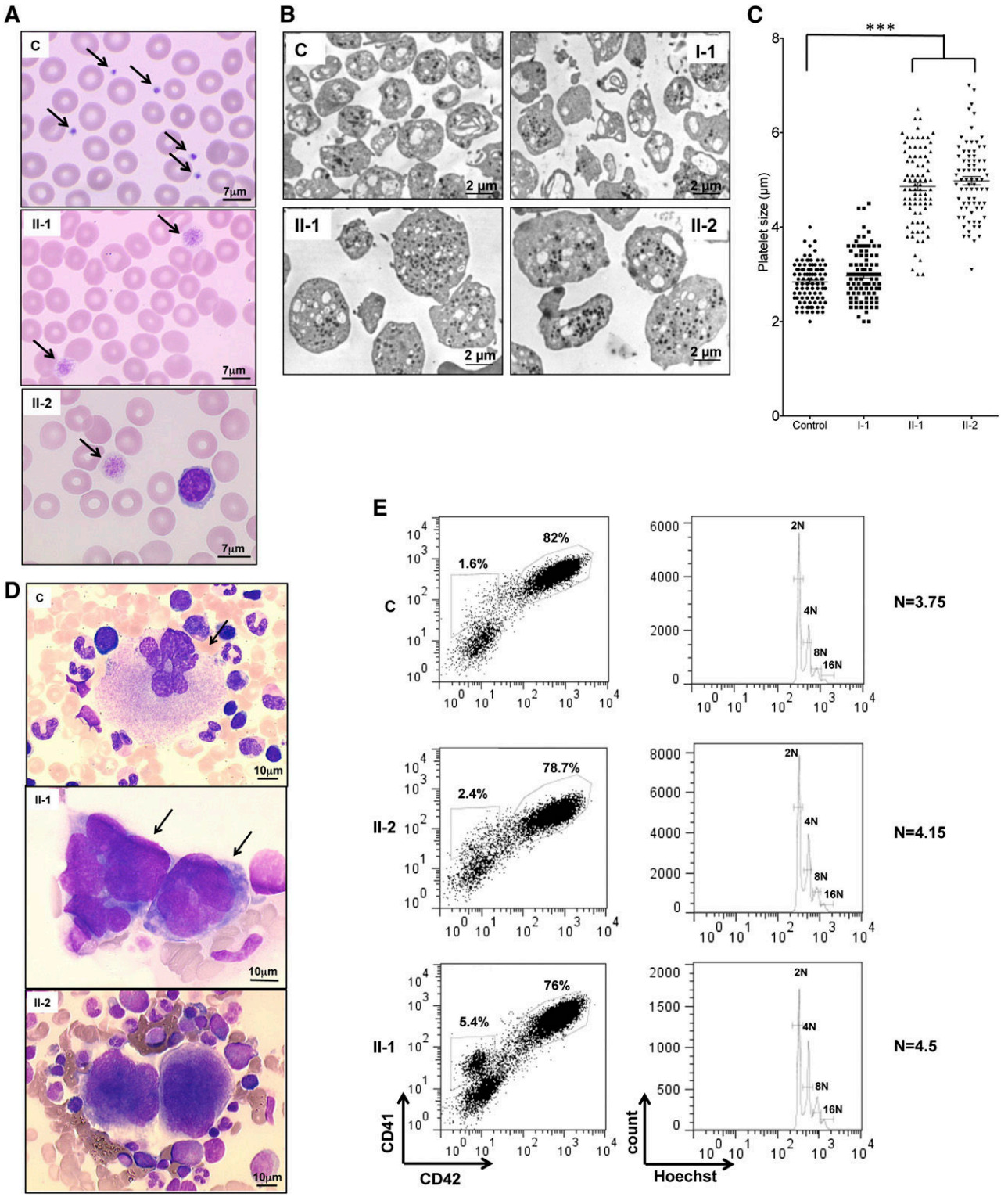

Figure 2. Platelet and MK analysis. (A) Cytological investigation of blood platelets. The black arrows point to platelets in the blood smears. Note the much larger platelet size for patients (II-1 and II-2) compared with control (C). (B) Ultrastructural aspect of blood platelets. Large platelets were detected in blood of II-1 and II-2 patients, and platelets of normal size were detected in 1 control and in a I-1 family member with the heterozygous *PRKACG* mutation. (C) The size of 100 platelets for control, I-1, II-1, and II-2 individuals was measured. The results represent mean ± SEM. ***$P < .0001$, unpaired Student *t* test (2-tailed). (D) Cytological investigations of the bone marrow of II-1 and II-2 patients and control. (E) MK differentiation was induced from control or patient peripheral blood $CD34^+$ cells and analyzed at day 10 of culture. Gates represent mature ($CD41^+CD42^+$) or immature ($CD41^+CD42^-$) MKs (left). The ploidy level (N) was analyzed in the gate of $CD41^+CD42^+$ MKs and was based on the percentage of cells in 8N, 16N, and 32N gates.

(proband II-1) at the age of 4 years. She presented with no syndromic features but many bleeding episodes during infancy, including epistaxis, spontaneous hematomas, menorrhagias inducing anemia, and, notably, 3 consecutive bleeding ruptures of ovarian cysts involving life prognosis and requiring platelet and blood cell transfusion. The World Health Organization bleeding score is 4 in this patient.

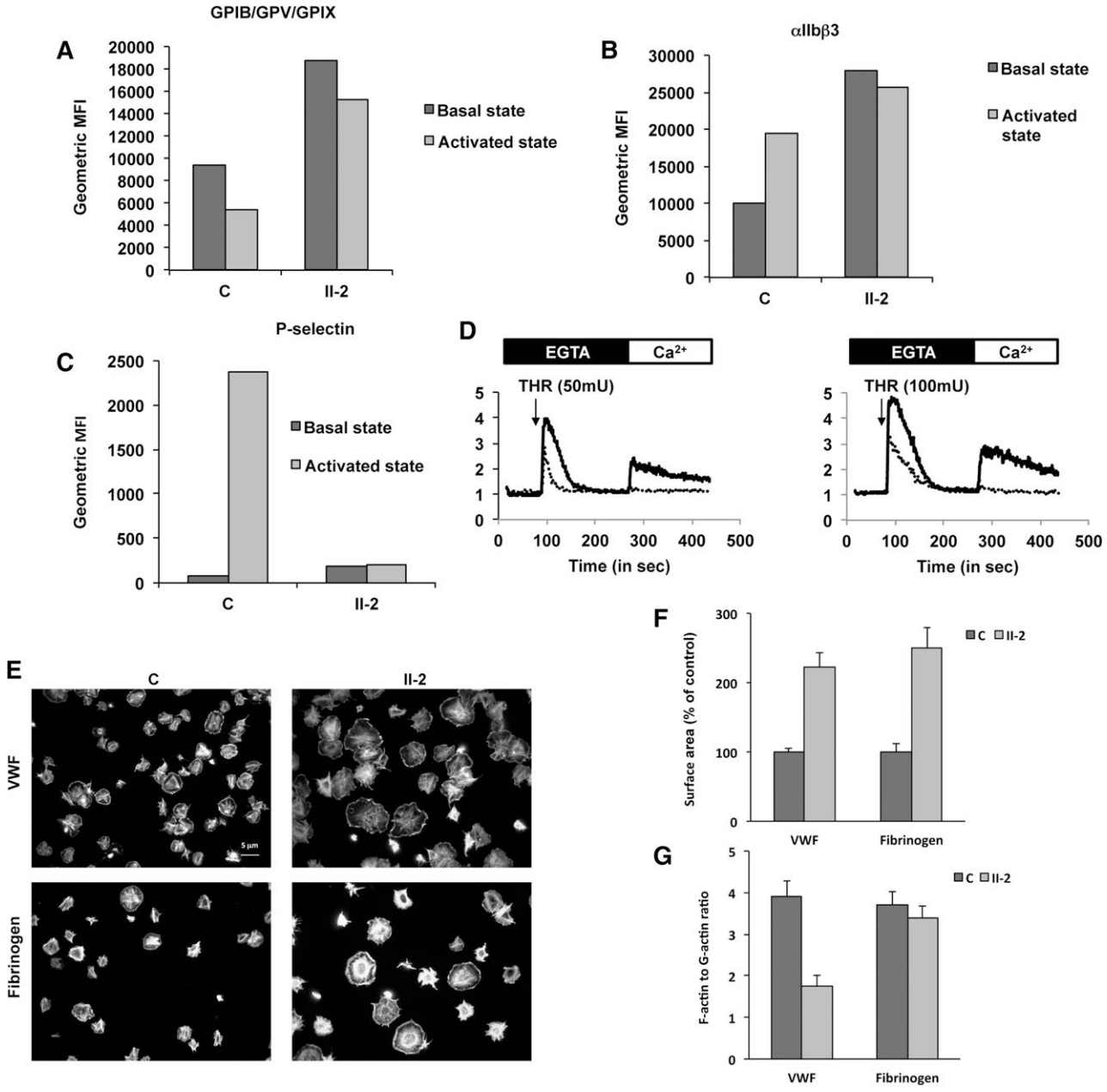

Figure 3. Platelet functions. (A-C) Fluorescence-activated cell sorter flow analysis of the (A) GPIb-IX-V complex (anti-CD42a), (B) αIIbβ3 complex (anti-CD41a), and (C) P-selectin (anti-CD62P) on control (C) and patient (II-2) platelets before (basal state) and after activation by thrombin receptor agonist peptide (activated state). Histograms present geometric mean fluorescence intensity (geometric MFI). (D) Typical traces representative of normalized (to basal level) fluorescence intensity of Oregon green 488 BAPTA1-AM (representative of the cytosolic Ca^{2+} concentration) recorded using Accury flow cytometer. Platelets from the control (black line) and from the patient (dotted line) were treated, in the absence of calcium (EGTA, 100 μM), with thrombin (THR, 50 or 100 mU/mL) and Ca^{2+} ($CaCl_2$, 300 μM). (E-G) Platelet spreading. (E) Platelets were adhered on fibrinogen or von Willebrand factor substrates and stained with both Alexa Fluor488-labeled phalloidin and Alexa Fluor594-labeled DNAse I. (F) Platelet surface area and (G) ratio of F-actin to G-actin were measured by ImageJ version 1.42k.

Genealogical studies (Figure 1) showed that her brother (II-2) also exhibited severe thrombocytopenia (8×10^9 platelets/L; Table 1) and life-long moderate bleeding, epistaxis, and cutaneous hematomas (World Health Organization bleeding score of 3). Her mother (I-1) had a normal platelet count. Data from her father (I-2) were not available because he died prior to this study. However, his son (II-4) from his second wife (I-3) did not display any platelet defects.

Platelet and MK morphology

May-Grünwald-Giemsa staining of peripheral blood smears of patients II-1 and II-2 (Figure 2A) showed 90% giant and macrocytic platelets. This was confirmed by electron microscopy. The diameter of platelets was 4.86 and 4.98 μm for II-1 and II-2, respectively, compared with 2.84 and 2.97 μm for control and I-1 platelets, respectively (Figure 2B-C). The morphology of the patient's bone marrow cells revealed the presence of MK clusters, which is absent in normal bone marrow (Figure 2D). An in vitro study of patient MKs derived from peripheral blood $CD34^+$ cells in the presence of TPO and SCF revealed no differences in percentage of mature $CD41^+CD42^+$ cells and in the ploidy level between patients II-1 and II-2 and a healthy donor (Figure 2E). Similar results were obtained for family members I-1 and III-1 (data not shown). Altogether, these results suggest no defect in MK differentiation and ploidization.

Patient platelets exhibit defective activation

Because the patients exhibit a bleeding score of 3 to 4, suggesting a profound defect in platelet function, we first analyzed the effects of stimulating platelets. Quantification of integrin αIIbβ3 and GPIb/IX/V by flow cytometry showed that their levels in the unstimulated patient platelets was 2.7- and 2-fold higher than in control platelets, respectively (Figure 3A-B), consistent with their large size. After stimulation with protease-activated receptor 4-activating peptide (25 μM), GPIb/XI/V underwent poor activation-dependent internalization (18% of the level of resting platelets) in patient platelets compared with control platelets (44.2% of the level of resting platelets; Figure 3A). Moreover, although surface expression of integrin αIIbβ3 in control platelets, as expected, was upregulated (193% compared with unstimulated control platelets), no change in αIIbβ3 surface expression was observed for patient platelets after stimulation (Figure 3B). Finally, no surface expression of P-selectin, a marker of α granule mobilization, on activation was observed in patient platelets (Figure 3C). Altogether, these results are consistent with patient platelets being unable to undergo activation.

Consistent with altered activation, Ca^{2+} mobilization from internal stores and Ca^{2+} influx elicited by added extracellular Ca^{2+} were much lower in patient platelets upon stimulation with thrombin (50 and 100 mU) than in control platelets (Figure 3D).

Finally, we analyzed platelet spreading with VWF (10 μg/mL) and fibrinogen (100 μg/mL) and quantified actin polymerization by measuring the F-actin/G-actin ratio. Immunofluorescence imaging showed that patient platelets were heterogeneous in morphology (Figure 3E). The majority of the platelets were giant, whereas some of them were of normal size and aspect. Moreover, patient platelets exhibited ruffles, which were absent from the control platelets. Quantification showed that the extent of patient platelet spreading was 2.2- and 2.5-fold that of control platelets with VWF and fibrinogen, respectively (Figure 3F). This larger size is the likely consequence of the larger diameter of the patient platelets vs control platelets. In contrast, a low F-actin/G-actin ratio of patient platelets was observed with VWF (44% of the control), whereas the ratios were comparable with fibrinogen (Figure 3G) between control and patient platelets.

Altogether, these results show an unexpected defect in activation and in cytoskeleton reorganization of patient platelets.

Homozygous *PRKACG* and *GNE* mutations are present in affected family members

The absence of genetic defects in GPIbα, GPIbβ, and GPIX (expressed as a GPIb-IX complex) excluded Bernard-Soulier syndrome (BSS), and the absence of neutrophil inclusions excluded an MYH9-related disease.[11] Therefore, to identify a genetic factor leading to this new form of macrothrombocytopenia, we performed whole-exome sequencing of family members I-1, II-1, II-2, II-3, and III-1. A total of 57 447 single nucleotide variations (SNVs) and 6781 insertion-deletions (indels) were detected in I-1; 58 351 SNVs and 6968 indels in II-1; 57 341 SNVs and 6832 indels in II-2; 58 129 SNVs and 7077 indels in II-3; and 57 863 SNVs and 7012 indels in III-1. After excluding variants present in public databases at a frequency of >1%, by keeping only nonsynonymous mutations and by imposing an autosomal recessive mode of transmission for the mutation (I-1 and III-1, heterozygous for the mutation; II-1 and II-2, homozygous for the mutation; II-3, homozygous wild type due to the consanguinity between I-1 and I-2 pedigrees and the fact that pedigrees II-4 and III-1 have a normal platelet count), only 2 variations remained. Both are localized on chromosome 9. The first one, c.1675G>A, is in the gene *GNE* and corresponds to the substitution of the amino acid glycine for arginine at position 559

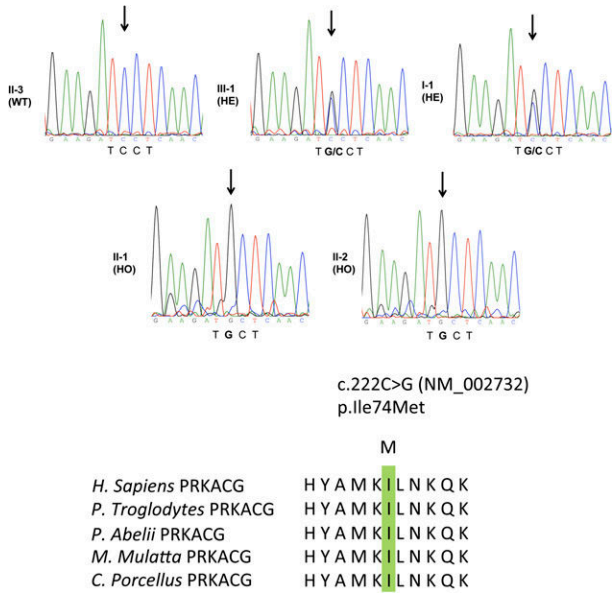

Figure 4. Germ-line *PRKACG* mutation. Electrophoregram of *PRKACG* gene (NM_00273), as sequenced by the Sanger method, revealed no mutation in individual II-3 designed as wild type (WT). Individuals III-1 and I-1 were found to be heterozygous (HE) for the c.222C>G mutation, without clinical features of macrothrombocytopenia. Patients II-1 and II-2 were found to be homozygous for the c.222C>G mutation and exhibited macrothrombocytopenia. The c.222C>G mutation caused substitution of the evolutionarily conserved Ile amino acid. Homologous sequences were aligned using the CLUSTALW Web site.

(p.559G>R-NM_005476). The second mutation, c.222C>G, was found in the *PRKACG* gene and substitutes isoleucine for methionine at position 74 (p.74I>M-NM_002732; Figure 4). None of the mutations were found in the SNPdb database, indicating they are not polymorphisms. Furthermore, when analyzed using PolyPhen2, both the GNE p.559G>R mutation and the PRKACG p.74I>M mutation were predicted to be damaging with high probability. Additionally, both residues are well conserved through evolution, further suggesting a strong impact for the mutations. *GNE* encodes a bifunctional enzyme that initiates and regulates the biosynthesis of *N*-acetylneuraminic acid, and *PRKACG* encodes the γ isoform of the catalytic subunit (Cγ) of cAMP-dependent PKA. Among PKA substrates, FLNa and GPIbβ are present in MKs and platelets and are potential candidates involved in thrombocytopenia. Indeed, genetic alterations of FLNa and GPIbβ were found to be associated with macrothrombocytopenia,[1,12] whereas *GNE* mutations result in myopathy or sialuria[13,14] without thrombocytopenia. Because neither myopathy nor sialuria was detected in the patients, we further focused on PRKACG.

PRKACG homozygous mutation leads to a functional defect of PKA

To ascertain the role or *PRKACG* mutation in the induction of this new autosomal recessive macrothrombocytopenia with giant platelets, we first investigated mutant protein function. First, we found that the *PRKACG* mutation did not lead to the degradation of PRKACG in MKs or platelets (supplemental Figure 1). Then, the phosphorylation status of GPIbβ at Ser^{166} in patient MKs was investigated using $CD34^+$ progenitors cultured in the presence of TPO and SCF and $CD41^+CD42^+$ MKs for 12 days. Quantification showed no difference in P-Ser^{166}-GPIbβ levels between homozygous patients and controls in mature MKs (Figure 5A). Moreover, phosphorylation of GPIbβ at Ser^{166} in homozygous patient platelets was comparable to control platelets (Figure 5B). These results suggest that

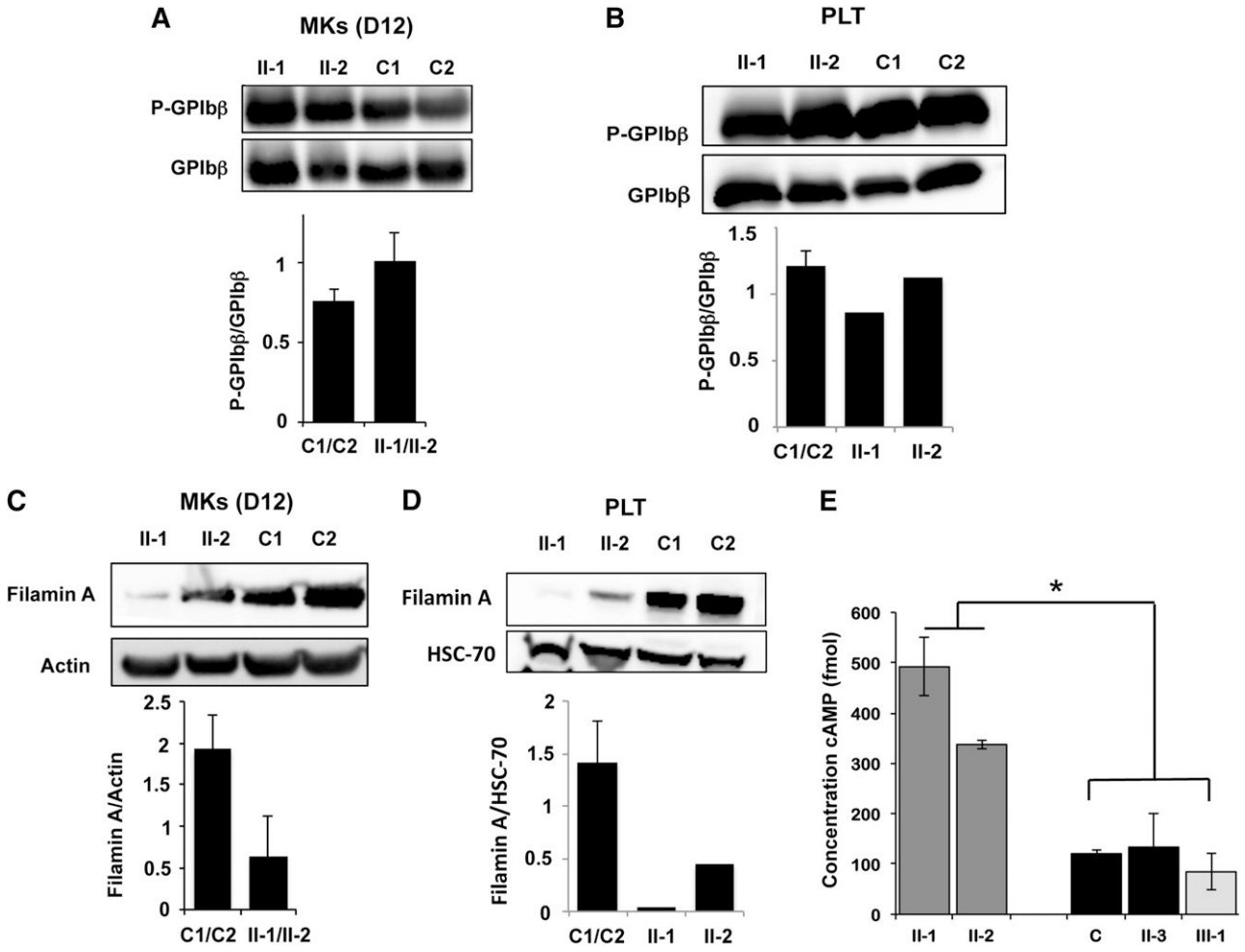

Figure 5. Analysis of PKA activity in patient platelets and megakaryocytes. (A-B) Western blot analysis and quantification of GPIbβ phosphorylated at Ser^{166} in MKs derived in vitro from (A) blood $CD34^+$ progenitors and (B) in platelets of patients homozygous (II-1 and II-2) for the PRKACG p.74I>M mutation. Two external controls (C1 and C2) were analyzed. Total GPIbβ was used as a control of protein loading. MKs were investigated at (A) day 12 of culture. (C-D) Western blot analysis and quantification of filamin A in (C) MKs and (D) platelets of patients carrying the homozygous (II-1 and II-2) mutation. Two external controls (C1 and C2) were used. Actin or HSC70 was used as a control of protein loading. (E) Analysis of cAMP level in platelets isolated from one external (C1) and one internal control (II-3) and from 2 patients homozygous (II-1 and II-2) and 1 heterozygous for the PRKACG p.74I>M mutation (III-1). Error bars represent mean ± SD of triplicate. Experiments were performed 2 times with similar results. *$P <$ .05, 2-tailed Mann-Whitney test.

PRKACG is not responsible for GPIbβ phosphorylation in mature MKs and platelets. Finally, because the phosphorylation of FLNa by PKA at Ser^{2152} has been suggested to protect FLNa from proteolysis,[15,16] we examined the level of total FLNa in MKs and platelets. FLNa was almost completely absent from mature MKs (harvested at day 12 of culture) (Figure 5C) and from platelets (Figure 5D) of homozygous patients compared with controls, strongly suggesting that PRKACG is required for FLNa phosphorylation.

The phosphorylation of many substrate proteins by PKA depends on cAMP. PKA regulates the concentration of cAMP as part of a feedback mechanism.[17] First, PKA can induce degradation of cAMP through activation of phosphodiesterases, which catalyze the conversion of cAMP into AMP. Second, PKA can inhibit cAMP synthesis by inhibiting adenylyl cyclase, which catalyzes the conversion of ATP into cAMP. Hence, we hypothesized that the p.74I>M PRKACG mutation alters PKA activity, thereby leading to a high intracellular level of cAMP. Therefore, we measured the cAMP levels in platelets from 1 external and 1 internal control (II-3), from 2 patients homozygous for the PRKACG p.74I>M mutation (II-1 and II-2), and from 1 individual heterozygous for the mutation (III-1). A three- to fivefold higher level of cAMP was detected for patients homozygous for the mutation compared with controls or with a heterozygous individual (Figure 5E).

In conclusion, low amounts of FLNa in both megakaryocytes and platelets and higher cAMP levels in platelets of homozygous patients are strikingly consistent with the PRKACG p.74I>M mutation inactivating PKA.

PPT formation is defective in patient MKs and is rescued by wild-type PRKACG overexpression

Finally, because the thrombocytopenia was not associated with defective MK differentiation or ploidization (Figure 2D-E), we investigated the ability of patient MKs to produce PPTs. A 2.5-fold lower percentage of PPT-bearing MKs ($CD41^+CD42^+$) was evidenced in patients homozygous for the mutation (II-1 and II-2) compared with controls or with patients heterozygous for the mutation (I-1 and III-1; Figure 6A). To confirm the implication of the homozygous PRKACG p.74I>M mutation in the PPT formation defect, we cloned the wild-type *PRKACG* cDNA into a lentiviral vector and transduced $CD34^+$ cells isolated from peripheral blood of homozygous patients II-1 and II-2. Overexpression of wild-type

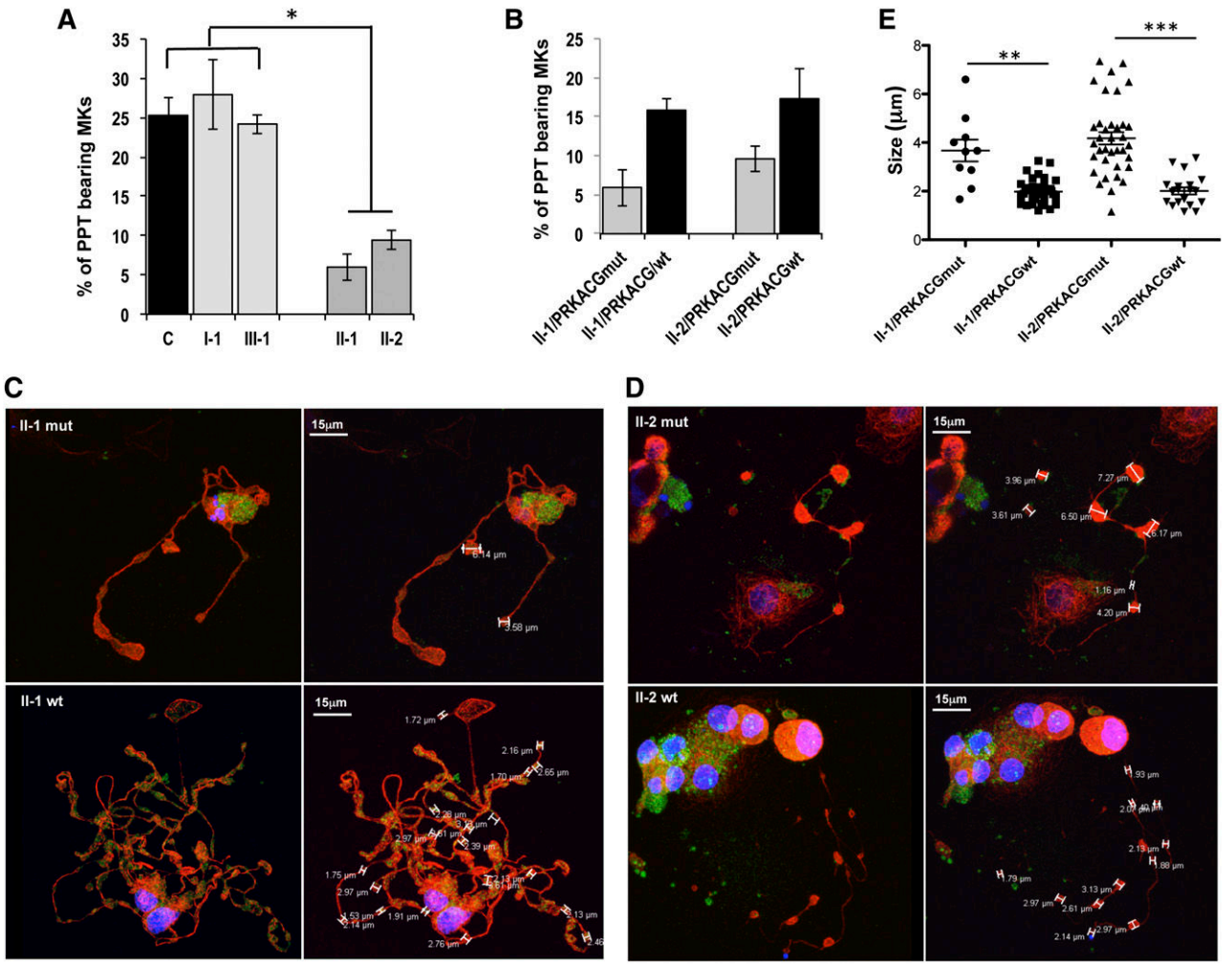

Figure 6. Mutant PRKACG leads to defective PPT formation, which is rescued by wild-type PRKACG overexpression. (A-E) In vitro MK differentiation was induced from control or patient peripheral blood $CD34^+$ progenitors in the presence of TPO and SCF. (B-E) $CD34^+$ cells of patients II-1 and II-2 were transduced with a lentiviral vector harboring wild-type (wt) or mutant PRKACG cDNA (used as a control of experiment) at days 1 and 2 of culture. (A-B) The percentage of PPT-forming MKs was estimated by counting MKs exhibiting ≥1 cytoplasmic processes with areas of constriction at day 13 of culture. A total of 200 cells per well were counted. The histograms show 1 of 2 independent experiments with similar results. Each experiment was performed in triplicate. Data represent mean ± SD of triplicate. $^*P < .05$, 2-tailed Mann-Whitney test. (C-D) Immunoconfocal analysis of platelet-like structures formed by PPTs generated from patients (C) II-1 and (D) II-2. MKs overexpressing wt or mutant PRKACG PPT-forming MKs were allowed to adhere on fibrinogen for 2 hours at day 13 of culture and stained with anti-tubulin (red) and rabbit anti-VWF (green) antibodies. Confocal imaging was performed on a Leica TCS SP8 inverted laser scanning confocal microscope (Leica Microsystems, Heidelberg, Germany), equipped with a 405-nm UV laser diode and visible optically pumped semiconductor lasers (488 and 552 nm). All images were acquired using an oil immersion 63× objective (1.4 numeric aperture). (E) At least 5 MKs for each condition were analyzed, and the size of platelet-like structures was measured by LAS AF version 2.4.1 software. Data are presented ± SEM. $^{**}P < .005$ and $^{***}P < .0001$, unpaired Student *t* test with Welch's correction.

PRKACG significantly increased PPT formation by MKs of both patients II-1 and II-2 (Figure 6B). The mutant PRKACG cDNA was used in parallel as a negative control. No rescue in PPT formation was observed in the MKs of patients II-1 and II-2, which already express endogenous mutant PRKACG. Moreover, after overexpression of wild-type PRKACG in patient MKs, the average diameter of platelet-like structures occurring along the PPTs decreased from 3.67 to 1.68 µm for patient II-1 and from 4.17 to 2.01 µm for patient II-2 (Figure 6C-E). This result strongly suggests that the defect in PKA is responsible for the thrombocytopenia.

Discussion

Here we report a new autosomal recessive macrothrombocytopenia characterized by a severe thrombocytopenia (5-8 × 10^9 PLT/L) and a severe thrombopathy with a bleeding score of 3 to 4. Exome sequencing revealed homozygous mutations in the coding exons of 2 genes: *GNE* and *PRKACG*. The corresponding GNE p.559G>R and PRKACG p.74I>M missense mutations were predicted by PolyPhen2 to be damaging with high probability, at positions with well-conserved residues, and not corresponding to polymorphisms. GNE is predominantly expressed in the liver and placenta. *GNE* mutations can result in 2 human disorders: myopathy with mutations in epimerase and/or kinase domains or sialuria linked to the mutations in the epimerase domain.[13,14] The GNE p.559G>R mutation located within the kinase domain was reported in 1 patient with myopathy in association with the V572L mutation on the other allele, which is the most frequent mutation associated with this disorder.[18] No thrombocytopenia was ever reported in patients with myopathy and, conversely, the patients described here have no signs of myopathy, suggesting that the GNE p.559G>R mutation induces no major functional defect. Thus, the PKA mutation appears more relevant to explain this thrombocytopenia. PKA is composed of

2 catalytic subunits and 2 regulatory subunits. After cAMP binding to the regulatory subunits, the catalytic subunits dissociate and phosphorylate their substrates. The 3 catalytic subunit isoforms, Cα, Cβ, and Cγ, are present in platelets, with a twofold lower level for Cγ compared with Cα and Cβ.[19] Among the major platelet PKA substrates, 2 groups were identified. The first group includes signaling regulators (Rap1B, Rap1GAP2, $G\alpha_{13}$, IP_3-R, TRPC6, and GPIbβ), whereas the second includes actin-binding proteins (VASP, LASP, HSP27, FLNa, and caldesmon).[20] We focused our attention on 2 PKA substrates: FLNa and GPIbβ. Indeed, genetic alterations of these substrates led to different forms of macrothrombocytopenia. Mutations in the *FLNA* gene localized on chromosome X result in a moderate thrombocytopenia with a mix of normal and giant platelets and with a defect in PPT formation.[12] We demonstrated here that the level of total FLNa in PKA patient platelets was drastically low. This could be a consequence of a decrease in FLNa phosphorylation at Ser^{2152} in platelets and MKs due to the defect in PKA activity. This nonprotection of FLNa from proteolysis could then lead to thrombocytopenia. Indeed, we previously showed in patients with mutated FLNa that low levels of remaining FLNa in platelets (30%) are correlated with abnormal fragmentation of the cytoplasm, leading to a defect in PPT formation.[12]

In platelets, GPIb-IX-V, the major receptor for VWF, is constitutively associated with FLNa. This FLNa-GPIbα interaction is required for adhesion of platelets onto VWF at high shear conditions, probably via dimerization and/or links with the actin networks,[21-24] and seems to regulate the mechanical stability of the platelet plasma membrane. In the patient homozygous for the PRKACG p.74Ile>Met mutation, a decrease in F-actin polymerization was observed after platelet spreading on the VWF matrix. This defect is the likely consequence of the absence of stabilization of actin networks by the remaining FLNa.

GPIb-IX-V is another PKA substrate, essential for platelet activation and formation. Indeed, mono-allelic mutations in *GP1BB* are at the origin of autosomal dominant macrothrombocytopenia in BSS characterized by the presence of large platelets.[1] In platelets, PKA mediates GPIbβ phosphorylation at Ser^{166}, which leads to the negative regulation of VWF binding to GPIb-IX-V.[9] Moreover, phosphorylation of GPIbβ inhibits actin polymerization during platelet activation through reorganization of the GPIb-IX–associated membrane skeleton.[25] In platelets from the patient homozygous for the PRKACG p.74Ile>Met mutation, GPIbβ phosphorylation was normal; thus, the defect in actin polymerization is not the result of altered GPIbβ but more likely of the degradation of FLNa.

Is the markedly altered activation of platelets, as evidenced by impaired Ca^{2+} mobilization, no αIIbβ3 and P-selectin externalization, and poor GPIb internalization, consistent with PKA inactivation? An attractive hypothesis is that increased intracellular cAMP, observed in patient platelets and a long-time recognized physiological negative regulator of platelet responses,[26-28] alters platelet functions. However, another hypothesis, not exclusive from the first one, is that the defect in FLNa alters actin cytoskeletal reorganization on platelet stimulation, inducing defective externalization or internalization of receptors or even Ca^{2+} translocation. Further experiments are required to test these hypotheses.

GPIb-IX-V central involvement in platelet formation has been demonstrated in 2 ways: antibodies directed against GPIb-IX-V have been shown to strongly inhibit PPT production, and MKs derived from patients with BSS (lacking normal expression of GPIb-IX-V) do not develop PPTs in vitro.[29-31] However, no defect in the phosphorylation of GPIbβ was observed at 12 days of culture, a stage where MKs start to generate PPTs and to release platelets. This suggests that another PKA catalytic subunit rather than PRKACG is involved in GPIbβ phosphorylation.

In conclusion, a new homozygous mutation in the *PRKACG* gene affecting PKA function results in a new form of severe macrothrombocytopenia designated here as *PRKACG*-related disease. This study further demonstrates the potential diagnostic value of exome sequencing in human thrombocytopenia, as well as providing unique evidence for a key role for PKA in normal platelet production and platelet functions.

Acknowledgments

The authors thank the patients and their families for participation in this study, Genethon (Evry, France) for the sinpRRL-PGK-GFP lentivirus vector, and the Laboratoire Français de Fractionnement et Biotechnologies (LFB, Courtaboeuf, France) for human purified von Willebrand factor.

This work was supported by French grants from the Agence Nationale de la Recherche (Jeunes Chercheurs) (to H.R.) and the Ligue Nationale Contre le Cancer (équipe labellisée 2013) (to H.R.). R.F., N.D., and W.V. are recipients of a research fellowship from Assistance Publique-Hôpitaux de Paris-Institut National de la Santé et de la Recherche Médicale (R.F.), Centre Hospitalier Universitaire Bordeaux (N.D.), and Institut Gustave Roussy-Institut National de la Santé et de la Recherche Médicale (W.V.).

Authorship

Contribution: V.T.M., M.H., E.B., S.S., G.P., and P.R. performed experiments and analyzed data; Z.E. and S.B. performed experiments; A.A. performed clinical and biological follow-up of patients; R.A., F.L., and W.V. discussed results and wrote the paper; J.-P.R. analyzed data, discussed results, and wrote the paper; R.B., M.B., and N.D. performed experiments, analyzed data, discussed results, and wrote the paper; R.F. performed clinical and biological follow-up of patients, performed experiments, and wrote the paper; and H.R. designed the work, performed and supervised experiments, and wrote the paper.

Conflict-of-interest disclosure: The authors declare no competing financial interests.

Correspondence: Hana Raslova, INSERM, UMR1009, Gustave Roussy, 114 rue Edouard Vaillant, 94805 Villejuif Cedex, France; e-mail: hraslova@igr.fr.

References

1. Balduini CL, Savoia A, Seri M. Inherited thrombocytopenias frequently diagnosed in adults. *J Thromb Haemost.* 2013;11(6):1006-1019.
2. Stevenson WS, Morel-Kopp MC, Chen Q, et al. GFI1B mutation causes a bleeding disorder with abnormal platelet function. *J Thromb Haemost.* 2013;11(11):2039-2047.
3. Albers CA, Cvejic A, Favier R, et al. Exome sequencing identifies NBEAL2 as the causative gene for gray platelet syndrome. *Nat Genet.* 2011;43(8):735-737.
4. Kunishima S, Okuno Y, Yoshida K, et al. ACTN1 mutations cause congenital macrothrombocytopenia. *Am J Hum Genet.* 2013;92(3):431-438.
5. Gnirke A, Melnikov A, Maguire J, et al. Solution hybrid selection with ultra-long oligonucleotides

for massively parallel targeted sequencing. *Nat Biotechnol.* 2009;27(2):182-189.

6. Debili N, Massé JM, Katz A, Guichard J, Breton-Gorius J, Vainchenker W. Effects of the recombinant hematopoietic growth factors interleukin-3, interleukin-6, stem cell factor, and leukemia inhibitory factor on the megakaryocytic differentiation of CD34+ cells. *Blood.* 1993;82(1): 84-95.
7. Lordier L, Bluteau D, Jalil A, et al. RUNX1-induced silencing of non-muscle myosin heavy chain IIB contributes to megakaryocyte polyploidization. *Nat Commun.* 2012;3:717.
8. Gilles L, Guièze R, Bluteau D, et al. P19INK4D links endomitotic arrest and megakaryocyte maturation and is regulated by AML-1. *Blood.* 2008;111(8):4081-4091.
9. Bodnar RJ, Xi X, Li Z, Berndt MC, Du X. Regulation of glycoprotein Ib-IX-von Willebrand factor interaction by cAMP-dependent protein kinase-mediated phosphorylation at Ser 166 of glycoprotein Ib(beta). *J Biol Chem.* 2002;277(49): 47080-47087.
10. Anderson DR. A method of preparing peripheral leucocytes for electron microscopy. *J Ultrastruct Res.* 1965;13(3):263-268.
11. Savoia A, De Rocco D, Panza E, et al. Heavy chain myosin 9-related disease (MYH9 -RD): neutrophil inclusions of myosin-9 as a pathognomonic sign of the disorder. *Thromb Haemost.* 2010;103(4):826-832.
12. Nurden P, Debili N, Coupry I, et al. Thrombocytopenia resulting from mutations in filamin A can be expressed as an isolated syndrome. *Blood.* 2011;118(22):5928-5937.
13. Argov Z, Mitrani-Rosenbaum S. The hereditary inclusion body myopathy enigma and its future therapy. *Neurotherapeutics.* 2008;5(4):633-637.
14. Bork K, Reutter W, Weidemann W, Horstkorte R. Enhanced sialylation of EPO by overexpression of UDP-GlcNAc 2-epimerase/ManAc kinase containing a sialuria mutation in CHO cells. *FEBS Lett.* 2007;581(22):4195-4198.
15. Jay D, García EJ, Lara JE, Medina MA, de la Luz Ibarra M. Determination of a cAMP-dependent protein kinase phosphorylation site in the C-terminal region of human endothelial actin-binding protein. *Arch Biochem Biophys.* 2000;377(1): 80-84.
16. Chen M, Stracher A. In situ phosphorylation of platelet actin-binding protein by cAMP-dependent protein kinase stabilizes it against proteolysis by calpain. *J Biol Chem.* 1989;264(24):14282-14289.
17. Brown KM, Lee LC, Findlay JE, Day JP, Baillie GS. Cyclic AMP-specific phosphodiesterase, PDE8A1, is activated by protein kinase A-mediated phosphorylation. *FEBS Lett.* 2012; 586(11):1631-1637.
18. Cho A, Hayashi YK, Monma K, et al. Mutation profile of the GNE gene in Japanese patients with distal myopathy with rimmed vacuoles (GNE myopathy). *J Neurol Neurosurg Psychiatry.* 2013.
19. Burkhart JM, Vaudel M, Gambaryan S, et al. The first comprehensive and quantitative analysis of human platelet protein composition allows the comparative analysis of structural and functional pathways. *Blood.* 2012;120(15):e73-e82.
20. Smolenski A. Novel roles of cAMP/cGMP-dependent signaling in platelets. *J Thromb Haemost.* 2012;10(2):167-176.
21. Nakamura F, Pudas R, Heikkinen O, et al. The structure of the GPIb-filamin A complex. *Blood.* 2006;107(5):1925-1932.
22. Cranmer SL, Pikovski I, Mangin P, et al. Identification of a unique filamin A binding region within the cytoplasmic domain of glycoprotein Ibalpha. *Biochem J.* 2005;387(Pt 3):849-858.
23. Williamson D, Pikovski I, Cranmer SL, et al. Interaction between platelet glycoprotein Ibalpha and filamin-1 is essential for glycoprotein Ib/IX receptor anchorage at high shear. *J Biol Chem.* 2002;277(3):2151-2159.
24. Cranmer SL, Ashworth KJ, Yao Y, et al. High shear-dependent loss of membrane integrity and defective platelet adhesion following disruption of the GPIbα-filamin interaction. *Blood.* 2011;117(9): 2718-2727.
25. Fox JE, Berndt MC. Cyclic AMP-dependent phosphorylation of glycoprotein Ib inhibits collagen-induced polymerization of actin in platelets. *J Biol Chem.* 1989;264(16):9520-9526.
26. Salzman EW. Cyclic AMP and platelet function. *N Engl J Med.* 1972;286(7):358-363.
27. Siess W. Molecular mechanisms of platelet activation. *Physiol Rev.* 1989;69(1):58-178.
28. Noé L, Peeters K, Izzi B, Van Geet C, Freson K. Regulators of platelet cAMP levels: clinical and therapeutic implications. *Curr Med Chem.* 2010; 17(26):2897-2905.
29. Takahashi R, Sekine N, Nakatake T. Influence of monoclonal antiplatelet glycoprotein antibodies on in vitro human megakaryocyte colony formation and proplatelet formation. *Blood.* 1999;93(6): 1951-1958.
30. Balduini A, Malara A, Balduini CL, Noris P. Megakaryocytes derived from patients with the classical form of Bernard-Soulier syndrome show no ability to extend proplatelets in vitro. *Platelets.* 2011;22(4):308-311.
31. Machlus KR, Italiano JE Jr. The incredible journey: From megakaryocyte development to platelet formation. *J Cell Biol.* 2013;201(6): 785-796.

2014 124: 2554-2563
doi:10.1182/blood-2014-01-551820 originally published online July 24, 2014

A new form of macrothrombocytopenia induced by a germ-line mutation in the *PRKACG* gene

Vladimir T. Manchev, Morgane Hilpert, Eliane Berrou, Ziane Elaib, Achille Aouba, Siham Boukour, Sylvie Souquere, Gerard Pierron, Philippe Rameau, Robert Andrews, François Lanza, Regis Bobe, William Vainchenker, Jean-Philippe Rosa, Marijke Bryckaert, Najet Debili, Remi Favier and Hana Raslova

Blood (print ISSN 0006-4971, online ISSN 1528-0020), is published weekly by the American Society of Hematology, 2021 L St, NW, Suite 900, Washington DC 20036.

Chapter 14
The Calcium Entry-Calcium Refilling Coupling

Ziane Elaib, Francois Saller, and Regis Bobe

Abstract Calcium ions (Ca^{2+}) are versatile messengers that need to be tidily regulated in time and space in order to create a large number of signals. The coupling between Ca^{2+} entry and Ca^{2+} refilling is playing a central role in this Ca^{2+} homeostasis. Since the capacitative Ca^{2+} entry has been described, different mechanisms have been proposed in order to explain how the Ca^{2+} entry could be under control of intracellular store Ca^{2+} depletion. Today, in addition of STIM1 and Orai1, the two major elements of SOCe, increasing attention is put on the role of the transient receptor potential canonical (TRPC), that can form protein clusters with Orai1, and Sarco/endoplasmic reticulum Ca^{2+}ATPases (SERCAs), that refill the stores and are also located in the same environment than SOC clusters. Altogether, these proteins elaborate either Ca^{2+} microdomains in the vicinity of the membrane or larger Ca^{2+} increases overtaking the whole cell. The coupling between Ca^{2+} entry and Ca^{2+} refilling can possibly act much further away from the plasma membrane. Ca^{2+}, uptaken by SERCAs, have been described to move faster and further in the ER than in the cytosol and to create specific signal that depends on Ca^{2+} entry but at longer distance from it. The complexity of such created Ca^{2+} currents resides in the heteromeric nature of channels as well as the presence of different intracellular stores controlled by SERCA2b and SERCA3, respectively. A role for mitochondria has also been explored. To date, mitochondria are other crucial compartments that play an important role in Ca^{2+} homeostasis. Although mitochondria mostly interact with intracellular stores, coupling of Ca^{2+} entry and mitochondria cannot be completely rule out.

Keywords SERCA • STIM1 • Orai1 • TRPC channels

Z. Elaib • F. Saller • R. Bobe (✉)
Inserm U1176, Le Kremlin Bicetre, France

UMR_S 1176, Univ Paris Sud, Le Kremlin Bicetre, France
e-mail: regis.bobe@inserm.fr

J.A. Rosado (ed.), *Calcium Entry Pathways in Non-excitable Cells*, Advances in Experimental Medicine and Biology 898, DOI 10.1007/978-3-319-26974-0_14

14.1 Introduction

Calcium ions (Ca^{2+}) are universal second messengers that create a ubiquitous signal transduction pathway that is functional in every cellular type and species. Ca^{2+} signal regulates various processes including cell proliferation, response to the environment, death and apoptosis…

In a review published in 2006, R.J.P. Williams presented a paradigm in which the role of calcium as second messenger could be the result of evolution to adapt cells to life in an oxidized environment [1]. When cyanobacteria changed the face of the world and killed nearly all living species (mostly prokaryotic cells), surviving cells evolved to internally compartmentalized eukaryotic cells. These cells needed protection, ability to recognize their environment as well as to coordinate the internal activity of their new compartments; a new messenger was needed. As life had a long experience in dealing with calcium ions, widely common molecules that were rejected out cells for billions of years because of their ability to form insoluble salts (precipitates) with inorganic and organic anions carbon and phosphate, calcium ions became the messengers that not only coordinated the action of intracellular compartments but also triggered cell responses to the environment.

As Ca^{2+} signaling is very versatile, the question is to figure out how a single cation can code for a multitude of cellular responses, (i.e.) how distinct signals can be generated and how cell compartments can decipher specific messages.

The Ca^{2+} signal has, in order to be efficient and specific, to be tightly modulated in time and space. Multiple partners exist, forming cell specific calcium toolkits that are organized to control calcium flux and to translate Ca^{2+} signals into cellular activity. At rest, cytosolic Ca^{2+} is maintained around 50–200 nM. Upon activation its concentration will increase to create a global Ca^{2+} signal that can propagate over large distances (10–100 μm) in the range of μM and/or formation of microdomains with very high level of Ca^{2+} concentration (50–100 μM) in the vicinity of the Ca^{2+} channels. These latter events only spread over 20 nm and, Ca^{2+} concentration drops rapidly as ions are buffered and diluted in the cytosol [2, 3].

The increase in cytosolic calcium is due to its influx from the extracellular medium through the plasma membrane (PM) (extracellular Ca^{2+} concentration ranges between 1 and 2 mM in aqueous conditions) and its depletion from intracellular stores, mainly (but not only) the endoplasmic reticulum (ER). The storage capacity of the ER is limited and Ca^{2+} reuptake is performed by Ca^{2+} pumps termed Sarco/Endoplasmic Reticulum Ca^{2+}ATPases (SERCA) that control the Ca^{2+} concentration in the ER lumen. As SERCAs compete with other calcium transporters, such as Na/Ca exchangers or plasma membrane Ca^{2+}ATPases (PMCA) that extrude Ca^{2+} to the extracellular medium, a continuously loss of intracellular calcium storage would be observed if a subsequent calcium entry from extracellular medium was not organized to help cells to refill their intracellular stores in calcium. This Ca^{2+} entry is controlled by the ER lumen concentration and termed SOCe (Store operated calcium entry). If the SOC process was initially designed to maintain the concentration of stored Ca^{2+}, it now appears as a crucial actor that shapes the calcium signal within the cells.

14.2 Store Operated Calcium Entry (SOCe)

The classical way of non-excitable cell stimulation associates G protein coupled receptor and phospholipase activation. The newly formed inositol 1,4,5-trisphosphate (IP_3) will open its receptor channel (IP_3R) inserted in the endoplasmic reticulum (ER) membrane and will allow the mobilization of Ca^{2+} [4–6]. SOCe is a ubiquitous pathway in non-excitable cells as well as in some excitable cell types [7]. This event is associated to Ca^{2+} influx across the plasma membrane (PM). This paradigm of the existence of a store-dependent Ca^{2+} influx was proposed 30 years ago by J. W. Putney as Capacitive Calcium Entry (CCE) [8]. The use of Thapsigargin (Tg), a selective noncompetitive inhibitor of the SERCAs that is isolated from the plant *Thapsia garganica* and triggers a "passive" depletion of the ER stored Ca^{2+} without receptor activation, have permitted to establish that the store depletion by itself was responsible for a Ca^{2+} influx similar to those recorded as SOCe and, more important, independently of IP_3 [9, 10].

While the idea of having a Ca^{2+} entry from the extracellular medium under the control of intracellular organelles catches on, it was very difficult to have a clear insight into the underlying mechanisms until recently. Since, a number of studies have focused on the current specificities of this SOCe [11–14].

The first question was to understand how Ca^{2+} mobilization was able to activate the Ca^{2+} entry. At least three major hypothetic mechanisms have been advanced.

First, the existence of a soluble mediator from intracellular stores was proposed and termed "calcium influx factor" (CIF) [15]. This messenger was described to be released into the cytoplasm upon Ca^{2+} mobilization in Jurkat cells and is still unknown. Probably due to the lack of its molecular identity, very few studies are since focusing on CIF. Additionally, as CIF is "purified" or isolated after a long process, it is difficult to ascertain its specificity [16]. However, a recent publication showed that only CIF produced by agonists or Thapsigargin activation is able to induce a 2-APB (SOCe inhibitor) sensitive Ca^{2+} influx when injected in non-activated cells. Similar treatments, with components isolated in the same way than CIF but from non-activated cells, have no effect. Such data suggest in contrast, that the existence of a putative CIF is not ruled out [17].

The second proposed hypothesis was a conformational coupling between IP_3 receptor (IP_3R) and SOC channels in an ER-PM junction [18]. In this model, upon activation, IP_3R is able to activate Ca^{2+} channels and even to create a long channel that could transport Ca^{2+} directly from the extracellular medium into the ER lumen. While the idea of having the IP_3R working in a reverse mode was not established, it was later proposed that signaling clusters containing Transient receptor potential canonical channel type 1 (TRPC1) (see below for the roles of TRPC in SOCe) and IP_3R exist [19], both being able to bind directly through a CIRB domain positioned in the C-Terminal part of TRPC1 [20]. TRPC1 was described to associate with IP_3R in platelets upon store depletion, and to participate to extracellular Ca^{2+} influx into the cell [21, 22].

The last and most successful model was the existence of a direct interaction between ER resident proteins and Ca^{2+} channels.

14.2.1 Molecular Identity and Mechanism of Store Operated Channel

It took nearly 20 years to validate the whole concept of the SOC channel formation and the two key proteins involved in SOCe were almost concomitantly identified. First, the role of the Ca^{2+} sensor protein STIM1 (stromal interacting molecule 1) was highlighted in 2005 using a RNA interference-based screening in Drosophila and HeLa cells that showed that its knockdown strongly reduced SOCe [23, 24]. The second player, Orai1, was identified a year later also in Drosophila and human cells. Both RNAi screens in *Drosophila* and gene mapping on lymphocytes from a family with a severe combined immunodeficiency (SCID) revealed that Orai1 deficiency was associated to a defect in SOCe [25–27].

14.2.1.1 STIM1

STIM1 is a ubiquitously expressed protein which is widely expressed from Drosophila to mammalian cells. STIM1 is a single transmembrane protein of 77 kDa inserted predominantly in the ER [28] and distributed evenly along its membrane [29]. This protein is the crucial link between ER and Ca^{2+} channel in the PM. The luminal part of the protein contains two EF-hand (canonical and hidden EF-hand domains (cEF) and (hEF), respectively) domains and an adjacent sterile α motif (SAM) (Fig. 14.1a). Only the cEF domain can bind Ca^{2+} and confers to STIM1 its sensor function [23, 30, 31].

When Ca^{2+} stores are at rest, the estimated luminal Ca^{2+} concentration is about 500 μM [32]. At this level, Ca^{2+} binding to cEF allows the formation of a stable complex between EF and SAM domains. Upon ER depletion, Ca^{2+} dissociates from the STIM1 EF-hand domain, thus destabilizing the EF-hand-SAM complex (Fig. 14.1c). Both EF-hand and SAM domain will then expose their hydrophobic regions leading to the oligomerization of STIM1 [31, 33, 34]. It seems that the clustering of

Fig. 14.1 (continued) are composed of four transmembrane domains (TM1 (*blue*), TM2 (*purple*), TM3 *dark red*) and TM4 (*green*)). Two regions (CAD binding domains) are exposed into the cytosol and localized at both extremities of the proteins. On the right part of the figure using the same color code for the transmembrane domains of Orai is a top down schematic view of the hexameric Orai structure inserted into the plasma membrane with a Ca^{2+} (*red dot*) in the channel. (**c**) STIM1/Orai1 activation model. (*a*) Under resting conditions, the STIM1 Ca^{2+} binding to EF-hand domain masks SAM domains and keeps cytosolic domains folded and inactive. (*b*) Depletion of Ca^{2+} within the ER induces structural reorganization that uncovers SAM domains allowing oligomerization of STIM1. This also extends binding/activating domains towards the plasma membrane and (*c*) leads to clustering of Orai through interaction between SOAR and CAD domains

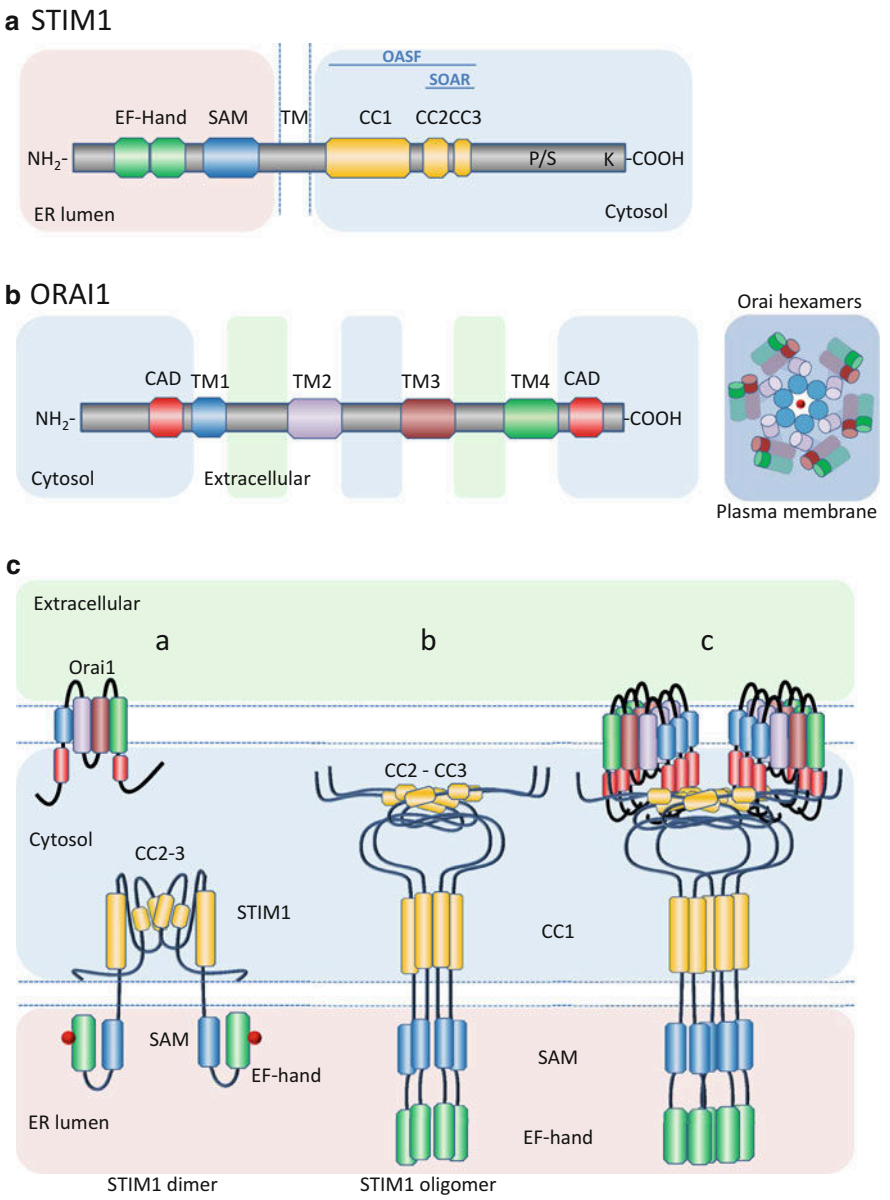

Fig. 14.1 Functional domains of STIM1 and Orai1 and model of coupling between STIM1 and Orai1. (**a**) Schematic representation of the main functional domains of STIM1. The N-terminal part of STIM1 (amino acids 1–214) is in the ER lumen and includes both EF-Hand domains (canonical and hidden EF-hand) and a sterile α motif (*SAM*) followed by transmembrane domain. In the cytosolic part of the protein are the coiled coil domains (CC1, CC2 and CC3) that form the region involved in the binding and activation of Orai (STIM-Orai activation region (SOAR, amino acids 345–444) or Orai activating small fragment (OASF, amino acids 233–450) and. The C-terminal part of STIM1 includes a serine/proline rich domain (P/S) and a lysine-rich domain (K). (**b**) Schematic representation of the main functional domains of Orai1. Orai monomers

EF-hand and SAM is critical, as similar oligomerization resulting in SOC activation was obtained by replacing EF-hand domain with FKBP-rapamycin binding domain under rapamicyn analogue stimulation [35].

To activate the Ca^{2+} channel, STIM1 clusters have to translocate to the plasma membrane to form punctate structures <25 nm from the plasma membrane (which corresponds to ER-PM junctions) [36]. It has been suggested that STIM1 could be preferentially localized within specific regions into the ER membrane, the so called "precortical subdomains" that will form cortical ER upon Ca^{2+} depletion [37]. A role for microtubule and F-actin polymerization seems to be involved, depending on the ER stores involved in the SOC (see below).

Of note, STIM2 shares similar structure with STIM1 and although its Ca^{2+} dissociation constant (Kd) is higher that of STIM1 (400 μM vs 200 μM respectively) [38], which could make STIM2 a better sensor for Ca^{2+} depletion [38], the unfolding of EF-hand – SAM domains for STIM2 appears to be much slower resulting in a lower SOC activation than STIM1 [39].

14.2.1.2 ORAI1

In mammalian cells, three genes code for three homologs: Orai1, Orai2 and Orai3. Orai monomers include four transmembrane domains (TM1–TM4) with a particular role of TM1 in the pore formation of the channel [40], the N- and C-terminal tails being cytoplasmic. Recent biochemical and fluorescence studies suggest that the SOC channel is composed of 6, and not 4 [41, 42] monomers that can form homo or heteromers of Orai (although Orai1 seems to be critical for the channel activity [43, 44]). The hexamer is organized in a concentric form with the most aqueous transmembrane α helice (TM1) in the central part of the pore (Fig. 14.1b) [42, 45, 46]. Orai proteins are inserted homogenously in the PM in resting cells but rapidly associate in clusters inside raft domains of the PM upon Ca^{2+} depletion and co-localize above the STIM1 clusters [47, 48]. The clustering by itself is not sufficient to open the channel and the direct interaction between STIM1 and Orai1 also leads to its activation.

14.2.2 Coupling Between STIM1 and Orai1

The coupling between STIM1 and Orai1 involves several domains of these proteins, all localized in the cytosol. Various regions named CAD, SOAR, OASF or Ccb9, all similarly located in the cytosolic part of STIM, have been identified in 2009 as being critical for the Orai activation (Fig. 14.1a) [48–51]. All of them cover the CC2 (aa 363–389) and CC3 (aa 399–423) regions of STIM1 that form a hairpin motif.

Two regions termed "CRAC activation domain" (CAD) have been proposed to bind STIM1 based on mutations in Orai and in silico studies; one is N-terminal (aa 73–85) and one is C-Terminal (aa 272–292) [52–54]. Whether this two CAD form

distinct binding regions or can form a unique binding site for STIM1 is still unknown and has to be determined. Interestingly, these regions seem to share structural homology with the STIM1 CC2 and CC3 domains, suggesting the possible formation of complex structure between the domains of both proteins [54].

The proposed mechanism suggests that, at rest, activation sites of STIM1 are masked by interaction with other flanking domains (possibly CC1 domain) of STIM1, thus preventing any interaction with Orai1. Upon Ca^{2+} depletion, lack of Ca^{2+} binding to EF-hand leads to homo association of CC1 (similarly to the SAM domains). This structural reorganization unmasks the CC2–CC3 domains and allows a physical extension of these domains in the cytoplasm [55] letting them to become available for Orai1 binding [52]. When binding to STIM1, Orai proteins will also change their structural conformation and either open their gates to Ca^{2+} or become highly specific for Ca^{2+} [56, 57] (Fig. 14.1c). Indeed, Orai channels display a selectivity for Ca^{2+} that is 1000 times higher than that for Na^{+} [58] when they are activated by STIM1. However, the mutant V102C/A, which appears to be constitutively activated, displays a poorly selective activity in absence of STIM1 and can regain its selectivity when co-expressed with STIM1 [59].

This first part of the chapter explained the relationship between ER and SOCe activation via STIM1 and ORAI1. Although STIM1 and Orai1 are crucial in coupling between ER and SOCe activation, other players participate in SOCe. First, a number of regulators of SOCe interact with either STIM1 or Orai1 (for review see [60, 61]). In addition other proteins can also form Ca^{2+} channels. A special attention was given to TRPC, that role as SOCe was strongly considered, until Orai1 was identified, a matter of debate.

14.2.3 TRPC

Transient receptor potential canonical (TRPC) are members of the superfamily of Transient receptor potential proteins. Since the discovery of its role as Ca^{2+} channel downstream of PLCγ2 activation, the TRPC proteins were proposed to be part of the SOC channel complex [62]. Probably because TRPC family is large and presents members with distinct functional capacities, whether TRPC function as SOCe has been highly debated [63, 64]. Among the TRPC family (TRPC1-7), TRPC1 is the most often associated to SOCe and was described to act as a STIM1-dependent Ca^{2+} channel in many studies [65–69]. Its expression in cell lines potentiates SOCe induced either by PLC activation or pharmacological (Tg) Ca^{2+} depletion [70].

It is however possible that TRPC form a macro-complex with Orai1 which therefore would explain their impact on SOCe without forming the channel by itself. Accordingly, direct association of Orai1 with TRPC3 and TRPC6 has been observed in HEK293 and COS1 cells [71, 72].

Most likely, as it has been described in blood platelets for TRPC1, TRPC play multiple role in the Ca^{2+} entry and their participation implies a higher level of complexity in the regulation of the Ca^{2+} entry controlled by store depletion [73].

Activation of TRPC1 downstream of Ca^{2+} depletion and their direct association with STIM1 has very recently been confirmed with a new single ion channel detection technique which further ascertains their possible role as SOCe [74].

Additionally to their action as SOCe, some members of the family, TRPC3, 4 6 and 7 have been described to be activated via diacylglycerol (DAG) upon PLC activation by G-protein coupled receptor stimulation. These activations are parallel to the Ca^{2+} mobilization but independent of Ca^{2+} depletion [67, 75, 76] and behave as ROC. Moreover, some authors suggest a direct link between IP_3R and TRPC, which lets suppose another way of store dependent Ca^{2+} entry regulation [19, 65, 77].

Thus, these three distinct pathways all activate TRPC channels, two being dependent on Ca^{2+} store depletion and one being parallel to the activation pathway of the Ca^{2+} depletion, might co-exist in the same cells (Fig. 14.2). Therefore, some TRPC members appear to be more inclined to participate to the SOC, like TRPC1, while some others seem to be more sensitive to DAG or IP_3R depending on their level of expression, their stoichiometry with STIM1 expression and the cellular models.

Finally, the whole system complexity increases again as TRPC can form heterodimer, thus sharing the properties of the different subunits that constitute the channels.

The paradigm of the crosstalk between Ca^{2+} entry and Ca^{2+} refilling is based on the observation that the fundamental reason for store-operated Ca^{2+} entry is that cells loose Ca^{2+} during signaling, Ca^{2+} mobilized from the ER to the cytoplasm is later transported outside the cell by plasma membrane Ca^{2+}ATPases (PMCA) or by the Na^{+}/Ca^{2+} exchanger (NCX). To ensure sustained signaling, the Ca^{2+} ions that have been extruded must return back to the store. Direct measurements of Ca^{2+} concentrations inside different organelles using nucleus, mitochondria or ER targeted aequorins have established that the impact of Ca^{2+} influx (by increasing extracellular Ca^{2+}) on Ca^{2+} uptake was 30 times larger in the ER than in other organelles [78]. Therefore, the third (or fourth taking into account TRPC) player in the coupling between Ca^{2+} entry – Ca^{2+} refilling has to be the Ca^{2+} pumps inserted in the ER membrane, the sarco/endoplasmic reticulum Ca^{2+}ATPase (SERCA).

14.3 SERCA

The SERCA family is composed of three genes giving rise to multiple isoforms though alternative splicing. SERCA2b isoform is ubiquitously expressed and plays a housekeeping function in the Ca^{2+} homeostasis. SERCA3 isoforms were firstly observed in non-muscular cells but some SERCA3 isoforms have now been described in smooth muscle as well [79–81].

The function of SERCA is to transport cytosolic Ca^{2+} into the ER, an action that will affect SOCe in two different ways depending on the point of view. From the ER point view, SERCA increase luminal ER Ca^{2+} concentration and allow STIM1 to return back to its inactivate status [82]. At the same time, Ca^{2+} uptake from the

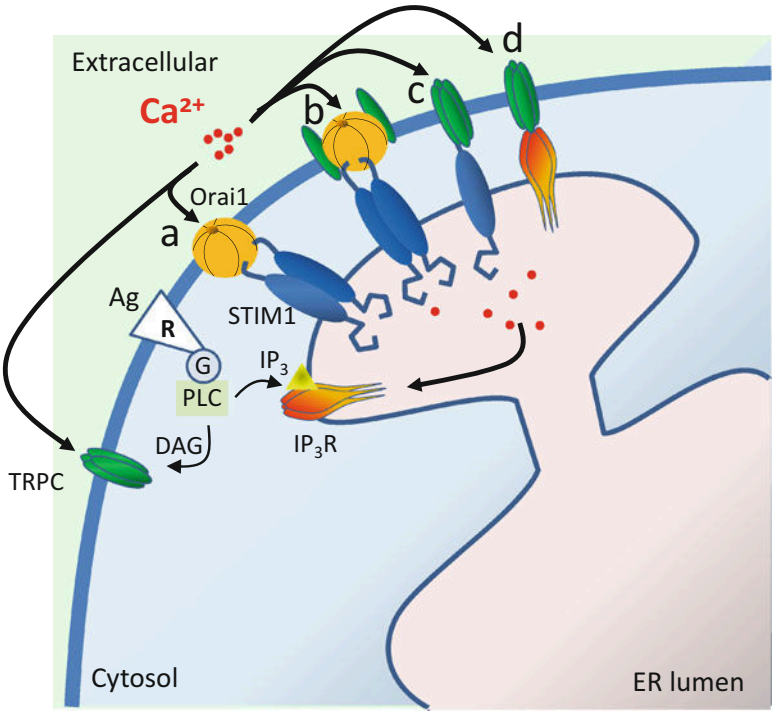

Fig. 14.2 Possible mechanism of store operated Ca^{2+} influx involving Orai1 and TRPc. Upon agonist stimulation of its receptor, PLC activation generates IP_3 and DAG. The latter is able to directly activate Ca^{2+} influx via TRPC channels. Produced IP_3 results in the depletion of Ca^{2+} from the ER via IP3R. (*a*) STIM1, the Ca^{2+} sensor inserted in the ER membrane oligomerizes and translocated to the ER-MP junction where it binds to and activates Orai1. (*b*) TRPC have been proposed to associate with Orai1 in a multiprotein complex or (*c*) to act as SOC channel when directly activated by STIM1. (*d*) Finally it has also been suggested that TRPC could be directly activated by IP_3R to directly refill the ER store. Abbr. 1,2-diacylglycerol (*DAG*); inositol trisphosphate (*IP_3*); inositol trisphophaste receptor (*IP_3R*); G protein-couple receptors (*R*); Ca^{2+} release-activate Ca^{2+} channel protein 1 (*Orai1*); phophoslipase (*PLC*); stromal interaction molecule 1 (*STIM1*); transient receptor potential cation channel (*TRPC*)

cytosol will avoid formation of high Ca^{2+} concentration microdomains at the mouth of channel and therefore will prevent channel inactivation [83, 84]. The combination of both actions explains why SERCA are so important in the shaping of Ca^{2+} signals. When over-expressed in cells, SERCA proteins are very efficient in reducing the need for Ca^{2+} entry. In agreement with this paradigm, it has been observed in smooth muscle cells that increased in SERCA2a expression leads in higher Ca^{2+} uptake and decrease in Ca^{2+} entry, showing a direct link between cell Ca^{2+} uptake capacity and SOCe activation [85].

Interestingly, recent reports show evidence that SERCA2 or SERCA3 associated with STIM1 upon Ca^{2+} depletion. This was inferred by confocal colocalization and co-immunoprecipitation [63, 86–88], although no FRET could have been obtained when SERCA-GFP and STIM1-CFP were co-expressed in HEK293T [89].

Additionally, while reduction in STIM1 expression using siRNA does not regulate SERCA activity in permeabilized cells, it decreased both SOCe and Ca^{2+} transport into ER in intact cells, which suggests that STIM1-SERCA association is more a spatial organization than a functional cluster [78, 90]. The current paradigm is that SERCA proteins form a crown around STIM1 when STIM1 is activated and associated with ORAI1 (Fig. 14.3b). Therefore, the Ca^{2+} pumps are localized just under the Ca^{2+} entry in order to refile the Ca^{2+} store from the high Ca^{2+} concentration microdomains formed at the mouth of the SOC.

In addition, Lemonnier et al. also demonstrated an association between SERCA and TRPC7, which appears to preserve the non capacitative Ca^{2+} influx (which is dependent on DAG) of the channel and suggests that the inhibition of TRPC7 by high cytosolic Ca^{2+} concentrations is suppressed by Ca^{2+} uptake into the stores similarly to what is described for SOC. Of note, the fact that the interaction between SERCA and TRPC7 is not disrupted in the presence of high concentrations of BAPTA indicates a more intimate relation between both proteins [83].

The fact that both SERCA2 and SERCA3 proteins have been involved in the regulation of SOCe and associated with STIM1, adds a new level of complexity in the organization of the crosstalk between Ca^{2+} influx and Ca^{2+} refilling. Since 1997, it has been proposed that both Ca^{2+} pump types could be part of distinct stores [91]. Based on electronical imaging and using inhibitors that could preferentially inhibit SERCA2 (Tg) or SERCA3 (tBHQ) associated to F-actin polymerization disruption by Cytochalisin-D or Latrunculin-A, the presence of at least two distinct SOCe has been observed in platelets (Fig. 14.4) [92, 93].

Acidic granules have been associated to SERCA3 [87, 94]. These granules are thought to be localized near the plasma membrane even in basal conditions. Therefore, formation of the ER-MP junction, necessary for activation of SOCe, does not need cytoskeleton reorganization. This was enlightened by the absence of effect (although some potentialization was actually observed) of F-actin polymerization inhibitors, on the SOCe induced by Ca^{2+} depletion using tBHQ that specifically inhibits SERCA3 [93]. These acidic granules have also been proposed to be sensitive to nicotinic acid adenine dinucleotide phosphate (NAADP), whose associated channel seems to be the two pores channels (TPC) [95, 96]. These granules are supposed to play a role of trigger of Ca^{2+} signaling starting before intracellular Ca^{2+} events that are sensitive IP_3R [97].

It is possible to imagine that these granules also act as SOCe trigger. Their submembrane localization can lead to a rapid association between STIM1 and Orai1 and the fast SERCA3 Ca^{2+} pumps can also participate preventing to reach high Ca^{2+} concentration in microdomains that could block the channel (Fig. 14.4a).

In contrast, SERCA2b-associated stores are strongly dependent on the actin polymerization and the similar experiments (pretreatments of cells with F-actin polymerization inhibitors) result in a decreased SOCe in response to Ca^{2+} depletion by Tg which preferentially inhibits SERCA2b [93]. This suggests a deeper insertion in the cytosol that could be associated to a slower process of activation in which STIM1 proteins has to relocalize to the ER-PM junctions, as observed in RBL cells (a tumor mast cell line) wherein STIM1 oligomers diffusion rate was evaluated to

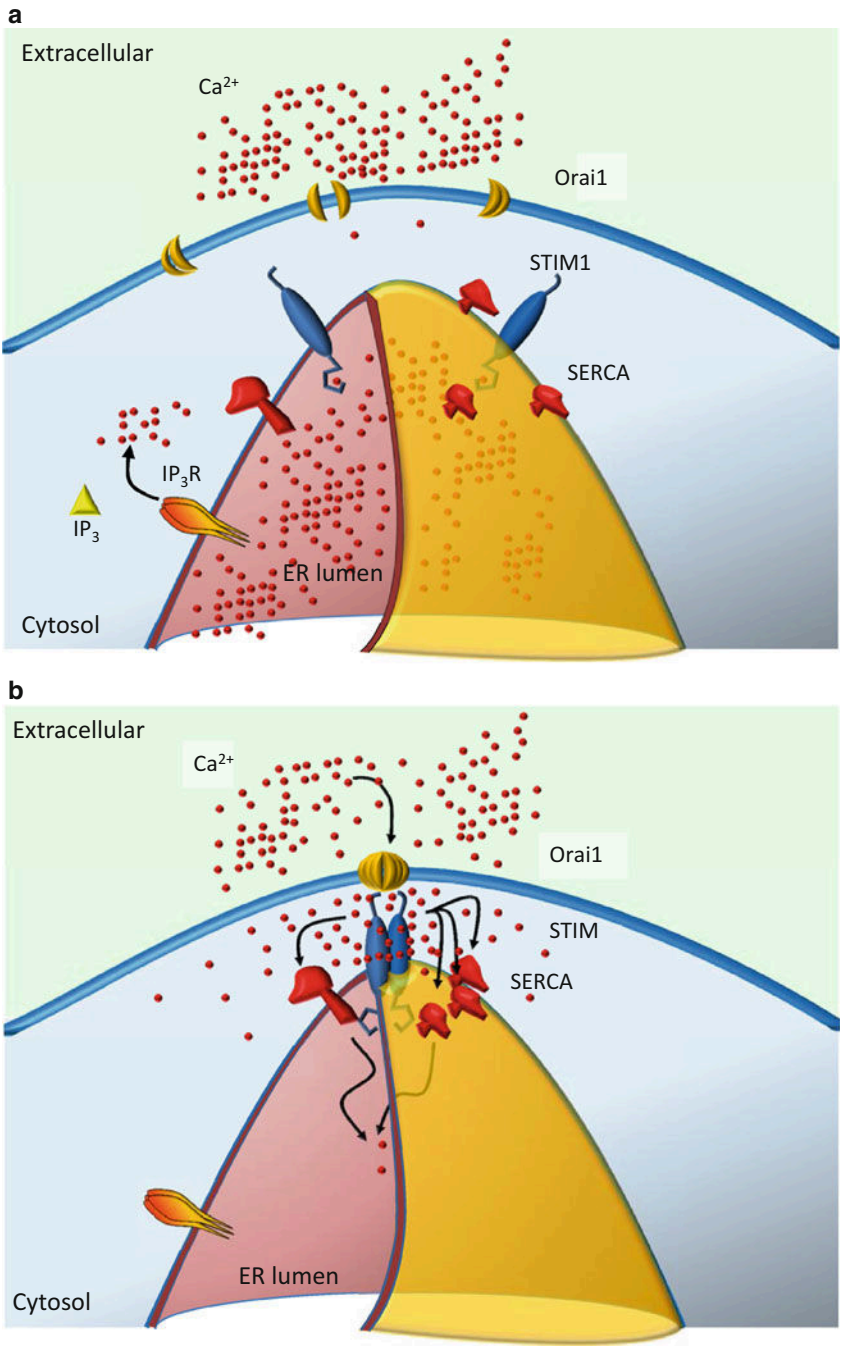

Fig. 14.3 Spatial organization of the SOC partners Orai1, STIM1 and SERCA. (**a**) Under resting conditions, high Ca^{2+} concentrations in the ER lumen keep SERCA and STIM1 homogenously at the surface of the ER membrane. Similarly, Orai is diffusely organized on the plasma membrane (*PM*). (**b**) Upon Ca^{2+} depletion though IP3R, STIM1 proteins oligomerise and translocate to form cluster under PM raft domains wherein Orai1 also form hexamers. SERCA pumps are also concentrated around STIM1 oligomers. Such organisation will avoid massive diffusion of Ca^{2+} ions in the cytosol and Ca^{2+} are re-uptaken by the pumps as soon as they reach the cytosol

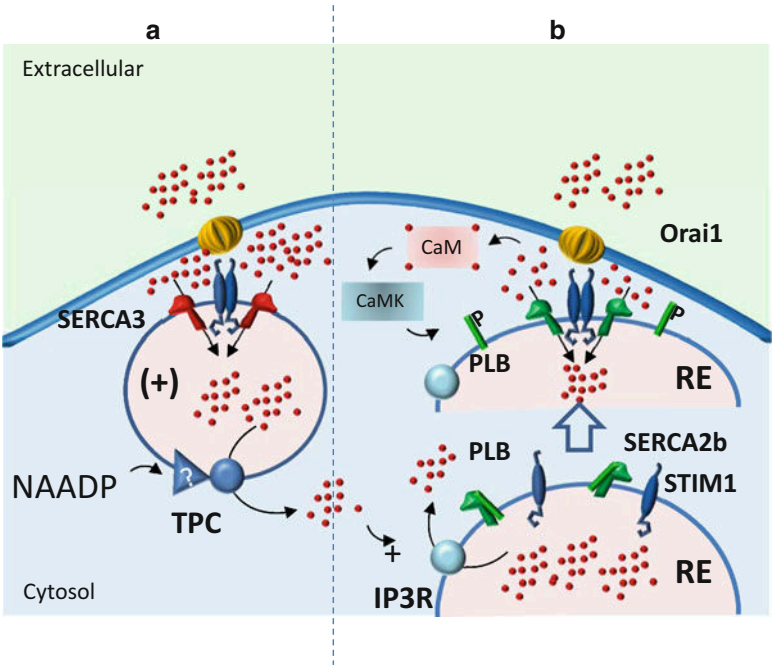

Fig. 14.4 Hypothetical representation of two SERCA3 and SERCA2b associated SOCe pathways. (**a**) Acidic granules (+) are enriched in SERCA3 and localized near the plasma membrane. Ca^{2+} depletion can produce a rapid activation of SOC as STIM1 is already close to the ER-PM junction. Presence of SERCA that are activated in high Ca^{2+} environment will also rapidly capture cytosol Ca^{2+} back into the granule avoiding its diffusion to the whole cell. Alternatively, depletion though TPC channels (NAADP receptor?) can act as trigger to potentialize IP_3R. (**b**) Ca^{2+} depletion through IP3R will induced STIM1 activation and translocation to the ER-PM junction. Orai1 activation will produce high Ca^{2+} microdomains that can activate Calmodulin (*Cam*)-dependent kinase (*CamK*) leading to the phosphorylation of phospholamban (*PLB*) and its dissociation from SERCA2b resulting in the activation of SERCA

be 0.05 $\mu m^2/s$. As the authors estimated that STIM1 will only form a cluster at a distance of 2 μm, STIM1 oligomers would take about 40s to achieve such a relocalization [82].

Additionally, it is important to keep in mind that SERCA3 and SERCA2 activities are differently regulated. SERCA2b has a much higher affinity for Ca^{2+} and this could allow those pumps to work at basal cytosolic Ca^{2+} level unless to be negatively controlled by phospholamban (PLB), a cAMP-dependent kinase whose phosphorylation by PKA and CAMKII kinase can disrupt its association with SERCA2b and can increase the SERCA affinity [98, 99]. This signaling cascade can provide a useful mechanism that specifically controls the SERCA2b Ca^{2+} uptake (Fig. 14.4b). Here, the Ca^{2+} uptake involves different signaling cascades including protein movements on membrane and in the cytosol, which could take a longer time to be func-

tional. It is therefore possible that the resulting SOCe is larger than the one depending on SERCA3-associated granule and overtakes the whole cytosol.

14.4 Coupling Response Between Mitochondria and SOCe

Mitochondria are multifunctional organelles that control a large number of cellular processes. Mitochondria are the cell energy factories that burn oxygen during oxidative phosphorylation to produce the cellular ATP used for biochemical reactions. They contain two membranes. In contact with the cytosol, is an outer membrane that is permeable, due to the abundant expression of voltage dependent anion selective channel (VDAC), acting as a general diffusion pore for small hydrophilic molecules such as ADP and ATP [100]. The larger Ca^{2+} uptake into the mitochondrial matrix occurs predominantly through the impermeable inner membrane via the ruthenium red-sensitive mitochondrial Ca^{2+} uniporter (MCU) complex.

Therefore, mitochondria are another crucial compartment that plays an important role in Ca^{2+} homeostasis.

Early models even proposed mitochondria as intermediate stores for Ca^{2+} originating from the extracellular medium before being transferred into the ER [101–103]. To do so, mitochondria should be located between the PM and ER. With the latter demonstration of the ER-PM junction and the direct interaction between STIM1 and Orai1 it is now hard to imagine such a role [104, 105].

Nevertheless, Mitochondria adjacent to ER and in the proximity of the SOCe channel, could take large amount of Ca^{2+} which dissipates high Ca^{2+} concentration in the ER-PM environment, facilitating STIM1 oligomerization and preventing Orai1 inactivation by Ca^{2+} [106, 107].

Ca^{2+} pumping by both SERCA and PMCA is an ATP-dependent process that is favored by the presence of activated mitochondria. By supplying ATP to the PMCA, mitochondria favor the transport of Ca^{2+} ions from the lumen of the ER to the extracellular medium when signaling is triggered, and thus favor SOCE activation. In contrast, by energizing SERCA, mitochondria improve store refilling and prevent SOCE activation (for review see [108]. Whether mitochondria enhance or reduce the level of ER depletion thus depends on the spatial organization of the organelles and on the relative contribution of mitochondria in buffering Ca^{2+} action (in the vicinity of Ca^{2+} depletion and Ca^{2+} entry channels) and in supplying ATP for SERCA and PMCA.

However, In more recent reports, it seems that Ca^{2+} uptake by mitochondria is essentially independent of SOC [78] and is much more sensitive to Ca^{2+} release by the ER than Ca^{2+} originating from the extracellular medium [109, 110]. Both organelles are finely tuned and interact one with each other. Although no direct link has ever been established between STIM1 and mitochondria, mitochondria and ER stores have been reported to be in close contact and to be able to exchange Ca^{2+} [111–113].

Additionally, recent findings also suggest that mitochondria can control the SOC independently of the Ca^{2+} buffering action through its action on STIM1 trafficking. Some authors have proposed that under depolarization, mitochondria might have a positive effect of STIM1 migration and subsequent SOC activation, a mechanism that appears to be dependent on mitofusin 2 (Mfn2) [114].

14.5 Ca^{2+} Tunnelling: Link Between SOCe and Store Depletion

Lastly, an important part of the relationship between ER refilling and SOC Ca^{2+} entry could rely on the Ca^{2+} tunnelling which has been described preferentially in highly polarized cells; i.e. pancreatic acinar cells. Such a mechanism allows the intracellular propagation of Ca^{2+} signals from a local entry at the basolateral membrane to distant targets several μm away. In these cells, Ca^{2+} across the cytosol would have been blocked by the greater buffering capacity of the cytosol, including mitochondria [115]. This supports the concept that entering Ca^{2+} is taken up into the ER by the SERCA, where it rapidly diffuses to the apical region and it is released through IP_3R. In the ER, Ca^{2+} ions can travel much easier (lower Ca^{2+} buffer activities and lower capacities of Ca^{2+} binding proteins of the ER lumen compared to the cytosol) [116, 117]. A similar mechanism is also proposed for induction of SOCe dependent Ca^{2+} signalling activation, such as NFAT, without induction of a global Ca^{2+} signal and faraway of the SOCe Ca^{2+} microdomains [118].

14.6 Conclusions

In a great number of cell types, Ca^{2+} signal is a message coded by change in Ca^{2+} concentration from steady increase to high oscillation frequencies with a period ranging from a few seconds to a few minutes. These Ca^{2+} oscillations are thought to control a wide variety of cellular processes, and are often organized into intracellular and intercellular Ca^{2+} waves.

SOCe plays a crucial part in those processes. Although the first goal of this Ca^{2+} influx into the cytosol via SOCe is to refill intracellular stores after their depletion, the impact of SOCe is major under physiological conditions. The existence of the SOC process is based on the crosstalk between distinct compartments. SERCA, the ER Ca^{2+} pump, STIM1 and Orai1 and TRPC1 can be localized at the ER-PM junction. This results in a very efficient refilling of intracellular stores.

The crosstalk between SOCe and intracellular stores allows a complex and finely tuned regulation of Ca^{2+} events either at the mouth of the channel, between distinct Ca^{2+} stores including mitochondria, or even far more distant from the SOC clusters into the cell via the diffusion of the message inside the ER. This is why this crosstalk appears much more than a simple process that refills intracellular stores but is recognized as a crucial member of the Ca^{2+} signalling.

References

1. Williams RJ (2006) The evolution of calcium biochemistry. Biochim Biophys Acta 1763(11):1139–1146
2. Parekh AB (2008) Ca2+ microdomains near plasma membrane Ca2+ channels: impact on cell function. J Physiol 586(13):3043–3054
3. McCarron JG, Chalmers S, Bradley KN, MacMillan D, Muir TC (2006) Ca2+ microdomains in smooth muscle. Cell Calcium 40(5–6):461–493
4. Taylor CW, Berridge MJ, Cooke AM, Potter BV (1989) Inositol 1,4,5-trisphosphorothioate, a stable analogue of inositol trisphosphate which mobilizes intracellular calcium. Biochem J 259(3):645–650
5. Berridge MJ (2004) Calcium signal transduction and cellular control mechanisms. Biochim Biophys Acta 1742(1–3):3–7
6. Berridge MJ (2006) Calcium microdomains: organization and function. Cell Calcium 40(5–6):405–412
7. Tojyo Y, Morita T, Nezu A, Tanimura A (2014) Key components of store-operated Ca2+ entry in non-excitable cells. J Pharmacol Sci 125(4):340–346
8. Putney JW (1986) A model for receptor-regulated calcium entry. Cell Calcium 7:1–12
9. Takemura H, Hughes AR, Thastrup O, Putney JWJ (1989) Activation of calcium entry by the tumor promoter thapsigargin in parotid acinar cells. J Biol Chem 264:12266–12271
10. Thastrup O, Cullen PJ, Drobak BK, Hanley MR, Dawson AP (1990) Thapsigargin, a tumor promotor, discharges intracellular Ca^{2+} stores by specific inhibition of the endoplasmic reticulum Ca^{2+} -ATPase. Proc Natl Acad Sci U S A 87:2466–2470
11. Lewis RS, Cahalan MD (1989) Mitogen-induced oscillations of cytosolic Ca2+ and transmembrane Ca2+ current in human leukemic T cells. Cell Regul 1(1):99–112
12. von Tscharner V, Prod'hom B, Baggiolini M, Reuter H (1986) Ion channels in human neutrophils activated by a rise in free cytosolic calcium concentration. Nature 324(6095):369–372
13. Kuno M, Gardner P (1987) Ion channels activated by inositol 1,4,5-trisphosphate in plasma membrane of human T-lymphocytes. Nature 326(6110):301–304
14. Penner R, Matthews G, Neher E (1988) Regulation of calcium influx by second messengers in rat mast cells. Nature 334(6182):499–504
15. Randriamampita C, Tsien RY (1993) Emptying of intracellular Ca2+ stores releases a novel small messenger that stimulates Ca2+ influx. Nature 364(6440):809–814
16. Smani T, Zakharov SI, Csutora P, Leno E, Trepakova ES, Bolotina VM (2004) A novel mechanism for the store-operated calcium influx pathway. Nat Cell Biol 6(2):113–120
17. Dramane G, Akpona S, Besnard P, Khan NA, Pt A (2014) Cell mechanisms of gustatory lipids perception and modulation of the dietary fat preference. Biochimie 107 Pt A:11–14
18. Irvine R (1990) 'Quantal' Ca^{2+} release and the control of Ca^{2+} entry by inositol phosphates. A possible mechanism. FEBS Lett 263:5–9
19. Redondo PC, Jardin I, Lopez JJ, Salido GM, Rosado JA (2008) Intracellular Ca(2+) store depletion induces the formation of macromolecular complexes involving hTRPC1, hTRPC6, the type II IP(3) receptor and SERCA3 in human platelets. Biochim Biophys Acta 1783(6):1163–1176
20. Tang J, Lin Y, Zhang Z, Tikunova S, Birnbaumer L, Zhu MX (2001) Identification of common binding sites for calmodulin and inositol 1,4,5-trisphosphate receptors on the carboxyl termini of trp channels. J Biol Chem 276(24):21303–21310
21. Rosado JA, Sage SO (2001) Activation of store-mediated calcium entry by secretion-like coupling between the inositol 1,4,5-trisphosphate receptor type II and human transient receptor potential (hTrp1) channels in human platelets. Biochem J 356(Pt 1):191–198
22. Rosado JA, Brownlow SL, Sage SO (2002) Endogenously expressed Trp1 is involved in store-mediated Ca2+ entry by conformational coupling in human platelets. J Biol Chem 277(44):42157–42163

23. Liou J, Kim ML, Heo WD, Jones JT, Myers JW, Ferrell JE Jr, Meyer T (2005) STIM is a Ca2+ sensor essential for Ca2+-store-depletion-triggered Ca2+ influx. Curr Biol 15(13):1235–1241
24. Roos J, DiGregorio PJ, Yeromin AV, Ohlsen K, Lioudyno M, Zhang S, Safrina O, Kozak JA, Wagner SL, Cahalan MD, Velicelebi G, Stauderman KA (2005) STIM1, an essential and conserved component of store-operated Ca2+ channel function. J Cell Biol 169(3):435–445
25. Feske S, Gwack Y, Prakriya M, Srikanth S, Puppel SH, Tanasa B, Hogan PG, Lewis RS, Daly M, Rao A (2006) A mutation in Orai1 causes immune deficiency by abrogating CRAC channel function. Nature 441(7090):179–185
26. Vig M, Beck A, Billingsley JM, Lis A, Parvez S, Peinelt C, Koomoa DL, Soboloff J, Gill DL, Fleig A, Kinet JP, Penner R (2006) CRACM1 multimers form the ion-selective pore of the CRAC channel. Curr Biol 16(20):2073–2079
27. Zhang SL, Yeromin AV, Zhang XH, Yu Y, Safrina O, Penna A, Roos J, Stauderman KA, Cahalan MD (2006) Genome-wide RNAi screen of Ca(2+) influx identifies genes that regulate Ca(2+) release-activated Ca(2+) channel activity. Proc Natl Acad Sci U S A 103(24):9357–9362
28. Spassova MA, Soboloff J, He LP, Xu W, Dziadek MA, Gill DL (2006) STIM1 has a plasma membrane role in the activation of store-operated Ca(2+) channels. Proc Natl Acad Sci U S A 103(11):4040–4045
29. Shen WW, Frieden M, Demaurex N (2011) Local cytosolic Ca2+ elevations are required for stromal interaction molecule 1 (STIM1) de-oligomerization and termination of store-operated Ca2+ entry. J Biol Chem 286(42):36448–36459
30. Zhang SL, Yu Y, Roos J, Kozak JA, Deerinck TJ, Ellisman MH, Stauderman KA, Cahalan MD (2005) STIM1 is a Ca2+ sensor that activates CRAC channels and migrates from the Ca2+ store to the plasma membrane. Nature 437(7060):902–905
31. Stathopulos PB, Zheng L, Li GY, Plevin MJ, Ikura M (2008) Structural and mechanistic insights into STIM1-mediated initiation of store-operated calcium entry. Cell 135(1):110–122
32. Demaurex N, Frieden M (2003) Measurements of the free luminal ER Ca(2+) concentration with targeted "cameleon" fluorescent proteins. Cell Calcium 34(2):109–119
33. Stathopulos PB, Li GY, Plevin MJ, Ames JB, Ikura M (2006) Stored Ca2+ depletion-induced oligomerization of stromal interaction molecule 1 (STIM1) via the EF-SAM region: an initiation mechanism for capacitive Ca2+ entry. J Biol Chem 281(47):35855–35862
34. Zheng L, Stathopulos PB, Schindl R, Li GY, Romanin C, Ikura M (2011) Auto-inhibitory role of the EF-SAM domain of STIM proteins in store-operated calcium entry. Proc Natl Acad Sci U S A 108(4):1337–1342
35. Luik RM, Wang B, Prakriya M, Wu MM, Lewis RS (2008) Oligomerization of STIM1 couples ER calcium depletion to CRAC channel activation. Nature 454(7203):538–542
36. Wu MM, Buchanan J, Luik RM, Lewis RS (2006) Ca2+ store depletion causes STIM1 to accumulate in ER regions closely associated with the plasma membrane. J Cell Biol 174(6):803–813
37. Orci L, Ravazzola M, Le Coadic M, Shen WW, Demaurex N, Cosson P (2009) STIM1-induced precortical and cortical subdomains of the endoplasmic reticulum. Proc Natl Acad Sci U S A 106(46):19358–19362
38. Brandman O, Liou J, Park WS, Meyer T (2007) STIM2 is a feedback regulator that stabilizes basal cytosolic and endoplasmic reticulum Ca2+ levels. Cell 131(7):1327–1339
39. Stathopulos PB, Zheng L, Ikura M (2009) Stromal interaction molecule (STIM) 1 and STIM2 calcium sensing regions exhibit distinct unfolding and oligomerization kinetics. J Biol Chem 284(2):728–732
40. McNally BA, Yamashita M, Engh A, Prakriya M (2009) Structural determinants of ion permeation in CRAC channels. Proc Natl Acad Sci U S A 106(52):22516–22521
41. Penna A, Demuro A, Yeromin AV, Zhang SL, Safrina O, Parker I, Cahalan MD (2008) The CRAC channel consists of a tetramer formed by Stim-induced dimerization of Orai dimers. Nature 456(7218):116–120

42. Madl J, Weghuber J, Fritsch R, Derler I, Fahrner M, Frischauf I, Lackner B, Romanin C, Schutz GJ (2010) Resting state Orai1 diffuses as homotetramer in the plasma membrane of live mammalian cells. J Biol Chem 285(52):41135–41142
43. Vig M, Peinelt C, Beck A, Koomoa DL, Rabah D, Koblan-Huberson M, Kraft S, Turner H, Fleig A, Penner R, Kinet JP (2006) CRACM1 is a plasma membrane protein essential for store-operated Ca2+ entry. Science 312(5777):1220–1223
44. Prakriya M, Feske S, Gwack Y, Srikanth S, Rao A, Hogan PG (2006) Orai1 is an essential pore subunit of the CRAC channel. Nature 443(7108):230–233
45. Mercer JC, Dehaven WI, Smyth JT, Wedel B, Boyles RR, Bird GS, Putney JW Jr (2006) Large store-operated calcium selective currents due to co-expression of Orai1 or Orai2 with the intracellular calcium sensor, Stim1. J Biol Chem 281(34):24979–24990
46. Hou X, Pedi L, Diver MM, Long SB (2012) Crystal structure of the calcium release-activated calcium channel Orai. Science 338(6112):1308–1313
47. Smyth JT, Dehaven WI, Bird GS, Putney JW Jr (2008) Ca2+-store-dependent and -independent reversal of Stim1 localization and function. J Cell Sci 121(Pt 6):762–772
48. Park CY, Hoover PJ, Mullins FM, Bachhawat P, Covington ED, Raunser S, Walz T, Garcia KC, Dolmetsch RE, Lewis RS (2009) STIM1 clusters and activates CRAC channels via direct binding of a cytosolic domain to Orai1. Cell 136(5):876–890
49. Yuan JP, Zeng W, Dorwart MR, Choi YJ, Worley PF, Muallem S (2009) SOAR and the polybasic STIM1 domains gate and regulate Orai channels. Nat Cell Biol 11(3):337–343
50. Muik M, Fahrner M, Derler I, Schindl R, Bergsmann J, Frischauf I, Groschner K, Romanin C (2009) A cytosolic homomerization and a modulatory domain within STIM1 C terminus determine coupling to ORAI1 channels. J Biol Chem 284(13):8421–8426
51. Kawasaki T, Lange I, Feske S (2009) A minimal regulatory domain in the C terminus of STIM1 binds to and activates ORAI1 CRAC channels. Biochem Biophys Res Commun 385(1):49–54
52. Korzeniowski MK, Manjarres IM, Varnai P, Balla T (2010) Activation of STIM1-Orai1 involves an intramolecular switching mechanism. Sci Signal 3(148):ra82
53. Zhou Y, Meraner P, Kwon HT, Machnes D, Oh-hora M, Zimmer J, Huang Y, Stura A, Rao A, Hogan PG (2010) STIM1 gates the store-operated calcium channel ORAI1 in vitro. Nat Struct Mol Biol 17(1):112–116
54. Stathopulos PB, Schindl R, Fahrner M, Zheng L, Gasmi-Seabrook GM, Muik M, Romanin C, Ikura M (2013) STIM1/Orai1 coiled-coil interplay in the regulation of store-operated calcium entry. Nat Commun 4:2963
55. Zhou Y, Srinivasan P, Razavi S, Seymour S, Meraner P, Gudlur A, Stathopulos PB, Ikura M, Rao A, Hogan PG (2013) Initial activation of STIM1, the regulator of store-operated calcium entry. Nat Struct Mol Biol 20(8):973–981
56. Derler I, Plenk P, Fahrner M, Muik M, Jardin I, Schindl R, Gruber HJ, Groschner K, Romanin C (2013) The extended transmembrane Orai1 N-terminal (ETON) region combines binding interface and gate for Orai1 activation by STIM1. J Biol Chem 288(40):29025–29034
57. McNally BA, Somasundaram A, Yamashita M, Prakriya M (2012) Gated regulation of CRAC channel ion selectivity by STIM1. Nature 482(7384):241–245
58. Hoth M, Penner R (1992) Depletion of intracellular calcium stores activates a calcium current in mast cells. Nature 355(6358):353–356
59. Demuro A, Penna A, Safrina O, Yeromin AV, Amcheslavsky A, Cahalan MD, Parker I (2011) Subunit stoichiometry of human Orai1 and Orai3 channels in closed and open states. Proc Natl Acad Sci U S A 108(43):17832–17837
60. Shim AH, Tirado-Lee L, Prakriya M (2015) Structural and functional mechanisms of CRAC channel regulation. J Mol Biol 427(1):77–93
61. Majewski L, Kuznicki J (2015) SOCE in neurons: signaling or just refilling? Biochim Biophys Acta 1853(9):1940–1952
62. Montell C (2005) The TRP superfamily of cation channels. Sci STKE 2005(272):re3
63. DeHaven WI, Jones BF, Petranka JG, Smyth JT, Tomita T, Bird GS, Putney JW Jr (2009) TRPC channels function independently of STIM1 and Orai1. J Physiol 587(Pt 10):2275–2298

64. Putney JW (2009) Capacitative calcium entry: from concept to molecules. Immunol Rev 231(1):10–22
65. Beech DJ (2005) TRPC1: store-operated channel and more. Pflugers Arch 451(1):53–60
66. Vaca L, Sampieri A (2002) Calmodulin modulates the delay period between release of calcium from internal stores and activation of calcium influx via endogenous TRP1 channels. J Biol Chem 277(44):42178–42187
67. Salido GM, Jardin I, Rosado JA (2011) The TRPC ion channels: association with Orai1 and STIM1 proteins and participation in capacitative and non-capacitative calcium entry. Adv Exp Med Biol 704:413–433
68. Zeng W, Yuan JP, Kim MS, Choi YJ, Huang GN, Worley PF, Muallem S (2008) STIM1 gates TRPC channels, but not Orai1, by electrostatic interaction. Mol Cell 32(3):439–448
69. Lopez JJ, Salido GM, Pariente JA, Rosado JA (2006) Interaction of STIM1 with endogenously expressed human canonical TRP1 upon depletion of intracellular Ca2+ stores. J Biol Chem 281(38):28254–28264
70. Liu X, Wang W, Singh BB, Lockwich T, Jadlowiec J, O'Connell B, Wellner R, Zhu MX, Ambudkar IS (2000) Trp1, a candidate protein for the store-operated Ca(2+) influx mechanism in salivary gland cells. J Biol Chem 275(5):3403–3411
71. Liao Y, Erxleben C, Yildirim E, Abramowitz J, Armstrong DL, Birnbaumer L (2007) Orai proteins interact with TRPC channels and confer responsiveness to store depletion. Proc Natl Acad Sci U S A 104(11):4682–4687
72. Liao Y, Erxleben C, Abramowitz J, Flockerzi V, Zhu MX, Armstrong DL, Birnbaumer L (2008) Functional interactions among Orai1, TRPCs, and STIM1 suggest a STIM-regulated heteromeric Orai/TRPC model for SOCE/Icrac channels. Proc Natl Acad Sci U S A 105(8):2895–2900
73. Redondo PC, Harper AG, Harper MT, Brownlow SL, Rosado JA, Sage SO (2007) hTRPC1-associated alpha-actinin, and not hTRPC1 itself, is tyrosine phosphorylated during human platelet activation. J Thromb Haemost 5(12):2476–2483
74. Asanov A, Sampieri A, Moreno C, Pacheco J, Salgado A, Sherry R, Vaca L (2015) Combined single channel and single molecule detection identifies subunit composition of STIM1-activated transient receptor potential canonical (TRPC) channels. Cell Calcium 57(1):1–13
75. Hofmann T, Obukhov AG, Schaefer M, Harteneck C, Gudermann T, Schultz G (1999) Direct activation of human TRPC6 and TRPC3 channels by diacylglycerol. Nature 397(6716):259–263
76. Gudermann T, Mederos y Schnitzler M, Dietrich A (2004) Receptor-operated cation entry – more than esoteric terminology? Sci STKE 2004(243):pe35
77. Jardin I, Lopez JJ, Salido GM, Rosado JA (2008) Functional relevance of the de novo coupling between hTRPC1 and type II IP3 receptor in store-operated Ca2+ entry in human platelets. Cell Signal 20(4):737–747
78. Alonso MT, Manjarres IM, Garcia-Sancho J (2012) Privileged coupling between Ca(2+) entry through plasma membrane store-operated Ca(2+) channels and the endoplasmic reticulum Ca(2+) pump. Mol Cell Endocrinol 353(1–2):37–44
79. Burk SE, Lytton J, MacLennan DH, Shull GE (1989) cDNA cloning, functional expression, and mRNA tissue distribution of a third organellar Ca^{2+} pump. J Biol Chem 264(31):18561–18568
80. Bobe R, Bredoux R, Wuytack F, Quarck R, Kovacs T, Papp B, Corvazier E, Magnier C, Enouf J (1994) The rat platelet 97-kDa Ca^{2+}ATPase isoform is the sarcoendoplasmic reticulum Ca^{2+}ATPase 3 protein. J Biol Chem 269(2):1417–1424
81. Dally S, Monceau V, Corvazier E, Bredoux R, Raies A, Bobe R, del Monte F, Enouf J (2009) Compartmentalized expression of three novel sarco/endoplasmic reticulum Ca^{2+}ATPase 3 isoforms including the switch to ER stress, SERCA3f, in non-failing and failing human heart. Cell Calcium 45(2):144–154
82. Liou J, Fivaz M, Inoue T, Meyer T (2007) Live-cell imaging reveals sequential oligomerization and local plasma membrane targeting of stromal interaction molecule 1 after Ca2+ store depletion. Proc Natl Acad Sci U S A 104(22):9301–9306

83. Lemonnier L, Trebak M, Lievremont JP, Bird GS, Putney JW Jr (2006) Protection of TRPC7 cation channels from calcium inhibition by closely associated SERCA pumps. FASEB J 20(3):503–505
84. Redondo PC, Salido GM, Pariente JA, Sage SO, Rosado JA (2008) SERCA2b and 3 play a regulatory role in store-operated calcium entry in human platelets. Cell Signal 20(2):337–346
85. Bobe R, Hadri L, Lopez JJ, Sassi Y, Atassi F, Karakikes I, Liang L, Limon I, Lompre AM, Hatem SN, Hajjar RJ, Lipskaia L (2011) SERCA2a controls the mode of agonist-induced intracellular Ca^{2+} signal, transcription factor NFAT and proliferation in human vascular smooth muscle cells. J Mol Cell Cardiol 50(4):621–633
86. Sampieri A, Zepeda A, Asanov A, Vaca L (2009) Visualizing the store-operated channel complex assembly in real time: identification of SERCA2 as a new member. Cell Calcium 45(5):439–446
87. Lopez JJ, Jardin I, Bobe R, Pariente JA, Enouf J, Salido GM, Rosado JA (2008) STIM1 regulates acidic Ca2+ store refilling by interaction with SERCA3 in human platelets. Biochem Pharmacol 75(11):2157–2164
88. Jousset H, Frieden M, Demaurex N (2007) STIM1 knockdown reveals that store-operated Ca2+ channels located close to sarco/endoplasmic Ca2+ ATPases (SERCA) pumps silently refill the endoplasmic reticulum. J Biol Chem 282(15):11456–11464
89. Vaca L (2010) SOCIC: the store-operated calcium influx complex. Cell Calcium 47(3):199–209
90. Manjarres IM, Alonso MT, Garcia-Sancho J (2011) Calcium entry-calcium refilling (CECR) coupling between store-operated Ca(2+) entry and sarco/endoplasmic reticulum Ca(2+)-ATPase. Cell Calcium 49(3):153–161
91. Kovacs T, Berger G, Corvazier E, Paszty K, Brown A, Bobe R, Papp B, Wuytack F, Cramer EM, Enouf J (1997) Immunolocalization of the multi-sarco/endoplasmic reticulum Ca^{2+}ATPase system in human platelets. Br J Haematol 97(1):192–203
92. Lopez JJ, Redondo PC, Salido GM, Pariente JA, Rosado JA (2006) Two distinct Ca(2+) compartments show differential sensitivity to thrombin, ADP and vasopressin in human platelets. Cell Signal 18(3):373–381
93. Rosado JA, Lopez JJ, Harper AG, Harper MT, Redondo PC, Pariente JA, Sage SO, Salido GM (2004) Two pathways for store-mediated calcium entry differentially dependent on the actin cytoskeleton in human platelets. J Biol Chem 279(28):29231–29235
94. Lopez JJ, Camello-Almaraz C, Pariente JA, Salido GM, Rosado JA (2005) Ca2+ accumulation into acidic organelles mediated by Ca2+- and vacuolar H+-ATPases in human platelets. Biochem J 390(Pt 1):243–252
95. Churchill GC, Okada Y, Thomas JM, Genazzani AA, Patel S, Galione A (2002) NAADP mobilizes Ca(2+) from reserve granules, lysosome-related organelles, in sea urchin eggs. Cell 111(5):703–708
96. Ruas M, Davis LC, Chen CC, Morgan AJ, Chuang KT, Walseth TF, Grimm C, Garnham C, Powell T, Platt N, Platt FM, Biel M, Wahl-Schott C, Parrington J, Galione A (2015) Expression of Ca2+-permeable two-pore channels rescues NAADP signalling in TPC-deficient cells. EMBO J 34(13):1743–1758
97. Patel S (2015) Function and dysfunction of two-pore channels. Sci Signal 8(384):re7
98. Simmerman HK, Jones LR (1998) Phospholamban: protein structure, mechanism of action, and role in cardiac function. Physiol Rev 78(4):921–947
99. Bhupathy P, Babu GJ, Periasamy M (2007) Sarcolipin and phospholamban as regulators of cardiac sarcoplasmic reticulum Ca2+ ATPase. J Mol Cell Cardiol 42(5):903–911
100. Betz C, Stracka D, Prescianotto-Baschong C, Frieden M, Demaurex N, Hall MN (2013) Feature Article: mTOR complex 2-Akt signaling at mitochondria-associated endoplasmic reticulum membranes (MAM) regulates mitochondrial physiology. Proc Natl Acad Sci U S A 110(31):12526–12534
101. Bernardi P (1999) Mitochondrial transport of cations: channels, exchangers, and permeability transition. Physiol Rev 79(4):1127–1155

102. Malli R, Frieden M, Osibow K, Zoratti C, Mayer M, Demaurex N, Graier WF (2003) Sustained Ca2+ transfer across mitochondria is Essential for mitochondrial Ca2+ buffering, sore-operated Ca2+ entry, and Ca2+ store refilling. J Biol Chem 278(45):44769–44779
103. Hoth M, Button DC, Lewis RS (2000) Mitochondrial control of calcium-channel gating: a mechanism for sustained signaling and transcriptional activation in T lymphocytes. Proc Natl Acad Sci U S A 97(19):10607–10612
104. Park MK, Ashby MC, Erdemli G, Petersen OH, Tepikin AV (2001) Perinuclear, perigranular and sub-plasmalemmal mitochondria have distinct functions in the regulation of cellular calcium transport. EMBO J 20(8):1863–1874
105. Lewis RS (2007) The molecular choreography of a store-operated calcium channel. Nature 446(7133):284–287
106. Gilabert JA, Parekh AB (2000) Respiring mitochondria determine the pattern of activation and inactivation of the store-operated Ca(2+) current I(CRAC). EMBO J 19(23):6401–6407
107. Parekh AB, Putney JW Jr (2005) Store-operated calcium channels. Physiol Rev 85(2):757–810
108. Demaurex N, Poburko D, Frieden M (2009) Regulation of plasma membrane calcium fluxes by mitochondria. Biochim Biophys Acta 1787(11):1383–1394
109. Csordas G, Varnai P, Golenar T, Roy S, Purkins G, Schneider TG, Balla T, Hajnoczky G (2010) Imaging interorganelle contacts and local calcium dynamics at the ER-mitochondrial interface. Mol Cell 39(1):121–132
110. Giacomello M, Drago I, Bortolozzi M, Scorzeto M, Gianelle A, Pizzo P, Pozzan T (2010) Ca2+ hot spots on the mitochondrial surface are generated by Ca2+ mobilization from stores, but not by activation of store-operated Ca2+ channels. Mol Cell 38(2):280–290
111. Rizzuto R, Pinton P, Carrington W, Fay FS, Fogarty KE, Lifshitz LM, Tuft RA, Pozzan T (1998) Close contacts with the endoplasmic reticulum as determinants of mitochondrial Ca^{2+} responses. Science 280:1763–1766
112. Arnaudeau S, Kelley WL, Walsh JV Jr, Demaurex N (2001) Mitochondria recycle Ca^{2+} to the endoplasmic reticulum and prevent the depletion of neighboring endoplasmic reticulum regions. J Biol Chem 276(31):29430–29439
113. Li B, Xiao L, Wang ZY, Zheng PS (2014) Knockdown of STIM1 inhibits 6-hydroxydopamine-induced oxidative stress through attenuating calcium-dependent ER stress and mitochondrial dysfunction in undifferentiated PC12 cells. Free Radic Res 48(7):758–768
114. Singaravelu K, Nelson C, Bakowski D, de Brito OM, Ng SW, Di Capite J, Powell T, Scorrano L, Parekh AB (2011) Mitofusin 2 regulates STIM1 migration from the Ca2+ store to the plasma membrane in cells with depolarized mitochondria. J Biol Chem 286(14):12189–12201
115. Tinel H, Cancela JM, Mogami H, Gerasimenko JV, Gerasimenko OV, Tepikin AV, Petersen OH (1999) Active mitochondria surrounding the pancreatic acinar granule region prevent spreading of inositol trisphosphate-evoked local cytosolic Ca(2+) signals. EMBO J 18(18):4999–5008
116. Mogami H, Nakano K, Tepikin AV, Petersen OH (1997) Ca2+ flow via tunnels in polarized cells: recharging of apicl Ca2+ stores by focal Ca2+ entry through basal membrane patch. Cell 88:49–55
117. Mogami H, Tepikin AV, Petersen OH (1998) Termination of cytosolic Ca^{2+} signals: Ca^{2+} reuptake into intracellular stores is regulated by the free Ca^{2+} concentration in the store lumen. EMBO J 17(2):435–442
118. Courjaret R, Machaca K (2014) Mid-range Ca2+ signalling mediated by functional coupling between store-operated Ca2+ entry and IP3-dependent Ca2+ release. Nat Commun 5:3916